

Eidesstattliche Erklärung

Ich erkläre an Eides statt, dass ich die vorliegende Arbeit selbstständig verfasst, andere als die angegebenen Quellen/Hilfsmittel nicht benutzt, und die den benutzten Quellen wörtlich und inhaltlich entnommenen Stellen als solche kenntlich gemacht habe.

Graz, am

.....

(Unterschrift)

Statutory declaration

I declare that I have authored this thesis independently, that I have not used other than the declared sources / resources, and that I have explicitly marked all material which has been quoted either literally or by content from the used sources.

Graz,

.....

(signature)

Preface of the author

First of all I would like to express the deepest gratitude to my thesis supervisor Univ.-Prof. Dipl.-Ing. Dr.techn. Roman Marte from the Institute of Soil Mechanics and Foundation Engineering at TU Graz for his assistance, support and valuable comments. Without his help I would not have been able to get my first real experience in the geotechnical engineering. Thank you for sharing your knowledge during the exciting and inspiring lectures.

I would also like to thank the experts Dipl.-Ing. Dr.techn. Christoph Wiltafsky and Dipl.-Ing. Herbert Gaube. Their advices, critical opinions and help were extremely important not only for this thesis, but as well for my personal and professional development.

Finally, I must express my very profound gratitude to my parents and my dear friends Katharina and Matthew for providing me with unfailing support and continuous encouragement through the process of writing this thesis. This accomplishment would not have been possible without them. Thank you.

Kurzfassung

In der gegenständlichen Arbeit wird für ein Projekt an der Mittelmeerküste das dort zur Anwendung kommende Verfahren zur Bodenverbesserung näher untersucht.

Um die Konsolidierung zu beschleunigen und die Setzungen in der Phase nach den Bauarbeiten zu reduzieren, sollen zur Bodenverbesserung vertikale Drains in Kombination mit einer Überlastschüttung für einen großflächigen Bereich angewendet werden. Das Bodenverbesserungskonzept wird in Übereinstimmung mit den erwarteten Betriebslasten und mit den Anforderungen optimiert, die vom Auftraggeber vorgegeben sind.

Um die Setzungen im vielschichtigen Berechnungsmodell auszuwerten, werden numerische Analysen durchgeführt. Die Geometrie des Berechnungsmodells wird mittels der Implementierung des CUR 191 (1997) Ansatzes vereinfacht dargestellt. Weil zwei Typen der Randbedingungen - drainierte und undrainierte - für den unteren Bereich zugeordnet werden können, wurde der Einfluss der darunter liegenden Boden auf die Setzungen untersucht und ausgewertet.

Die Untergrunderkundungskampagne auf dem großflächigen Baufeld wurde mittels CPTu-Sondierungen ausgeführt. Die ersten acht CPTu Tests sind als Investigation- 1 genannt. Die gewonnenen Daten werden als die Basiswerte für die Beurteilung des Untergrundmodells benutzt, das im Lauf des Projektes in numerischen Simulationen verwendet wird. Im Laufe des Untergrunderkundungsprogramms werden die zusätzlich gewonnenen Daten mit den ersten acht Tests verglichen, um ein erweitertes Verständnis über den Untergrund zu bekommen und das für die Modellierung geeignete Untergrundmodell zu verbessern, wenn eine solche Notwendigkeit erforderlich ist. Der Vergleich wird mit Hilfe von programmierten Excel Tabellenblättern durchgeführt.

Abstract

“In the wide array of existing ground improvement methods, the use of vertical drains with preloading is considered as one of the most effective and economical methods for improving soft clays (normally consolidated to lightly over-consolidated) prior to construction of infrastructure. Vertical drains installed to significant depths promote radial flow inducing consolidation rapidly enhancing the shear strength of the compressed ground” (Indraratna et al 2012).

The ground improvement method with prefabricated vertical drains and excess preloading is applied for the area of great extent, for the located in the North Africa, in order to accelerate the consolidation and to reduce the post-construction settlement. The ground improvement concept was optimized in accordance to the expected service loads and requirements for settlement, stated by the Client.

The numerical analyses with the software *GGU CONSOLIDATE 5* are conducted to estimate the settlement in the multi-layered calculation model. The CUR 191 (1997) approach is implemented in these calculations in order to simplify the geometry of the model. As two different types of boundary conditions – drained and undrained – can be assigned for the bottom edge of the calculation model, the influence of underneath laying soils on the settlement rate is investigated and evaluated.

The subsurface investigation program in the area of the project is performed by means of piezocone tests. The first eight CPTu tests are named as Investigation-1. The obtained data was used as the basis for the assessment of a calculations model, later used in numerical simulations. With the continuation of the subsurface investigation program, the received supplementary data is compared to the first tests in order to obtain the enhanced understanding about the subsurface and to improve the underground model used in calculations, if necessary. The comparison is performed by the means of programmed spreadsheets.

Keywords: ground improvement, settlements; saturated soils; soft soils; consolidation; fine grained; modelling; *GGU CONSOLIDATE 5*; vertical drains; PVD; preloading; CUR 191 (1997); CPTu; piezocone test.

Table of contents

1	Introduction	1
2	Theoretical part	2
2.1	Fundamentals of consolidation	2
2.1.1	General information	2
2.1.2	Interpretation of typical void ratio- effective stress plot.....	6
2.1.3	The settlement – log time plot from the oedometer test	11
2.1.4	1-D Consolidation theory by Terzaghi	13
2.2	Ground improvement	16
2.2.1	Classification of ground improvement techniques	17
2.2.2	Preloading.....	19
2.2.3	Vertical drains used for the ground improvement	24
2.3	Modelling of vertical drains	31
2.3.1	Generalities.....	31
2.3.2	Axisymmetric and plane strain model.....	32
2.3.3	Grid based influence zone of drains	33
2.3.4	Approach according to CUR 191 (1997).....	35
2.4	In-situ geotechnical subsurface investigation tests	39
2.4.1	In-situ geotechnical tests	39
2.4.2	Interpretation of results for CPTu test.....	47
3	Practical part	55
3.1	Introduction to the Project.....	55
3.2	Geological conditions.....	55
3.2.1	Literature research.....	55
3.2.2	Subsurface investigation campaign	56
3.3	Development of design	58
3.3.1	Preliminary Design.....	58
3.3.2	Investigation-1	65

3.4	Settlement calculation with the idealized subsoil model	71
3.4.1	General design considerations	71
3.4.2	Modelling with the software <i>GGU CONSOLIDATE 5</i>	72
3.4.3	Predicted settlement	77
3.4.4	Settlement with the drained bottom boundary	85
3.4.5	Comparison of effective settlement	90
3.5	Piezocone test evaluation	93
3.5.1	Programmed spreadsheets for CPTu evaluation.....	95
3.5.2	Delimitating lines.....	100
3.5.3	Investigation-2	123
3.5.4	Comparison of dissipation tests.....	130
3.5.5	Comparison of time – settlement curves from the new CPTu data with the delimitating lines.....	133
3.6	Discussion.....	140
4	Summary of results	150
5	Conclusions	157
6	Literature	158
	Appendix A.....	161
	Appendix B.....	167
	Appendix C.....	173
	Appendix D.....	198
	Appendix E	202
	Appendix F	211

List of figures

Figure 1 Phase 1: initial loading (UMass Lowell 2013)	3
Figure 2 Phase 2: consolidation takes place(UMass Lowell 2013)	3
Figure 3 Phase 3: consolidation process is completed (UMass Lowell 2013)	4
Figure 4 Variations of total, pore water and effective pressures during the consolidation (UMass Lowell 2013).....	5
Figure 5 Comparison of dissipation process in cohesionless soils and clays	6
Figure 6 Definition of voids and solids in a specimen (UMass Lowell 2013).....	8
Figure 7 Oedometer apparatus (GDS 2017)	9
Figure 8 Typical $e - \log \sigma'$ relationship plot (UMass Lowell 2013)	10
Figure 9 Typical <i>settlement</i> – <i>log time</i> plot (UMass Lowell 2013)	13
Figure 10 Initial variations of excess pore water pressure (Knappett & Craig 2012)	16
Figure 11 Relationships between average degree of consolidation and time factor (Knappett & Craig 2012).....	16
Figure 12 Resulting settlement due to preloading (Stapelfeldt 2000)	21
Figure 13 Time – settlement behaviour under preloading and overloading (Veder and Prinzi 1983)	23
Figure 14 Benefit of vertical drains (Indraratna 2002)	24
Figure 15 Type of PVD filter (Arizona Geosynthetics 2017).....	25
Figure 16 Type of PVD filter (Tencate 2015).....	26
Figure 17 Type of PVD filter (Geoengineer 2017).....	26
Figure 18 Roll of PVD (Keller 2017)	26
Figure 19 Installation of vertical drains (Menard 2017)	29
Figure 20 Axisymmetric and plane strain models (Indraratna 2002).....	33
Figure 21 Triangle and square patterns (Geoengineer 2017)	34
Figure 22 Sequence of driving the SPT sampler (UONBI).....	41
Figure 23 Terminology for the cone penetrometer (Robertson 2012)	43
Figure 24 Examples of commercial piezocones with two types of built-in filters (Mayne 2000)	44
Figure 25 Example of dissipation test to determine t_{50} (Robertson 2012)	45
Figure 26 Layout of downhole seismic cone system (Robertson 2006).....	46
Figure 27 $Q_t - F_r$ chart (Robertson, 2006).....	51
Figure 28 Soil behavior type zones (Robertson, 2006)	52
Figure 29 The ranges of hydraulic permeability based on I_c (Robertson, 2012)	53
Figure 30 Summary of properties obtained with the investigation campaign	57
Figure 31 Sketch of typical embankment design developed for the Project.....	62

Figure 32 Construction process of embankment with vertical drains	63
Figure 33 Layout of piezocone tests	65
Figure 34 Data about performed piezocone tests	66
Figure 35 Idealized underground model.....	67
Figure 36 Variations of constrained modulus M values versus depth for the executed eight CPTu considering factor I_c	68
Figure 37 Variations of constrained modulus M values versus depth for the executed eight CPTu considering factor $\alpha=6$	69
Figure 38 Guidelines from FHWA RD-86/168	70
Figure 39 Loading scenario for roads.....	72
Figure 40 Loading scenario for structures.....	72
Figure 41 Applied loading for roads with 20kPa life load	73
Figure 42 Underground model with 11 layers	75
Figure 43 Idealized underground model.....	76
Figure 44 Input option in the software	77
Figure 45 Log time – settlement curves for roads with 0kN/m ² life load.....	81
Figure 46 Log time – settlement curves for roads with 10kN/m ² life load.....	81
Figure 47 Log time – settlement curves for roads with 20kN/m ² life load.....	82
Figure 48 Log time – settlement curves for roads with 30kN/m ² life load.....	82
Figure 49 The variations of log time – settlement curves for all four life load for roads	83
Figure 50 Log time – settlement curve for structures	84
Figure 51 Resulting effective settlement for roads and structures	85
Figure 52 Variations of log time – settlement curves for roads with four different life loads	88
Figure 53 Log time – settlement curve for structures with 16kN/m ² life and structural load	89
Figure 54 Resulting effective settlement for calculations with the drained bottom boundary	90
Figure 55 Comparison of effective settlement for simulations with the drained and undrained bottom boundary	91
Figure 56 Delimitating lines for constrained modulus M	101
Figure 57 Delimitating lines for horizontal coefficient of permeability k_h	103
Figure 58 Delimitating lines for SBT.....	105
Figure 59 Estimated permeabilities of the upper group.....	108
Figure 60 Estimated permeabilities of the lower group	109
Figure 61 Delimitations for the upper group.....	110
Figure 62 Delimitations for the lower group.....	111

Figure 63 The comparison of delimitating lines obtained from dissipation tests and approximated with correlations by Robertson (2012).....	112
Figure 64 Delimitating lines for settlement with 0kN/m ² for roads.....	121
Figure 65 Delimitating lines for settlement with 10kN/m ² for roads.....	122
Figure 66 Delimitating lines for settlement with 20kN/m ² for roads.....	122
Figure 67 Delimitating lines for settlement with 30kN/m ² for roads.....	123
Figure 68 Delimitating lines for settlement with 16kN/m ² for structures.....	123
Figure 69 Sketched locations of Investigation-1 and Investigation-2.....	124
Figure 70 Comparison of new CPTu tests with the delimitating lines.....	125
Figure 71 Comparison of new CPTu tests with delimitating lines.....	127
Figure 72 Comparison of generated soil behavior type (SBT) based on the soil behavior type index I_c graph for new CPTu tests with previously plotted delimitating lines.....	129
Figure 73 Comparison of dissipation tests for CPTu_132-152 with the delimitating lines.....	133
Figure 74 Comparison of log time - settlement curves for the eight new CPTu with the delimitating lines for roads with 0kN/m ² life load.....	136
Figure 75 Comparison of log time - settlement curves for the eight new CPTu with the delimitating lines for roads with 10kN/m ² life load.....	136
Figure 76 Comparison of log time - settlement curves for the eight new CPTu with the delimitating lines for roads with 20kN/m ² life load.....	137
Figure 77 Comparison of log time - settlement curves for the eight new CPTu with the delimitating lines for roads with 30kN/m ² life load.....	137
Figure 78 Comparison of log time - settlement curves for the eight new CPTu with the delimitating lines for structures with 16kN/m ² life load.....	138
Figure 79 Influence of Eur/E ratio on settlement (undrained bottom of the model).....	142
Figure 80 Influence of Eur/E ratio on settlement (drained bottom of the model).....	142
Figure 81 Comparison of effective settlement.....	143
Figure 82 Gradual decrease of the applied loading.....	144
Figure 83 Stress distribution models due to different embankment' parameters.....	145
Figure 84 Influence of opened bottom boundary and narrowing of layers.....	146
Figure 85 CPTu_1 settlement with two types of permeability.....	148
Figure 86 Comparison of effective settlement with the closed and opened bottom boundary.....	151
Figure 87 Comparison of new CPTu tests with the delimitating lines.....	152
Figure 88 Comparison of new CPTu tests with delimitating lines.....	153
Figure 89 Comparison of generated soil behavior type (SBT) based on the soil behavior type index I_c graph for new CPTu tests with previously plotted delimitating lines.....	154

Figure 90 Comparison of log time - settlement curves for the eight new CPTu with the delimitating lines for roads with 20kN/m² life load156

List of tables

Table 1 Input parameters for settlement calculations in Preliminary Design.....	58
Table 2 Loads generated by embankments for roads and structures	64
Table 3 Load increase expressed in percent's for each simulation case	74
Table 4 Evaluated settlement ratio for roads with 0kN/m ² life load	78
Table 5 Evaluated settlement ratio for roads with 10kN/m ² life load	79
Table 6 Evaluated settlement ratio for roads with 20kN/m ² life load	79
Table 7 Evaluated settlement ratio for roads with 30kN/m ² life load	79
Table 8 Evaluated settlement ratio for structures with 16kN/m ² life and constructional load	83
Table 9 Summarized effective settlement	85
Table 10 Evaluated settlement ratio for roads with 0kN/m ² life load and the drained bottom boundary	86
Table 11 Evaluated settlement ratio for roads with 10kN/m ² life load and the drained bottom boundary	87
Table 12 Evaluated settlement ratio for roads with 20kN/m ² life load and the drained bottom boundary	87
Table 13 Evaluated settlement ratio for roads with 30kN/m ² life load and the drained bottom boundary	87
Table 14 Evaluated settlement ratio for structures with 16kN/m ² life load and the drained bottom boundary	88
Table 15 Resulting effective settlement for calculations with the drained bottom boundary	89
Table 16 Comparison of effective settlement for simulations with drained and undrained bottom boundary.	91
Table 17 Settlement comparison for calculations with and without the effective drain diameter	93
Table 18 Results of 32 dissipation tests.....	107
Table 19 Delimitations of horizontal coefficient of hydraulic permeability obtained from dissipation tests.....	110
Table 20 Approximated stiffness used for CPTu_1 – CPTu_8.....	116
Table 21 Approximated input values of permeability.....	119
Table 22 Effective settlement evaluated for all eight CPTu with variable loading conditions	120
Table 23 Values of hydraulic permeability for dissipation tests, approximated with the programmed spreadsheets	132

Table 24 Input stiffness for CPTu_135- 152 [MPa]	134
Table 25 Input permeability for CPTu_135 – 152 [m/s].....	135
Table 26 Effective settlement [cm] approximated for CPTu_135 – 152 and the delimitating lines.....	139
Table 27 Calculated settlement with gradually decreasing loading.....	144
Table 28 Comparison of effective settlement for CPTu_1.....	148
Table 29 Comparison of final settlement for CPTu_1	148
Table 30 Comparison of effective settlement with the closed and opened bottom boundary	150
Table 31 Effective settlement [cm] approximated for CPTu_135 – 152 and the delimitating lines.....	155

List of symbols and abbreviations

Capital letters

A	[m ²]	Area of specimen
A_c	[m ²]	Projected area of the cone
A_s	[m ²]	Surface area of the sleeve
A_{sb}	[m ²]	Cross- section area of sleeve at base
A_{st}	[m ²]	Cross- section area of sleeve at top
B	[m]	Width of unit cell
D	[m]	Influence zone
D_{cell}	[m]	Diameter of unit cell
ER	[m/s]	Rod energy ratio
F_r	[%]	Normalized friction ratio
F_s	[MN]	Frictional force acting on the sleeve
H_s	[m]	Equivalent thickness of solids at start of test
H_v	[m]	Equivalent thickness of voids at start of test
ΔH_1	[m]	Change of specimen thickness at the end of first increment period
ΔH_2	[m]	Change of specimen thickness at the end of second increment period
ΔH_i	[m]	Change of specimen thickness at the end of any increment period
I_c	[-]	Soil behavior type index
M	[MPa]	Constrained modulus
N_m	[blows]	Measured N – value of blows
N_{60}	[blows]	Corrected N – values
OCR	[-]	Overconsolidation ratio
P_a	[MPa]	Atmospheric pressure (100kPa)
P_{a2}	[MPa]	Reference pressure, in general same as P_a
Q_c	[MN]	Force acting on the cone
Q_t	[-]	Normalized cone resistance
Q_{tn}	[-]	Normalized cone resistance
R_f	[%]	Friction ratio
$S_{triangular}$	[m]	Distance between drain centers in the triangular grid
S_{square}	[m]	Distance between drain centers in the square grid
T_h	[-]	Time factor for the radial flow
T_v	[-]	Dimensionless time factor
U	[%]	Degree of consolidation
U_h	[%]	Degree of consolidation due to the radial flow
U_v	[-]	Degree of consolidation for parallel flow

V_V	[m ³]	Equivalent volume of voids at start of test
V_S	[m ³]	Equivalent volume of solids at start of test

Small letters

a	[-]	The net area ratio determined from laboratory calibration with a typical value between 0.70 and 0.85
b	[m]	Thickness of band-shaped drain
c_h	[m ² /s]	Horizontal coefficient of consolidation
c_v	[m ² /s]	Vertical coefficient of consolidation
d	[m]	Length of drainage path
d_w	[m]	Equivalent diameter of band-shaped drain
e	[-]	Void ratio at the end of consolidation for $t = \infty$
e_i	[-]	Void ratio at the end of any increment period
e_{i-1}	[-]	Void ratio at the end of any minus one increment period
e_0	[-]	Initial void ratio
e_1	[-]	Void ratio at the end of first increment period
e_2	[-]	Void ratio at the end of second increment period
Δe_i	[-]	Change of void ratio at the end of any increment period
Δe_1	[-]	Change of void ratio at the end of first increment period
Δe_2	[-]	Change of void ratio at the end of second increment period
f_s	[MPa]	Sleeve friction
f_t	[MPa]	Corrected sleeve friction
h	[m]	Height of embankment
k	[m/s]	Hydraulic permeability
k_h	[m/s]	Horizontal coefficient of permeability
k'_h	[m/s]	Equivalent horizontal coefficient of permeability
k_v	[m/s]	Vertical coefficient of permeability
k'_v	[m/s]	Equivalent vertical coefficient of permeability
n	[-]	Stress exponent
p_{50}	[kPa]	50% pressure of dissipation test
q_c	[MPa]	Cone resistance
q_t	[MPa]	Corrected cone resistance
s_i	[m]	Settlement at any time
$s_{eff,roads}$	[cm]	Effective settlement for roads
$s_{eff,struct}$	[cm]	Effective settlement for structures
$s_{50,years}$	[cm]	Settlement 50 years after preloading

$s_{20,years}$	[cm]	Settlement 20 years after preloading
$s_{preload}$	[cm]	Settlement at the end of preloading stage
s_{final}	[m]	Final settlement
t	[s]	Consolidation time
t_y	[years]	Time
t_{50}	[s]	Time of 50% completion of dissipation test
u_0	[kPa]	In-situ equilibrium pore water pressure
u_1	[kPa]	Pressure in the beginning of the dissipation test
u_2	[MPa]	Pore pressure measured in the filter just behind the cone
u_3	[MPa]	Pore pressure measured at the top of sleeve
Δu	[MPa]	Excess pore water pressure
w	[m]	Width of band-shaped drain

Greek letters

α	[-]	Function of degree of consolidation
α_M	[-]	The coefficient which varies with the type of soil
γ	[kN/m ³]	Soil unit weight
$\gamma_{material}$	[kN/m ³]	Unit weight of embankment material
∂u	[%]	Change in void ratio
∂t	[m]	Change in time
∂z	[m]	Change in the elevation head
μ	[-]	Correlation coefficient
σ_c'	[MPa]	Preconsolidation stress
σ'	[MPa]	Effective vertical stress
σ_{v0}	[MPa]	In-situ vertical stress
σ'_{v0}	[MPa]	In-situ effective vertical stress
$\sigma_{vertical}$	[kN/m ²]	Vertical stress

Abbreviations

CPT	Cone Penetration Test
CPTu	Piezocone Penetration Test
FEM	Finite Element Method
SPT	Standard Penetration Tests
SCPTu	Seismic Piezocone Penetration Test

1 Introduction

“Coastal clays often have low bearing capacity and high compressibility, causing excessive and differential settlements upon loading” (Indraratna et al 2007). Due to their fine size of particles, clays, peat and silts, as typically found in coastal areas, possess low permeability, what has a negative influence on the consolidation time. Thus, the ground improvement methods applied for such areas are designed in the way to accelerate the ground water dissipation from soils.

Within this thesis a case study of a practical project in North Africa is discussed. The aim of the Project is to use the ground improvement method with prefabricated vertical drains and excess preloading in order to accelerate the consolidation time and to reduce the post-construction settlement. For this practical project, this method is applied over a large area, to be called the area of great extent within this Thesis. The ground improvement method must fulfill the requirements set by the Client. Some confidentiality is required for this practical project, thus some changes in names are made by the author of this Thesis.

The goals of this Thesis are related to the aim of the project and are as follows:

- To gain the necessary theoretical background;
- To create a settlement calculation model based on a proposed subsoil model;
- To calculate settlements according to different loading conditions;
- To check the influence of boundary conditions on settlements;
- To check if estimated settlements fulfill the requirement;
- To develop a CPTu evaluation system to compare incoming CPTu results;
- To check whether the area of great extent has varying geotechnical properties;
- To use new CPTu results to confirm the project’s calculation model.

This Thesis describes the steps taken to achieve above mentioned goals and is divided into two major parts: the necessary theory is presented in the first part, while the second part has a focus on practical project-related tasks.

The first part is composed of four chapters, which cover the required theoretical background. In the first chapter the theory of consolidation is presented in four subdivisions. The second chapter provides the overview of ground improvement with preloading and prefabricated vertical drains. The third chapter covers the modelling principles of vertical drains. The last, fourth, chapter deals with the methods of in-situ

geotechnical subsurface investigation and the interpretation of gained data, based on the publication “Guide to Cone Penetration Testing for Geotechnical Engineering” by Robertson (2012).

The second part covers the practical project related calculations. The generalities about the Project and geological conditions are summarized in the first two chapters. The third chapter explains in details the development of ground improvement design concept. The fourth chapter focuses on the calculation and the comparison of predicted settlement with different boundary conditions. The fifth chapter describes the method developed for the evaluation and comparison of CPTu test results. The sixth section summarizes some points of interest, as well as unanswered questions, which arise from the results of settlement calculations and performed evaluation of piezocone tests

Finally, the most significant results and conclusions are summarized and presented as separate chapters.

2 Theoretical part

2.1 Fundamentals of consolidation

“Consolidation settlement is the vertical displacement of the soil surface corresponding to the volume change at any stage of the consolidation process” (Knappett & Craig 2012).

The focus of this chapter is to provide the basic theoretical background about the consolidation and the commonly used equations to evaluate the consolidation settlement.

2.1.1 General information

“Consolidation is the gradual reduction in volume of a fully saturated soil of low permeability due to the change of effective stress” (Knappett & Craig 2012). The consolidation process is generated by the gradual decrease of excess pore water pressure and results in the increment of effective stress in soil skeleton.

Generally, the consolidation process is divided into three major phases, which are directly related to time:

1. Phase 1: initial loading

The first phase with the corresponding equations is depicted in Figure 1.

In the first phase the initial loading $\Delta\sigma$ is instantaneously applied on saturated soil. This instant application of loading $\Delta\sigma$ on saturated soils generates the increment of excess pore pressure p_w , which is the sum of initial pore water pressure $p_{w,0}$ and of the change of pore water pressure $\Delta p_{w,p=0}$. The change of pore water pressure $\Delta p_{w,p=0}$ is equal to the change of vertical stress $\Delta\sigma$ and is carried by the water, assuming it is incompressible. In the first phase the effective stress in the soil skeleton σ' is equal to the initial effective stress σ'_0 .

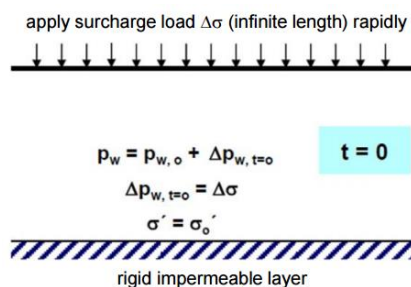


Figure 1 Phase 1: initial loading (UMass Lowell 2013)

2. Phase 2: consolidation takes place

The second phase with corresponding equations is shown in Figure 2.

As time goes on, water runs out of voids due to the applied stress. The excess pore water pressure will dissipate ($\Delta p_{w,t} = \Delta\sigma - \Delta\sigma_t'$) and some of the stress increment will be carried by the soil skeleton ($\Delta\sigma' = \Delta\sigma_o' + \Delta\sigma_t'$). The volume of soils decreases and this reduction of volume generates settlement.

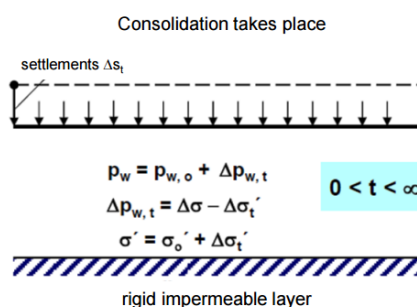


Figure 2 Phase 2: consolidation takes place(UMass Lowell 2013)

3. Phase 3: consolidation process is completed

The third phase with the corresponding equations is shown in Figure 3.

When the excess pore water pressure due to the initial loading p_w completely dissipates, soil skeleton takes the whole loading. As a result, now the increase of effective stress in the soil skeleton is equal to the applied vertical stress ($\sigma' = \sigma_o' + \Delta\sigma$). After the consolidation process is completed, settlement reach the maximal value.

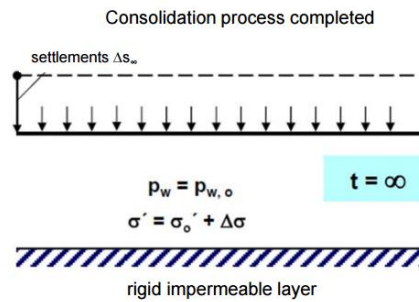


Figure 3 Phase 3: consolidation process is completed (UMass Lowell 2013)

When the consolidation takes place, total, effective and pore water pressures vary with respect to time and the drainage conditions at the bottom and the top of consolidated soil layer. The variations of total, pore water and effective pressures with respect to time in the clay layer, which is surrounded by the two permeable layers, are illustrated in Figure 4. The sequence of variations agrees with the above described three phases of consolidation process with respect to time.

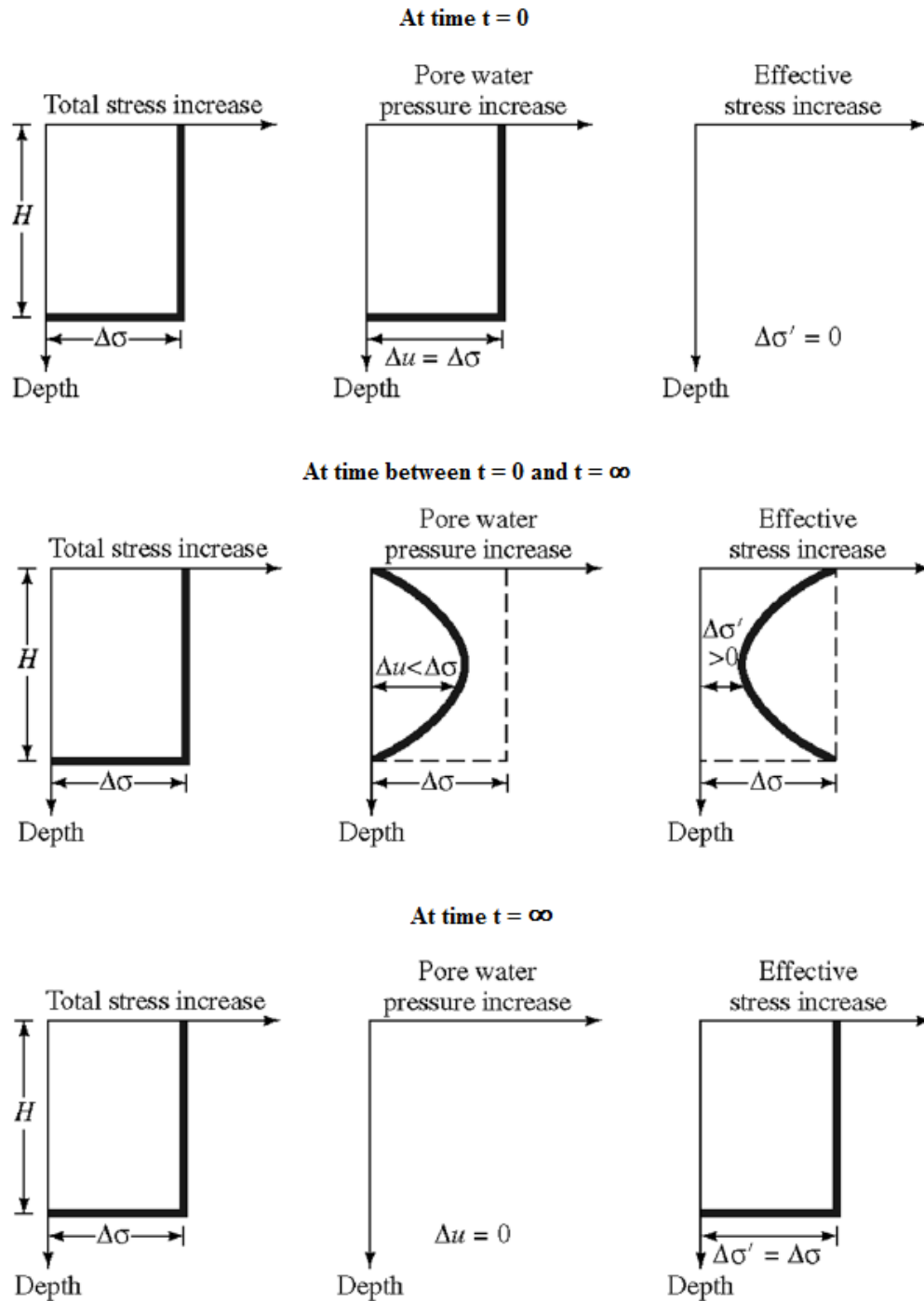


Figure 4 Variations of total, pore water and effective pressures during the consolidation (UMass Lowell 2013)

The average velocity of excess pore water pressure dissipation is strongly dependent on the soil type, grain size and permeability. For saturated cohesionless soils as sands pore

pressure increase decays rapidly due to the high permeability. In saturated clays the consolidation takes much longer time because of the low permeability in general. Typical time – settlement curves for cohesionless soils and clays are compared in Figure 4.

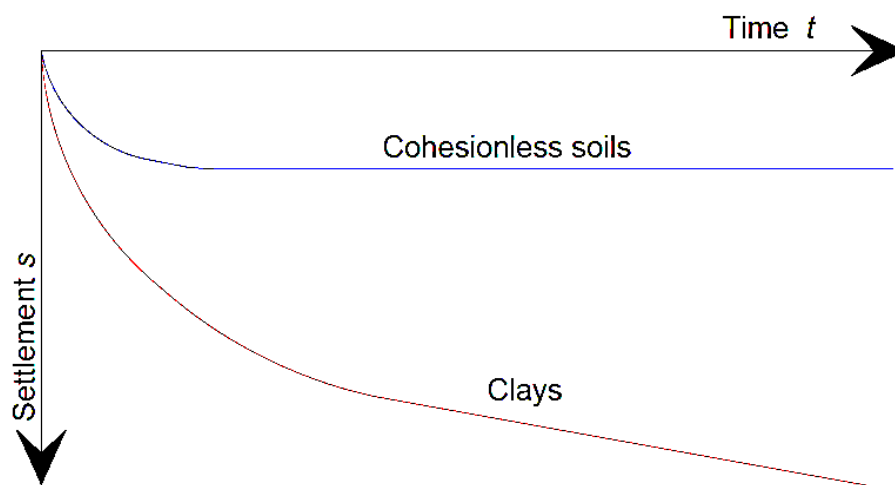


Figure 5 Comparison of dissipation process in cohesionless soils and clays

“The process of swelling, the reverse of consolidation, is the gradual increase in volume of a soil under negative excess pore water pressure“(Knappett & Craig 2012). In general, the process of swelling is sub-divided into mechanical and chemical swelling. The mechanical swelling is linked with the time-dependent stress conditions (loading-unloading), while the volume change caused by expandable clay minerals is known as the chemical swelling. In this Thesis only the mechanical swelling is considered in settlement calculations. In geotechnics the mechanical swelling is defined as heave and from now on this definition will be used to describe the increase in volume of a soil.

2.1.2 Interpretation of typical void ratio- effective stress plot

One of the key results of the consolidation process is the reduction in volume. The expulsion of pore water from loading allows soil particles to redistribute. The void ratio is estimated every time the load is applied on the sample and each current void ratio is estimated on the basis of previous result. For example, the void ratio for the first loading is calculated on the basis of initial void ratio, however the void ratio for the second loading is based on the results from the first loading. The change of volume can be evaluated with Equation (1) - (5). Figure 6 visualizes the input parameters for these calculations.

$$e_0 = \frac{V_V}{V_S} = \frac{H_V A}{H_S A} = \frac{H_V}{H_S} \quad (1)$$

e_0	[-]	Initial void ratio
A	[m ²]	Area of specimen
V_V	[m ³]	Equivalent volume of voids at start of test
V_S	[m ³]	Equivalent volume of solids at start of test
H_V	[m]	Equivalent thickness of voids at start of test
H_S	[m]	Equivalent thickness of solids at start of test

$$\Delta e_1 = \frac{\Delta H_1}{H_S} \quad (2)$$

Δe_1	[-]	Change of void ratio at the end of first increment period
ΔH_1	[m]	Change of specimen thickness at the end of first increment period

$$e_1 = e_0 - \Delta e_1 = e_0 - \frac{\Delta H_1}{H_S} \quad (3)$$

e_1	[-]	Void ratio at the end of first increment period
-------	-----	---

$$\Delta e_2 = \frac{\Delta H_2}{H_S} \quad (4)$$

Δe_2	[-]	Change of void ratio at the end of second increment period
ΔH_2	[m]	Change of specimen thickness at the end of second increment period

$$e_2 = e_1 - \Delta e_2 = e_1 - \frac{\Delta H_2}{H_S} \quad (5)$$

e_2	[-]	Void ratio at the end of second increment period
-------	-----	--

General equation for estimation of void ratio at the end of any increment period is derived and presented as Equation (6):

$$e_i = e_{i-1} - \Delta e_i = e_{i-1} - \frac{\Delta H_i}{H_S} \quad (6)$$

e_i	[-]	Void ratio at the end of any increment period
e_{i-1}	[-]	Void ratio at the end of any minus one increment period
Δe_i	[-]	Change of void ratio at the end of any increment period
ΔH_i	[m]	Change of specimen thickness at the end of any increment period

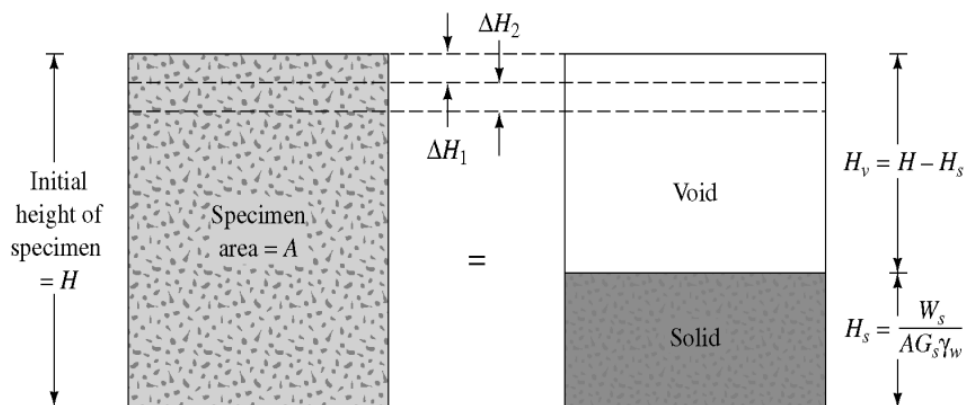


Figure 6 Definition of voids and solids in a specimen (UMass Lowell 2013)

The progress of the consolidation process under a particular total stress increment can be explained through a change of void ratio with Equation (7). The estimated value is denoted as the degree of consolidation U and it indicates how far the consolidation process in comparison to the initial state is gone.

$$U = \frac{e_0 - e_i}{e_0 - e} \times 100\% \quad (7)$$

U	[%]	Degree of consolidation
e	[-]	Void ratio at the end of consolidation for $t = \infty$

If the degree of consolidation U is equal to zero, it indicates that consolidation process has not yet begun. If this value U is equal to 100%, it indicates that consolidation is complete.

The degree of consolidation can be expressed as the settlement ratio, if the final settlement is known. The degree of consolidation at any time U with the incorporation of settlement is expressed in Equation (8).

$$U = \frac{s_i}{s_{final}} \times 100\% \quad (8)$$

s_i	[m]	Settlement at any time
s_{final}	[m]	Final settlement

As Equation (7) and (8) are used to estimate the result of the same process, it means that components of equations can be compared. The settlement due to the consolidation

are the result of volume reduction or more specifically, the reduction of pore volume. In both equations the numerator indicates the consolidation stage at any time, while the denominator corresponds the end result of the process.

An example of oedometer apparatus used to carry out consolidation tests is shown in Figure 7.



Figure 7 Oedometer apparatus (GDS 2017)

In the oedometer test a soil sample is tested with two types of load application– loading and unloading. Final plots consist of results of numerous loading and unloading increments, evaluated with respect to the void ratio and the effective stress. For clays the relationship between void ratio and effective stress depends on the stress history of soil. According to Knappett et al. (2012), clays are divided into two groups, based on the stress history:

1. Normally consolidated clays (NC)

The present overburden pressure or in-situ effective stress is the highest loading the clay sample has ever seen.

The $e - \log \sigma'$ relationship for a normally consolidated soil is linear (nearly so), and is called the virgin (one-dimensional) compression line. During compression along this line, permanent irreversible changes in soil structure continuously take place and soil does not revert to the original structure during expansion.

2. Overconsolidated clays (OC)

The present overburden pressure or in-situ effective stress is lower than the soil has seen in the past.

In the $e - \log \sigma'$ relationship plot the resulting curve has one additional loop, which is called the swelling- recompression part. The changes of soil structure along this loop are almost totally recoverable and the recompression line ultimately rejoins the virgin line.

A typical result of void – effective stress plot for normally and overconsolidated clay samples is presented in Figure 8. In the normally consolidated soil the compression occurs only along a – b – c – g part, while in the overconsolidated soil the swelling- recompression part c – d – f must be considered.

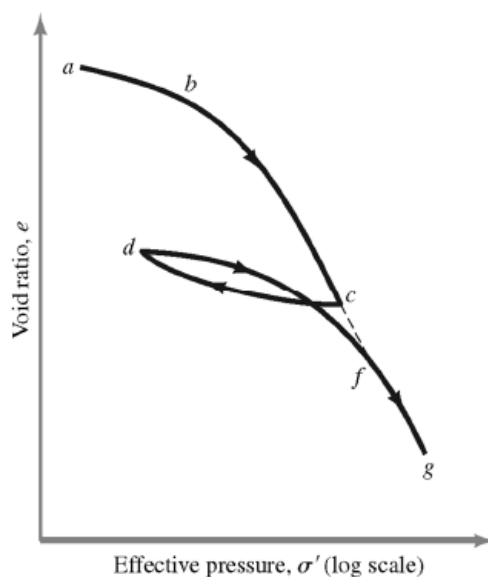


Figure 8 Typical $e - \log \sigma'$ relationship plot (UMass Lowell 2013)

Figure 8 suggests that a soil in the overconsolidated state will be less compressible than that in the normally consolidated state, because of the presence of recoverable components of volume changes, which are in general smaller than irrecoverable.

The preconsolidation pressure, which is referred to the maximum stress the soil has ever experienced, can be defined by Casagrande's graphical method (Knappett & Craig 2012). When the preconsolidation pressure or the maximum past pressure is known, the overconsolidation ratio (OCR) for this soil is estimated as in Equation (9).

$$OCR = \frac{\sigma'_c}{\sigma'} \quad (9)$$

OCR [-] Overconsolidation ratio

σ_c' [MPa] Preconsolidation stress

σ' [MPa] Effective vertical stress

General guidelines suggest to evaluate soils as normally consolidated (NC), when overconsolidation ratio *OCR* does not exceed or is equal to 1. Above this value, an investigated soil falls into the category labeled as overconsolidated (OC).

Possible causes of overconsolidation are the fluctuation of ground water, preloading generated by thick sediments, glaciers or weight of previously existing structures, secondary compression and desiccation above the ground water table.

2.1.3 The settlement – log time plot from the oedometer test

“Consolidation settlement is the vertical displacement of the soil surface corresponding to the volume change at any stage of the consolidation process” (Knappett & Craig 2012).

The typical experimental curve obtained by plotting the dial gauge readings of settlement in the oedometer test against logarithm of time is shown in Figure 9. According to the theory of consolidation, this curve consists of three main parts:

1. Initial compression

The initial compression is the part of consolidation curve, where the degree of saturation stays close to constant (marginally below 100%). The difference is mainly based on the compression of air bubbles in water. In this stage the elastic or recoverable deformations occur in the soil sample. The deformations are said to be recoverable, because as explained above the degree of saturation stays close to the constant and the loading is mainly carried by the water and not by the soil skeleton.

In the cohesive, fine-grained soils it is assumed that no initial settlement is generated in the initial compression stage due to the low permeability.

2. Primary consolidation

In this stage the volume change of the soil sample is caused by the expulsion of water from voids between particles due to the constant loading. The expulsion of water from voids between particles results in the dissipation of excess pore water pressure and rearrangement of soil particles (since the volume of water in the sample decreases, it creates the empty space between soil particles). Thus, the volume of

sample reduces (the sample is being compacted by the applied loading) and settlement is generated.

The final point in this stage corresponds the degree of consolidation equal to 1. This point is an intersection of linear extents of two parts of the curve.

3. Secondary compression

This secondary compression is the part of consolidation curve, which follows the primary compression. The general assumption suggests that the secondary compression should not begin until the primary compression is completed ($U = 1$).

The secondary compression is related to the cohesive soils with the low permeability. Due to the low permeability, it continues at the very slow rate for an indefinite period of time. This part of consolidation process is as well known as creep – deformations under the constant loading with no change of pore water pressure.

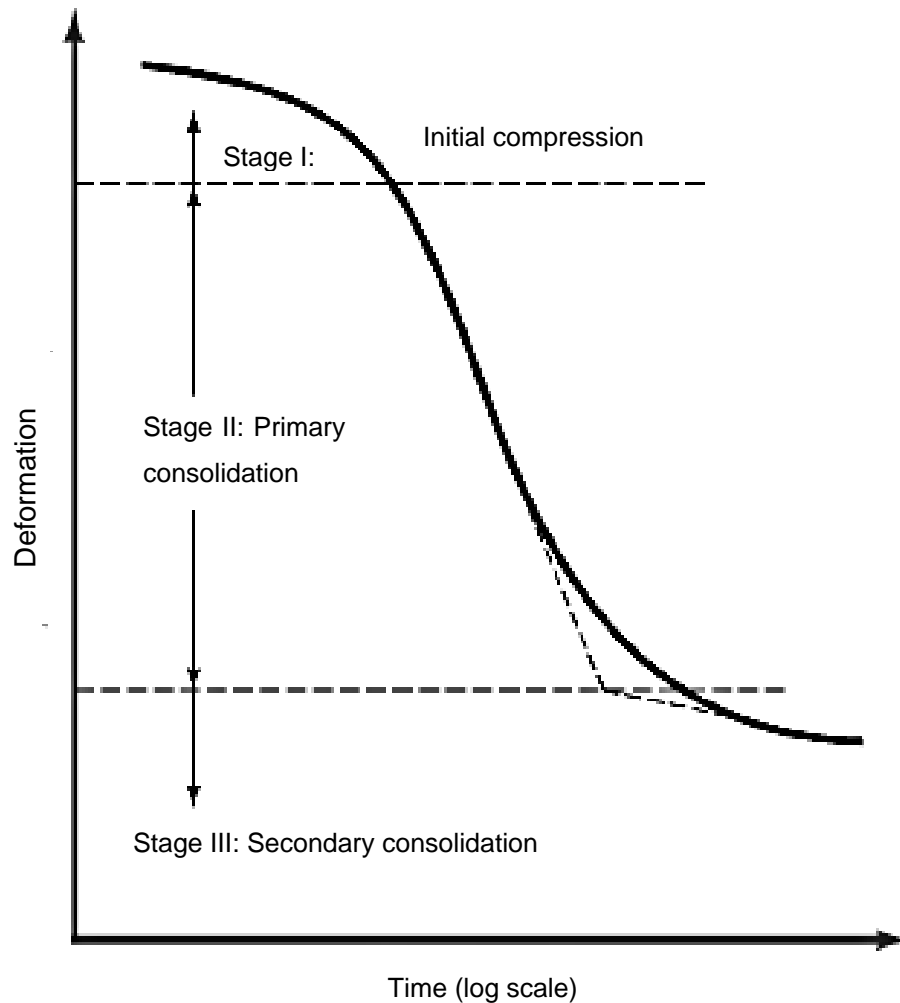


Figure 9 Typical *settlement* – *log time* plot (UMass Lowell 2013)

2.1.4 1-D Consolidation theory by Terzaghi

“Terzaghi (1943) developed an analytical model for determining the degree of consolidation within soil at any time t ” (Knappett & Craig 2012). The product of this theory is the one-dimensional governing equation for pore pressure dissipation (Equation (10)):

$$\frac{\partial u}{\partial t} = c_v \frac{\partial^2 u}{\partial z^2} \quad (10)$$

∂u	[%]	Change in void ratio
∂t	[m]	Change in time
∂z	[m]	Change in the elevation head
c_v	[m ² /s]	Vertical coefficient of consolidation

The vertical coefficient of consolidation is expressed with Equation (11):

$$c_v = \frac{k_v}{\gamma_w m_v} \quad (11)$$

k_v	[m/s]	Vertical coefficient of permeability
γ_w	[kN/m ³]	Effective vertical stress
m_v	[kN/m ²]	Coefficient of compressibility

For derivation of Equation (11) the assumptions made in the theory are:

- The soil is homogenous.
- The soil is fully saturated.
- The soil particles and water are incompressible.
- Compression and flow are one-dimensional (vertical).
- Strains are small.
- Darcy's law is valid at all hydraulic gradients.
- The coefficient of permeability k and the coefficient of volume compressibility remain constant throughout the process.
- There is a unique relationship, independent of time, between void ratio and effective stress.

As well, the theory relates the three quantities:

- The excess pore water pressure u .
- The depth z .
- Time t from the sudden application of the constant load.

Since the vertical coefficient of permeability k_v and the coefficient of compressibility m_v are assumed as constants (based on the assumption that soil skeleton is incompressible), the vertical coefficient of consolidation c_v is constant during the consolidation.

After the load is applied instantaneously, the excess pore water pressure is generated. The decay of excess pore water pressure is caused by the water discharge between soil particles. Terzaghi solved the consolidation equation (Equation (10)) as he presumed, that the volume change of soil element and settlement rate induced by volumetric changes and soil particle redistribution is equal to the volume of expelling water. The result is provided as Equation (12).

$$T_v = \frac{c_v t_y}{d^2} \quad (12)$$

T_v	[-]	Dimensionless time factor
t_y	[years]	Time
d	[m]	Length of drainage path

Variations of excess pore water pressure and the length of the drainage path in the layer are influenced the surrounding soils, as it is illustrated in Figure 10:

- a) A layer for which both upper and lower boundaries are free-draining is described as an open layer (Knappett & Craig 2012).
- b) A layer for which only one boundary is free-draining is a half-closed layer (Knappett & Craig 2012).

The free draining boundary allows the rapid dissipation of the excess pore water pressure, while the dissipation through the closed boundary requires much more time.

Curve (1), curve (2), curve (3) under the illustrated initial variations of excess pore water pressure in Figure 10 are related to the three curves, shown in Figure 11. Curve (1), curve (2) and curve (3) in Figure 11 are used to solve the equation of consolidation (Equation (12)) for the cases with opened and half-closed layers. In order to solve Equation (12), the length of the drainage path d is estimated based on the drainage conditions from Figure 10. Then the curve with the matching number is chosen in Figure 11. Lastly, the degree of consolidation U is estimated from this graph.

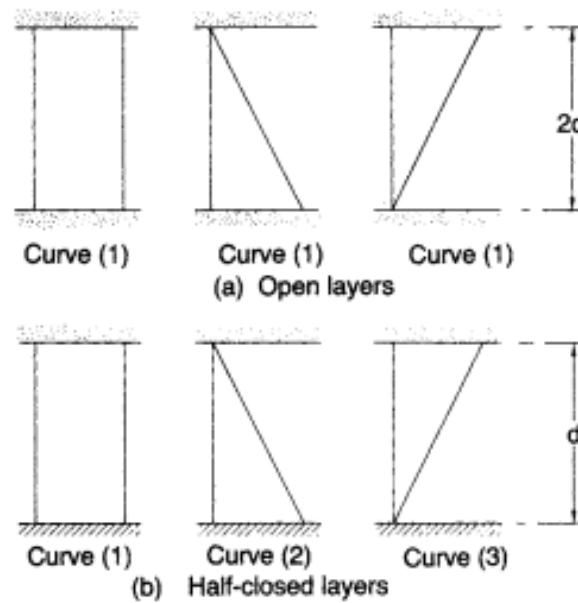


Figure 10 Initial variations of excess pore water pressure (Knappett & Craig 2012)

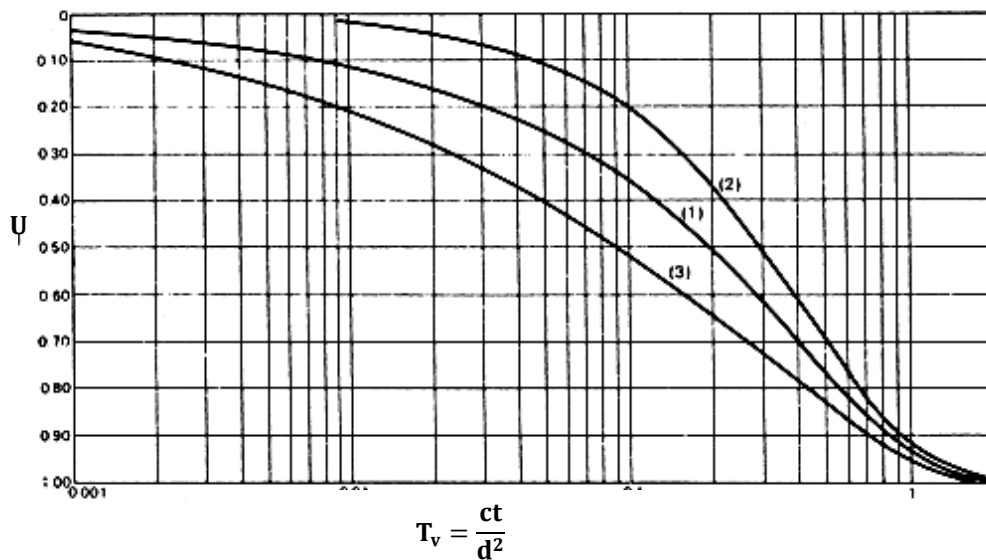


Figure 11 Relationships between average degree of consolidation and time factor (Knappett & Craig 2012)

2.2 Ground improvement

Ground improvement is used to stabilize soft, compressible soils, increase their bearing capacity and stiffness. Some techniques are more applicable for saturated soils, as the

ground improvement induces the reduction of ground water in the soil matrix and thus increases the consolidation ratio (see chapter 2.1). Overall, the goal of ground improvement techniques is a densification of a soil layer with or without special additives.

This chapter provides the general overview of commonly used ground improvement methods and then focuses on the principles of the ground improvement with preloading and vertical drains.

2.2.1 Classification of ground improvement techniques

Chu et al (2009) has listed and grouped commonly used ground improvement techniques according to TC17 in the following way:

A. Ground improvement without admixtures in non-cohesive soils or fill materials

- Dynamic compaction;
- Vibrocompaction;
- Explosive compaction;
- Electric pulse compaction;
- Surface compaction (including rapid impact compaction).

B. Ground improvement without admixtures in cohesive soils

- Replacement/displacement (including load reduction using lightweight materials);
- Preloading using fill (including the use of vertical drains);
- Preloading using vacuum (including combined fill and vacuum);
- Dynamic consolidation with enhanced drainage (including the use of vacuum);
- Electro-osmosis or electro-kinetic consolidation;
- Thermal stabilization using heating or freezing;
- Hydro-blasting compaction;

C. Ground improvement with admixtures or inclusions

- Vibro replacement or stone columns;
- Dynamic replacement;
- Sand compaction piles;
- Geotextile confined columns;
- Rigid inclusions (or composite foundation);
- Geosynthetic reinforced column or pile supported embankment;
- Microbial methods;
- Other methods (mostly unconventional methods or use of natural materials, like bamboo, timber and etc.).

D. Ground improvement with grouting type admixtures

- Particulate grouting;
- Chemical grouting;
- Mixing methods (including premixing or deep mixing);
- Jet grouting;
- Compaction grouting;
- Compensation grouting.

E. Earth reinforcement

- Geosynthetics or mechanically stabilized earth (MSE);
- Ground anchors or soil nails;
- Biological methods using vegetation.

All in all, main purposes of ground improvement can be summarized as:

- To increase the bearing capacity;

- To increase stiffness;
- To control deformations;
- To accelerate consolidation;
- To provide lateral stability;
- To form seepage cut-offs;
- To increase resistance to liquefaction.

Better results can be achieved combining two techniques. For example, it is common to couple vertical drains or the vacuum consolidation with preloading for saturated, very soft to soft, fine grained soils of low permeability.

In the context of this Thesis only the ground improvement with vertical drains and preloading is discussed with respect to the practical Project.

2.2.2 Preloading

2.2.2.1 General information about preloading

“It is well known that the compressibility and shear strength of soil can be greatly improved if the water content in the soil can be significantly reduced. One common method for improving soft soil is to reduce the water content of the soil through consolidation” (Chu et al 2014).

The introduction of the additional (equal to or higher than the weight of structure) loading on soils for a defined range of time prior to the placement of structure in order to increase the stiffness and bearing capacity of soils, decrease their volume due to the weight of structure generated settlements is noted as preloading. When the higher weight than the weight of the structure is applied on soil prior to the construction process, it is known as the overloading or excess preloading (over-loading).

In the most elementary case, additional vertical stresses are generated by the embankment, constructed on the site. This method is known as a conventional preloading. Vertical stresses are influenced by the height of embankment and weight of fills and calculated as in Equation (13).

$$\sigma_{vertical} = h \cdot \gamma_{material} \quad (13)$$

$\sigma_{vertical}$ [kN/m²] Vertical stress

h	[m]	Height of embankment
$\gamma_{material}$	[kN/m ³]	Unit weight of embankment material

“Depending on how a preload is applied, the preloading methods can be subdivided into preloading using fill, preloading using vacuum pressure and combined fill, and vacuum preloading methods” (Chu et al 2014).

The applied preloading prior to the construction generates the excess pore water pressure. With time, the generated excess pore water pressure dissipates, because water is being expelled from soils. It results in the decrease of volume and consequently, settlement due to the preloading (see section 2.1.1). Thus, this compacted soil has the higher bearing capacity and this increase in the soil strength results in the reduction of the post- construction settlement (the settlement, defined as the difference between the final settlement generated by the construction and settlement generated by the preloading applied prior to this construction).

After the required degree of consolidation is reached, the embankment can be totally or partially removed or used as a new surface, building platform.

2.2.2.2 Principles of the mechanism

The aim of the preloading is to achieve a required amount of settlement prior to the placement of constructions. The basic principle of the mechanism is to estimate how much and how long loading must be applied on soils prior to the placement of constructions in order to achieve this required amount of settlement.

The design steps, which lead to the estimation of this loading, can be summarized as follows:

1. To define design loads and the final settlement, generated by these loads. Additionally, the resulting log time – settlement curve for these loads should be plotted in order to estimate, how many settlement are generated at the specific time ranges. In Figure 12 the dashed curve corresponds the log time – settlement curve, generated by the design loads.
2. To define the type of preloading: at this step it should be defined, whether the applied preloading is equal to the design loads or is higher than these design loads (excess preloading). When the excess preloading is applied, the resulting log time – settlement lays underneath the log time – settlement curve due to the design loads (in Figure 12 this is the continuous curve underneath the dashed curve). That

corresponds higher settlements. In Figure 12 it is shown that higher than design loads are achieved with the applied surcharge.

3. To define the duration of the preloading. The excess loading (or surcharge as in Figure 12) can be removed, when the desired settlement due to the preloading is reached.
4. To estimate what combination of embankment's and surcharge's heights and used material will correspond the applied preloading (see Equation (13)).
5. This iteration loop (steps 1-4) may be repeated several times in order to achieve the optimization of design.

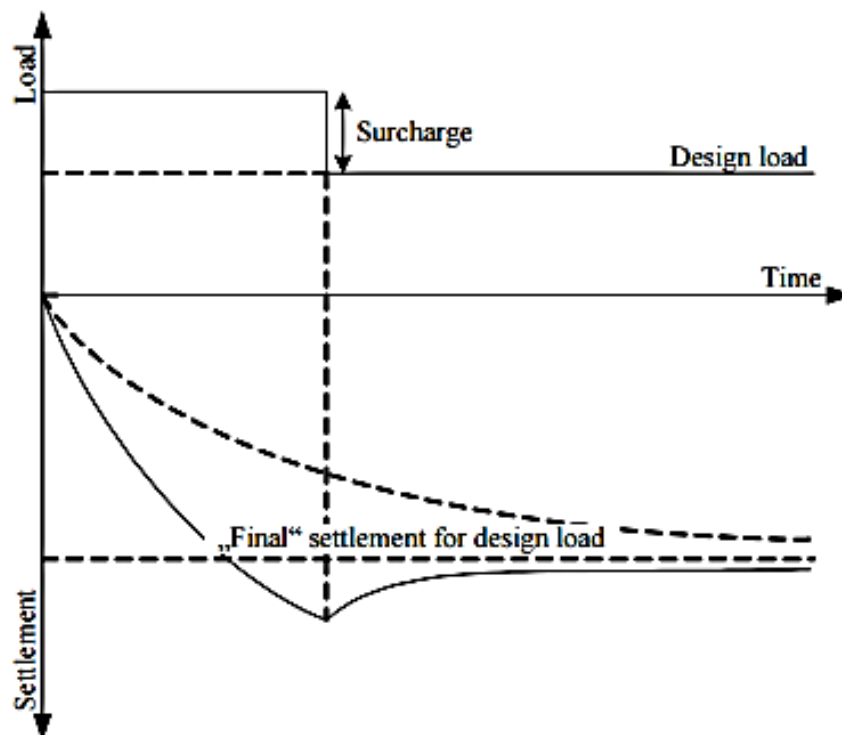
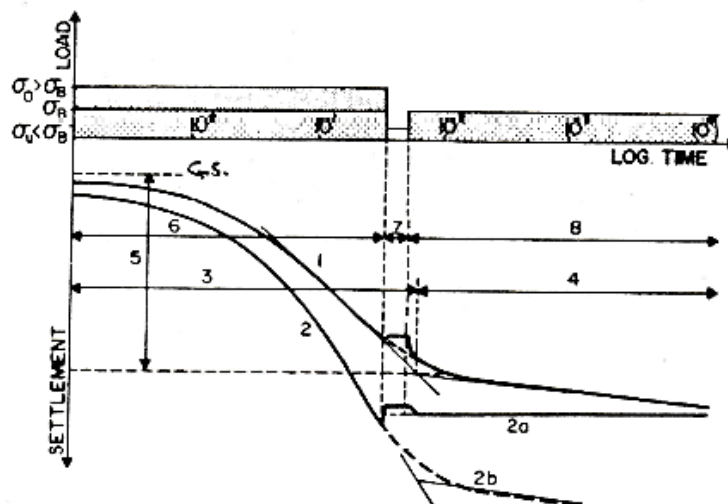


Figure 12 Resulting settlement due to preloading (Stapelfeldt 2000)

In general, it is more common to use the ground improvement with the excess preloading in order to reduce the post-construction settlement. The more detailed working principle of the excess preloading is illustrated in Figure 13, where the concept of time – settlement behavior under preloading and over-loading is visualized. Time – settlement curve 1 depicts the soil behavior, if in the preloading and reloading stages the maximal applied stress is equal to the service load σ_B . Time – settlement curve 2 shows soil behavior with

overloading σ_O in the preloading stage and service load σ_B in the reloading. For both curves the stress σ_U in the unloading stage is lower than the service load σ_B . In the unloading stage the time – settlement curve 1 indicates heave, but later returns to the initial settlement curve while it reaches the value of final settlement. In the time – settlement curve 2 a value higher than expected portion of final settlement is already reached in the preloading stage due to the applied over-loading. After the part of overloading is removed, soil stays in the overconsolidated state and secondary settlements in the reloading stage do not exceed the settlement predicted with the service load σ_B .



- 1 Time-settlement Curve: load σ_B
- 2 Time-settlement Curve: load $\sigma_0 > \sigma_B$
- 2a Unloading to $\sigma_0 < \sigma_B$ and reloading to σ_B
- 2b $\sigma_0 < \sigma_B$ without unloading
- 3 Period for initial and primary settlement of curve 1
- 4 Period for secondary settlement of curve 1
- 5 Total initial and primary settlement
- 6 Preloading, overloading period, respectively
- 7 Unloading and construction period
- 8 Period under final load of building
- G.S. Zero point of settlement

G_B service load
 G_0 overload

Figure 13 Time – settlement behavior under preloading and overloading (Veder and Prinzi 1983)

2.2.2.3 Pros and cons of the technique

Advantages of preloading:

- Economical technique (but depends on the availability of material for the preloading);
- Suitable for large areas;
- Suitable for saturated, compressible soils, such as soft silts, clays, silty clays;
- Fill can be later re-used as a construction material, if required.

Disadvantages of preloading:

- A time – consuming technique, if it is applied for low permeable soils without additional means of consolidation acceleration;
- Irregularity of settlements due to the size of embankment;
- Stability of embankment slopes must be considered in the design phase of embankment.

2.2.3 Vertical drains used for the ground improvement

2.2.3.1 General information about vertical drains

Vertical drains are artificially introduced drainage ways into the soils, designed to increase the permeability of soils and thus to reduce the excess pore water pressure and accelerate the consolidation in soft, cohesive, fine grained soils. In praxis, vertical drains are combined with conventional or vacuum preloading, because vertical drains do not work on their own without the excess pore water pressure. The potential benefit of application of vertical drains for the acceleration of settlement is sketched in Figure 14.

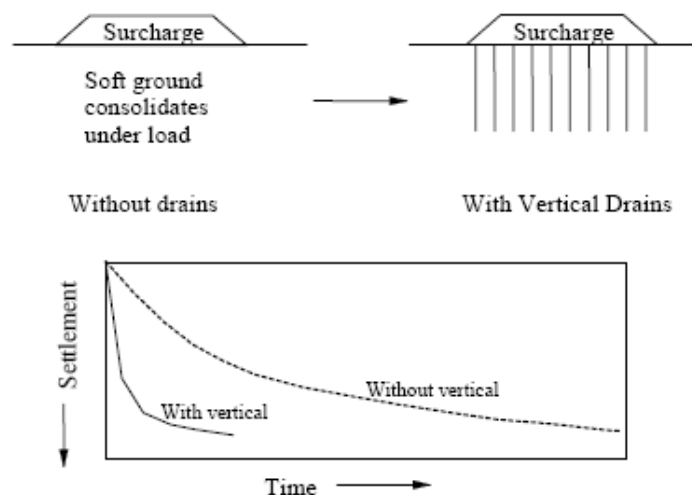


Figure 14 Benefit of vertical drains (Indraratna 2002)

First vertical drains were installed in California in 1934. Until the early 1970s, mainly large diameter sand drains were used. These were installed by means of close-ended mandrels and such installation method was causing the smear zone of considerable thickness around drains. The problem was solved with the invention of jetted sand drains in the Netherlands. As negative aspects of this method the additional costs of jetting pumps and the disposal of massive quantities of water were mentioned.

The development of synthetic materials and improvement of technical equipment resulted in the invention of principal alternative to large diameter sand drains, known as prefabricated vertical drains (PVD). The mechanism of prefabricated vertical drains is the same as in large diameter sand drains, but they are prefabricated in bands.

Today in geotechnical engineering the following types of vertical drains are used:

- **Sand drains**

Traditionally sand drains are sand filled holes in the soil, prepared by a displacement, drilling or washing method. Naturally, the permeability of sand is much higher than the permeability of the surrounding soil.

- **Sand wicks**

Pre-packed drains in a filter stocking are placed in a predrilled hole or into a mandrel. It saves the used amount of sand and reduces the soil disturbance around a drain during the installation. The fabric stockings allow sand drains to be extremely flexible and tenacious, thus allowing to stretch and compress at various points along their length to compensate lateral and vertical deformations. The granular soil filling in sand wicks ensures that the drain remains open irrespective of the external soil pressure.

- **Prefabricated band – shaped drains**

Such drains consist of flat plastic core, wrapped in thin layer of geotextile. Today several types of cores of various parameters and, consequently, efficiencies are used. Examples of flat plastic cores are presented in Figure 15 - Figure 17 .

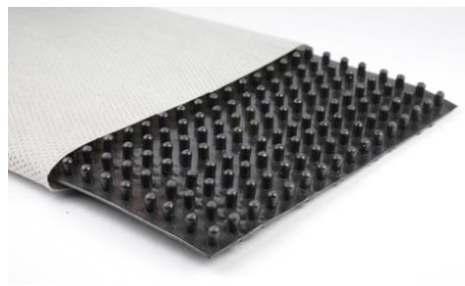


Figure 15 Type of PVD filter (Arizona Geosynthetics 2017)

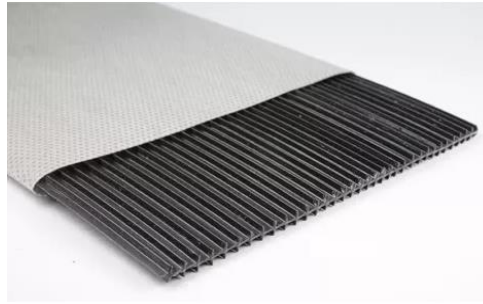


Figure 16 Type of PVD filter (Tencate 2017)



Figure 17 Type of PVD filter (Geoengineering 2017)

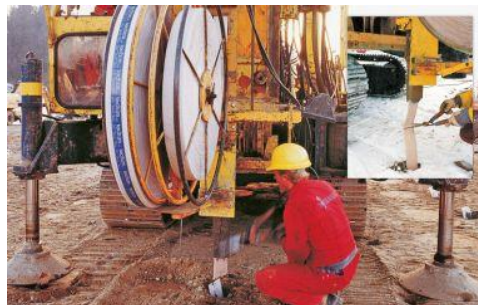


Figure 18 Roll of PVD (Keller 2017)

2.2.3.2 Principle of operation

Vertical drains are artificial drainage paths, pushed into a soil, to increase the settlement rate through the accelerated consolidation. The acceleration of consolidation ratio is achieved through two main features of drains:

- The groundwater flows in horizontal direction to a single drain:

Water always looks for the easiest route to the free surface. After the implementation of vertical drains a faster way for the water flow to reach the surface is to flow in horizontal direction towards a drain and then dissipate vertically through it. Here, the higher horizontal permeability of soils is capitalized, too.

- Deployed grid of vertical drains over construction area provokes a fairly distributed water inflow towards a single drain from the surrounding soil.

2.2.3.3 Properties of vertical drains

a) Equivalent drain diameter for band – shaped drains

The conventional theory of consolidation with vertical drains assumes that the vertical drains are circular in their cross-section. As most of the prefabricated drains are rectangular in cross-section (band-shaped), the rectangular drain for purposes of design only has to be converted into an equivalent cylindrical shape. That implies that the equivalent diameter has the same theoretical radial drainage capacity as the band-shaped drain. Hansbo (1979) suggested that both band-shaped and circular drains lead to practically the same degree of consolidation if their circumferences are equal. Thus, the equivalent drain diameter is evaluated with Equation (14).

$$d_w = \frac{2(w + b)}{\pi} \quad (14)$$

d_w	[m]	Equivalent diameter of band-shaped drain
w	[m]	Width of band-shaped drain
b	[m]	Thickness of band-shaped drain

b) Properties of filter

“In general, the drain material of a sand drain and the filter jacket of a prefabricated drain have to perform two basic but contrasting requirements, which are retaining the soil particles and at the same time allowing the pore water to pass through” (Stapelfeldt 2000).

The geotextile used for the filter jacket must ensure proper permeability, retain fine soil particles, be strong enough to withstand later pressures of soil and not to break during the installation process. Apparent opening size (AOS) is a criterion introduced to the filter design and is related to the size of fabric pores. For example, O_{95} is the AOS of the filter, where 95% of fabric pores are smaller than defined O_{95} . $O_{95} \leq 0,075$

mm is often specified for vertical drains. More information about requirements is provided in ASTM D4751.

c) Discharge capacity

Release of excess pore water pressure and discharge of ground water are main purposes of using vertical drains. Higher discharge capacity ensures better discharge properties. The discharge capacity is influenced by the lateral earth pressure, the occurrence of large settlements, clogging of drains and hydraulic gradient of soils.

2.2.3.4 Installation methods of PVD

In many cases a sand blanket filling is placed on the existing original ground surface before the installation. The blanket ensures the accessibility to a construction site for the heavyweight rigs and serves as a drainage layer for dissipating water.

As the drain is placed in the steel mandrel lining, an anchor plate is fixed on its end. The anchor plate serves two purposes in the operation. First, it prevents soil from entering and clogging the mandrel as it is being driven into the ground, and secondly, it anchors the drain in place at the desired depth as the mandrel is being retracted. When the mandrel has been withdrawn, the wick is cut off above the ground surface, leaving a tail. Then a new anchor plate is installed, the mast is repositioned over the next location and the cycle is repeated.

The installation process is illustrated in Figure 19.

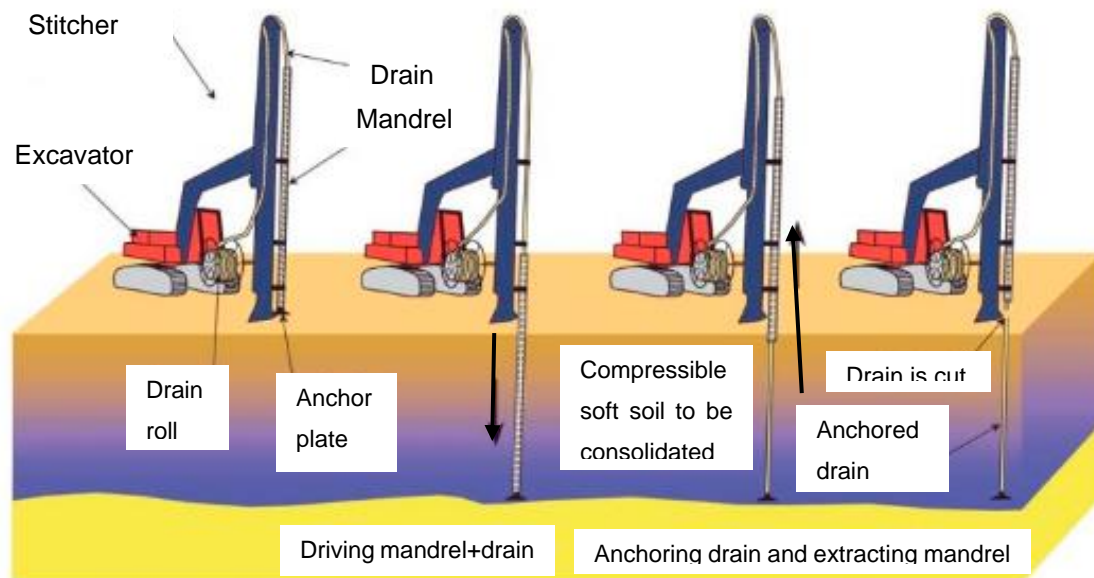


Figure 19 Installation of vertical drains (Menard 2017)

2.2.3.5 Factors affecting the performance of PVD

Installation and operation of vertical drains requires a constant monitoring. A nonconformity with expected settlements can be a results of many factors such as:

- **Smear effect**

As a mandrel with an anchor plate is being driven into the soil or later the same mandrel is removed, a portion of material around a mandrel is being compacted, what causes a reduction of hydraulic conductivity within a certain radius. This reduction of permeability around a drain due to the installation is called the smear effect. The smear effect can be implemented into calculations of settlements, however a significance of this effect on the total amount of settlement is debatable.

- **Well resistance**

“The relevant features for the design and performance of vertical drains are their hydraulic properties: the discharge capacity of the cross-section and their filter permeability. If during the consolidation period the discharge capacity of the drain is reached, the overall consolidation process is retarded. In such cases, the drains exhibit a resistance to water flow into them what is known as the well resistance. It can develop and increase as the deterioration of the drain filter may lead to a significant reduction of the cross-section. Furthermore, fine soil particles may pass

through the filter and decrease the area available for flow. Finally, folding of the drain because of large settlements may result in a reduced discharge capacity” (Holtz et al. 1991).

- **Threat of clogging when prefabricated vertical drains are pushed in the soil**

Even though at the end of mandrel a steel anchor plate is placed, which serves two purposes during the operation - prevent soils from entering and anchors the plate at the desired depth, the risk, that an anchor plate is weakly attached to a mandrel or is damaged during the installation, remains.

- **Bending of drains**

Bending may occur due to the consolidation process. Bending of drains due to the lateral earth pressure may distort the effective cross-section of vertical drains and that is likely to influence the overall effectivity of drain properties.

- **Sensitivity of geotextile to the chemical properties of soils**

Installation and use of vertical drains for improvement of contaminated soils might have a negative impact on geotextile wrapping. If the geotextile is not compatible with aggressive chemical particles in soil, a strongly damaged drain can lose its function.

2.2.3.6 Pros and cons of the technique

Advantages of the technique:

- Decrease of overall time required for completion of primary consolidation due to preloading;
- Decrease the amount of excess surcharge required to achieve the desired amount of precompression in the given time;
- Prefabricated vertical drains can withstand considerable lateral displacement or buckling under vertical or horizontal soil movement;
- Suitable for a rapid consolidation with varying spacing;
- Prefabricated vertical drains can be installed underwater and in a non-vertical orientation;

- In comparison to sand drains, prefabricated vertical drains are installed faster, do not require the source of water for jetting and ensure continuous vertical drainage path.

Disadvantages and design considerations:

- If the compression layer is overlain by dense fills or sands, very stiff clay or other obstructions, drain installation could require predrilling, jetting, and/or use of a vibratory hammer, or may not even be feasible;
- Where sensitive soils are present or where stability is of concern, disturbance of the soil due to drain installation may not be tolerable.

2.3 Modelling of vertical drains

As it is explained in section 2.2.3, vertical drains are commonly used in fine-grained soils in order to accelerate the consolidation. Nowadays settlement predictions are performed with various softwares and FEM programs, where vertical drains can be implemented in simulation models.

In the first three sections of this chapter provide general information about the software used for the calculations in this Thesis and modelling of vertical drains. The fourth section describes one of the many ways to implement vertical drains, which was specifically chosen for this Thesis.

2.3.1 Generalities

Implementation of vertical drains in the ground model adds significant difference in the modelling procedure. Application of vertical drains to the model results in the more complexed geometry and consequently longer time steps, required by the program to perform the simulation.

For this Thesis, simulations are carried out with the *GGU CONSOLIDATE 5* software, which performs calculations based on the elasticity theory.

The software *GGU CONSOLIDATE 5* offers two possible switches for simulations with vertical drains:

- Analytical simulation of a unit cell with one vertical drain, where parameters of this cell are equal to the effective radius and length of the single drain.

- Numerical simulation of multi-layered underground model with installed vertical drains within the whole thickness of model.

Due to preloading a generated excess pore water pressure can dissipate anytime through the opened upper edge of drain element.

However, the software *GGU CONSOLIDATE 5* has a limitation for numerical simulations with multi-layered soil models: the underground model cannot be divided into the upper part with vertical drains and lower without them. This problem can be solved if two following conditions are applied:

- The opened upper bound is prescribed for the model as an equivalent condition for drains with opened upper edges.
- For calculations in this model, the natural, radial inflow of the vertical drainage must be converted into a parallel inflow by means of suitable approaches.

2.3.2 Axisymmetric and plane strain model

“Most finite element analyses are conducted based on the plane strain model, even though actual consolidation around vertical drains is axisymmetric. Therefore, to employ a realistic 2-D (plane strain) finite element analysis for vertical drains, the equivalence between the plane strain and axisymmetric analysis needs to be established, in order to ensure the correct time-settlement relationship” (Indraratna 2012).

In comparison to the axisymmetric consolidation model, where drains are modelled as well elements, in the plane strain consolidation model a vertical drain is a rectangular element of very small thickness. Respectively, the effective radius of a single drain corresponds the change in geometry. Thus, the water inflow towards drain is considered as parallel rather than radial. It results in the change of flow area. This aspect is illustrated in Figure 20.

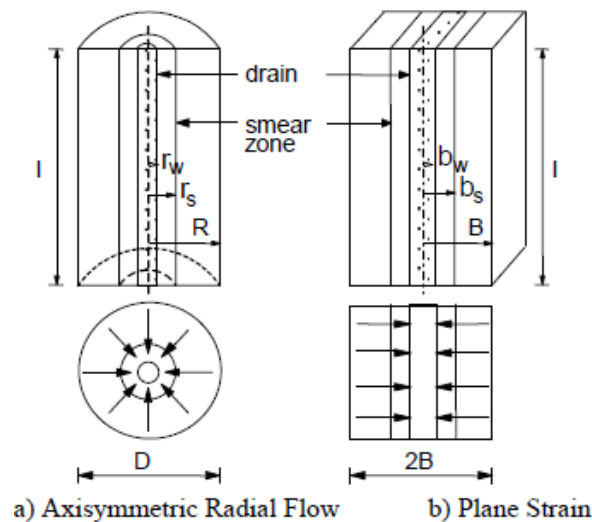


Figure 20 Axisymmetric and plane strain models (Indraratna 2002)

The equivalence of axisymmetric and plane strain conditions can be executed in three ways:

1. “Geometric matching approach – the spacing between drains is made equivalent while keeping the permeability the same “ (Indraratna 2002);
2. “Permeability matching approach - permeability coefficient is made equivalent while keeping the spacing of drains the same” (Indraratna 2002).
3. “Combination of permeability and geometric matching approach – plane strain permeability is calculated for a convenient drain spacing” (Indraratna 2002).

2.3.3 Grid based influence zone of drains

Influence zone D around a single drain is a function of the drain spacing and the grip type.

Two for ground stabilization applicable grids (patterns) – triangle and square – are shown in Figure 21.

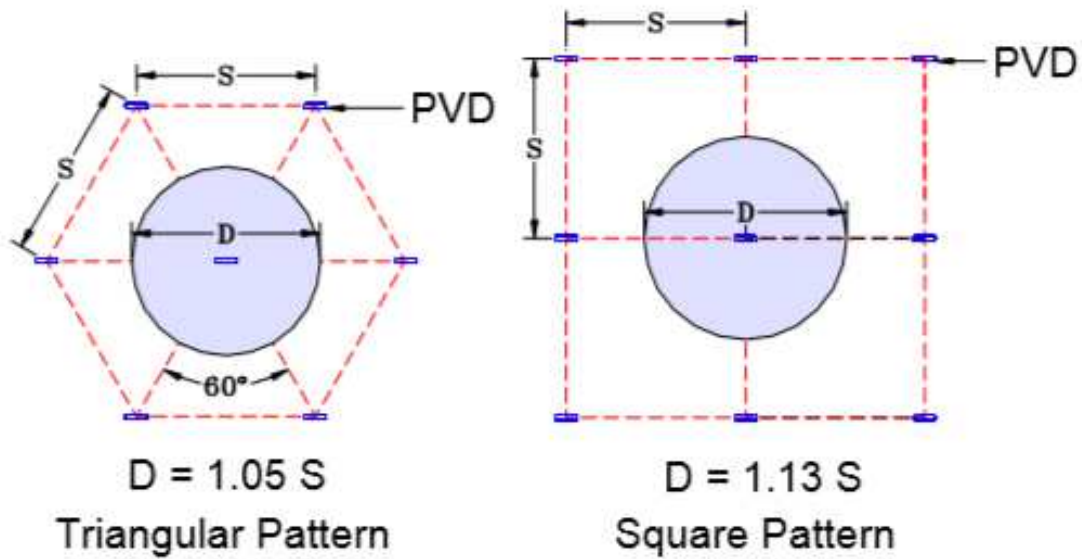


Figure 21 Triangle and square patterns (Geoengineering 2017)

In modelling following values are prescribed for above shown grids:

- Triangular grid: 1.05
- Square grid: 1.13

Hence, the influence zone D can be controlled and calculated with Equation (15) and (16):

$$D = 1.05S_{triangular} \quad (15)$$

D [m] Influence zone
 $S_{triangular}$ [m] Distance between drain centers in the triangular grid

$$D = 1.13S_{square} \quad (16)$$

S_{square} [m] Distance between drain centers in the square grid

“A square pattern is often easier to lay out during field installations, however, a triangular pattern is usually preferred since it provides a more uniform consolidation between drains” (Indraratna 2002).

2.3.4 Approach according to CUR 191 (1997)

In the unit cell the consolidation process is influenced by two conditions: horizontal inflow towards a single drain and a simultaneous decay of excess pore water pressure in the vertical direction along the drain towards an opened (drained) boundary.

To convert the radial inflow towards the radial drainage element into a parallel flow, the method proposed by CUR 191 (1997) is chosen for calculations in this Thesis. The main advantage of CUR 191 (1997) method is a significant simplification of the calculation model.

CUR 191 (1997) describes the methodology of consolidation simulation with vertical drains with an explicit modeling of drain elements. It is achieved through the estimation of equivalent vertical permeability for a homogenous soil layer. Likewise, CUR 191 (1997) provides a simplified approach for the estimation of equivalent horizontal permeability.

The main difference of CUR 191 (1997) methodology in comparison to other approaches, for example, to the solution proposed by Hansbo (1979), lays in the estimation of the consolidation rate for a perfect drain without the consideration of smear and well-resistance effects, implicated in the method proposed by Hansbo (1979).

2.3.4.1 Equations for radial inflow

Kjellman (1952) proposed a solution for an average degree of consolidation due to the radial flow towards a sand or prefabricated vertical drain. In this case the excess pore water pressure dissipated in the horizontal direction via a drain in a unit cell. The proposed solution is shown in Equation (17).

$$U_h = 1 - e^{-\frac{8T_h}{\mu}} \quad (17)$$

U_h	[%]	Degree of consolidation due to the radial flow
T_h	[-]	Time factor for the radial flow
μ	[-]	Correlation coefficient as in Equation (19)

Here:

$$T_h = \frac{c_h t}{D_{cell}^2} \quad (18)$$

t	[s]	Consolidation time
-----	-----	--------------------

D_{cell} [m] Diameter of unit cell
 c_h [m²/s] Horizontal coefficient of consolidation

And

$$\mu = \frac{n^2}{n^2 - 1} \left[\ln(n) - \frac{3}{4} + \frac{1}{n^2} \left(1 - \frac{1}{4n^2} \right) \right] \quad (19)$$

with $n = \frac{D_{cell}}{d_w}$

The drain diameter d_w is design dependent parameter. For sand drains d_w is equal to the designed drain diameter, while for prefabricated vertical band drains this diameter should be recalculated with respect to the width and length of cross-section as in Equation (20):

$$d_w = \frac{(2w + 2b)}{\pi} \quad (20)$$

2.3.4.2 Equations of parallel flow path

Based on the dimensionless time factor T_v and the assumption that during the consolidation process the flow paths of pore water are parallel to each other, the following solutions (Equation (21) and Equation (22)) were derived to estimate the consolidation degree U_v :

$$U_v \approx 2 \sqrt{\frac{T_v}{\pi}} \quad \text{if } T_v \leq 0.2 \quad (21)$$

U_v [-] Degree of consolidation for parallel flow

Or

$$U_v \approx 1 - e^{-\frac{\pi^2}{4} T_v - 0.21} \quad \text{if } T_v > 0.2 \quad (22)$$

With

$$T_v = \frac{c_v t}{D_{cell}^2} \quad (23)$$

Vertical coefficient of consolidation c_v is calculated based on Equation (11).The implemented permeability must conform the chosen direction, in which the coefficient of consolidation is determined.

2.3.4.3 Combination

However, in reality the water flow between soil particles towards drains is a combination of two earlier described flow mechanisms. Water always looks for the “easiest” route to the free surface. In soils the easiest route is as well the shortest, because the water can penetrate through voids between grains. For this reason if a soil layer has a boundary with another layer of higher permeability or lays near the ground surface, water close to the edge of this bound tends to flow in the vertical direction. On the other hand, within the layer, water will flow in the horizontal direction, in parallel to each other currents. Here the radial or horizontal flow dominates over the vertical.

Carillo (1942) considered these conditions in the one Equation (24):

$$U_{vh} = 1 - (1 - U_v)(1 - U_h) = U_v + U_h - U_v U_h \quad (24)$$

U_{vh} [-] Degree of consolidation for combined flow

The substitution of U_v and U_h with Equation (25) and (26) provides following solutions:

$$U_{vh} = 1 - (1 - 2 \sqrt{\frac{T_v}{\pi}}) e^{-\frac{8}{\mu} T_h} \quad \text{if } T_v \leq 0.2 \quad (25)$$

$$U_{vh} = 1 - e^{-\left(\frac{\pi^2}{4} T_v + 0.21 + \frac{8}{\mu} T_h\right)} \quad \text{if } T_v > 0.2 \quad (26)$$

2.3.4.4 Equivalent horizontal permeability according to CUR 191 (1997)

Figure 20 in section 2.3.2 which introduces a brief description of two different modeling concepts shows the unit cell with a vertical drain in axisymmetric and plane strain modes. This figure depicts, how the change in geometry modifies the modeling concept and shapes flow conditions.

In both cases the ground water flows in the direction perpendicular to a drainage element, what corresponds to the shortest way. However, in the plane strain drainage

elements function as plate elements, located perpendicular to the calculation plane with unlimited extent in the opposite to the viewer direction. Due to the rectangular cross-section of drains and unlimited length the water flow is converted into parallel. Thus, the consolidation in the vertical direction plays a subordinate role in this scenario.

Taking into account above mentioned conditions, the horizontal coefficient of consolidation is now defined as equivalent horizontal coefficient of permeability k_h' . The implementation of an equivalent horizontal coefficient of permeability k_h' allows to equate the combined flow with the parallel flow, and it results in the Equation (27)

$$k_h' = \alpha \frac{B^2}{\mu d^2} k_h \quad (27)$$

k_h'	[m/s]	Equivalent horizontal coefficient of permeability
k_h	[m/s]	Horizontal coefficient of permeability
α	[-]	Function of degree of consolidation
B	[m]	Width of unit cell
k_v'	[m/s]	Equivalent vertical coefficient of permeability
k_v	[m/s]	Vertical coefficient of permeability

α is a function of the degree of consolidation. As it is explained in the previous chapters, the degree of consolidation is a time-dependent parameter. This suggests that the α factor is as well governed by time, and estimated as shown in Equation (28). However, the Equation (28) reveals that in order to estimate the equivalent horizontal permeability the degree of consolidation must be prescribed in advance.

$$\alpha = 3.24 \frac{\ln(1 - U) + 0.21}{\ln(1 - U)} \quad (28)$$

Even though the method with the equivalent horizontal permeability allows to switch from the axisymmetric to the plane strain model, nonetheless it does not result in the simplification of the model geometry, because the need to vertical drains in the model still remains.

2.3.4.5 Equivalent vertical permeability according to CUR 191 (1997)

The fundamental idea of this approach is to simplify the geometry of calculation model with vertical drains. Thus, the effect of vertical drains on the soil permeability is considered and in modeling replaced with the equivalent vertical permeability.

As it was discussed in the previous section, the water flow around a single drain is considered to be radial. As it reaches the drain, it is directed to the surface and results in dissipation of excess pore water pressure. Based on this pore water dissipation mechanism with vertical drains, in the contrast to the consolidation without vertical drains the horizontal permeability of soils is the governing input parameter.

According to CUR 191 (1997) the equivalent vertical permeability is estimated under assumption that both of the above described models reach the same degree of consolidation at the same time. This can be expressed as $U_v = U_{vh}$. This is equivalent to comparison of Equation (22) and (26). The estimated result is shown as Equation (29)

$$k'_v = k_v + \frac{32}{\pi^2} \frac{d^2}{\mu D_{cell}^2} k_h \quad \text{with } k'_h = k_h \quad (29)$$

All in all, if the equivalent vertical permeability is estimated with the CUR 191 (1997) approach, the calculation model can be simplified and there is no need to model vertical drains.

2.4 In-situ geotechnical subsurface investigation tests

In geotechnics there are two common ways, how soil properties can be defined: in the laboratory or in-situ. The in-situ subsurface investigation is performed “locally”, “on the construction site” and provides the direct measurement of soil properties and geotechnical parameters. The purpose of the in-situ subsurface investigation is to obtain the understanding of soil properties, the soil stratigraphy (if possible) and the hydrogeological conditions.

This chapter provides a brief introduction of adopted in-situ geotechnical tests: Standard Penetration Test (SPT), cone penetration test (CPT), piezocone penetration test (CPTu) and seismic piezocone penetration test (SCPT). The chapter contains two sections: the first section gives the short description of each of the above mentioned tests; the second section has an emphasis on empirical correlations proposed by Robertson (2012), which are recently used in the praxis of CPTu testing.

2.4.1 In-situ geotechnical tests

The aim of this section is to provide a brief overview of four popular in-situ subsurface investigation tests: Standard Penetration Test (SPT), Cone Penetration Test (CPT), Piezocone Penetration Test (CPTu) and Seismic Piezocone Penetration Test (SCPT).

The first three types of in –situ subsurface investigation tests mentioned above are chosen due to their popularity and due to the reason, that the main literature source used for this Thesis “Guide to cone penetration testing” (Robertson, 2012) provides correlations derived specifically for these tests. The fourth type of tests is the extension of CPTu tests, which provides the enhanced understanding of subsurface.

a) Standard Penetration Test (SPT)

The Standard Penetration Test (SPT) is performed during the advancement of a soil boring to obtain an approximate measure of the dynamic soil resistance, as well as a disturbed drive sample.

The development of the Standard Penetration Test origins from early beginning of the 20th century, when Colonel Charles R. Gow introduced the exploratory boring technique with the 1-inch diameter drive sampler.

Nowadays this test involves driving a standard hollow thick-walled sample tube (outside diameter of 50,8 mm and an inside diameter of 35 mm, and a length of around 650 mm) into the ground by blows of a slide hammer. The fall height of the standardized 63,5kg hammer is 0,76m. Then the dynamic soil resistance is evaluated with a number of blows (N-value). This hammer falls repeatedly from the fall height and must achieve three successive increments of 0,15m each. According to (UONBI), the first increment is recorded as a “seating”, while the number of blows to advance the second and the third increments are summed to give the N-value or SPT-resistance (reported in blows/0,30m or blows/foot).

The test sequence as it is standardized in ASTM D 1586 is shown in Figure 22.

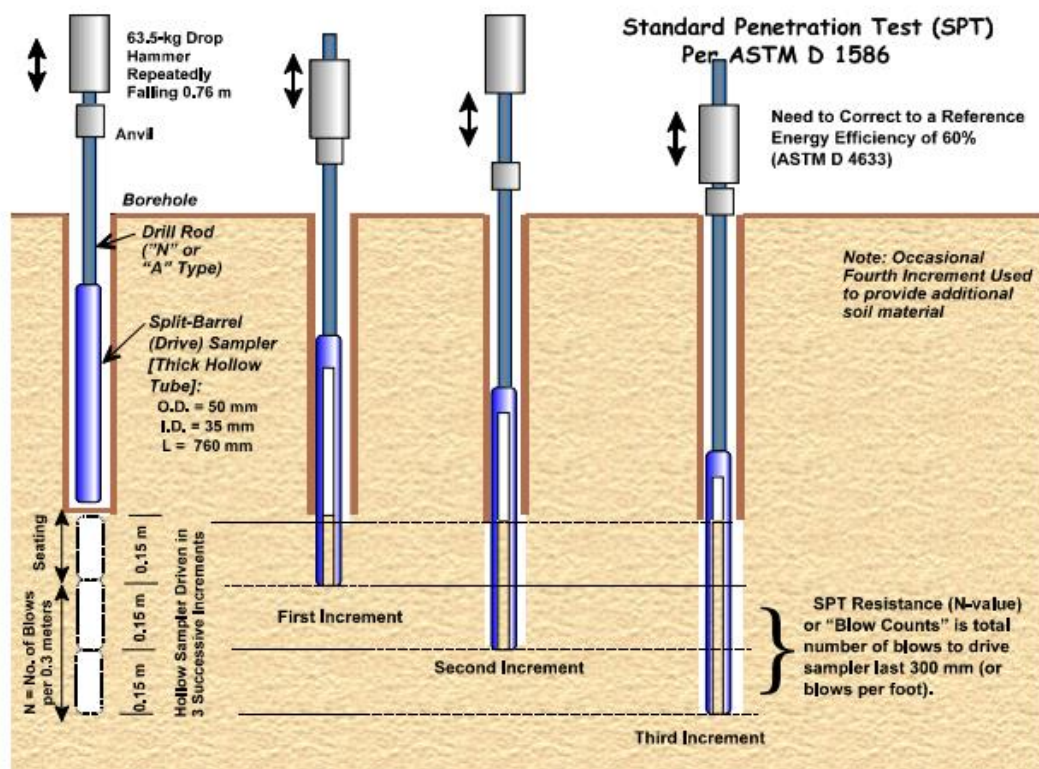


Figure 22 Sequence of driving the SPT sampler (UONBI)

The N-value provides an indication of the relative density of the specific driving interval, and it is used in the empirical correlation to estimate the approximate shear strength properties in that specific driving interval.

The SPT N-value should be corrected with respect to the energy efficiency. "The main way to assess the influence of test equipment on the SPT-N value has been through the measurement of the energy delivered to the SPT rods from the hammer/anvil system. The energy delivered to SPT rods is normally expressed in terms of the rod energy ratio (ER). An energy ratio of 60% has generally been accepted as the reference value [...]" (Robertson 2006). This corrected N-value is designated N_{60} and estimated with Equation (30):

$$N_{60} = \left(\frac{ER}{60}\right)N_m \quad (30)$$

N_{60} [blows] Corrected N – values

N_m [blows] Measured N – value of blows

ER [m/s] Rod energy ratio

According to Robertson (2006), the corrected SPT N – value is used for interpretations of the relative density, friction angle, stiffness, undrained shear strength, stress history and overconsolidation ratio OCR.

The main advantage of this in-situ test is the simplicity of its procedure, which provides numbers suitable for further correlations, such as the strength and the density. This in-situ test is applicable to many soil types (most often in granular materials) and even weak rocks, with exception of soft clays and silts, because the act of driving the sampler results in the significant disturbance of the soil and gives results based on the disturbed soil properties rather than the intact. If the disturbed sample is received, it is suitable for index tests only.

The main disadvantage of this method is its roughness, because the received numbers are limited to the specific driving interval, and the need to “normalize” the received data with respect to the drilling and borehole technique, sampling technique, SPT equipment and test procedure and the overburden stress.

b) Cone penetration test (CPT)

The cone penetration test (CPT) is an in-situ testing method, which additionally to the estimation of geotechnical soil properties assess the subsurface stratigraphy. This method is as well known as the Dutch Cone test, because it originates from the Gouda vicinity, Netherlands. The CPT apparatus dates from 1932 and was designed by the civil servant Mr. Peter Berentsen. He performed the first CPT test with a 10cm^2 cone, pushing it into the ground by his own body weight.

Today standardized CPT apparatus has following parameters: cross-section area of 10cm^2 , apex angle of 60° , sleeve of 150cm^2 . The ASTM Standard as well allows to use a larger body of cone (cross-section area of 15cm^2 , sleeve of 200cm^2). The main parts of the CPT penetrometer are shown in Figure 23.

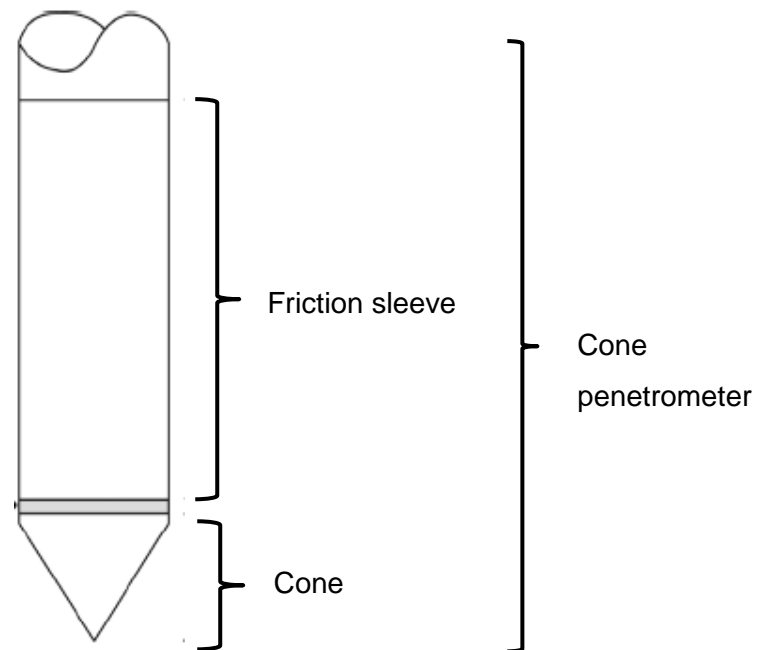


Figure 23 Terminology for the cone penetrometer (Robertson 2012)

The test is carried out by first pushing the cone into the ground at a standard velocity of 1 to 2cm/s while keeping the sleeve stationary. This procedure is repeated and the measurements are made at regular depth intervals, generally 2cm interval are applied, during penetration. For any depth the resistance of the cone tip q_c and the sleeve resistance f_s are monitored. Later these two resistance values are correlated to shear strength parameters using proposed empirical curves and prescribed for different soil behavior types.

The CPT test provides a fast and continuous profiling of the subsoil, based on the measured tip and sleeve resistance. This test is applicable for very soft clays to dense sands. The investigation of gravely soils may be carried out with cones of larger parameters, but the received data must be correlated with respect to the standardized cones. However, no soil samples can be obtained with the CPT test.

c) Piezocone penetration test (CPTu)

Piezocone penetration test (CPTu) is an extension of above mentioned cone penetration test. In this method additionally to the values of the cone tip resistance q_c and the sleeve resistance f_s the pore pressure measurement is carried out.

The pore pressure monitoring is enabled through two filters – u_1 and u_2 – built into the measurement apparatus. In commercial penetrometers the filter u_1 is located at the midface and the filter u_2 is located at the shoulder, just behind the tip. In general, the measured pore pressure at the filter u_1 is higher than at the filter u_2 . Locations of filters is depicted in Figure 24.

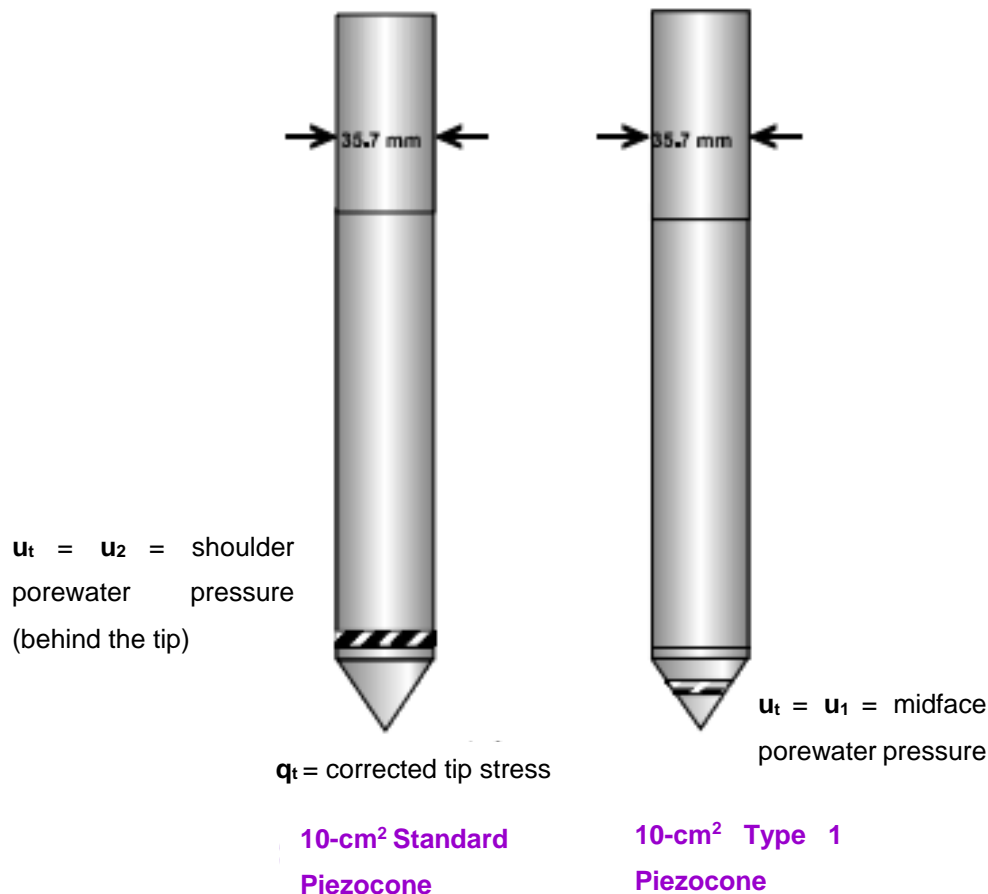


Figure 24 Examples of commercial piezocones with two types of built-in filters (Mayne 2000)

In most of the cases, the subsoil investigation is performed with piezocones, where the filter is located in the shoulder, because of the necessary correction for the measured tip resistance q_c .

The output of CPTu measurement - q_c , f_s and u_1 or u_2 - are plotted with respect to depth. As the continuous records are provided, the general changes of stratigraphy (the change

of soil type) and the presence of lenses can be investigated in details. As well, these output values are used in correlations to estimate other related soil properties (they are discussed in section 2.4.2).

The advantage of CPTu test is possibility to combine it with the dissipation test. Each time the penetration of the cone is stopped, the excess pore water pressure starts to dissipate. The rate of dissipation depends on the permeability and compressibility of soils. "A dissipation test can be performed at any required depth by stopping the penetration and measuring the decay of pore pressure with time" (Robertson 2012). In general it is required to reach the 50% dissipation time t_{50} – the time, which corresponds to the pore water pressure p_{50} (Equation (31)). The example of dissipation time t_{50} estimation is presented in Figure 25.

$$p_{50} = u_0 + \left(\frac{u_1 - u_0}{2} \right) \quad (31)$$

- p_{50} [kPa] 50% pressure of dissipation test
- u_0 [kPa] In-situ equilibrium pore water pressure
- u_1 [kPa] Pressure in the beginning of the dissipation test

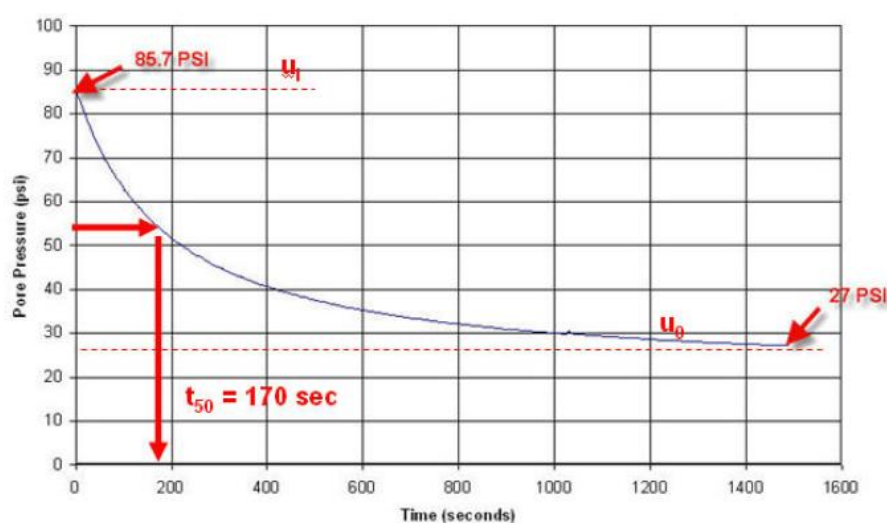


Figure 25 Example of dissipation test to determine t_{50} (Robertson 2012)

The dissipation time t_{50} is lower for coarse grained soils and occurs rapidly. For fine grained soils as clay and silts it may take up to several hours for the dissipation to reach the time t_{50} .

The relationship between t_{50} and the hydraulic permeability is proposed by Mayne (2002) and is approximated as in Equation (32):

$$k = \left(\frac{1}{251 \times t_{50}} \right)^{1.25} \quad (32)$$

t_{50} [s] Time of 50% completion of dissipation test

However, in this test the dissipation rate depends on the size of the probe: the dissipation rate decreases with the increase of the probe diameter.

d) Seismic piezocone penetration test (SCPTu)

The addition of a geophone in the piezocone body enables the collection of seismic wave data, and the calculation of shear and compressional wave velocities during the cone penetration test.

For SCPTu testing, the selected energy source depends on field conditions and the specific data which is to be collected for a project. Figure 26 illustrates the typical layout for a downhole seismic cone test.

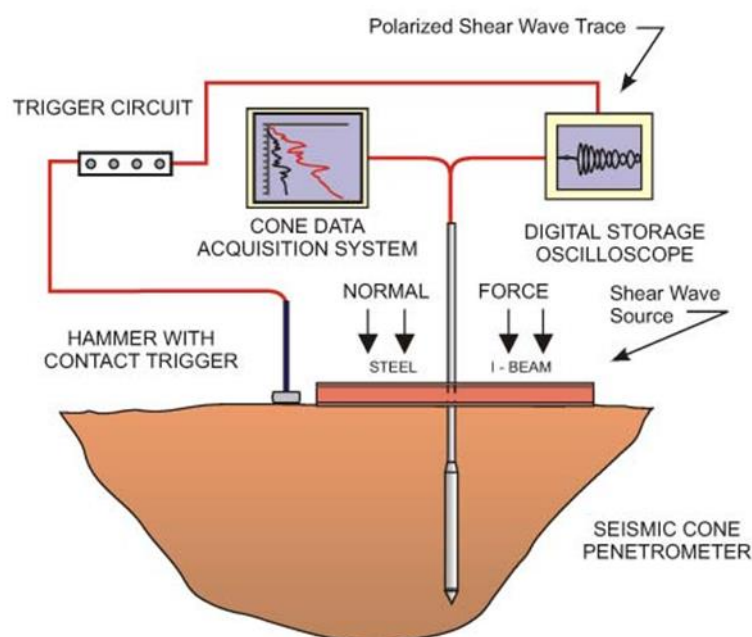


Figure 26 Layout of downhole seismic cone system (Robertson 2006)

e) Other methods

The in-situ underground investigation can be as well for example performed by mean of:

- Flat Dilatometer Test (DMT);
- Field Vane Test (FVT);
- Pressuremeter Test (PMT).

2.4.2 Interpretation of results for CPTu test

This section summarizes the empiric correlations used for the interpretation of data, obtained with piezocone tests. The summarized empiric correlations are taken from the publication “Guide to Cone Penetration Testing for Geotechnical Engineering” (2012) by P. K. Robertson.

2.4.2.1 Raw data

The initial records obtained with the piezocone test include measurements of tip resistance q_c , sleeve friction f_s and excess pore water pressure u_2 .

a) Cone resistance q_c [MPa]

Cone resistance q_c is the quotient of the force acting on the cone Q_c with the projected area of the cone A_c :

$$q_c = \frac{Q_c}{A_c} \quad (33)$$

q_c	[MPa]	Cone resistance
Q_c	[MN]	Force acting on the cone
A_c	[m ²]	Projected area of the cone

In general, the higher cone resistance is observed in sands than in clays.

b) Sleeve friction f_s [MPa]

The sleeve friction f_s is the quotient of the frictional force acting on the sleeve F_s with the surface area of the sleeve A_s :

$$f_s = \frac{F_s}{A_s} \quad (34)$$

f_s	[MPa]	Sleeve friction
F_s	[MN]	Frictional force acting on the sleeve

A_s [m²] Surface area of the sleeve

In general, the higher sleeve friction is observed in fine – grained soils than in coarse grained sediments.

c) Excess pore pressure (net pressure) Δu [MPa]

The excess pore pressure (net pressure, shoulder pressure) Δu is a temporal dynamic increase of in-situ equilibrium ground water pore pressure, generated by the applied external load:

$$\Delta u = u_2 - u_0 \quad (35)$$

Δu [MPa] Excess pore water pressure

u_2 [MPa] Pore pressure measured in the filter just behind the cone

2.4.2.2 Values derived from CPTu

1. Corrected values

“Due to the inner geometry of the cone the ambient water pressure acts on the shoulder behind the cone and on the ends of the friction sleeve. This effect is often referred to as the unequal end area effect” (Campanella et al., 1982). The influence of pore water pressure acting on the cone geometry must be considered in calculations and improved values are named as corrected.

In sandy soil, which distinguish themselves with the higher permeability, calculated cone resistance must not be corrected for pore water pressures acting on the cone geometry. Thus, the cone resistance q_c does not differ from the corrected cone resistance q_t ($q_c = q_t$).

“In soft clays and silts and in over water work, the measured q_c must be corrected for pore water pressures acting on the cone geometry, thus obtaining the corrected cone resistance, q_t ” (Robertson 2012) (see Equation (36)):

$$q_t = q_c + u_2(1 - a) \quad (36)$$

q_t [MPa] Corrected cone resistance

a [-] The net area ratio determined from laboratory calibration with a typical value between 0,70 and 0,85

It is desired to use the penetrometers with the net area ratio $a > 0,80$, because it minimizes the correction. The value should be provided by the manufacturer.

Correction for the sleeve friction is applied under the same consideration of the ground water influence:

$$f_t = f_s - (u_2 A_{sb} - u_3 A_{st}) / A_s \quad (37)$$

f_t	[MPa]	Corrected sleeve friction
u_3	[MPa]	Pore pressure measured at the top of sleeve
A_{sb}	[m ²]	Cross- section area of sleeve at base
A_{st}	[m ²]	Cross- section area of sleeve at top
A_s	[m ²]	Surface area of the sleeve

“However, the ASTM standard requires that cones have an equal end area friction sleeve that reduces the need for such a correction. All cones should have equal end area friction sleeves with small end areas to minimize the effect of water pressure on the sleeve friction measurements” (Robertson 2012).

2. Evaluation of geotechnical properties

The evaluation of geotechnical properties starts with the approximation of normalized values.

a) Friction ratio R_f [%]

“The ratio, expressed as a percentage, of the sleeve friction, f_s , to the cone resistance, q_t , both measured at the same depth” (Robertson 2012)

(Equation (38)):

$$R_f = \frac{f_s}{q_t} \times 100\% \quad (38)$$

R_f	[%]	Friction ratio
-------	-----	----------------

“Since both the penetration resistance and sleeve friction increase with depth due to the increase in effective overburden stress, the CPT data requires normalization for overburden stress for very shallow and/or very deep soundings” (Robertson 2012).

b) Normalized cone resistance Q_t [-]

Normalized cone resistance Q_t is the expression of cone resistance in non-dimensional units, which takes into account the in-situ vertical stresses

(Equation (39)):

$$Q_t = \frac{q_t - \sigma_{v0}}{\sigma'_{v0}} \quad (39)$$

Q_t [-] Normalized cone resistance

σ_{v0} [MPa] In-situ vertical stress

σ'_{v0} [MPa] In-situ effective vertical stress

c) Normalized cone resistance Q_{tn} [-]

“The cone resistance expressed in a non- dimensional form taking account of the in-situ vertical stresses and where the stress exponent (n) varies with soil type and stress level. When $n=1$, $Q_{tn} = Q_t$ ” (Robertson 2012) (Equation (40)):

$$Q_{tn} = \left(\frac{q_t - \sigma_{v0}}{P_{a2}} \right) \left(\frac{P_a}{\sigma'_{v0}} \right)^n \quad (40)$$

Q_{tn} [-] Normalized cone resistance

P_a [MPa] Atmospheric pressure (100kPa)

P_{a2} [MPa] The reference pressure, in general same as P_a

n [-] Stress exponent

d) Normalized friction ratio F_r [%]

The sleeve friction ratio tends to decrease with the increasing number of fines in the soil. The same tendency is observed with the normalized friction ratio, calculated with Equation (41):

$$F_r = \frac{f_s}{(q_t - \sigma_{v0})} \times 100\% \quad (41)$$

F_r [%] Normalized friction ratio

e) The soil behavior type index I_c [-]

The normalized values are used to estimate the soil behavior type index I_c , as in Equation (42):

$$I_c = ((3.47 - \log Q_t)^2 + (\log F_r + 1.22)^2)^{0.5} \quad (42)$$

I_c [-] Soil behavior type index

The obtained soil behavior type index I_c is a tool to identify the soil type. The Q_t - F_r chart (Figure 27) identifies general trends of ground response, where smaller

numbered zones corresponds the resulting soil behavior index. However, it must be noted that this chart should be used as the guidelines for the soil type estimation. The description of zones are given in Figure 28.

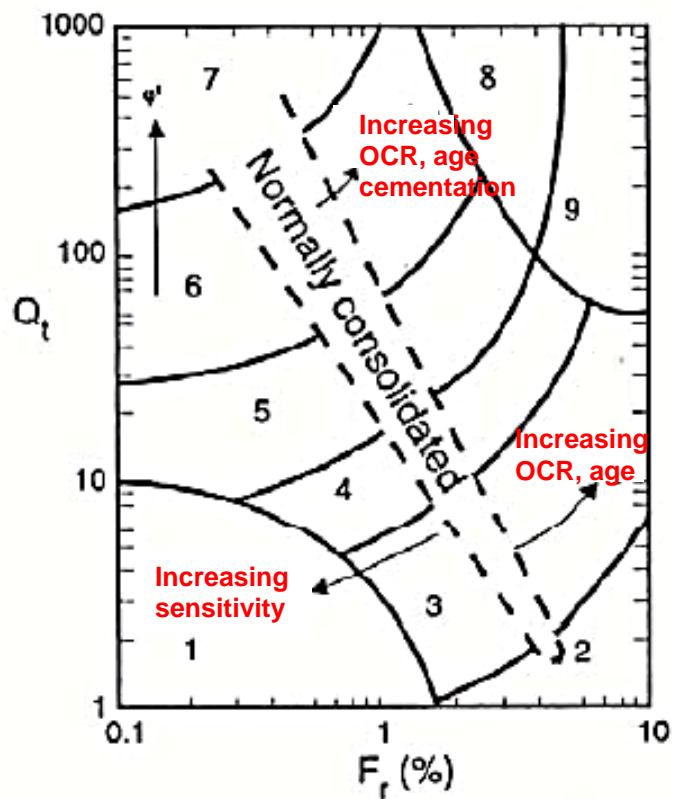


Figure 27 $Q_t - F_r$ chart (Robertson 2006)

Zone	Soil Behavior Type
1	Sensitive fine grained
2	Organic material
3	Clay
4	Silty Clay to clay
5	Clayey silt to silty clay
6	Sandy silt to clayey silt
7	Silty sand to sandy silt
8	Sand to silty sand
9	Sand
10	Gravelly sand to sand
11	Very stiff fine grained*
12	Sand to clayey sand*

* Overconsolidated or cemented

Figure 28 Soil behavior type zones (Robertson 2006)

f) Soil unit weight γ [kN/m³]

The best way to estimate the soil unit weight is obtaining it from the relatively undisturbed sample. However, the subsoil investigation with CPT or CPTu does not provide the soil sample. Robertson (2012) suggests the following correlation (Equation (43)) to estimate the soil unit weight:

$$\frac{\gamma}{\gamma_w} = 0.27[\log R_f] + 0.36 \left[\log \left(\frac{q_t}{P_a} \right) \right] + 1.236 \quad (43)$$

γ [kN/m³] Soil unit weight
 γ_w [kN/m³] Water unit weight

g) Constrained modulus M [MPa]

The general evaluation of the constrained modulus M is based on Equation (44):

$$M = \alpha_M(q_t - \sigma_{v0}) \quad (44)$$

M [MPa] Constrained modulus
 α_M [-] A coefficient which varies with the type of soil

Different correlations of estimation of constrained modulus M are proposed and used for interpretations, such as:

- Meigh (1987): $2 < \alpha_M < 8$;

- Mayne (2001): suggested the general value of 5;
- Robertson (2012): α_M varies with Q_t and I_c as follows:

When $I_c > 2,2$ (fine grained soils):

$$\alpha_M = Q_t, \text{ if } Q_t < 14 \text{ or } \alpha_M = 14, \text{ if } Q_t > 14$$

When $I_c < 2,2$ (coarse - grained soils):

$$\alpha_M = 0.0188 \left[10^{(0.55I_c + 1.688)} \right] \quad (45)$$

Note that the evaluated constrained modulus M is the approximate value. It can be corrected by the qualified geotechnical engineer if necessary.

h) Hydraulic permeability k [m/s]

The dependency of the hydraulic permeability on the soil type is considered in the correlations proposed by Robertson (2012). The hydraulic conductivity is estimated based on the soil behavior type index I_c . The estimated ranges of hydraulic permeability based on the CPT soil behavior type chart (this chart is shown above) are shown in Figure 29.

SBT Zone	SBT	Range of k (m/s)	SBT I_c
1	Sensitive fine-grained	3×10^{-10} to 3×10^{-8}	NA
2	Organic soils - clay	1×10^{-10} to 1×10^{-8}	$I_c > 3.60$
3	Clay	1×10^{-10} to 1×10^{-9}	$2.95 < I_c < 3.60$
4	Silt mixture	3×10^{-9} to 1×10^{-7}	$2.60 < I_c < 2.95$
5	Sand mixture	1×10^{-7} to 1×10^{-3}	$2.05 < I_c < 2.60$
6	Sand	1×10^{-5} to 1×10^{-3}	$1.31 < I_c < 2.05$
7	Dense sand to gravelly sand	1×10^{-3} to 1	$I_c < 1.31$
8	*Very dense/ stiff soil	1×10^{-8} to 1×10^{-3}	NA
9	*Very stiff fine-grained soil	1×10^{-9} to 1×10^{-7}	NA

*Overconsolidated and/or cemented

Figure 29 The ranges of hydraulic permeability based on I_c (Robertson 2012)

According to Robertson (2012), the average relationship between soil permeability and soil behavior type index I_c can be represented by following equations:

- When $1,0 < I_c \leq 3,27$:

$$k = 10^{(0.952-3,04I_c)} \quad (46)$$

k [m/s] Hydraulic permeability

- When $3,27 < I_c < 4,00$:

$$k = 10^{(-4.52-1.37I_c)} \quad (47)$$

“Since the normalized CPT parameters respond to the mechanical behavior of the soil and depend on many soil variables, the suggested relationship between k and I_c is approximate and should only be used as a guide” (Robertson 2012).

Additionally to above described soil parameters, the empirical correlations were proposed to identify following soil parameters:

- Undrained shear strength s_u
- Sensitivity index S_t
- Undrained shear ratio s_u/σ'_{v0}
- Overconsolidation ratio OCR
- In- situ stress ratio K_0
- Relative density D_r
- Friction angle φ'
- Coefficient of consolidation c

The correlations used to estimate all above mentioned soil properties are summarized in the same publication. However, they are not discussed in details in this Thesis, because they were not directly applied to the evaluation of CPTu data, described in chapter 3.5.

All in all, the interpretation of data, obtained with various in this section described in-situ investigation methods, is a tricky part of the project. The general statement of Robertson suggests that the results obtained with empirical correlations should be used only as guidelines. The estimated numbers should be reconsidered and if necessary corrected based on the experience and knowledge of the engineer.

3 Practical part

This second part of the Thesis presents the calculations performed with the data obtained from a construction site, located in North Africa.

The practical part of the Thesis consists of two main tasks: the estimation of consolidation settlement and interpretations of CPTu test data.

The goal of calculations is to estimate the settlement generated by various loading scenarios. Simulations are performed with the software *GGU CONSOLIDATE 5*.

The interpretations of CPTu data involve the development of evaluation methods with spreadsheets, so the taken raw data would provide a set of geotechnical properties derived from the single test.

3.1 Introduction to the Project

It is planned to build on a territory of great dimensions roads and lightweight buildings, however local soils do not possess the suitable bearing capacity. For this reason, to withstand loads, geotechnical properties of soils must be improved.

In order to reduce the construction time, the construction area is divided into smaller zones, which later were allocated to several companies. One of bids has been submitted to GENCO, subsidiary of Keller Grundbau GmbH. Austrian Consultant GDP, in coordination with Keller Grundbau GmbH, is responsible for the development of the ground improvement design concept. The Client has set the requirement for the ground improvement concept- construction of prefabricated vertical drains (PVD) with preloading.

Even though the ground improvement design is developed for the whole zone, foremost it will be tested on the smaller piece within the allocated zone. This test ground is called the Trial field. There is no available data about the Trial field so far. Thus, the ground improvement design is not connected to any selected area, but gives design rules in general.

3.2 Geological conditions

3.2.1 Literature research

The area under development suggests the presence of relative soft, saturated soils of lacustrine and marine origin.

The study area and its environs are occupied by sedimentary rocks of Quaternary age of fluvial and coastal environments.

The stratigraphic succession of the study area is represented by the surface recent sediments which overlie fluvial deposits.

The region overlies a large depression filled with 55 meters of silt and mud, indicating that fluvial branches have been running through the area and that is still obvious in the borehole data. The data indicated that about 50m of recent and relatively soft deposits overlie harder soil.

The fluvial deposits in the study area are defined by two formations of Pleistocene-Holocene age. The Upper unit is the Holocene which is mainly composed of massive soft clays and evaporates that represent shallow marine environment. The Lower unit is the Pleistocene formations which are composed of coarsening upward brown sand and mudstone that represented the shallow delta lobes.

The Holocene formation is as well-known as the Tinh Formation. It underlies about 0,5 – 1m of soft clays and sand with evaporates of Sabkha deposits. It attains about 30 – 40m and composed entirely of soft mud with evaporates and contains shell and shell fragments that indicate its shallow marine origin.

3.2.2 Subsurface investigation campaign

The literature review for this certain region provides only a basic and general overview of geological characteristics. The development of ground improvement requires more factual evidences about the underground status. The geotechnical investigation campaign explored the area with the following geotechnical services:

- Drilling, sampling and in- situ testing of seven onshore boreholes
- Undisturbed sampling of cohesive soils utilizing core barrel and Shelby tubes
- Disturbed sampling of granular soils utilizing core barrel and the Standard Penetration Test (SPT), whenever applicable
- Installation and monitoring of groundwater levels
- Performing seven electrical Cone Penetration (ECPTU) tests
- Labeling, boxing, transportation and examination of selected representative sampled in the laboratory.

The scope of laboratory testing includes:

- Classification of soils
- Grain size distribution analysis
- Atterbergs' limits analysis
- Estimation of unit weight
- Estimation of natural water content
- One dimensional consolidation analysis
- Direct shear test
- Unconfined compression test
- Unconsolidated undrained and consolidated drained triaxial tests
- Chemical analysis of groundwater

However, the results of this complex subsoil investigation are discussed in details in the Thesis, because all further calculations are based on the supplementary subsoil investigation (Investigation-1) performed in a localized area. Figure 30 shows the summary of the received data from the general subsurface investigation campaign.

Layer	Level		Layer thickness [m]	Soil description	OCR	Unit weight [kN/m ³]	PI
	Top	Bottom					
Formation A	0	10	10	Clayey silt/silty clay with sand interlayers, very soft to soft, dark grey, traces of broken shells	1	15-16.5	28-30
Formation B	10	48	38	Silty clay	1	15.5-16.5	30-60; increase with depth
Formation C	48	60	12	Silty clay with interlayers of silty sand(fine, very dense)	-	-	-

Figure 30 Summary of properties obtained with the investigation campaign

The supplementary subsoil investigation (Investigation-1) is discussed within the next sections.

3.3 Development of design

This chapter describes the first results of settlement calculations (named as Preliminary Design), performed with the underground model, which is derived from the data of the subsurface investigation campaign, and the proposed ground improvement design.

The second section of this chapter deals with the localized site investigation (Investigation-1) performed with CPTu tests. The result of this site investigation is the idealized underground model, used in the settlement calculations in section 3.4.

3.3.1 Preliminary Design

The Preliminary Design, as it is suggested by its name, summarizes the first results of settlement calculations, based on the proposed ground improvement strategy with vertical drains and preloading.

3.3.1.1 Underground model

The underground model developed for the Preliminary Design is based on the data, obtained from the subsurface investigation campaign. The obtained data was interpreted and summarized in the way it can be used for calculations. Table 1 shows geotechnical properties used for settlement evaluation in the Preliminary Design.

This summarized subsurface model extends to 50m depth and consists of three major layers. The calculation methodology is developed so, that the only input parameters of soils necessary for settlement evaluation are stiffness modulus E_s , unit weight γ , vertical coefficient of consolidation c_v and Poisson's ratio ν .

Table 1 Input parameters for settlement calculations in Preliminary Design

Depth [m]		Input parameters			
From	to	E_s [MPa]	c_v [m ² /year]	ν [-]	γ [kN/m ³]
0	15	2,00	0,65	0,25	18,00
15	25	2,50	0,65	0,25	18,00
25	50	3,00	1,00	0,25	18,00

3.3.1.2 Loads and loading conditions

In the beginning of the development of the ground improvement concept, the Client expressed interest in building two types of constructions – roads and lightweight structures - with the following loads:

1. For roads

Life loads of up to 30 kN/m². The total design stress for unloading is a sum of the life load and the remaining load from the surcharge.

2. For structures

- Foundation loads :
- For light-weight structures: floor loads 10 kN/m² and 6kN/m² life load; in total 16 kN/m².

The excess preloading with the surcharge lasts 6 months. After 6 months, the surcharge is removed and additionally to the remaining load, the life loads and construction loads must be considered.

3.3.1.3 Requirements for settlement

Since the goal of the preliminary design has been to develop a general scheme for the ground improvement works, the requirements are defined in a general way as follows:

- For total settlements for building areas (structures) a requirement of < 15cm within 50 years has been set by the client.
- For total settlements for road areas (roads) a requirement of < 15cm within 20 years has been set by the client.

At this point the Client has implemented the concept of effective settlement in to the design and requirements. In the case for roads, the effective settlement is a difference between the settlement 20 years after preloading and the settlement monitored at the end of the excess preloading stage.

$$S_{eff\ roads} = S_{20years} - S_{preload} \quad (48)$$

$S_{eff,roads}$ [cm] Effective settlement for roads

$S_{20,years}$ [cm] Settlement 20 years after preloading

$S_{preload}$ [cm] Settlement at the end of preloading stage

In the case for structures, the effective settlement is a difference between the settlement 50 years after preloading and the settlement monitored at the end of the excess preloading stage.

$$S_{eff\ struct} = S_{50years} - S_{preload} \quad (49)$$

$S_{eff,struct}$ [cm] Effective settlement for structures

$S_{50,years}$ [cm] Settlement 50 years after preloading

$S_{preload}$ [cm] Settlement at the end of preloading stage

Maximum differential settlements caused by foundation of columns / structure is limited with 25 mm assuming a 10% criteria within the settlement calculations (final approach to limit the maximum differential settlements to 1/300 for the foundation of columns /structure).

3.3.1.4 Specific considerations set for the design

Besides above described requirements for loading conditions and settlement, further specifications were implemented into the design concept:

- A working platform has to be built by placing fillings (land fill) up to 1 m.a.s.l. in advance (see Figure 32).
- Requirement to reach 2 m.a.s.l. height after consolidation or preloading process. It will be achieved through division of embankment into two parts: the lower permanent part and the upper temporal part, which is called a surcharge and will be removed after the preloading (see Figure 32).
- From the original surface level up to the final surface level (ground level after removal of preloading material and after initial settlements) competent fillings must be placed in layers of maximal 0,5m (e.g. roller compacted layering of sands) in order to ensure competent foundation conditions. The quality of these fillings is essential for the expected differential settlements and it is the governing factor for the bearing capacity of the single footings.
- Vertical drains are going to be installed after the construction of the working platform is completed (see Figure 32).

3.3.1.5 Specific considerations for settlement evaluation

Further considerations are adopted for settlement prediction by the Consultant:

- The grid of vertical drains is kept constant for both roads and structures, because the exact locations of roads and structures are not specified.
- Calculations performed with the assumption of perfect drains: smear effect and well resistance is not considered in the preliminary design.
- Settlement estimation carried out under the assumption that beneath the investigated soil layers a soil of very low permeability is situated.

- The assumption of equivalent vertical permeability based on CUR 191 (1997) methodology is implemented in the calculations for the layer with vertical drains (see section 2.3.4).
- During the whole duration of the field investigation program, the measurements of stand – pipe piezometers in two ground water observation boreholes were taken. The water table measured from the existing ground level varies within the range of 1,3 – 1,9m. However, for design purposes the groundwater level is assigned to be at the sea level.

3.3.1.6 Ground improvement design proposed by the Consultant

The developed ground improvement design is going to be tested in the trial field and its accuracy will be evaluated based on the recorded settlement.

1. Solution for design of vertical drains

Triangle grid for vertical drains is chosen because of the higher efficiency compared to the square grid. The constant distance of 1,50m between drain centers for roads and structures is estimated.

The 50m thick underground model is divided into two parts: in the upper part the length of vertical drains matches the thickness of the layer (25m); the lower part of the underground model without vertical drains is 25m thick. In this lower part the drainage path of the ground water corresponds to the thickness of this layer (25m), because this layer is assumed to have an undrained bottom boundary. The diameter of single drain is chosen as 0,05m (supplementary results of settlement calculations with the effective drain diameter are shown in Table 17, section 3.4.5).

2. Solution for embankment design

In the ground improvement design proposed by the Consultant two types of embankments are planned. Each embankment consists of three parts (described from the bottom to the top, repeats the construction sequence):

- **Working platform**

This working platform is a layer made of draining granular material and placed on the construction site, so rigs have an access to the site. As well, this working platform build of granular material functions as a drainage layer underneath the constructed embankment for the ground water which reaches the ground surface through vertical drains.

- **Filling “wet“**

This part should cover the generated settlement. In the settlement calculation the ground water level is prescribed to be at the sea level and the filling is considered to be in constant contact with water, because at the end of the preloading stage it sinks underneath the water. Therefore, the effective unit weight of filling is used in calculations.

- **Filling**

This is the part which after the removal of surcharge and consolidation will be used as a 2m height building platform, required by the Client.

- **Surcharge**

This is the part of the embankment which is removed after 6 months, when the preloading stage is finished.

A sketch in Figure 31 visualizes the arrangement of layer without dimensions.

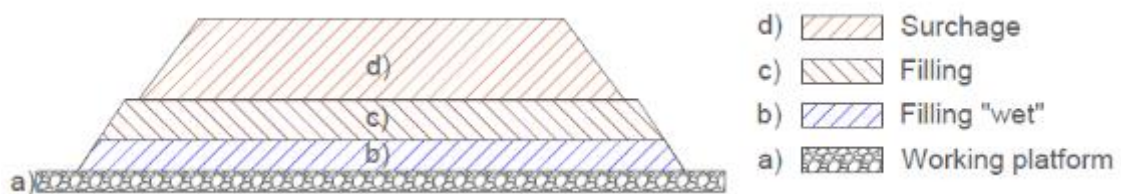


Figure 31 Sketch of typical embankment design developed for the Project

Construction process of embankment consists of following steps and is depicted in Figure 32.

1. A working platform is build.
2. Installation of vertical drains
3. Placement of "wet" filling.
4. Placement of filling.
5. Placement of surcharge.
6. After surcharge is placed, the apparent period of consolidation, important for evaluation of settlement, starts. After 6 months the surcharge is removed. Two lower layer of embankments serve further their design purposes.

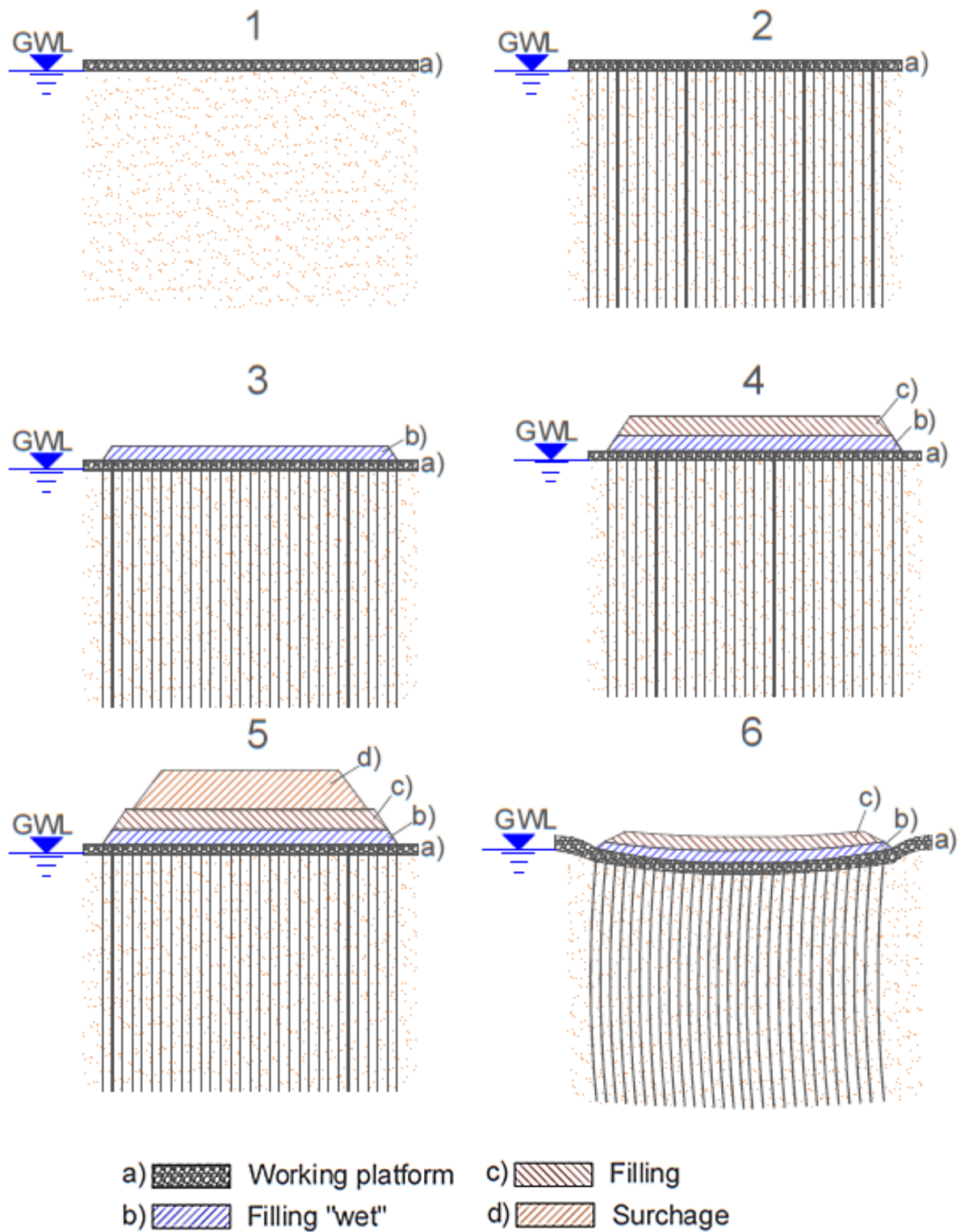


Figure 32 Construction process of embankment with vertical drains

Loads generated by embankments are summarized in Table 2.

Table 2 Loads generated by embankments for roads and structures

	Specific unit weight [kN/m ³]	Roads		Structures	
		h [m]	Stress [kN/m ²]	h [m]	Stress [kN/m ²]
Filling “wet“	10	1,00	10	1.50	15
Filling	20	2,00	40	2,00	40
Surcharge	18	2,5	45	4,00	72
Total preloading			95		127

The calculated preloading is higher than the sum of remaining loads (filling “wet” + filling + life loads), thus this method should be called the excess preloading.

The monitoring program for the Trial field is as well foreseen in the Preliminary Design. Four reference points are going to be installed in the corners of the square, where the embankment is constructed. 21 ground measurement points are planned to be installed at the ground surface. The displacements of the embankment are going to be monitored with two inclinometers and two extensometers. The data for generated pore water pressure is collected with two wire piezometers.

3.3.1.7 Results of Preliminary Design

Settlement evaluation in the Preliminary Design is performed with the previously described underground model (Table 1) and two types of excess preloading (Table 2). The stresses in soils are generated by embankments with the base area of 1.000.000m² (1000m x 1000m).

After the series of optimizations, the length of vertical drains was estimated and set to 25m. It is agreed that in the lower 25m thick part of the underground model the length of the drainage path corresponds to the thickness of this part. With the excess preloading as described in the previous section and the 25m long vertical drains the following effective settlements were calculated:

- For roads: with 0kN/m² life load 5,8cm; with 10kN/m² life load 7.5cm; with 20kN/m² life load 14,2cm and with 30kN/m² life load 27,4cm;

- For structures: with 16kN/m² life load 15,1cm.

It can be stated that based on the calculations with methods, approved in the Preliminary Design, only with the life load of 30kN/m² the requirement for the effective settlement is not fulfilled.

3.3.2 Investigation-1

Investigation-1 is the localized site investigation, performed in the reduced area within the whole are of great extent. It consists of 8 CPTu tests. The approximate location of the investigated area and the layout of piezocone tests is sketched in Figure 33. The average distance between two CPTu tests is 250m. Due to the confidentiality of the Project, only data about the top levels and depth of tests is provided in Figure 34. Note that the depth of the each of the performed CPTu test is given from the actual ground surface and in reality none of performed tests have reached the 50m.b.s.l. depth.

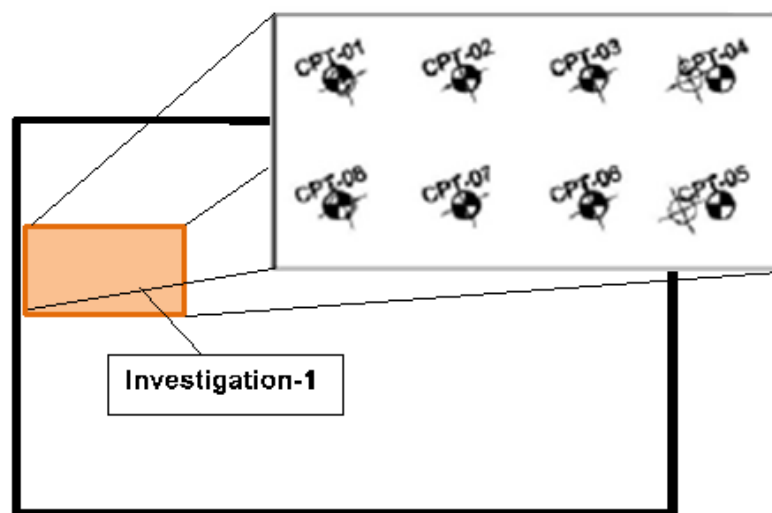


Figure 33 Layout of piezocone tests

CPT No.	Top Level	Depth (m)
CPTu-1	1.428	50.50
CPTu-2	1.155	50.58
CPTu-3	1.034	50.50
CPTu-4	1.024	50.56
CPTu-5	1.373	50.48
CPTu-6	1.065	50.52
CPTu-7	1.499	50.62
CPTu-8	1.256	50.52

Figure 34 Data about performed piezocone tests

For improved estimation, pore pressure dissipation tests should be performed additionally to piezocone tests. For each CPTu four dissipation tests were performed at different depths with a step of approximately 10m between each dissipation test. It sums up as 32 dissipation tests in total. Data from pore pressure dissipation tests is used to get an enhanced value of hydraulic conductivity and coefficient of consolidation.

The CPTu data was interpreted using CPeT-IT software and reviewed by the geotechnical engineer. The output of this site investigation is the idealized underground model, which is a result of performed piezocone tests. This model is shown in Figure 35.

Soil	Layer	Level		Layer thickness [m]	Unit weight [kN/m ³]	OCR	Constrained modulus <i>M</i> [MPa]		Time settlement parameters			
		Top	Bottom				<i>c_h</i> [m ² /s]	<i>c_v</i> [m ² /s]	<i>k_h</i> [m/s]	<i>k_v</i> [m/s]		
Silty clay/clayey silt with sand interlayers	1-A	0	10	10	16	2.25	5	3.22 E-7	3.22 E-8	3.22 E-9	3.22 E-10	
	1-B	10	15	5	16	1.1-1.2	2.5 3.5					
Silty clay	Formation B	15	50	35	17	1.1-1.2	3.5 6.5	9.66 E-8	3.22 E-8	2.41 E-10	8.04 E-11	

Figure 35 Idealized underground model

Compared to the underground model, used for settlement evaluation in the Preliminary Design Report, this new model has two clearly defined formations, with respect to prescribed soil types and the hydraulic conductivity. The upper formation of silty clay/clayey silt with interlayers of sand is 15m thick and can be further divided into two thinner layers: 1-A with constant 5,0MPa stiffness and 1-B with constantly increasing stiffness from 2,5 MPa to 3,0 MPa. Respectively, the first layer is 10m thick; the second is 5m thick. For the second formation of silty clay the increasing stiffness from 3,0 MPa to 6,5MPa is prescribed. According to the current report, the light overconsolidation is exhibited in both upper and lower formations.

The final values of stiffness for this idealized underground model are defined from two types of plotted constrained modulus curves: one estimated with the soil behavior type index I_c and another estimated with the coefficient α . The evaluated values of constrained modulus M for eight CPTu tests are summarized as the plot of data points in Figure 36 and Figure 37.

The results show that the average stiffness estimated with the factor I_c in the upper 10m thick layer is considered as 7,5 MPa. Below this depth, the constrained modulus increases gradually from 2,5 MPa to 5,0 MPa at depth of 50m. The 50m depth mentioned in the report is measured from the local ground level. The evaluation of tests with respect to the sea level shows that none of the executed tests have reached this level. The plot is provided in Figure 36.

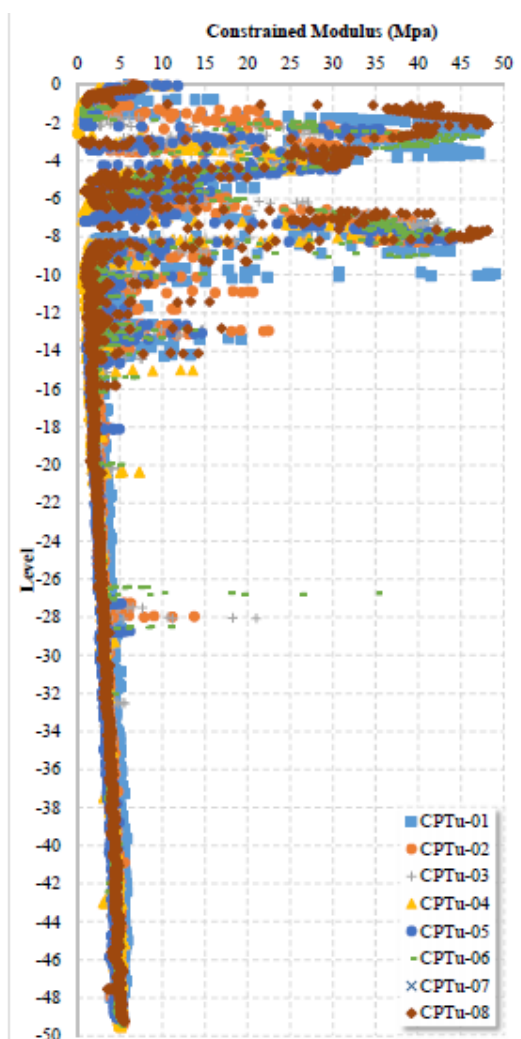


Figure 36 Variations of constrained modulus M values versus depth for the executed eight CPTu considering factor I_c

The report provides the second interpretation of constrained modulus M with the factor $\alpha = 6$. The graph as it is given in the report here is provided as Figure 37. Based on Figure 37, the constrained modulus for the upper 15m can be considered as 5,0 MPa.

Below this depth the modulus gradually increases from 2,5 MPa to 8.0 MPa at the depth close to 50m.

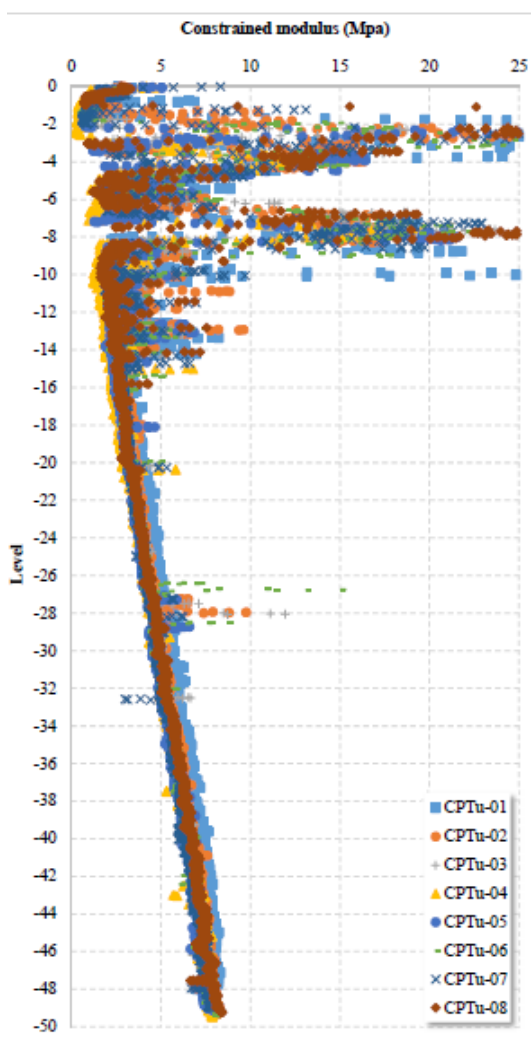


Figure 37 Variations of constrained modulus M values versus depth for the executed eight CPTu considering factor $\alpha=6$

For the resulting idealized model (Figure 35), the stiffness profile in the upper Formation A is entirely obtained from the evaluation with the coefficient $\alpha = 6$. The stiffness profile in the Formation B is obtained when the two of the above described stiffness evaluation methods were combined and this resulting profile is equal to the average value.

The horizontal coefficient of permeability for both soft formations is evaluated from dissipation tests. It varies from 0,1m/year in the upper formation to 0,0075m/year in the

lower formation, and according to Robertson (2012) soils of low permeability are indicated.

In general, the horizontal coefficient of permeability in soils is higher than the vertical permeability. In the current report the evaluation of the ratio between the vertical and horizontal coefficients of permeability is based on guidelines from FHWA RD-86/168. Representative ratios for soft clays are presented in Figure 38.

	k_h/k_v
1. No evidence of layering (Partially dried clay has completely uniform appearance)**	1.2 _{-0.2}
No or only slightly developed macrofabric (e.g. sedimentary clays with discontinuous lenses and layers of more permeable soil)***	1 to 1.5
2. Slight layering (e.g. sedimentary clays with occasional silt dustings to random silty lenses)**	2 to 5
Fairly well to well developed macrofabric (e.g. sedimentary clays with discontinuous lenses and layers of more permeable material)***	2 to 4
3. Varved clays in Northeastern US **	10 ₋₅
Varved clays and other deposits containing embedded and more or less continuous permeable layers***	3 to 15

Figure 38 Guidelines from FHWA RD-86/168

As the upper formation contains many continuous permeable sand lenses between clayey silt/ silty clay layers, category 3 is applied. The ratio between horizontal and vertical permeability is taken conservative as 10. For the lower formation category 2 is applied and ratio of 3 is chosen as a conservative evaluation. The same ratios are applied for estimation of vertical coefficient of consolidation.

Overall, the underground model obtained from the Investigation-1 indicates the presence of slightly stiffer soils, which are divided into two formations, based on the evaluated inhomogeneity and hydraulic conductivity.

3.4 Settlement calculation with the idealized subsoil model

This chapter compiles five smaller sections: the first is dedicated to general design considerations, used in the evaluation of settlements; the second describes the modelling procedure and the third summarizes the calculation results; the settlement results provided in the fourth section are obtained from calculations with modified drainage conditions; the last, fifth, section gives the comparison of settlement, obtained from calculations with two different drainage conditions.

3.4.1 General design considerations

3.4.1.1 Requirements for the ground improvement concept and effective settlement

The ground improvement concept and settlement requirements for roads and structures are adopted from the Preliminary Design without additional modifications.

Despite the initial agreement, this requirement might be reconsidered after results from the Trial field are obtained or the additional ground investigation reveals new data about geotechnical properties.

3.4.1.2 Loads and loading conditions

Originally approved loading conditions have undergone minor modifications. Differently than in the Preliminary Design, the total end loading generated by the remaining surcharge and various life load occurs 9 months after the completion of surcharge. The excess preloading with the surcharge still lasts 6 months, as defined in the Preliminary Design. Two quantifications of applied loads due to the embankment and various life loads are depicted in Figure 39 for roads and Figure 40 for structures.

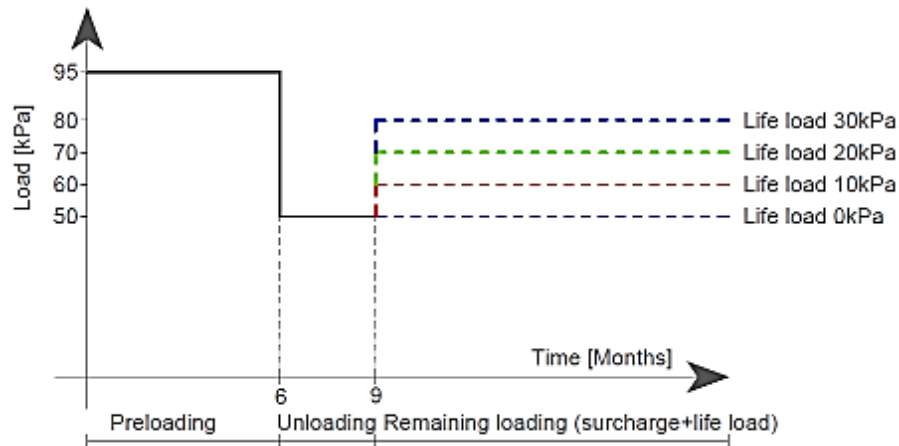


Figure 39 Loading scenario for roads

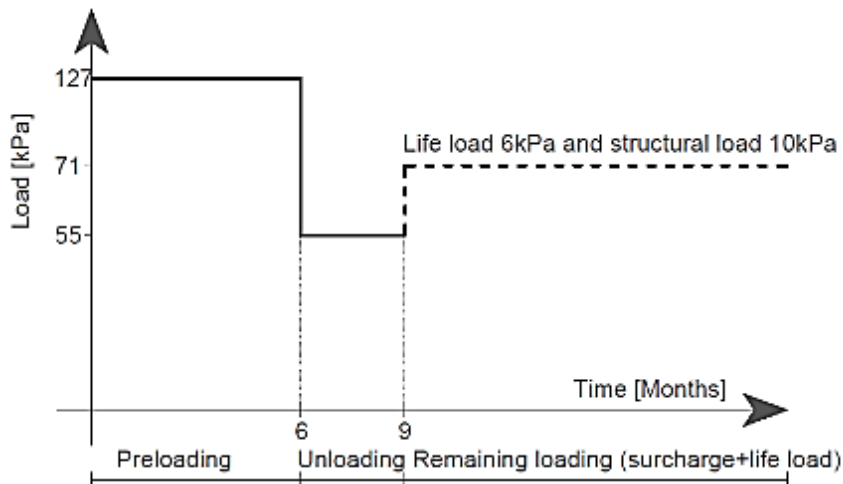


Figure 40 Loading scenario for structures

3.4.2 Modelling with the software *GGU CONSOLIDATE 5*

3.4.2.1 General switches

Settlement evaluation is performed via combination of constrained modulus and permeability. The coefficient of consolidation c_v is automatically calculated by the software from the constrained modulus E_s and permeability k .

Secondary settlements are not considered in the calculations in this Thesis. However, it is recommended to incorporate the calculations of secondary settlements for the future calculations (outside this Thesis) as a safety measure.

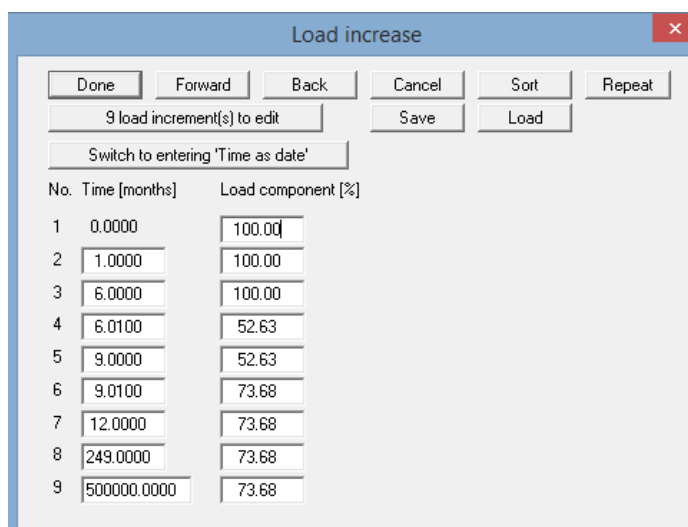
The numerical solution is chosen for simulations (see 2.3.1), because it allows the use of multi-layered system, load increase, implementation of vertical drains through the equivalent permeability and arbitrary pore water pressure distribution.

3.4.2.2 Loading conditions in the software

Even though the application of continuously increasing or decreasing loading due to the construction process can be considered in simulations with the software, in the used loading model the progressive decrease caused by the gradual removal of the surcharge between 6 and 9 months is neglected. Loads in all construction stages are applied instantaneously.

The initial loading, unloading and reloading are applied instantaneously instead of the gradually increasing/decreasing loading. It is considered as a conservative approach, because the scheme how the surcharge is going to be dismantled and when exactly the next construction phase starts is not approved.

The decrease of loading in the software is expressed as a percentage of the initially applied loading. Figure 41 shows how this change of loading is applied in the software with respect to time for the case with 20kPa for roads.



No.	Time [months]	Load component [%]
1	0.0000	100.00
2	1.0000	100.00
3	6.0000	100.00
4	6.0100	52.63
5	9.0000	52.63
6	9.0100	73.68
7	12.0000	73.68
8	249.0000	73.68
9	500000.0000	73.68

Figure 41 Applied loading for roads with 20kPa life load

Table 3 shows the loading is converted into percent and implemented into calculations.

Table 3 Load increase expressed in percent's for each simulation case

Life load	Roads				Structures
	With 0kN/m ²	With 10kN/m ²	With 20kN/m ²	With 30kN/m ²	With 16kN/m ²
0 - 6 months	100% 95kN/m ²	100% 95kN/m ²	100% 95kN/m ²	100% 95kN/m ²	100% 127kN/m ²
6 – 9 months	52.63% 50kN/m ²	52.63% 50kN/m ²	52.63% 50kN/m ²	52.63% 50kN/m ²	43.31% 55kN/m ²
From 9 months	52.63% 50kN/m ²	63.16% 60kN/m ²	73.68% 70kN/m ²	84.21% 80kN/m ²	55.91% 71kN/m ²

The initial loading curve is generated with ``Stresses due to foundation`` function. This function automatically generates the stress curve in the middle of the applied imaginary foundation, based on its geometry.

3.4.2.3 Idealized subsurface model

The modelled multi-layer underground consists in total of 11 layers. Based on the idealized underground model from section 3.3.2, the developed model is adapted to simulations by prescribed intermediate values of stiffness. The sketch of the underground model with 11 layers and stiffness values for each of these 11 layers used in further calculations is presented as Figure 42.

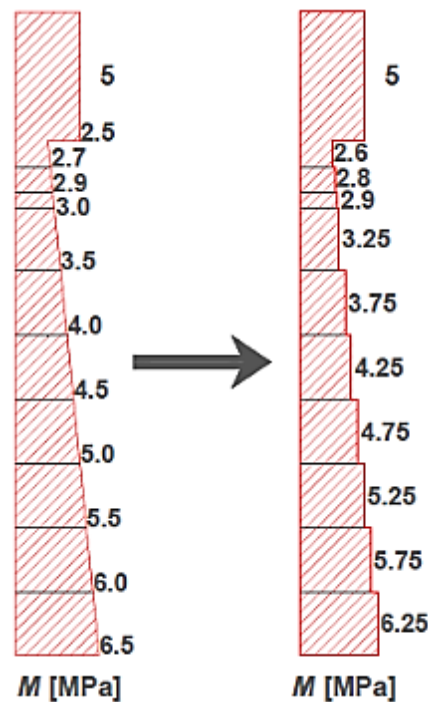


Figure 42 Underground model with 11 layers

Thus, the unloading – reloading stiffness in the software is evaluated through the defined ratio E_{ur}/E . The ratio $E_{ur}/E = 3$ is used in simulations as the most practice – oriented value.

The hydraulic conductivity in the Formation A is reevaluated in order to comply with the limitations, caused by the implementation of the CUR 191 (1997) approach. Designed vertical drains cross layers with variable vertical and horizontal hydraulic conductivity. However, in the CUR 191 (1997) approach the recalculated equivalent permeability is prescribed for the whole layer with drains, because the length of a single drain is used in the equation. Thus, the lower value of horizontal hydraulic conductivity from the Formation B is applied for the whole layer with drains as the conservative approach. A separate Excel spreadsheet is programmed to reevaluate permeability parameters for the part of subsurface model with vertical drains. The same diameter of drains ($a_{dw} = 0.05\text{m}^2$) is used in simulations as in the Preliminary Design.

Classical (numerical) consolidation switch (see 2.3.1) is used, because the presence of drains is prescribed through the recalculated equivalent vertical permeability with CUR 191 (1997).

Note that even though none of eight performed CPTu tests have reached the depth of 50m.b.s.l, for calculations the thickness of 50m is assigned for the model. At this point the undrained bottom boundary was assigned for the model under the assumption that the Formation B made of low permeable silty clay extends below 50m.b.s.l.

As well, the closed (undrained) bottom bound corresponds to the previously approved 25m drainage path in the layer without drains.

The idealized underground model with the closed bottom bound as it looks in the software is depicted in Figure 43.

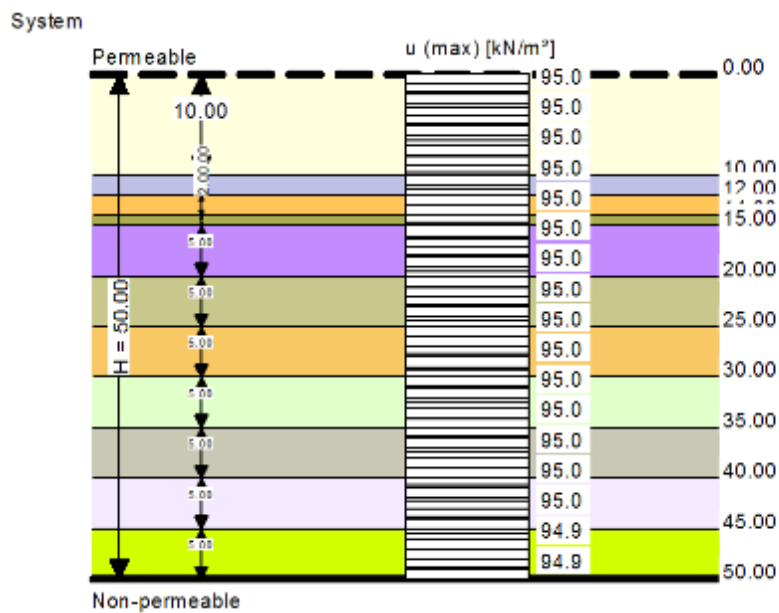
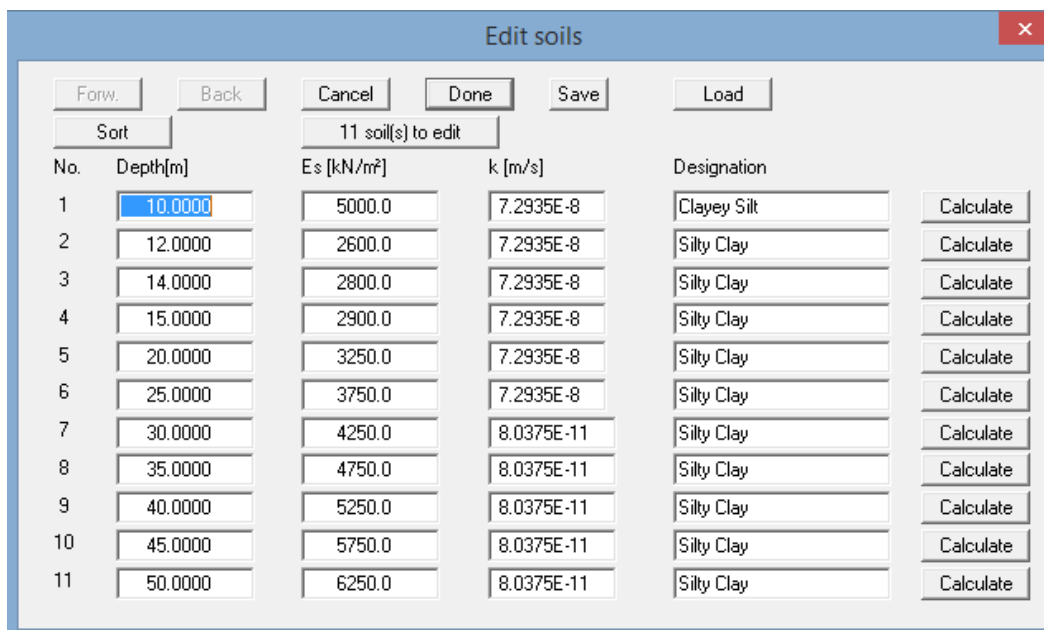


Figure 43 Idealized underground model

The screenshot with the input soil parameters for the idealized underground model is shown in Figure 44.



The screenshot shows the 'Edit soils' window with the following data:

No.	Depth[m]	Es [kN/m ²]	k [m/s]	Designation	Calculate
1	10.0000	5000.0	7.2935E-8	Clayey Silt	Calculate
2	12.0000	2600.0	7.2935E-8	Silty Clay	Calculate
3	14.0000	2800.0	7.2935E-8	Silty Clay	Calculate
4	15.0000	2900.0	7.2935E-8	Silty Clay	Calculate
5	20.0000	3250.0	7.2935E-8	Silty Clay	Calculate
6	25.0000	3750.0	7.2935E-8	Silty Clay	Calculate
7	30.0000	4250.0	8.0375E-11	Silty Clay	Calculate
8	35.0000	4750.0	8.0375E-11	Silty Clay	Calculate
9	40.0000	5250.0	8.0375E-11	Silty Clay	Calculate
10	45.0000	5750.0	8.0375E-11	Silty Clay	Calculate
11	50.0000	6250.0	8.0375E-11	Silty Clay	Calculate

Figure 44 Input option in the software

3.4.3 Predicted settlement

This section is dedicated to the summarized settlement from simulations. Data is submitted in tables and later compared in charts. The second column in each table shows the final settlement ($s_{50,50000}$), when consolidation process is completed. Settlement ratio after 6, 9, 249 months (corresponds to 20 years after the end of excess preloading, therefore 9months + 240months = 249months) or 609 months (corresponds to 50 years after the end of excess preloading, therefore 9months + 600months = 609months) is given with the corresponding degree of consolidation U . Note that 9 months are the sum of 6 months of preloading and 3 months of unloading (manipulation).

All output of calculations as it is given in the software is attached to this Thesis in Appendix A.

The results are summarized in Table 4 - Table 8. The data in these tables is presented in the same style. Note that in these tables:

- In the most upper road the loading conditions are summarized as **XX/XX/XX**. The first number corresponds the applied excess preloading for the first six months; the second number corresponds to the remaining loading in the period between 6 and 9

months, when the surcharge is removed; the last number corresponds the sum of remaining and life loads.

- Calculated settlement and the degree of consolidation in these tables are denoted as **s** and **U**. These abbreviations are given with two indices, where the first index correspond to the case with the sum of applied life and remaining load (for roads case with 0kN/m² corresponds to 50, 10kN/m² corresponds to 60, 20kN/m² corresponds to 70 and 30kN/m² to corresponds 80) and the second index indicates the time in months, when the settlement is calculated. For example, the **s_{50,9}** corresponds the settlement calculated for the case with 0kN/m² life load estimated 249 months after the beginning of calculations. The settlement calculated 50000 months after the beginning of consolidation corresponds to the final settlement generated with applied loading.
- The total settlement calculated for the 50m model after 6, 9, 249 or 609 and 50000 months is shown in the last row of each table. Additionally, it was investigated how many settlement is generated at the certain time in the upper part of the model with PVD (25m thick) and in the lower part without vertical drains (as well 25m thick, see specifications in section 3.4.2.3).
- The degree of consolidation for each case is calculated with respect to the generated final settlement due to the applied life load.

3.4.3.1 Roads

Results of simulations for roads with four different life loads are summarized in Table 4, Table 5, Table 6 and Table 7.

Table 4 Evaluated settlement ratio for roads with 0kN/m² life load

	95/50/50						
	S_{50,50000} [cm]	S_{50,6} [cm]	U_{50,6} [%]	S_{50,9} [cm]	U_{50,9} [%]	S_{50,249} [cm]	U_{50,249} [%]
Upper part with PVD	45,8	51,5	112,45	47,7	104,15	45,7	100
Lower part	24,3	1,0	4,12	1,4	5,76	6,3	26
Σ	70,1	52,5		49,1		52,0	

Table 5 Evaluated settlement ratio for roads with 10kN/m² life load

	95/50/60						
	S _{60,50000} [cm]	S _{60,6} [cm]	U _{60,6} [%]	S _{60,9} [cm]	U _{60,9} [%]	S _{60,249} [cm]	U _{60,249} [%]
Upper part with PVD	47,9	51,5	107,52	47,7	99,58	47,9	100
Lower part	29,2	1,0	3,42	1,4	4,79	7,5	26
Σ	77,1	52,5		49,1		55,4	

Table 6 Evaluated settlement ratio for roads with 20kN/m² life load

	95/50/70						
	S _{70,50000} [cm]	S _{70,6} [cm]	U _{70,6} [%]	S _{70,9} [cm]	U _{70,9} [%]	S _{70,249} [cm]	U _{70,249} [%]
Upper part with PVD	50,2	51,5	102,59	47,7	95,2	50,2	100
Lower part	33,9	1,0	2,95	1,4	4,13	8,6	26
Σ	84,1	52,5		49,1		58,8	

Table 7 Evaluated settlement ratio for roads with 30kN/m² life load

	95/50/80						
	S _{80,50000} [cm]	S _{80,6} [cm]	U _{80,6} [%]	S _{80,9} [cm]	U _{80,9} [%]	S _{80,249} [cm]	U _{80,249} [%]
Upper part with PVD	54,4	5,5	94,58	47,7	87,60	54,4	100
Lower part	38,9	1,0	2,57	1,4	3,60	9,9	25
Σ	93,3	52,5		49,1		64,30	

As it can be seen from the tables above, generated settlement between 9 and 249 months after the beginning of preloading stage ($s_{xx,249} - s_{xx,9}$) in the lower part is 3 to 5 times higher (it depends on the loading) than in the upper part with PVD. Only for the case with 30 kN/m² life load the settlement generated in the lower part in this period of time is almost equal to the settlement generated in the upper part with PVD. As well, it

can be seen from tables above that after 249 months the consolidation in the upper part with PVD is completed (degree of consolidation $U = 100\%$). In all four cases after the removal of the surcharge (it corresponds to the time period of 6 months), the volume of soils increases due to the unloading and following the settlement rate decreases (see columns in tables with the index "9"). Then, depending on the applied life load, within the next 240 months the soil undergoes further deformations (see columns in table with the index "249"). It is obvious from these tables that the higher applied life load leads to higher settlements after 249 months and after 50000 months, what corresponds the final settlement.

However, in the case with 0kN/m^2 life load the increase of soil volume – heave – continues in the period between 9 and 249 months (settlement decreases from 47,7 to 45,7cm).

Four figures below (Figure 45, Figure 46, Figure 47, Figure 48) provide an overview for each of the four cases with different life loads.

The following plots show that the expected log time – settlement curve (blue) fits between two curves: the green curve which indicates the expected settlement generated only by the load applied in the reloading stage and the red curve which indicates the expected settlements if the preloading was never removed.

Note that curves with the constant loading (50/50/50, 60/60/60, 70/70/70, 80/80/80 and 95/95/95) should not show two bendings. Log time – settlement curves due to the constant loading should indicate a smooth, constant increase of settlement (see line 2-2b in Figure 13). However, the reason why the software provides these curves was not defined (the following reasons were checked: input data, the way how time series were generated (linear, quadratic, exponential, etc.), loading conditions). The presence of two bends may be caused by the multiple layers, implemented in to the calculation model.

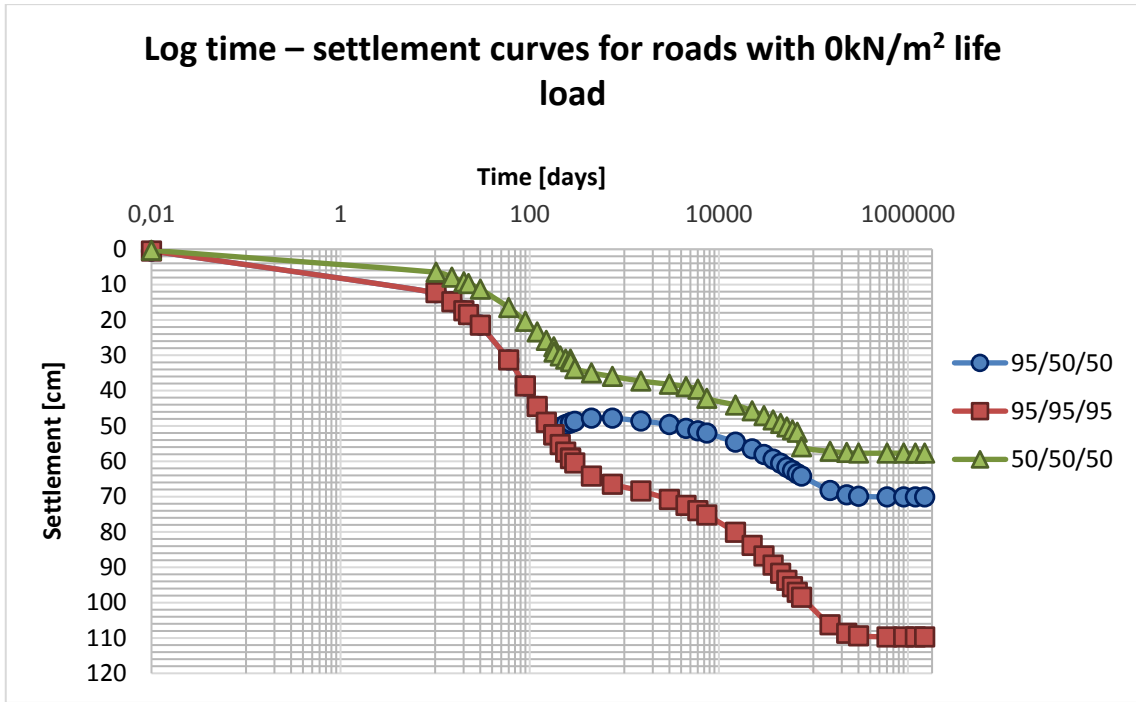


Figure 45 Log time – settlement curves for roads with 0kN/m² life load

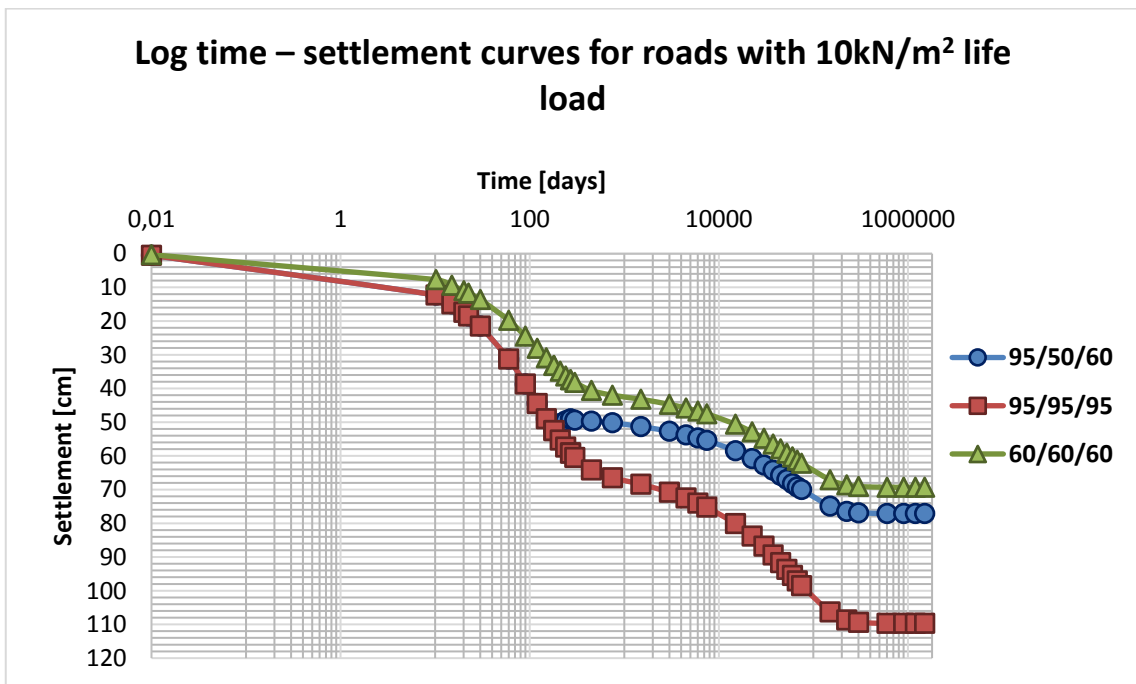
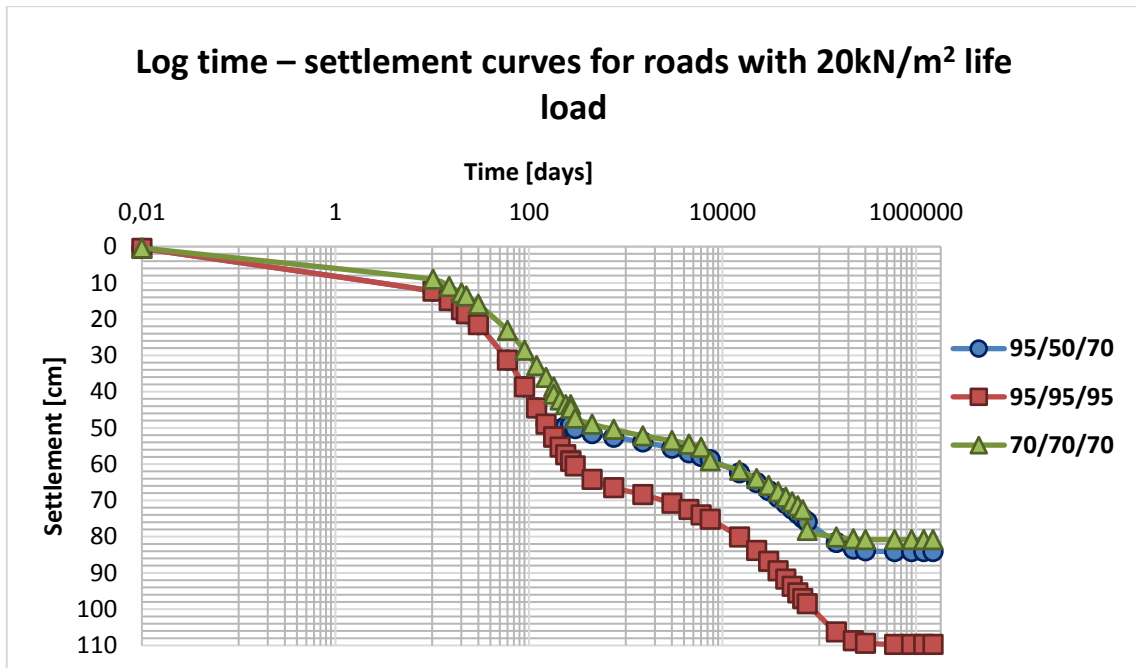
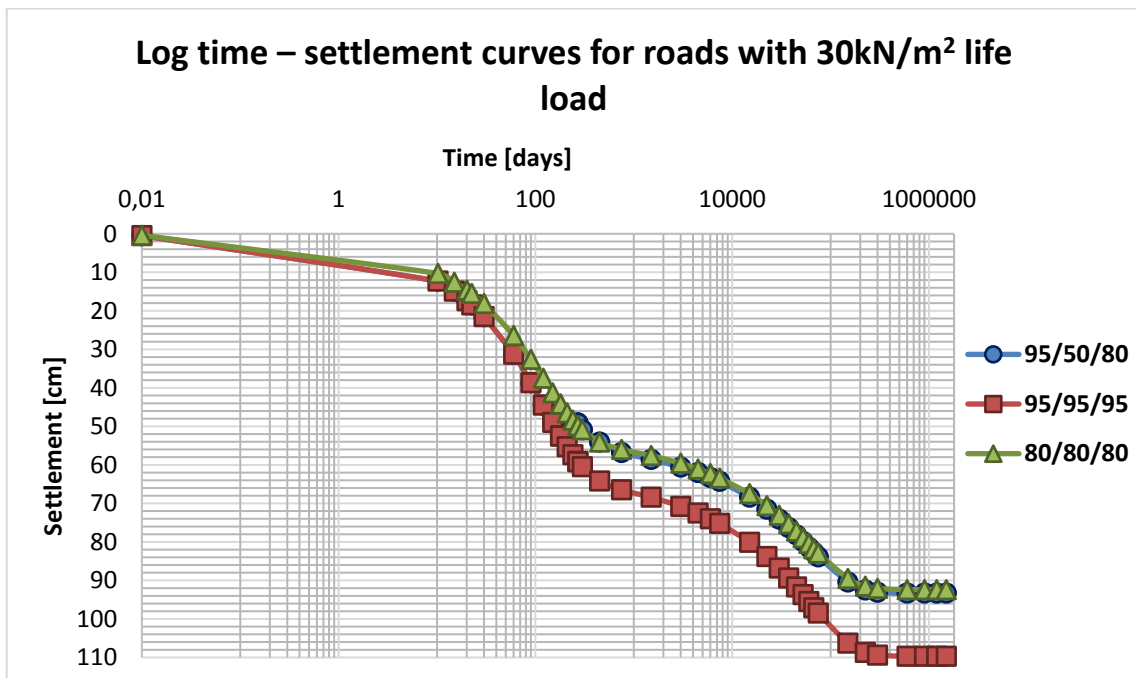


Figure 46 Log time – settlement curves for roads with 10kN/m² life load

Figure 47 Log time – settlement curves for roads with 20kN/m² life loadFigure 48 Log time – settlement curves for roads with 30kN/m² life load

It was expected that within the first 9 months all four log time – settlement curves indicates identical settlement, because loading conditions starts to differ only after the 9 months mark (see section 3.4.1.2). Independently from the settlement within the first 9

months, the end settlement after 50000 months must increase with the increase of loading. Following expectations are proved and presented in Figure 49.

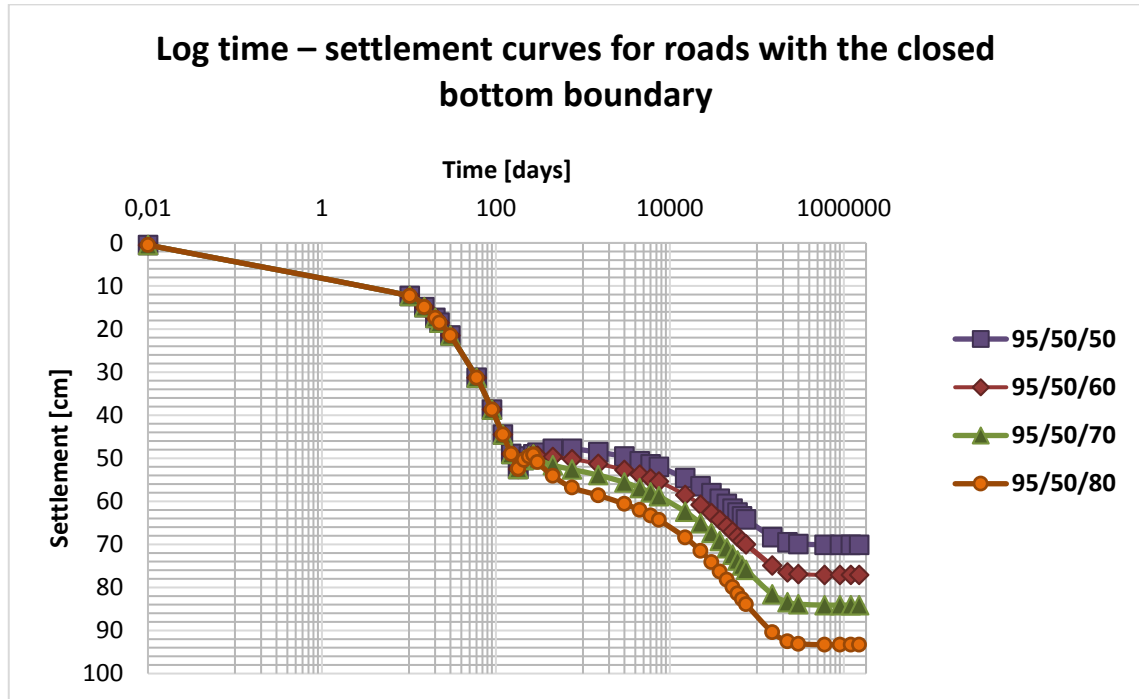


Figure 49 The variations of log time – settlement curves for all four life load for roads

3.4.3.2 Structures

The resulting settlement for structures is summarized in Table 8.

Table 8 Evaluated settlement ratio for structures with 16kN/m² life and constructional load

	127/55/71						
	S _{71,50000} [cm]	S _{71,6} [cm]	U _{71,6} [%]	S _{71,9} [cm]	U _{71,9} [%]	S _{70,609} [cm]	U _{71,609} [%]
Upper part with PVD	62,0	68,9	111,13	62,1	100,16	62,0	100,00
Lower part	34,5	1,3	3,77	1,8	5,22	13,8	40,00
Σ	96,5	70,2		63,9		75,8	

In this case in the time period between 9 and 609 months the upper part with PVD indicates close to the same value. However, it must be taken into account that the calculations are performed without consideration of the secondary settlement (or creep) and in reality, the additional settlement due to the constant loading may occur in the upper part.

The log time – settlement plot for the case with structures is given in Figure 50. The following plot shows that the expected log time – settlement curve (blue) fits between two curves: the green curve which indicates the expected settlement generated only by the load applied in the reloading stage and the red curve which indicates the expected settlements if the preloading was never removed.

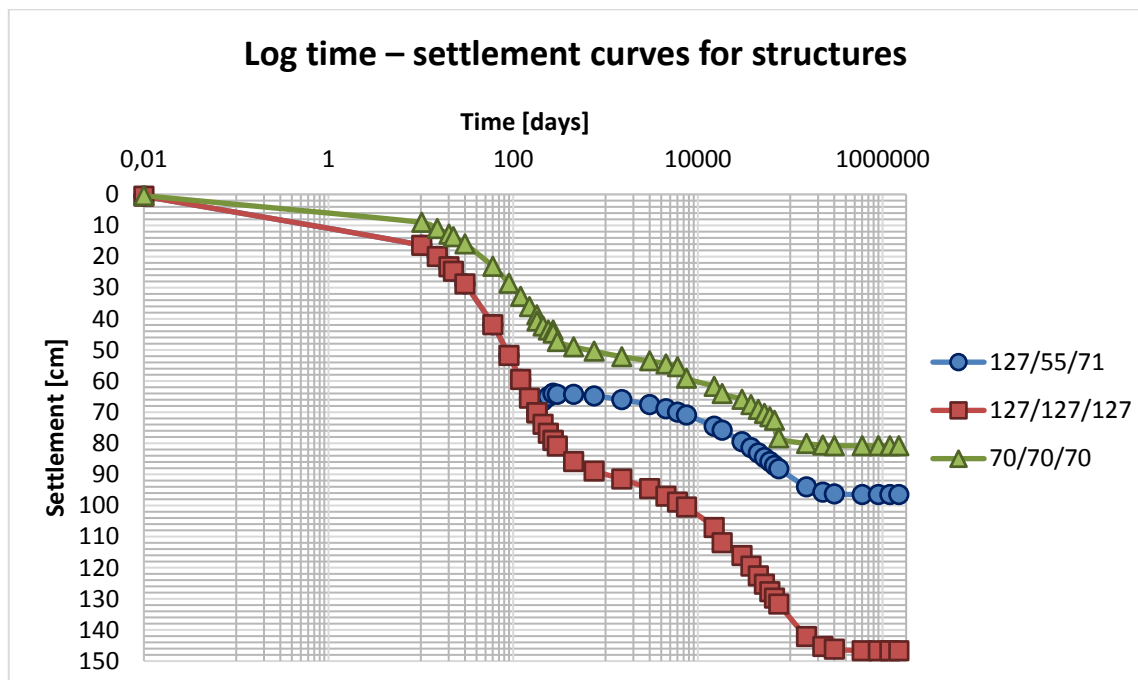


Figure 50 Log time – settlement curve for structures

3.4.3.3 Effective settlement

The requirement to keep the resulting effective settlement 20 years after preloading for roads and 50 years after preloading for structures below the 15cm limit is given by the Client. The explanation of the effective settlement concept and corresponding equations are given in the section 3.3.1.3.

Resulting effective settlement are summarized in Table 9. The effective settlement in Table 9 is calculated for the upper part with PVD, the lower part and as the sum of both parts (denoted as Σ in the table). The graphical comparison of resulting effective settlements for the whole 50m thick model is given in Figure 51.

Table 9 Summarized effective settlement

	Roads				Structures
	0 kN/m ²	10 kN/m ²	20 kN/m ²	30 kN/m ²	16 kN/m ²
Upper part with PVD	-2	0,2	2,5	6,8	-0,1
Lower part	4,9	6,1	7,2	8,4	12
Σ	2,9	6,3	9,7	15,2	11,9

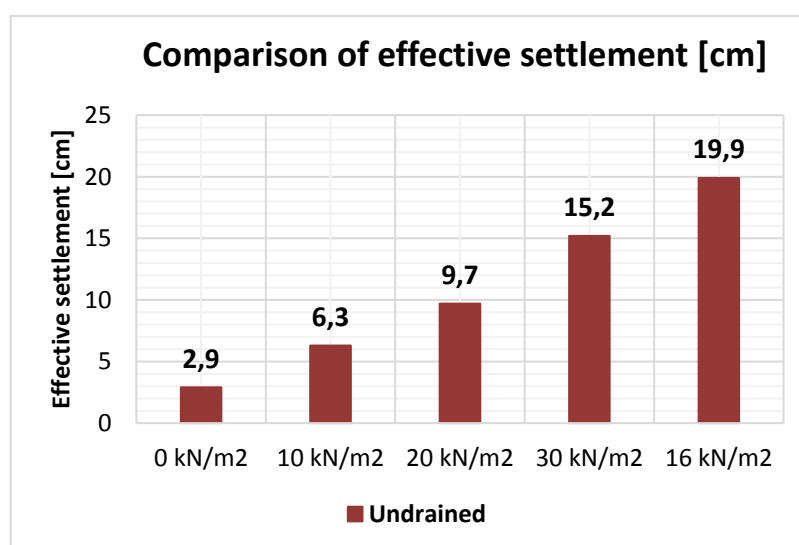


Figure 51 Resulting effective settlement for roads and structures

The summary of settlement calculations show in general a very good agreement with the requirement: only the case with 30kN/m² life load exceeds the required 15cm limit. Although, the evaluated settlement should be considered as conservative (these should be treated as recommendations) values.

3.4.4 Settlement with the drained bottom boundary

The idealized underground model used in calculations is estimated up to the 50m.b.s.l.depth with the 25m drainage path in the lower part of it, as it was agreed by the Client and the Contractor.

The subsoil investigation performed in various construction sites in the vicinity has revealed the likelihood of soil of high permeability underneath the 50m.b.s.l. mark. The

presence of such soils would affect the consolidation process. If the soil underneath the 50m.b.s.l. depth possesses significantly higher permeability properties than the defined hydraulic conductivity in the lower part of the used calculation model, the drainage path must be considered as the half of its initial length (see Chapter 2.1 with the theory of consolidation). Thus, the time required for consolidation reduces and the higher settlement rate is generated within the same amount of time.

The assumption of underground, framed by the permeable soil layer under the 50m.b.s.l. is applied for calculations. The calculations with the opened (drained) bottom bound are carried out for the same loading scenarios as described previously.

3.4.4.1 Roads

Results of simulations for roads with four variable life loads and the drained bottom boundary are summarized in Table 10, Table 11, Table 12 and

Table 13.

Table 10 Evaluated settlement ratio for roads with 0kN/m² life load and the drained bottom boundary

	95/50/50						
	S _{50,50000} [cm]	S _{50,6} [cm]	U _{50,6} [%]	S _{50,9} [cm]	U _{50,9} [%]	S _{50,249} [cm]	U _{50,249} [%]
Upper part with PVD	45,8	51,5	112,45	47,8	104,37	45,7	99,78
Lower part	24,5	2,6	10,61	2,9	11,84	11,8	48,16
Σ	70,3	54,1		50,7		57,5	

Table 11 Evaluated settlement ratio for roads with 10kN/m² life load and the drained bottom boundary

	95/50/60						
	S _{60,50000} [cm]	S _{60,6} [cm]	U _{60,6} [%]	S _{60,9} [cm]	U _{60,9} [%]	S _{60,249} [cm]	U _{60,249} [%]
Upper part with PVD	48,0	51,5	107,29	47,8	99,58	48,0	100,00
Lower part	29,2	2,6	8,90	2,9	9,93	13,9	47,60
Σ	77,2	54,1		50,7		61,9	

Table 12 Evaluated settlement ratio for roads with 20kN/m² life load and the drained bottom boundary

	95/50/70						
	S _{70,50000} [cm]	S _{70,6} [cm]	U _{70,6} [%]	S _{70,9} [cm]	U _{70,9} [%]	S _{70,249} [cm]	U _{70,249} [%]
Upper part with PVD	50,2	51,5	102,59	47,8	95,22	50,1	99,80
Lower part	34,0	2,6	7,65	2,9	8,53	16,1	47,35
Σ	84,2	54,1		50,7		66,2	

Table 13 Evaluated settlement ratio for roads with 30kN/m² life load and the drained bottom boundary

	95/50/80						
	S _{80,50000} [cm]	S _{80,6} [cm]	U _{80,6} [%]	S _{80,9} [cm]	U _{80,9} [%]	S _{80,249} [cm]	U _{80,249} [%]
Upper part with PVD	54,5	51,5	94,50	47,8	87,71	54,5	100,00
Lower part	38,9	2,6	6,68	2,9	7,46	18,2	46,79
Σ	93,4	54,1		50,7		72,7	

Figure 52 shows the log time – settlement curves generated by four cases of different life loads.

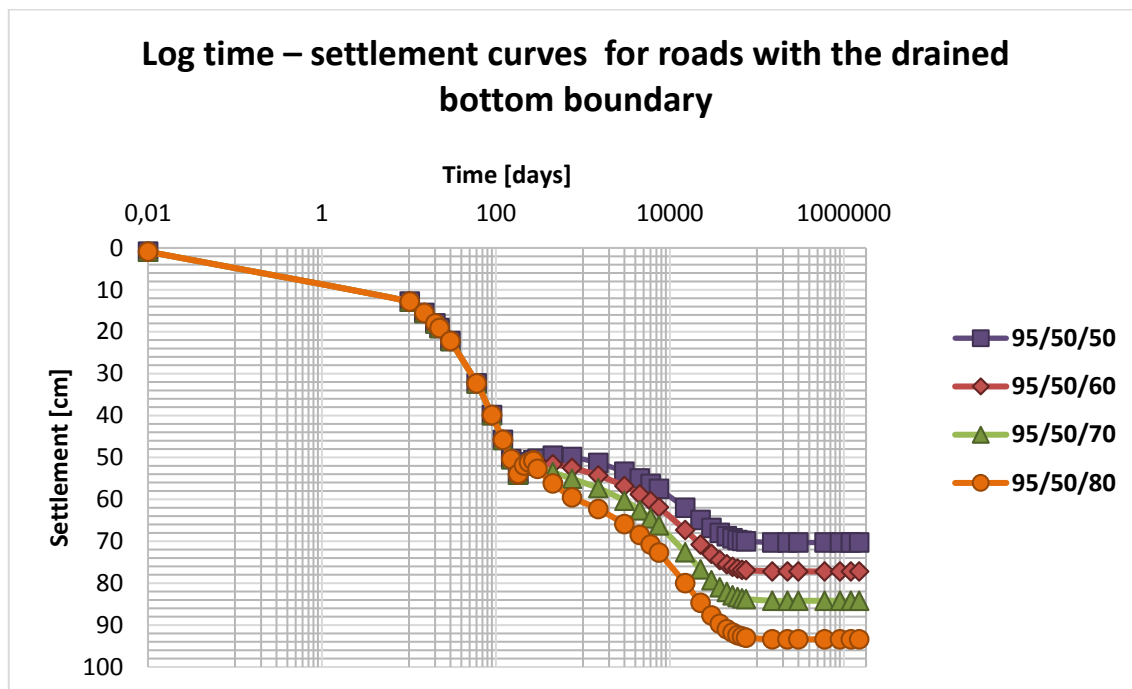


Figure 52 Variations of log time – settlement curves for roads with four different life loads

3.4.4.2 Structures

Results of settlement calculations for structures are summarized in Table 14 and presented in Figure 53.

Table 14 Evaluated settlement ratio for structures with 16kN/m² life load and the drained bottom boundary

	127/55/71						
	S _{71,50000} [cm]	S _{71,6} [cm]	U _{71,6} [%]	S _{71,9} [cm]	U _{71,9} [%]	S _{70,609} [cm]	U _{71,609} [%]
Upper part with PVD	62,1	68,9	110,95	62,1	100,00	61,9	99,68
Bottom part	34,7	3,4	9,80	3,9	11,24	25,1	72,33
Σ	96,8	72,3		66,0		87,0	

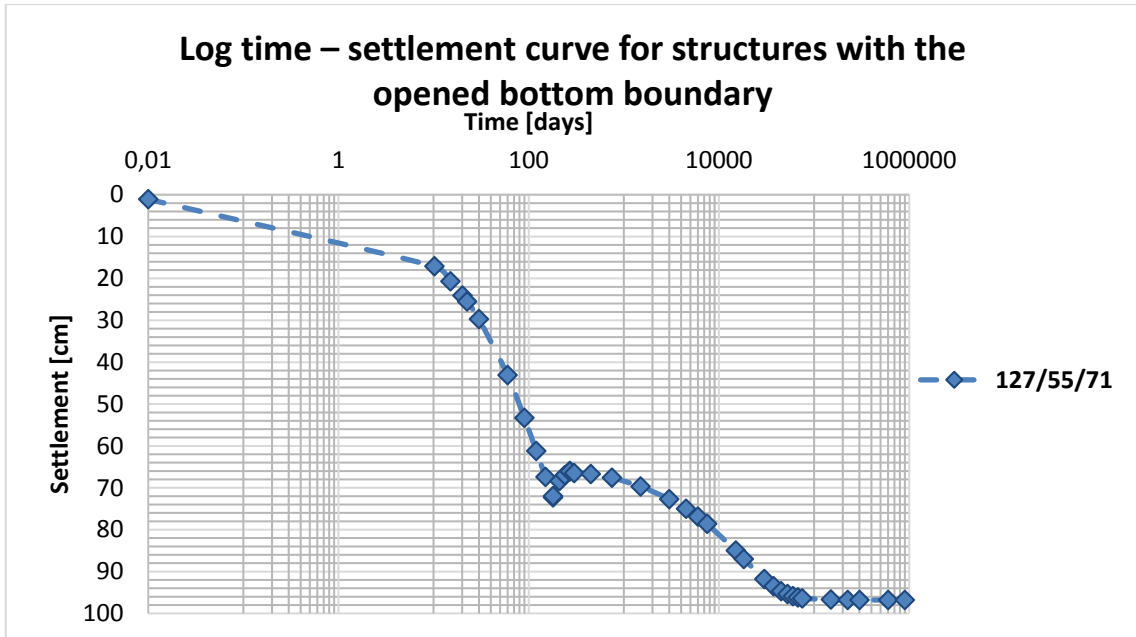


Figure 53 Log time – settlement curve for structures with 16kN/m² life and structural load

3.4.4.3 Effective settlement with the drained bottom bound

Results of settlement calculations with the drained bottom boundary are summarized in Table 15 and presented in Figure 54.

Table 15 Resulting effective settlement for calculations with the drained bottom boundary

	Roads				Structures
	0 kN/m ²	10 kN/m ²	20 kN/m ²	30 kN/m ²	16 kN/m ²
Upper part with PVD	-2,1	0,2	2,3	6,7	-0,2
Lower part	8,9	11,0	13,2	15,3	21,2
Σ	6,8	11,2	15,5	22,0	21,0

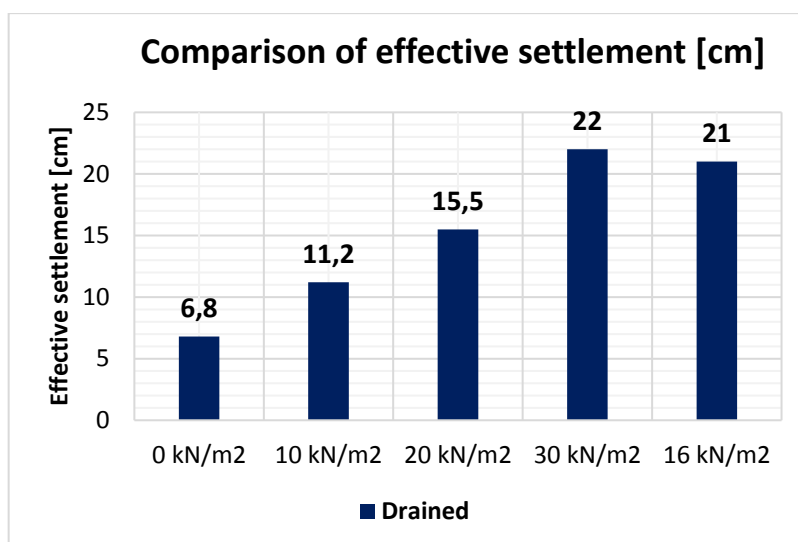


Figure 54 Resulting effective settlement for calculations with the drained bottom boundary

Simulations where the drained bottom boundary is applied reveal that the 15cm requirement is satisfied only in cases where the lowest life loads for roads – with 0 and 10kN/m². This is linked with the twice shorter drainage path in the lower layers from 25 to 50m.b.s.l, when the drained bottom boundary is assigned to the model.

3.4.5 Comparison of effective settlement

The effective settlement rate 20 or 50 years after unloading, depending on the type of construction, is compared in Table 16. The calculation results with the drained lower boundary are marked with the blue color and the abbreviation DR; the results with the closed bottom boundary are shown in red and marked with the abbreviation UNDR.

Table 16 Comparison of effective settlement for simulations with drained and undrained bottom boundary.

	Roads								Structures	
	0 kN/m ²		10 kN/m ²		20 kN/m ²		30 kN/m ²		16 kN/m ²	
	DR	UNDR	DR	UNDR	DR	UNDR	DR	UNDR	DR	UNDR
Upper part with PVD	2,1	-2	0,2	0,2	2,3	2,5	6,7	6,8	-0,2	-0,1
Lower part	8,9	4,9	11	6,1	13,2	7,2	15,3	8,4	21,2	12
Σ	6,8	2,9	11,2	6,3	15,5	9,7	22	15,2	21	11,9

Figure 55 presents the graphical comparison of the results (for the total effective settlement Σ), summarized in Table 16.

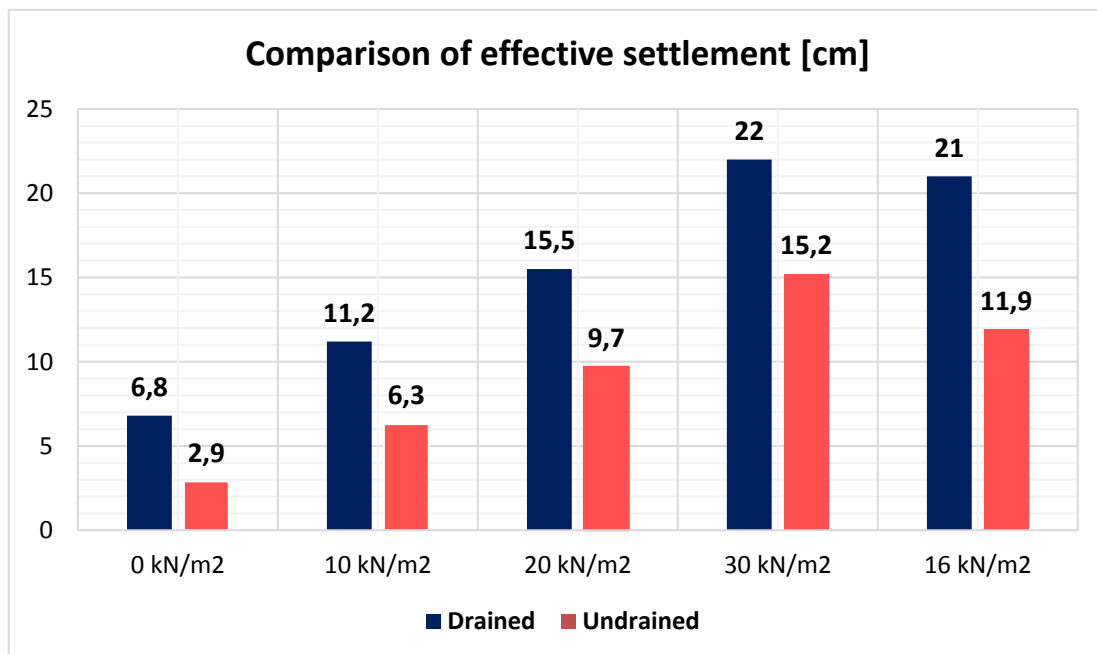


Figure 55 Comparison of effective settlement for simulations with the drained and undrained bottom boundary

The comparison of results show that the presence of permeable soils below 50m.b.s.l. increases the effective settlement:

- For roads with 0kN/m^2 life load settlements with the drained bottom boundary are 134% higher than in the case with the undrained bottom bound.
- For roads with 10kN/m^2 life load settlements with the drained bottom boundary are 178% higher than in the case with the undrained bottom bound.
- For roads with 20kN/m^2 life load life load settlements with the drained bottom boundary are 137% higher than in the case with the undrained bottom bound.
- For roads with 30kN/m^2 life load life load settlements with the drained bottom boundary are 145% higher than in the case with the undrained bottom bound.
- For structures with 16kN/m^2 life load life load settlements with the drained bottom boundary are 110% higher than in the case with the undrained bottom bound.

The following conclusions can be made from the present settlement comparison for the two types of simulation and can be considered as the major design concerns:

- a) The subsurface investigation must be performed below the 50m depth to estimate the soil characteristics, required for settlement calculation.
- b) The settlement evaluation was performed on the idealized underground model, which blends the range of stiffness and permeability parameters into the single values within the area of great extent. This can result in differential settlement under the constructed embankment with roads and structures.
- c) Negative settlement due to the unloading (where the negative excess pore water pressure is generated) is used in the estimation of effective settlement. In the case of negative outcome, the negative settlement may be overestimated, which results in the higher effective settlement rate. As well, the differential negative settlement may occur due to the sporadic construction of embankments and the irregular removal of the temporary surcharge.
- d) Because the construction sequence influences the generated settlement, detailed description how exactly the embankment with transition zones is going to be build, should be defined between the Client and Contractor.
- e) The starting time of the effective settlement measurements – whether immediately after the construction or after waiting until the design height of embankment is reached – should be defined in the contract.
- g) In this section simulations were carried out without the implementation of the effective drain diameter. The influence of this diameter must be considered in

further evaluations. The additional set of calculations with the effective drain diameter d_w was performed in order to assess this influence. The recalculated value of the effective drain diameter $d_w = 0,065\text{m}^2$ is higher than the value used in above described calculations. The comparison of results is summarized in Table 17 for the case with the closed bottom boundary.

Table 17 Settlement comparison for calculations with and without the effective drain diameter

	Cross-section area of a drain [m ²]	After 6 months	After 9 months	After 249 months	After 609 months	Effective settlement
0kN/m²	$a_{dw}=0,05\text{m}^2$	52,5	49,1	52		2,9
	$a_{dw}=0,065\text{m}^2$	54,3	50,3	53,1		2,8
10kN/m²	$a_{dw}=0,05\text{m}^2$	52,5	49,1	55,4		6,3
	$a_{dw}=0,065\text{m}^2$	54,3	50,3	56,5		6,2
20kN/m²	$a_{dw}=0,05\text{m}^2$	52,5	49,1	58,8		9,7
	$a_{dw}=0,065\text{m}^2$	54,3	50,3	59,9		9,6
30kN/m²	$a_{dw}=0,05\text{m}^2$	52,5	49,1	64,3		15,2
	$a_{dw}=0,065\text{m}^2$	54,3	50,3	64,5		14,2
16kN/m²	$a_{dw}=0,05\text{m}^2$	70,2	63,9		75,8	119
	$a_{dw}=0,065\text{m}^2$	72,6	65,5		77,2	11,7

The implemented effective drain diameter d_w results in the slight change of settlement ratio (vast majority below 1% difference and the case with 30kPa life load below 10%), which in general does not indicate the significant difference. It is likely to add the insignificant difference for the case with the drained bottom boundary. The main influence of the increase of the drain diameter is seen only in the upper part with PVD and, as it is mentioned previously, the drained bottom boundary does not have a strong influence on the drained upper part with PVD.

3.5 Piezocone test evaluation

For ground improvement projects, the effectiveness of design is highly dependent on the estimated underground model. The quality of performed work is defined by the

comparison of soil properties before and after the applied improvement technique. The ground improvement concept must include the goal to achieve the homogenous soil characteristics all over the area independently from the applied method.

Achievement of uniform soil characteristics is an important design criterion for areas of great extent. The larger the area is, the higher is the possibility of variable stratigraphy and the higher is the chance of the presence of sporadic underground features as lenses, boulders or cavities.

The estimation of reasonable underground model used for the development of ground improvement strategy is the essential of the effective design. The limitation to use a single underground model in areas of great extent can lead to the failure, because the effect of simplification to one set of values does not reflect all permutations of variable soil characteristics. The suitable solution would be the subdivision of the total area into smaller plots based on their found similarities.

As the proposed ground improvement design with vertical drains and preloading is going to be applied to the area of great extent, it is important to consider the possibility of variable underground conditions and their influence on settlement. The comparison of new data with the eight supplementary piezocone tests from the Investigation-1 (see section 3.3.2) can indicate the lower effectivity in areas, where the subsoil conditions vary.

To reduce possible geotechnical risks, the further investigation (Investigation-2) of this area of great extent with additional piezocone tests has been started in January, 2017. The data gained with these additional tests must be evaluated and then compared to the results of eight previous CPTu tests, which provide the basis for the used underground model. This comparison is significant for the further evaluation of settlement and the further work with the estimated calculation model. The previously used calculation model and the ground improvement design must be corrected, if the additional CPTu tests show different results than the Investigation-1. As well, the use of several calculation models, developed specifically for smaller areas, may be considered, if the further subsurface investigation shows that the area of great extent can be split into smaller parts with similar geological and geotechnical properties.

The evaluation of piezocone tests consists of six steps:

1. Recreation of constrained modulus M_{lc} , corrected cone resistance q_t , permeability k_h and soil behavior type I_c graphs from the Investigation-1 with the programmed

- spreadsheets and their comparison to the graphs provided in the results of this Investigation-1.
2. Delimitating lines for constrained modulus M , horizontal permeability k_h , soil behavior type SBT and settlements are generated.
 3. Evaluation of in-the-future received additional CPTu data with the previously programmed spreadsheets.
 4. Comparison of evaluated new data with defined delimitating lines for constrained modulus M , horizontal permeability k_h , and soil behavior type SBT.
 5. Comparison of time – settlement curves, if possible.
 6. Comparison of results, if the fifth step was completed.

These steps are described in details in the following sections in this section.

3.5.1 Programmed spreadsheets for CPTu evaluation

The underground model used for the calculation of settlement bases on the eight CPTu tests with correction from dissipation tests. CPe – IT takes the CPTu data and performs basic interpretation in terms of Soil Behavior Type (SBT) and various geotechnical soil design parameters using current published correlations based on the comprehensive review by Lunne, Robertson and Powel (1997), as well as recent updates by Professor Robertson. The correlations required for these basic interpretations are discussed in section 2.4.2.

The further subsurface investigation in the area will result in the new data, which must be compared to these eight CPTu tests. The initial idea is to create the relatively automated system which can be used in the future for evaluation of additional CPTu tests and their comparison to the first eight tests.

The idea of evaluation is realized as the set of spreadsheets. The spreadsheets take the raw data as input, calculate the raw data according to chosen correlations, and output graphs suitable for comparison to the graphs presented in results of the Investigation-1. The output can be only completed, if the access to the raw data is provided. The constants required for correlations (see section 2.4.2 with the theory and section 3.5.1.1) are calibrated to achieve the closest similar results to provided graphs, because these constant are not specified in the provided results for each test. A set of calibrated constants will be applied to future evaluations as default, if no further data is provided.

In the spreadsheet the constrained modulus M is evaluated with two different equations: the first with the net area ratio a and the second with the correlation constant α_M . As it is

explained in the Investigation-1 results, the final values of constrained modulus M proposed for the idealized underground model are the combination of these two calculations (see section 3.5.3).

3.5.1.1 The layout of spreadsheets

The programmed spreadsheet consist of two parts: the first part on the left hand side is used for input data and calculations; the second part located on the right hand side outputs the graphs.

In the part for input data and calculations constants prescribed for corresponding cells are summarized in the separate table. The constants and coefficients stay identical within the whole sheet and do not vary with depth. Unit weight of water is set to 10kN/m^3 for all spreadsheets. For the correlation constant α_M value of 6 is assigned, because this number is mentioned in the results of the Investigation-1. However, keeping the same α_M value of 6 for the whole underground model does not indicate the presence of various soils and it leads to the overestimation or underestimation of the stiffness (this should be considered for the future calculations). The atmospheric pressure is required in correlations and set to 100kPa , as it is suggested by Robertson (2012). The two ratios of the horizontal coefficient of permeability k_h to the vertical coefficient of permeability k_v (k_h/k_v) corresponds numbers and depth limitations provided in the Investigation-1. For the net area ratio a the chosen value varies between $0,7 - 0,85$.

The spreadsheets are programmed in the way that results are calculated with respect to the sea level. The data provided with respect to the local elevation and in $0,02\text{m}$ steps is adjusted to the 0m.a.s.l. if the local elevation at the time of test is known.

3.5.1.2 Input data

The output graphs are products of following raw data:

- Cone resistance q_c
- Sleeve friction f_s
- Pore pressure u_2

Additionally to them, the net area ratio a , the local ground level, the name and the date of test should be given.

For settlement calculations in this Project the soil properties of the working platform constructed on the original ground surface are not considered. The evaluation of soil characteristics starts at the sea level and continues to the end depth of test.

Note that during the manual input of raw data, the proper local elevation must be considered.

3.5.1.3 Analysis method and estimation of the net area ratio a

The comparison of graphs is performed in two steps.

In the first step the range of possible values of the net area ratio a is approximated. After the raw data is manually input in spreadsheets, the most suitable net area ratio a is assigned for the each test. The net area ratio a is estimated from the laboratory calibration with the typical values 0,7 – 0,85 and tuned till the recreated graphs of constrained modulus and corrected tip resistance show the best agreement with the graphs provided in the results of the Investigation-1.

The second step is based on the assumption that only one input number of net area ratio a is used for the set of tests and assigned for interpretations with the software. As the range of possible net area ratio a values is found, the median value of this ratio is chosen and repeatedly assigned for eight tests. The assigned a value will be applied for the future calculations as default, if no other calibration data are given.

3.5.1.4 Comparison of graphs

The resulting recreated graphs of eight CPTu tests are presented in Appendix C.

It can be stated that the recreated constrained modulus M , corrected cone resistance and soil behavior type SBT curves based on soil behavior type index I_c show the good agreement with the presented graphs, even then the single value of the net area ratio a was assigned for all eight tests.

For the eight CPTu tests from the Investigation-1, the range of approximated net area ratio a varies between 0,7 to 0,8. The tuned value a used for calculations is set to 0,75, because it has shown on average the better agreement with provided charts than other values in the approximated range. When the approximated net area ratio $a = 0,7$ was applied for all eight cases, the resulting constrained modulus M was overestimated in comparison to the provided graphs (in general, 5-10% higher); when the approximated net area ratio $a = 0,8$ was applied for all eight cases, the resulting constrained modulus M was underestimated in comparison to the provided graphs. The evaluated values of constrained modulus M for eight CPTu tests are summarized in the results of provided Investigation-1 as the plot of data points (see Figure 36).

The evaluation of stiffness with the factor l_c in the programmed spreadsheets shows that in the upper layer, where the interlayering of silty, clayey and sandy soils is defined by borehole drillings, the evaluated stiffness has the wide spread of values (0,5-48,0 MPa). In comparison to the presented in the results of the Investigation-1 graphs, in the recreated graphs the sharp increases of stiffness are slightly overestimated (approximately 5-10%). This overestimation may be caused by unit weight of water, which is set to 10kN/m³ for all spreadsheets, because the exact value of the unit weight of water used in the software is not known and might vary in the range of 9,5 - 10 kN/m³. Another possible cause of this overestimation may be the way, how the total and effective vertical stress is estimated. In the programmed spreadsheets the total and effective vertical stress in the 0,02m thick soil layer (this thickness is equal to the rate of penetration) is calculated using the calculated soil unit weight per each depth:

$$\sigma_{v0} = \sum (z_i \gamma_i) \quad (50)$$

σ_{v0}	[kPa]	Total vertical stress
z_i	[m]	Depth
γ_i	[kN/m ³]	Soil unit weight

In general, with exception of random interlayers of higher resistance, recreated constrained modulus M profiles from 10m down to 50m depth show constant, but not large increase of stiffness. At the 10m depth the approximated stiffness varies in the range of 2,0 – 3,1 MPa, while at the lowest end it increases to the range of 5,0 – 5,5 MPa.

The report provides the second interpretation of constrained modulus M with the factor $\alpha = 6$. The graph as it is given in the report here is provided as Figure 37.

Similar results are calculated in the spreadsheets with coefficient $\alpha_M = 6$. The constrained modulus profile approximated with the coefficient α_M shows similar behavior to the first profile evaluated with l_c . In the second profile from the ground level below to 10m depth the estimated values of constrained modulus have a wide spread (1,0 to almost 40,0 MPa), what suggests the presence of sands and fines interlayering. However, in general more data points within this depth interval tend to reach lower values of stiffness than in the first approximation. From 10m down to 15m depth the range of approximated stiffness values show a reasonably good agreement with the range evaluated in the first profile, but the evaluation $\alpha_M = 6$ indicates on average slightly higher values (2,5 – 4,0

MPa with $\alpha_M = 6$; 2,0 – 4,0 with I_c). Lastly, from 15m down to 50m depth the increase of approximated values is constant, but contrary to the first approximation more distinct, because the higher maximum value is reached (7,5 – 8,5 MPa contrary to 5,0 - 5,5 MPa).

All in all, it can be said that the stiffness values in the upper 10m thick layer, proposed for the idealized underground model, are approximated based on the lower values, obtained from the evaluation with the factor $\alpha = 6$. It can be considered as the conservative evaluation. The stiffness values for the depth interval 15-50m.b.s.l. are based on the average number, received from two evaluation methods.

The plots of corrected tip resistance, permeability, normalized friction ratio and soil behavior type SBT are assessed for the each separate CPTu tests. However, eight variations are not summarized in the one plot, as it is done with the stiffness. Therefore they are compared in the separate graphs and this comparison is shown in Appendix C.

The overall observation is that all eight corrected cone resistance plots in the upper layer (0-10m.b.s.l.) show a wide range of values (2,0-close to 7,0 MPa). All eight plots show the tendency of the sharp increases in the corrected cone resistance in the depth at approximately the 1-4m.b.s.l. It is likely to be due to the interlayer of sand, because this peak reaches 4,0-6,6 MPa resistance. In the depth 6-8m.b.s.l. all eight CPTu tests indicate the second peak of resistance. This peak is slightly lower than the first and reaches 2,5-4,3 MPa resistance.

The lower layer (10-50m.b.s.l.) shows the same behavior trend in all eight profiles: the corrected tip resistance has the constant increase from 0,5 MPa to 2,2 MPa.

The soil behavior type plots evaluated in the spreadsheets were compared to the original plots from the Investigation-1 and it can be said that they really precisely recreate the given graphs with following evaluation: in the upper layer due to the interlayering of soils the soil behavior type index I_c falls within the range 1,8-4,2; in the lower layer it falls within the range 3,2-3,6 and stays close to constant with respect to depth for eight out of eight tests.

The graphs of permeability and normalized friction ratio are compared to the provided graphs too. They show a good agreement. Both graphs prove the trend described above: the upper 15m thick layer with the soil interlayering and variable permeability and normalized skin friction; the lower layer 35m thick layer with the more constant evaluated soil parameters. In the upper layer two interlayers of higher permeability can be defined

in the depth intervals between 0-5m.b.s.l. and 7-9m.b.s.l. (these boundaries varies with different CPTu tests) and two less permeable intervals 5-7m.b.s.l. and 9-15m.b.s.l. In the lower layer the permeability is gradually decreasing from $1,5E-9$ to $8E-10$ m/s for CPTu_1, CPTu_2 and CPTu_8 or is constantly lower than $1E-9$ m/s for CPTu_3, CPTu_4, CPTu_5, CPTu_6 and CPTu_7. The normalized friction ratio graphs for all eight CPTU reveals an interesting trend: from the approximately 40m.b.s.l. depth the plot starts to bend and the normalized friction ratio starts to increase. "The increase of the normalized friction ratio is likely to indicate the increase of fines in soils and decrease of grain size" (Robertson 2012).

3.5.2 Delimitating lines

The next step in the evaluation is to mark out the extent of the data. The delimitating lines are created according the approximated data from the eight CPTus. The delimitating lines are a quick way to see, if evaluated data from new piezocone tests fit within the range thus far considered.

The extent of data is marked out with two lines: the first line picks out the absolute lowest values of evaluated properties and the second consists of the absolute highest values from eight piezocone tests.

The three types of delimitating lines are created on the basis of the eight programmed spreadsheets: for the constrained modulus M_{lc} , horizontal coefficient of permeability k_h and soil behavior type (SBT) based on the soil behavior type index I_c .

3.5.2.1 Delimitating lines for constrained modulus M_{lc}

After the good agreement of evaluated with the spreadsheets curves with results approved in the Investigation-1 was defined, the corresponding delimitating lines are created.

It was decided to create only one set of delimitating lines for the constrained modulus M_{lc} based on approximations with the soil behavior type index I_c .

The obtained plot of delimitating lines for the constrained modulus M_{lc} with the soil behavior type index I_c is shown in Figure 56. In order to improve the visual properties, the step 0,5m between points is taken. Two delimitating lines meet at one point at the depth of 49.5m.b.s.l., because this depth was reached only by one CPTu test.

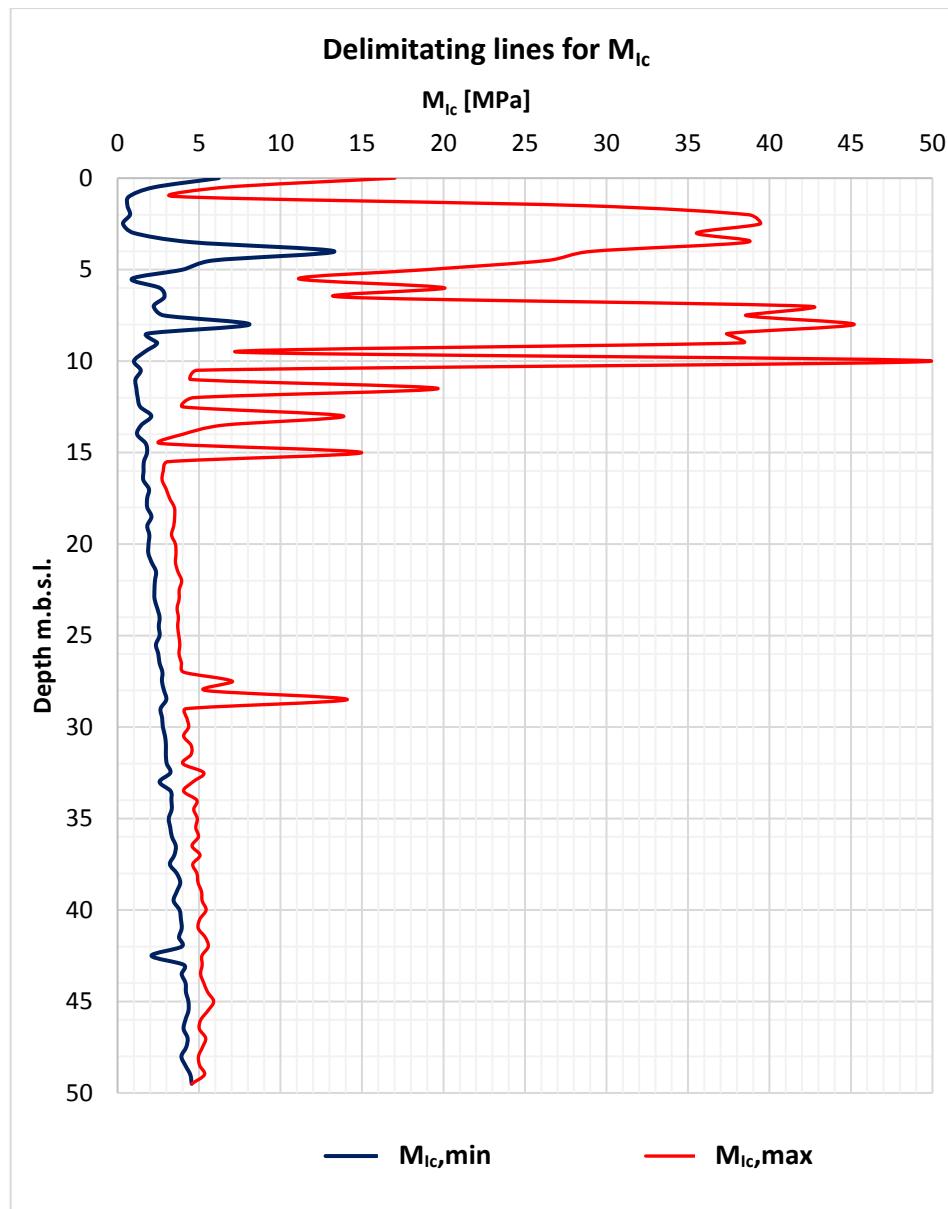


Figure 56 Delimitating lines for constrained modulus M_{Ic}

Based on the performed evaluation of raw data and considering the plots displayed in Figure 56, the following comments can be made:

- a) Considering the fact that the blue delimitating line (lower bound) consists only of absolutely lowest estimated values of constrained modulus M_{Ic} based on approximations with the soil behavior type index I_c and the red delimitating line (upper bound) consists only of absolutely highest values, both lines show the presence of soil interlayering in the upper 10m of deposit. It can be observed from the variety of spikes in these two lines.

- b) Below this depth, the delimitating lines run near parallel to each other with the exception of the stiffer part in the red profile between 26,20 and 28,40m.b.s.l. These spikes come from the results of CPTu_2, CPTu_3 and CPTu_6, which neighbors with each other (see Figure 33).
- c) The stratigraphy of deposit cannot be determined only on the estimated stiffness parameters. Other geotechnical properties must be attributed.

3.5.2.2 Delimitating lines for horizontal coefficient of permeability k_h

Based on the same principle of absolute lowest and highest values, two delimitating lines for the horizontal coefficient of permeability are plotted.

Figure 57 illustrated the results of evaluation. Originally the coefficient of horizontal permeability is estimated for each 0,02m step starting from the sea level. In order to improve the visual properties, the step 0,5m between points is taken. Two delimitating lines meet at one point at the depth of 49,5m.b.s.l, because this depth was reached only by one CPTu test. Like in the previous plot with delimitating lines, the lowest values of permeability is marked with the blue color and the highest- with the red.

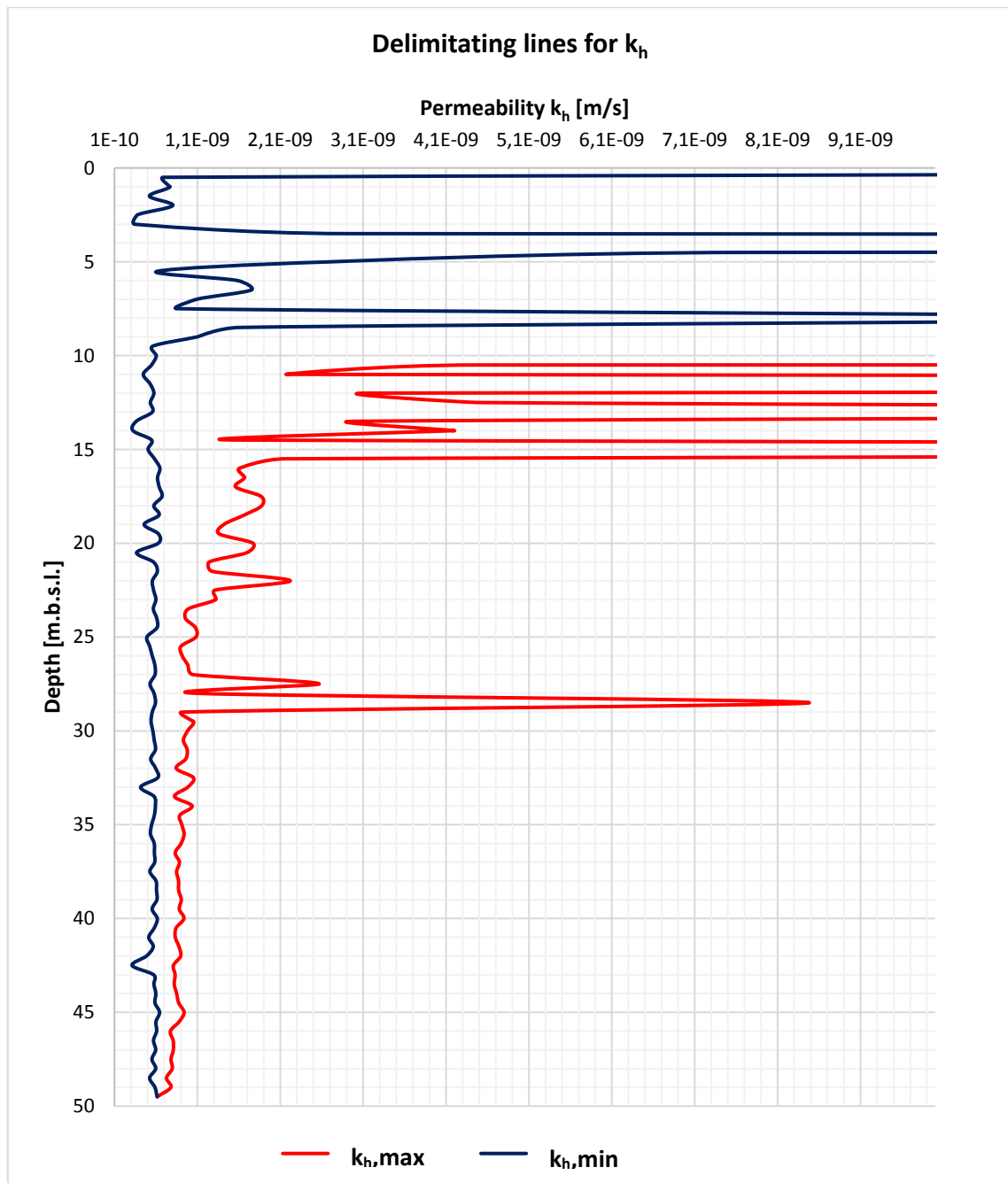


Figure 57 Delimitating lines for horizontal coefficient of permeability k_h

The following observations can be drawn from Figure 57:

- a) In the upper part the estimated variation of horizontal hydraulic conductivity falls within an extremely wide range. The absolute lowest value in the upper part is $1,2E-10$ m/s and the absolute highest value is $2,4E-03$ m/s. Such a wide range of

evaluated permeability values is likely due to the presence of inhomogeneous soil stratigraphy.

- b) In the depth interval from approximately 26 to 28m.b.s.l. the spikes of the red delimitating line from the graph of permeability show the really good agreement with the red delimitating line from the plot of constrained modulus M . It is likely to indicate the precedence of the permeable lens.
- c) From the 10m.b.s.l. to the almost 50m.b.s.l. depth the delimitating line of minimal values indicates considerably constant hydraulic permeability in the underground. There, values vary within the range of $1E-10$ m/s to almost $7,5E-10$ m/s. It is worth to mention that the minimal permeability increases over the depth.
- d) Contrary to the blue delimitating line, the red line shows about constant behavior from almost 30m.b.s.l. depth.

3.5.2.3 Delimitating lines for soil behavior type (SBT) based on soil behavior type index I_c

In general, soil properties depend on the soil type. For example, fine-grained soils show significantly lower permeability than the coarse-grained ones. In the evaluation methodology proposed by Robertson, the identification of soil behavior type is an important output of the underground investigation.

The comparison of soil behavior profile with the evaluated range is a helpful tool of quick identification of stratigraphy changes.

Based on the identical principles as earlier, the delimitating lines for soil behavior type are illustrated in Figure 58. In order to improve the visual properties, the step 0,5m between points is taken. Two delimitating lines meet at one point at the depth of 49,5m.b.s.l, because this depth was reached only by one CPTu test.

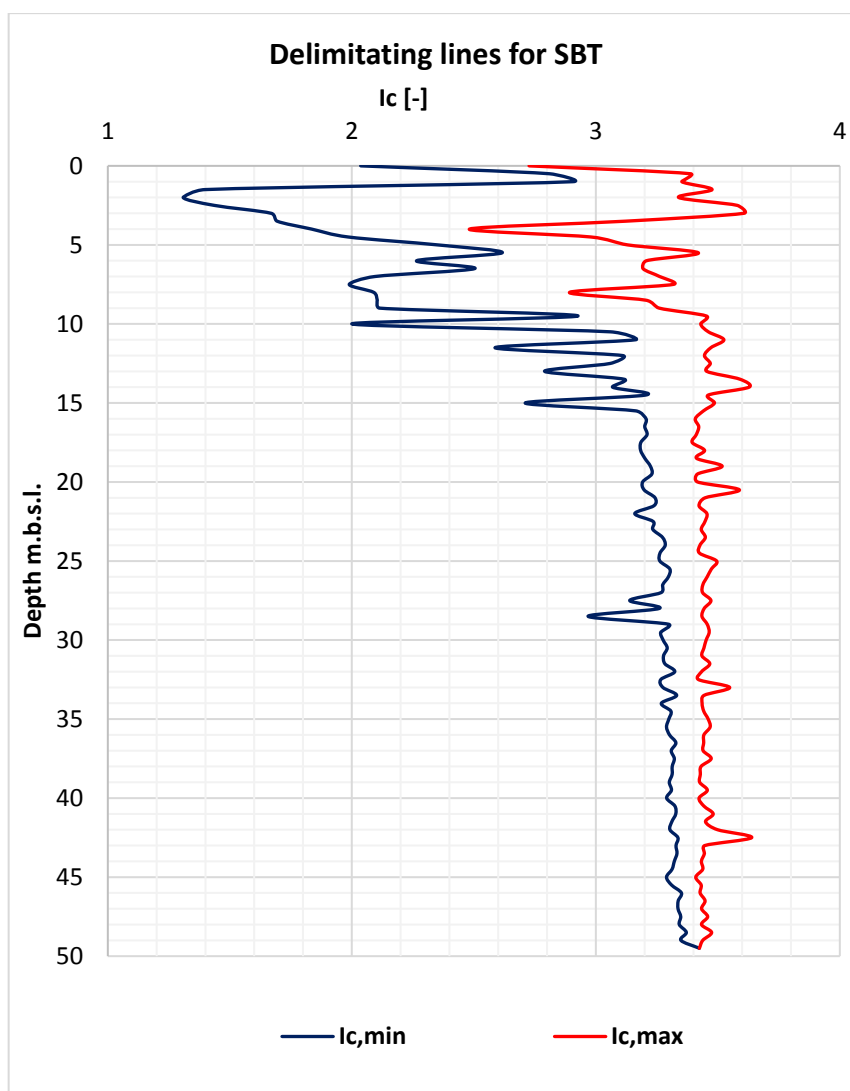


Figure 58 Delimitating lines for SBT

Based on Figure 58 the underground can be again divided into two formations: the upper (0-15m.b.s.l.) with soil behavior type index I_c varying from almost 1,1 to 3,9 and the lower (15-50m.b.s.l.), where with the exception of several higher than average values the index stays within the average range of 3,1 to less than 3,5.

Robertson estimated that the typical soil behavior type index I_c for sands falls within the range $1,31 < I_c < 2,05$ and for sand mixtures – $2,05 < I_c < 2,60$. That means that the lower is the estimated I_c value, the coarser are the particles. Respectively, the permeability of soils increases with the lower I_c .

The significant part of the blue delimitating line in the upper layer falls in the range, where investigated soil could be named as the sand or sand mixture based on the I_c index. The values of permeability for such soils should vary from $1E-07$ m/s to $1E-04$ m/s. From the depth approximately 4m.b.s.l. to 4,5m.b.s.l. and from the 7.m.b.s.l. to 8m.b.s.l. the red profile line peaks reach the index value of 2,2. The index values of the blue profile show really close agreement to the red profile within these intervals. It can be interpreted as the presence of continuous permeable layers in the tested area.

From 16m.b.s.l. to almost 50m.b.s.l. depth the distance between the delimitating lines reduces from 0,25 on the top to almost 0,1 in the bottom. The narrower the range between two delimitating lines is, the higher is the possibility of homogenous underground. In this depth interval both lines in general do not exceed the index limits of 3,10 and 3,50. The table with general trends of ground response shows that silty clay to clay fits within the range between 2,95 – 3,6, and the evaluated soils are in the good agreement with the proposed range.

Lastly, based on the soil behavior type index I_c and permeability correlations proposed by Robertson, the soil behavior type index I_c and horizontal hydraulic permeability curves approximated with correlations show good agreement with proposed ranges.

3.5.2.4 Delimitating lines for hydraulic permeability based on dissipation tests

The dissipation test is an additional test performed during the CPTu testing procedure in order to define the hydraulic properties of soils.

The eight CPTu tests used as the basis for the idealized underground model were performed with four dissipation tests for each. All together the results of 32 dissipation tests are available.

The results of these dissipation tests are summarized in Table 18 .

Table 18 Results of 32 dissipation tests

	Depth [m]	k_h [m/s]		Depth [m]	k_h [m/s]
CPTu_1	17	1,8E-09	CPTu_5	11.5	1,1E-10
	25	2,3E-10		21	3,8E-10
	33	1,7E-10		30	4,9E-10
	41	2,1E-10		38	2,0E-10
CPTu_2	15	3,2E-09	CPTu_6	16	5,6E-10
	23	3,3E-10		26	2,0E-10
	31	2,7E-10		34	1,6E-10
	42	4,5E-10		43	2,3E-10
CPTu_3	10	8,1E-09	CPTu_7	12	2,3E-08
	20	2,4E-10		24	2,2E-10
	30	2,5E-10		34	2,3E-10
	40	1,6E-10		45	7,4E-11
CPTu_4	13	3,1E-09	CPTu_8	14	2,2E-08
	27	2,8E-10		22	2,7E-10
	3	2,7E-10		30	2,5E-10
	44	2,3E-10		39	2,7E-10

The upper dissipation tests are performed within the range of approximately 10-17.m.b.s.l. depth; the lower dissipation tests are carried out from 17 to 47m.b.s.l. depth. The group of upper dissipation tests is comprised of one dissipation test per CPTu (resulting in 8), while the lower group is comprised of three tests per CPTu (resulting in 24). The calculated permeability values in the upper group in general are higher than in the lower. The same tendency is spotted in permeabilities, estimated in the spreadsheets (see section 3.5.1.4).

Figure 59 and Figure 60 summarize results of estimated permeabilities from dissipation tests.

Figure 59 is dedicated for the upper group, while Figure 60 is dedicated for the lower group. In these two figures the second number after the comma in the name of test corresponds the depth, where the test was carried out.

It is worth to mention that in the upper group the results of six tests with exception of CPTu_7 and CPTu_8 show a really good agreement and vary in the range from $1\text{E-}10$ to $8,1\text{E-}9$ m/s. CPTu_7 and CPTu_8 results show higher permeability (see Table 18). In the lower group two tests – CPTu_5 at depth 30m.b.s.l. (CPTU_5,30) and CPTu_2 at depth 42m.b.s.l. (CPTu_2,42) show higher permeabilities than other tests. However, these test are not excluded from the further investigation.

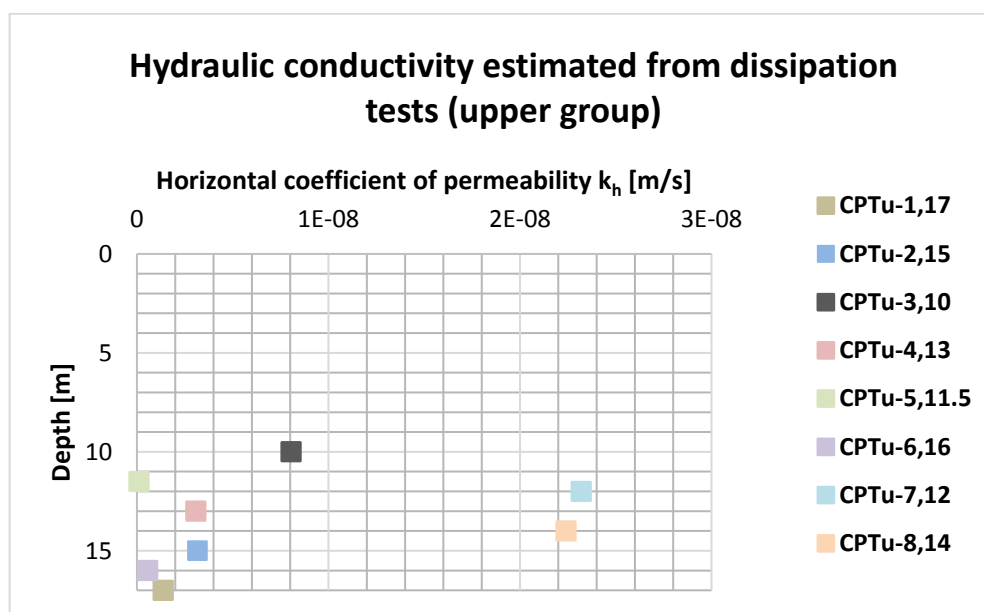


Figure 59 Estimated permeabilities of the upper group

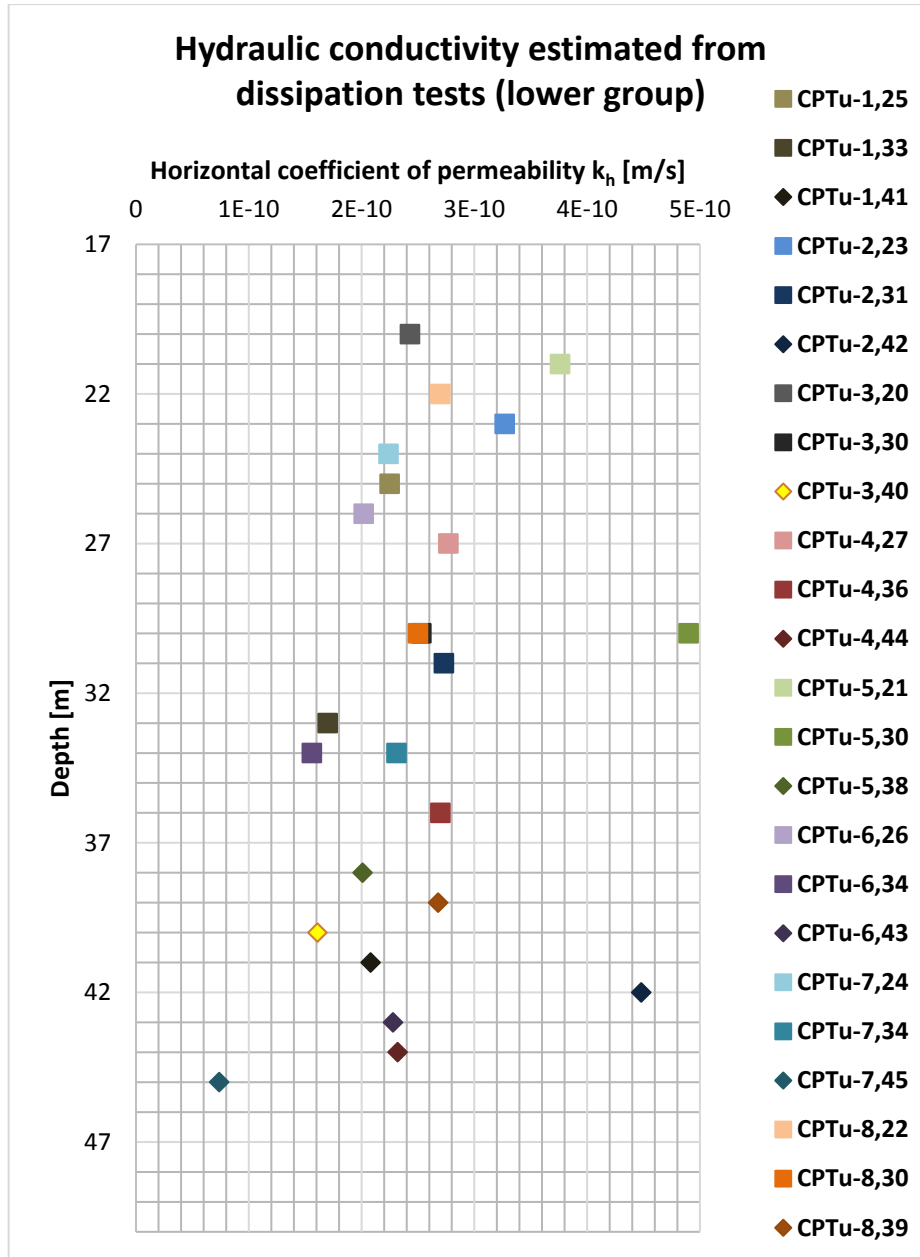


Figure 60 Estimated permeabilities of the lower group

3.5.2.5 Delimitating lines for the horizontal coefficient of permeability from the dissipation tests

The delimitating lines for hydraulic permeability from the dissipation tests are estimated based on the same principles as previously mentioned in this section. However, here the delimitations are set as single values for chosen depth ranges, as shown in Table 19. The estimated permeabilities are regrouped.

Table 19 Delimitations of horizontal coefficient of hydraulic permeability obtained from dissipation tests

Depth [m]	Prescribed depth interval [m]	$k_{h, \min}$ [m/s]	$k_{h, \max}$ [m/s]
10-17	0-15	1,1E-10	2,3E-08
20-25	15-25	2,0E-10	3,8E-10
30-36	25-35	1,6E-10	4,9E-10
40-45	35-49	7,4E-11	4,5E-10

The plots of the delimitations are presented in Figure 61 and Figure 62. Even though the dissipation tests carried out at 42m.b.s.l. depth with the CPTu_2 ant at the 30m.b.s.l. depth with the CPTu_5 have indicated difference from other values (see Figure 60), they are not excluded from the evaluation.

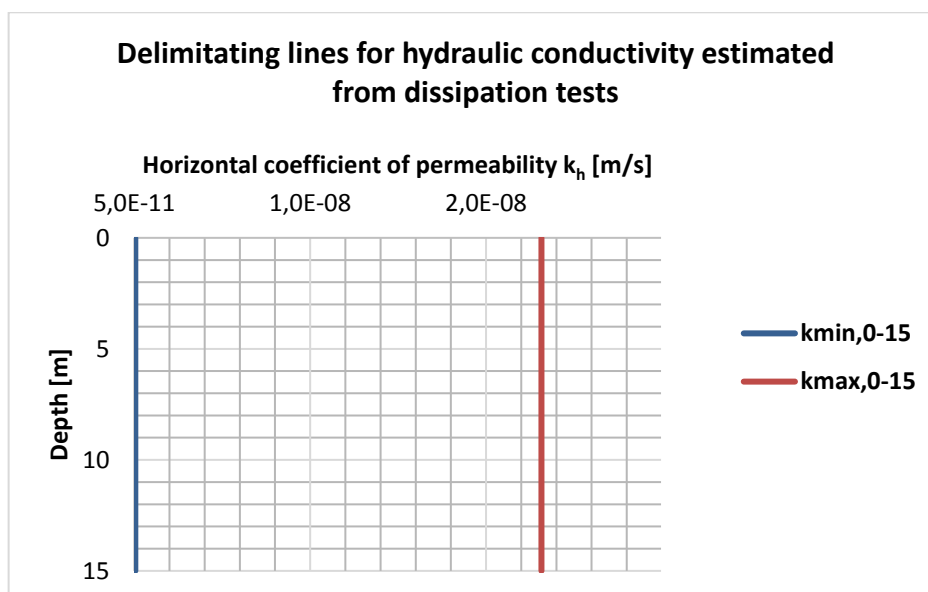


Figure 61 Delimitations for the upper group

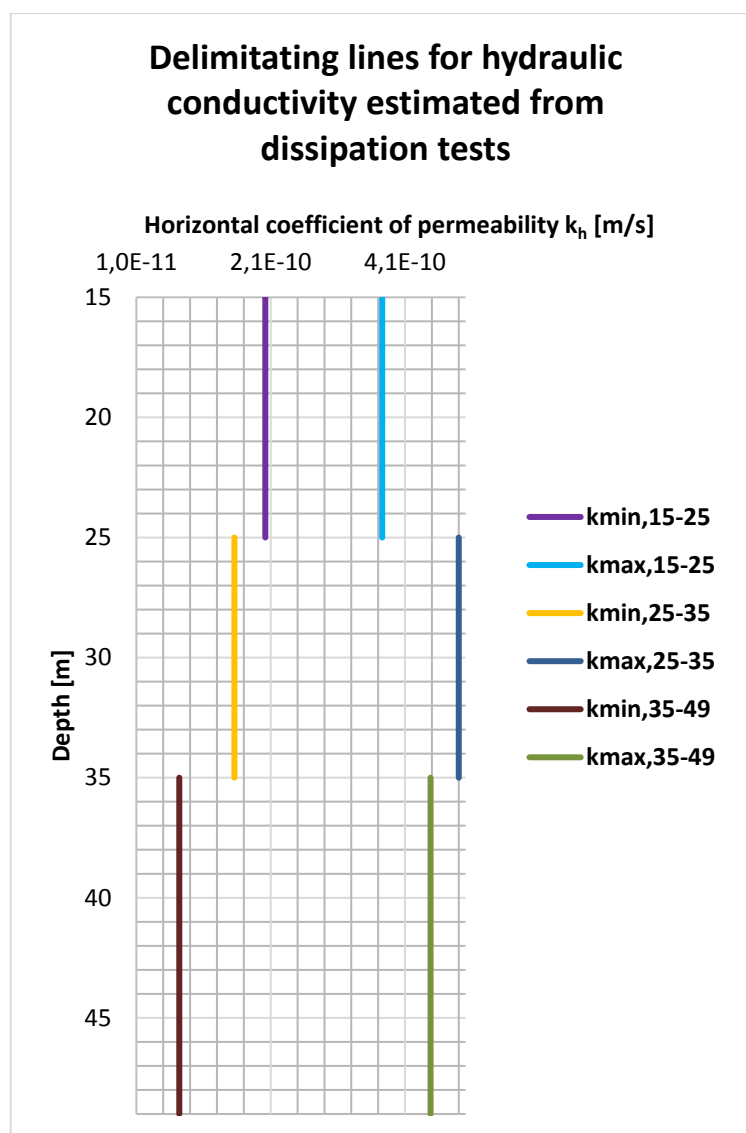


Figure 62 Delimitations for the lower group

3.5.2.6 Comparison of hydraulic permeability obtained with correlations and dissipation tests

Permeability values obtained from dissipation tests and derived from correlations are compared. Through this comparison the confidence of results can be assessed. The better the agreement, the higher is the confidence to use either one of these methods.

The comparison of results obtained with two described methods is illustrated in Figure 63.

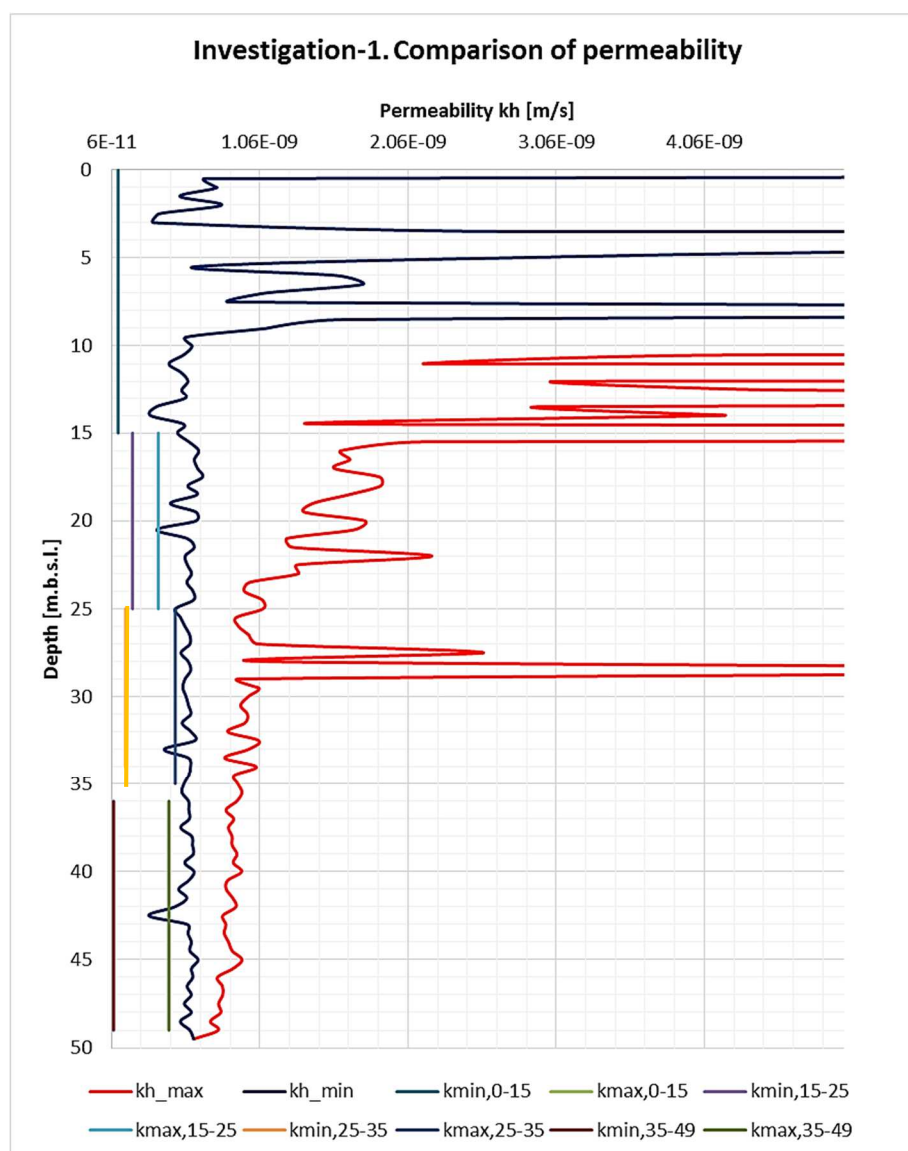


Figure 63 The comparison of delimitating lines obtained from dissipation tests and approximated with correlations by Robertson (2012)

As it is seen in Figure 63, the delimitating lines approximated in the spreadsheets show in general higher values of permeability than resulting delimitations from the dissipation test.

The delimitating lines obtained from the spreadsheets show good agreement with the delimitations from the dissipation tests only in the upper layer. The wider range seen in the upper layer is likely to be influenced by the interlayering of soils.

In the lower layer both sets of delimitating lines indicate the much narrower range of values. The narrow range between the delineations (for both sets) are likely due to the homogeneity of the lower layer (here the subsoil investigation data is considered). However, the two sets do not match. Indicating that only one set can be used in the estimation of settlement, the conservative approach is to use the set with higher values for the whole underground.

3.5.2.7 Delimitating lines for settlement

The estimated ratio of settlements is a function of permeability and stiffness with respect to time. While the stiffness governs the total amount of settlement, the permeability influences the rate of the process.

The time – settlement relationship varies with every single combination of hydraulic conductivity and stiffness. The proposed idealized underground model used for settlement calculation in chapter 3.4 provides its own unique time – settlement behavior curve and settlement ratio. However, the eight piezocone tests which were used to derive this idealized model do not possess exactly the same geotechnical soil properties. As it is expected, time – settlement curves calculated individually for each of eight CPTu tests do not produce the same results as the idealized underground model, which used the average numbers.

It is of interest to compare the results of individual CPTu tests to get the indication of the variety of results that may be seen over the whole site.

To perform the comparison of each individual CPTu to the idealized model, the assumptions with which the settlement calculations are performed must be the same for all simulations.

This section describes the process used to consolidate all the geotechnical properties into the single values, which are later used in the software. This process is specifically developed to estimate the input values of stiffness and permeability, and applied for all eight spreadsheets in the same way.

1. Stiffness evaluation

As discussed in section 3.4, the stratigraphy of idealized underground model has been idealized to allow the increase of stiffness with depth. Exactly the same discretization model with 11 thinner sublayers is applied for the eight CPTu to assess the better comparison.

The input values of stiffness are defined from the two types of plotted constrained modulus curves – the one estimated with I_c and another estimated with the coefficient α . Further stiffness evaluation is performed with the same logic as in the results of Investigation-1 (see section 3.3.2): in the upper Formation A the stiffness values are evaluated with the coefficient α ; in the lower Formation B the stiffness is the average of two numbers calculated with the soil behavior type index I_c and the coefficient α .

The used process of evaluation is divided into two parts with respect to the depth:

- **Formation A (0 – 15m.b.s.l.)**

In the idealized underground model from the Investigation-1 the stiffness defined for the first 15m is based on the lower numbers from clayey and silty soils, rather than on numbers from intrusions of higher resistance. The average stiffness obtained from the plot of constrained modulus based on the coefficient α in this report is lower than its average value from the evaluation with soil behavior type index I_c . The conservative approach was applied and the lower value of stiffness in the upper formation for the idealized underground model was chosen.

Applying the same logic, stiffness values for the upper Formation A are obtained from the M_α graph.

The stiffness values used as the input for calculations were approximated in the following way:

1. The visually approximated stiffness for each of 5 sublayers in the upper layer was used as the reference value for the next step.
2. Then a series of statistical variations was used to find the closest match to the reference value in all eight CPTu tests. The final approach was chosen due to the best match with the visually estimated stiffness and is described as follows: to calculate the average stiffness with all values lower than 15,0 MPa.

- **Formation B (15-50m.b.s.l.)**

All eight evaluated piezocone results indicate the constant increase of stiffness with an exception of several lenses of higher resistance. Thus, in the lower formation no specific limitations are applied as in the upper layer, and the constrained modulus is defined as the average value of the certain range.

Again, two plots of stiffness are considered in derivation of the average values. In the Investigation-1 the stiffness approximated on the basis of the soil behavior type index I_c is lower than the one estimated with the coefficient $\alpha = 6$. Applying the same logic (correction of the stiffness with consideration of higher values from the second method), the ranges of two methods are averaged.

Based on the available raw data obtained from the set of first eight CPTu tests and the performed evaluation of this data with the above described method, resulting input values of constrained modulus for the single tests are summarized in Table 20.

Table 20 Approximated stiffness E [MPa] used for CPTu_1 – CPTu_8

Depth m.b.s.l.	CPTu_1	CPTu_2	CPTu_3	CPTu_4
0-10	5,1	6,0	4,3	3,8
10-12	4,1	2,8	2,5	2,0
12-14	4,1	3,8	3,1	2,4
14-15	3,5	3,1	3,0	2,5
15-20	3,4	3,1	2,7	2,4
20-25	4,2	3,5	3,4	3,1
25-30	4,8	4,3	4,1	3,8
30-35	5,4	4,7	4,5	4,4
35-40	6,0	5,4	5,1	5,0
40-45	6,7	6,1	5,8	5,8
45-50	6,8	6,5	6,2	6,2
Depth m.b.s.l.	CPTu_5	CPTu_6	CPTu_7	CPTu_8
0-10	4,2	5,2	5,2	5,0
10-12	2,8	2,5	3,2	2,7
12-14	3,1	3,2	3,0	3,0
14-15	2,8	2,8	3,5	3,2
15-20	2,6	2,7	2,8	2,7
20-25	3,2	3,1	3,2	3,4
25-30	3,8	4,1	3,9	4,0
30-35	4,3	4,3	4,4	4,7
35-40	5,0	5,0	5,1	5,4
40-45	5,7	5,7	5,6	6,0
45-50	6,1	6,0	6,2	6,5

The following comments can be made with regard to the comparison of the idealized underground model with the evaluated data of the single test:

The following comments can be made with regard to the comparison of the idealized underground model with the evaluated data of the single test:

- a) Both types of recreated constrained modulus input data sets (the first with the net area ratio $a = 0,75$; the second with the coefficient $\alpha = 6$) show a reasonably good agreement with the evaluated average numbers from data points charts from the Investigation-1.
- b) The evaluation results given in the Investigation-1 state that in the upper part of deposit (0-15m) the stiffness values assessed with the coefficient $\alpha = 6$ are lower than the estimated with the soil behavior type index I_c . Contrary to this interpretation, the spreadsheet evaluation indicates following:
 - In the depth 0-10m, where the first layer is assigned, the stiffness in CPTu_1, CPTu_2, CPTu_3 and CPTu_5 evaluated with the coefficient $\alpha = 6$ is lower than the stiffness based on the soil behavior type index I_c ; in CPTu_4, CPTu_6 and CPTu_8 the stiffness evaluated with the coefficient $\alpha = 6$ is 110% higher than the stiffness based on the soil behavior type index I_c ; in CPTu_5 both methods show the same result.
 - In the depth 10-14m, where stiffness is evaluated and assigned for two 2m thick layers, in CPTu_1 and CPTu_2 and stiffness evaluated with the coefficient $\alpha = 6$ is lower than the stiffness based on the soil behavior type index I_c ; in other six CPTu the stiffness the stiffness evaluated with the coefficient $\alpha = 6$ is 110-130% higher than the stiffness based on the soil behavior type index I_c .
 - In the depth 14-15m the stiffness evaluated with the soil behavior type index I_c is lower for all eight CPTu. On the average, the stiffness estimated with the coefficient $\alpha = 6$ is 115-140% higher.
 - In the depth 15-50m the stiffness evaluated with both methods show a constant increase in all eight CPTu tests: with the soil behavior type index I_c from 2 MPa to 5,8 MPa; with the coefficient $\alpha = 6$ from 2,5 MPa to 8,2 MPa.

This difference may be attributed to the fact that the evaluation of stiffness with the soil behavior type index I_c includes directly measured parameters, such as cone resistance q_c and sleeve friction f_s , which provide better understanding of subsoil conditions. The evaluation with only one coefficient $\alpha = 6$ for the whole underground lacks precision and may be considered as less sensitive.

- c) The discrepancies between proposed average input values from the report and the values estimated in the spreadsheets can mainly be attributed to the evaluation method, which can be based on personal judgement.

Generally, the evaluated results from the programmed spreadsheets (where the net area ratio $a = 0,75$ and coefficient $\alpha = 6$ are assigned, because such numbers are provided in the report), show the reasonably good agreement with the provided stiffness profile of the idealized model.

2. Permeability

As discussed in section 3.5.2.4, the permeability values estimated with correlations do not show a good agreement compared to the results of dissipation tests. The conservative approach is to use the higher values. In this case, the higher numbers are obtained from the correlations.

As discussed in chapter 3.4, for simulations with the software two types of permeability are used: the equivalent vertical permeability determined with the CUR 191 (1997) method for the part of subsoil from the ground level to 25m.b.s.l. depth; the vertical coefficient of permeability for the part of the underground below 25m depth.

The principle of discretization used for the assignment of permeabilities does not consist of as many layer as the principle used for stiffnesses. Here, the equivalent vertical permeability defined with the CUR 191 (1997) method is estimated from the hydraulic properties of soil in the 15-25m.b.s.l. depth interval and then assigned for the whole layer, where vertical drains are planned. The implementation of equivalent vertical permeability based on the permeability in the 15-25m.b.s.l. depth interval, as it was as well done in Chapter 3.4, allows to skip the evaluation of the horizontal coefficient of permeability for the above laying soils. Thus, the average values of permeability are calculated for three depth intervals: 15-25, 25-35 and 35-50m.b.s.l. In turn, the same ratio of k_h/k_v calculations is assigned for all three depth intervals as in previous calculations for the lower layer.

Note that for the soil in the depth 25-50m.b.s.l. the vertical coefficient of permeability k_v must be used in the assessment of settlement in the software.

The resulting input values of permeability are given in Table 21.

Table 21 Approximated input values of permeability k [m/s]

Depth m.b.s.l.	CPTu_1	CPTu_2	CPTu_3	CPTu_4
0 - 25	5,3E-07	3,2E-07	2,7E-07	3,7E-07
25 - 35	3,2E-10	2,6E-10	2,9E-10	2,2E-10
35 - 50	2,8E-10	2,3E-10	2,9E-10	2,2E-10
Depth m.b.s.l.	CPTu_5	CPTu_6	CPTu_7	CPTu_8
0 - 25	2,3E-07	2,6E-07	2,4E-07	2,6E-07
25 - 35	2,0E-10	3,6E-10	2,0E-10	2,3E-10
35 - 50	2,1E-10	2,5E-10	2,0E-10	2,3E-10

3.5.2.8 Results

The input values for eight CPTu tests are presented summarized in Table 20 and Table 21.

Calculations are carried out with the applied condition of closed lower bound, as in chapter 3.4.

In total five cases are investigated. Four cases are dedicated for settlement due to roads with variable life loads, as it is defined by the Client; one case is dedicated for the settlement due to the structures.

In the Project the ratio of generated settlement 20 years after preloading for roads and 50 years after preloading for structures is limited with the maximum value of 15cm. The effective settlement (see the section 3.3.1.3) for all eight CPTu tests with different loadings are summarized in Table 22.

Table 22 Effective settlement evaluated for all eight CPTu with variable loading conditions

Effective settlement [cm]	Corresponding life loads for roads				Structures
	0kN/m ²	10 kN/m ²	20 kN/m ²	30 kN/m ²	16.00 kN/m ²
CPTu_1	8,4	12,4	16,5	20,7	20,6
CPTu_2	7,9	11,9	16	20,2	20,2
CPTu_3	8,2	12,8	17,5	22	22
CPTu_4	6,7	12,3	17,1	22,1	22,1
CPTu_5	6,7	11,1	15,5	20,1	20
CPTu_6	7,8	13,5	18,3	29,9	23,2
CPTu_7	6,9	11	15,2	19,5	19,4
CPTu_8	7,1	11,4	15,7	20,0	20,1

Resulting five sets of log time – settlement curves are presented in Appendix D with corresponding delimitating lines. These corresponding delimitating lines are illustrated in Figure 64, Figure 65, Figure 66, Figure 67 and Figure 68 below. In four cases with the different life loads for roads, the delimitating lines indicate the identical behavior until the reloading stage, because the applied loading do not change until then.

After these sets of log time – settlement curves and delimitating lines were compared, the following remarks are made:

- The blue delimitating line, which is composed of the lowest settlement values (lower bound), within the first two months of the excess preloading corresponds the part of the log time – settlement curve of CPTu_7 and after two months till the end of calculations it corresponds the log – time settlement curve of CPTu_1.
- The red delimitating line, which is composed of the highest settlement values (upper bound), almost entirely (with the exception of the first 10 days) repeats the log time – settlement curve of CPTu_4.
- Two above mentioned statements are applicable for all five loading cases.

The above mentioned remarks are likely to be influenced by:

- The stiffness profile evaluated for CPTu_4 has the lowest values of all eight CPTu tests. The lower is the stiffness, the higher is the final settlement. This explains, why the blue delimitating line corresponds the log time – settlement curve of CPTu_4.
- CPTu_7 stiffness profile show on average higher values in the upper 15m thick layer (Formation A) than other CPTu tests. As well, the lower permeability was evaluated within the whole thickness of this CPTu profile. This may be linked to the fact that evaluated settlement for CPTu_7 is lower than in other CPTu tests within first two months.
- CPTu_1 stiffness profile indicates the highest values of all eight evaluated CPTu tests. This is especially obvious in the Formation B (15-50m.b.s.l.). The higher is the stiffness, the lower is the final settlement. This may be used as an explanation, why the blue delimitating line partially corresponds the log time – settlement curve of CPTu_1.
- Note that the net area ratio $a = 0,75$ used in the estimation of settlement is not provided in the report and was calibrated (see section 3.5.1.3). The lower is the calibrated net area ration, the higher is the evaluated stiffness and the higher is the estimated permeability.

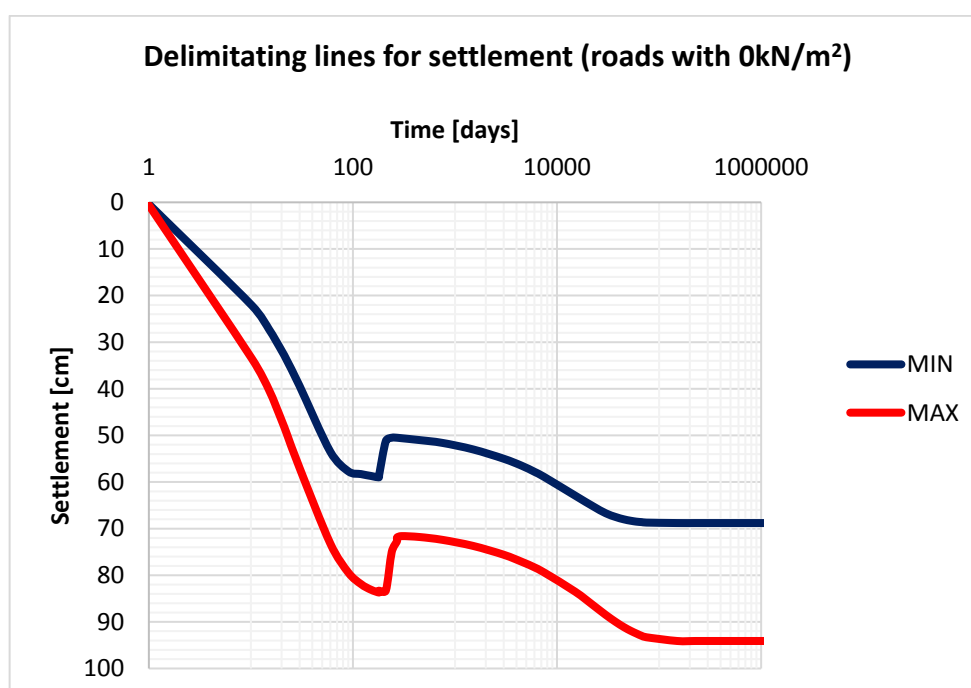
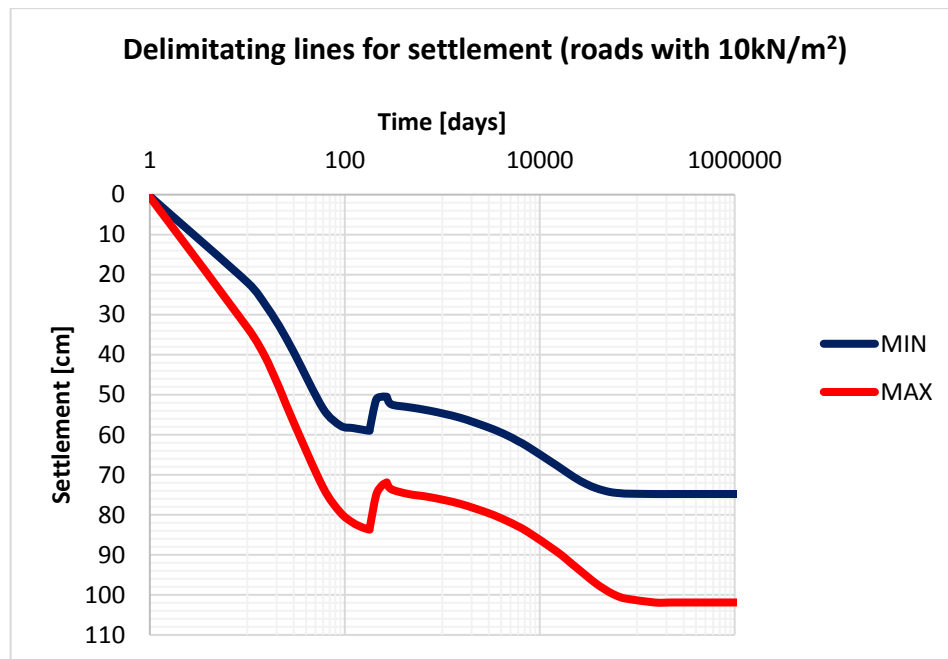
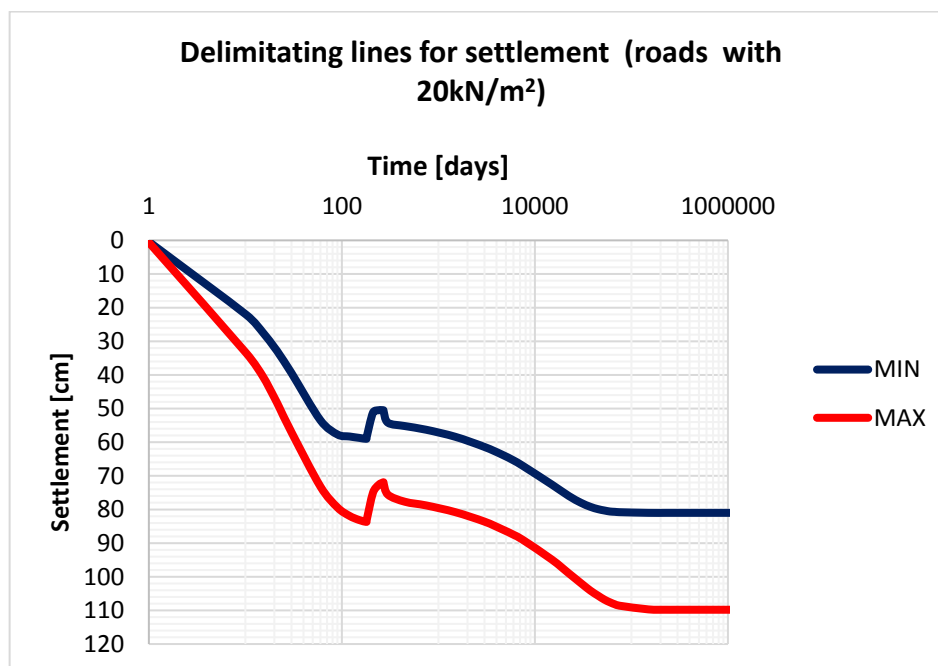


Figure 64 Delimitating lines for settlement with 0kN/m^2 for roads

Figure 65 Delimitating lines for settlement with 10kN/m² for roadsFigure 66 Delimitating lines for settlement with 20kN/m² for roads

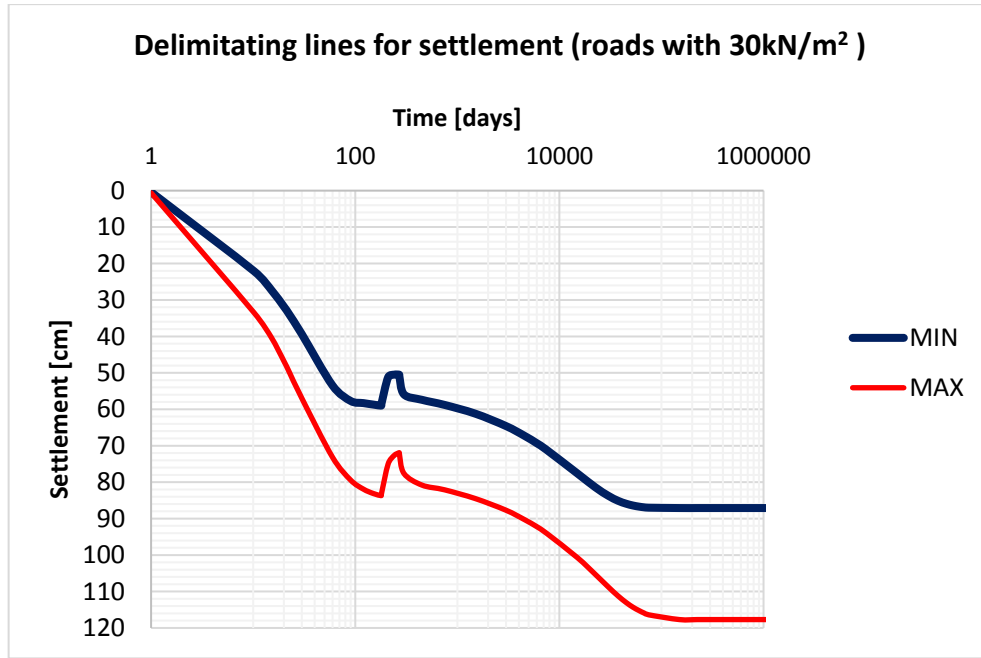


Figure 67 Delimitating lines for settlement with 30kN/m² for roads

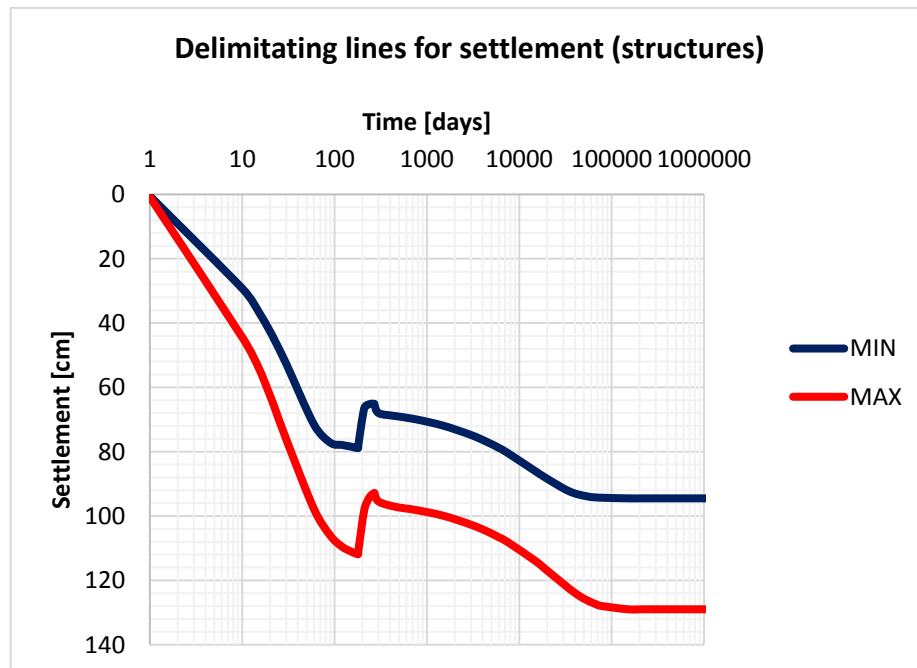


Figure 68 Delimitating lines for settlement with 16kN/m² for structures

3.5.3 Investigation-2

In January, 2017 eight additional CPTu tests (Investigation-2) were performed as a part of extended underground exploration study. The new tests have been numbered

according to the detailed division of the construction site into the smaller areas. Approximate locations of new tests are sketched in Figure 69.

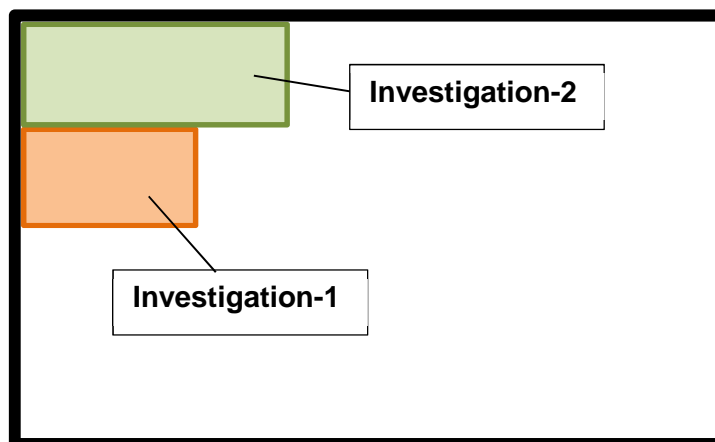


Figure 69 Sketched locations of Investigation-1 and Investigation-2

The tests are listed under following names: CPTu_135, Cptu_136, CPTu_137, CPTu_143, CPTu_144, CPTu_145, CPTu_151 and CPTu_151.

This section provides estimated geotechnical properties and calculated settlement rates, determined from these new eight piezocone tests. The estimation of geotechnical properties is carried out with the previously programmed spreadsheets.

3.5.3.1 Comparison of new CPTu data with delimitating lines for constrained modulus M_{lc}

The plots of constrained modulus M_{lc} , generated with the previously programmed spreadsheets, for the new data are compared with the previously determined delimitating lines. The comparison of each separate new CPTu with the delimitating lines is shown in Appendix E. Figure 70 shows the comparison of all eight new CPTu tests with delimitating lines in one picture.

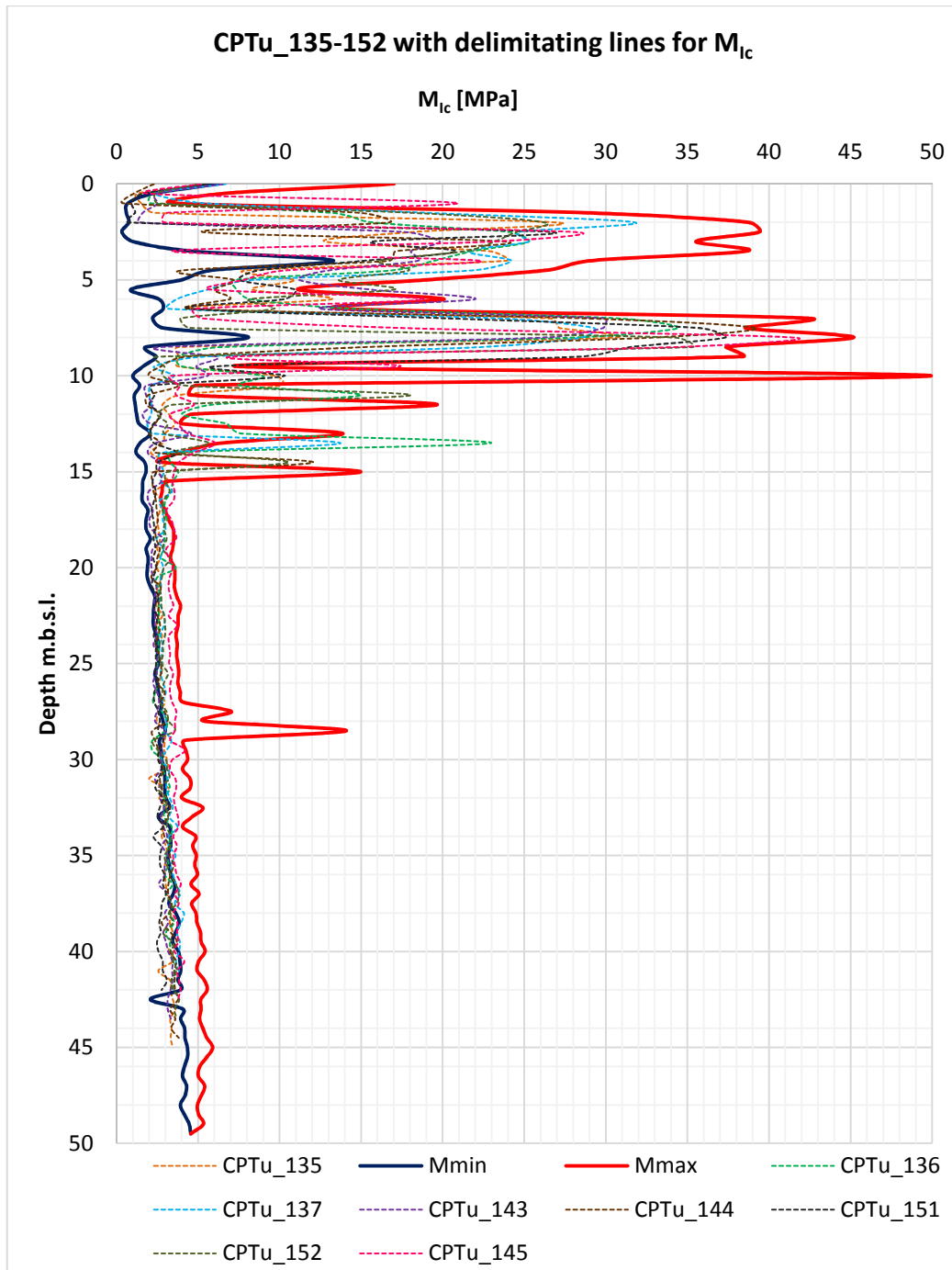


Figure 70 Comparison of new CPTu tests with the delimitating lines

The eight assessed CPTu tests show in general an average agreement with the created delimitating lines. The eight new interpretations indicate the presence of two layer: the upper with the average thickness of 15m contains the soil interlayering with the wide range of stiffness (from 1,0 to 47,0 MPa); the lower layer which starts approximately at

the depth of 15m.b.s.l. in the all eight cases indicates a slight increase in stiffness with depth.

In the upper layer the assessed graphs of constrained modulus M show the tendency to stay close to the middle part of the delimited area. In the lower part, the eight new generated graphs are either closer to the blue delimitating line, which defines the combination of lowest stiffness values from the first eight CPTu tests, or from the depth of 25m.b.s.l. they indicate the tendency to stay outside the area, limited by previous estimations. It suggests the lower stiffness in the upper layer in the new eight tests than in the idealized model.

The calculations with these eight tests are likely to show higher values of total settlement due to the lower stiffness in the bottom part.

3.5.3.2 Comparison of new CPTu data with delimitating lines for horizontal coefficient of permeability k_h

The plots of horizontal coefficient of permeability k_h , generated with the previously programmed spreadsheets, for the new data are compared with the previously determined delimitating lines. The comparison of each separate new CPTu with the delimitating lines is shown in Appendix E. Figure 71 shows the comparison of all eight new CPTu tests with delimitating lines in one picture.

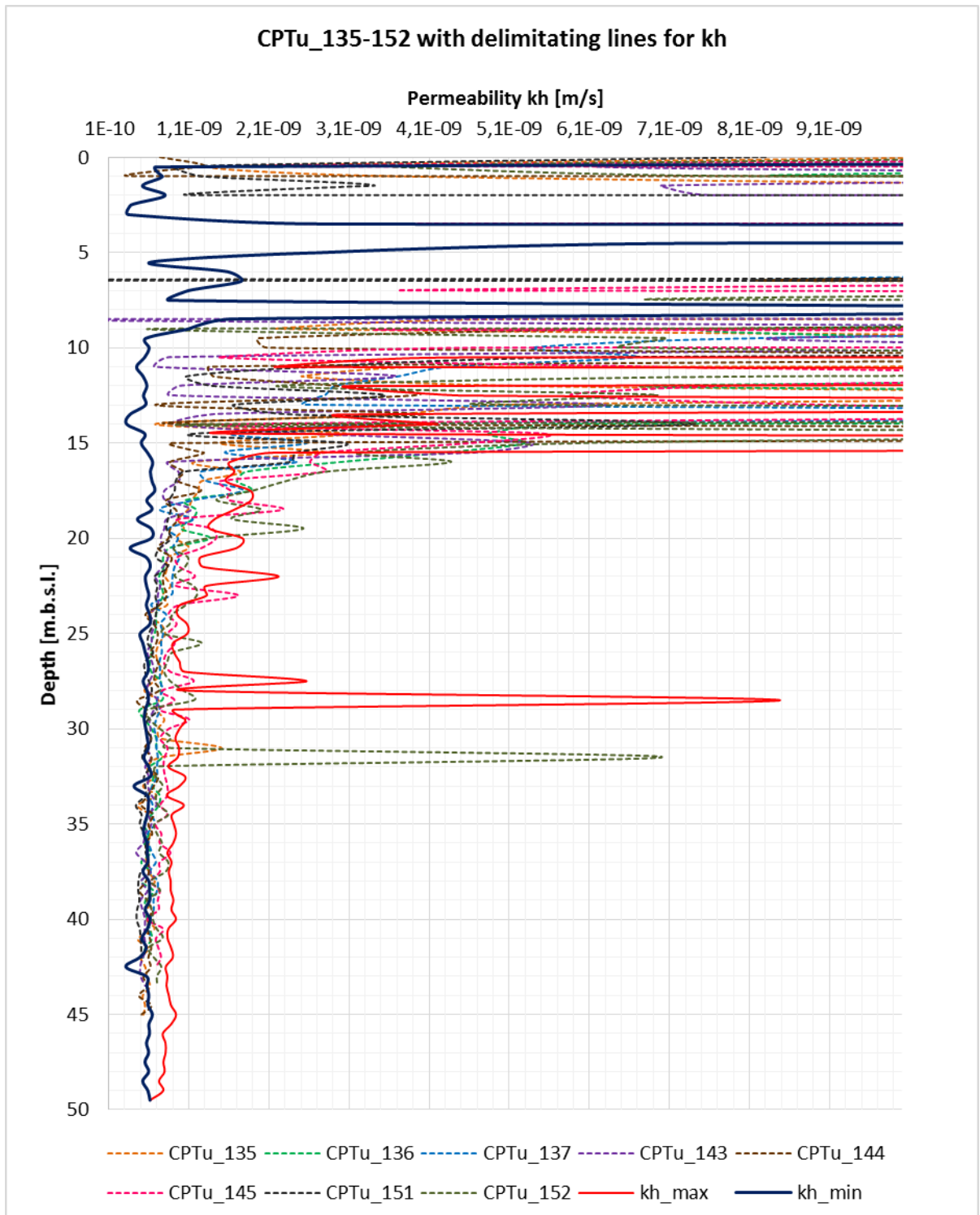


Figure 71 Comparison of new CPTu tests with delimitating lines

The assessed graphs of horizontal coefficient of permeability from the eight new piezocone tests are compared with the delimitating lines from the previous tests.

The assessment of the new tests has indicated that in the area, where these new tests were executed, the horizontal coefficient of permeability strongly varies with the depth. The three main depth intervals can be defined: the upper 0-15, the middle 15-25 and the lower 25-50m.b.s.l. In the upper part the hydraulic conductivity is strongly influenced by the interlayering of soils and shows the highest values. In the middle part the hydraulic conductivity gradually reduces and for the all evaluated tests at the bottom point of the middle part is lower than $1,0E-09$ m/s (with the exception to CPTu_145 and CPTu_152). In the bottom interval all eight cases indicate close to the constant permeability. Based on recommended permeability values by Robertson (2012), the permeabilities lower than $1,0E-09$ m/s are indicators of clayey soils. In the bottom part all eight cases show the tendency to be closer to the blue delimitating line than to the red. That suggest the general trend of lower permeability.

However, note that the horizontal coefficient of permeability assessed with empirical correlations is significantly higher than permeability values from the dissipation test.

3.5.3.3 Comparison of new CPTu data with delimitating lines for soil behavior type (SBT) based on the soil behavior type index I_c

The plots of soil behavior type (SBT), generated with the previously programmed spreadsheets, for the new data are compared with the previously determined delimitating lines. The comparison of each separate new CPTu with the delimitating lines is shown in Appendix E. Figure 72 shows the comparison of all eight new CPTu tests with delimitating lines in one picture.

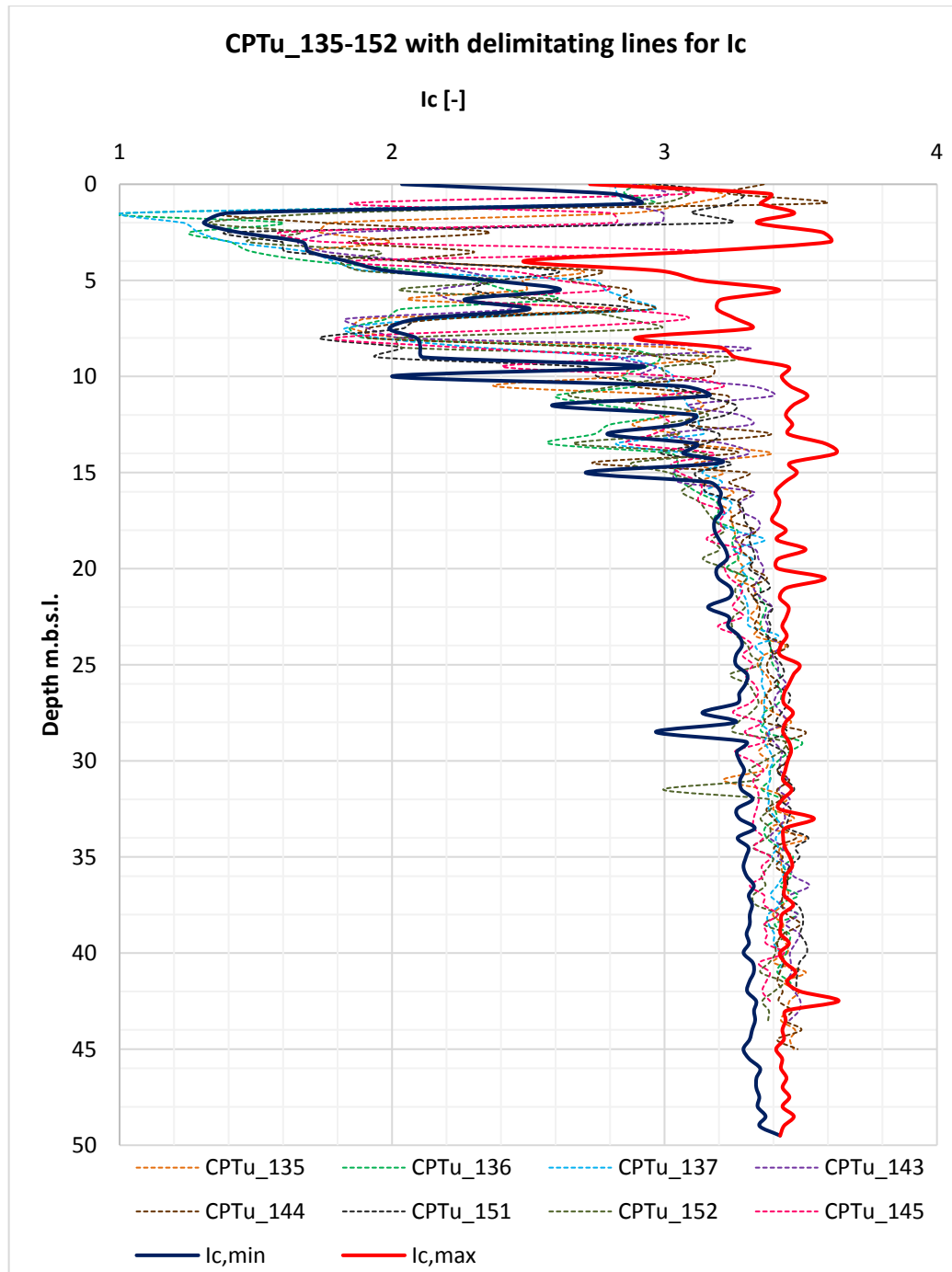


Figure 72 Comparison of generated soil behavior type (SBT) based on the soil behavior type index I_c graph for new CPTu tests with previously plotted delimitating lines

The soil behavior type index graphs obtained from the new eight CPTu tests show the general trend of lower index values in the upper layer and higher index values in the lower. In the Formation A the generated graphs are closer or partially overlap with the blue delimitating line. In the Formation B generated graphs tend to be closer to the red delimitating line or from the depth of approximately 25m.b.s.l. and later overlap with this

line or cross it. According to Robertson (2012), the higher is the soil behavior index I_c , the higher is the contain of fine particles in the soil.

3.5.4 Comparison of dissipation tests

Dissipation tests estimate the in-situ horizontal coefficient of permeability in soils. The permeability of soils is measured on the basis of excess pore water pressure decay, caused by mechanical penetration of the cone, when the test is stopped at the certain depth. The coefficient of permeability is a function of t_{50} (see section 2.4.1).

3.5.4.1 Dissipation tests from CPTu_135-152

After the new CPTu tests were performed in January 2017 (Investigation-2), the new dissipation test data was received in February.

As with the first piezocone tests, these recent CPTu tests were each followed by 4 dissipation tests. However, the recent dissipation tests were performed at different depths than previously. Also, the recent data does not include the evaluation of hydraulic permeability based on t_{50} .

Thus, the missing estimation of hydraulic conductivity from dissipation tests is performed by the means of programmed Excel spreadsheets, which go through the single dissipation test and check, whether it is complete or not. The dissipation test is complete, when the p_{50} is reached (see section 2.4.1). If this assumption is not satisfied, the hydraulic conductivity cannot be evaluated with the spreadsheet and must be extrapolated.

In the spreadsheets next considerations are adopted:

- a) Unit weight of groundwater is practice-oriented and prescribed as $\gamma_w=10\text{kN/m}^3$ for all calculations.
- b) The hydrostatic ground water pressure or ground water pressure at rest is a product of the unit weight of ground water and the depth, at which the tests are performed.
- c) Within the first seconds of a dissipation test the ground water is not in the balanced condition anymore. Due to this, first several values of measured excess pore water pressure might show a significant upswing contrary to the rest measurements. The initial measurements of questionable excess pore water pressure are excluded from interpretations.
- d) The $p_{50\%}$ is estimated as it is explained in section 2.4.1.

- e) Lastly, the data is filtered for possible false results- for example, if dissipation test was terminated and performed again, but the measurements were still recorded.

The graphs (output of spreadsheets) are presented in the Appendix F. Dissipation curves are plotted on the right hand side of the sheet. Curves are plotted twice: with regular and logarithmic horizontal x axis. The logarithmic plot is used as a tool to perform a rough estimation of OCR.

The graphs (see Appendix F) indicate the following results with dissipation test data:

1. The depth intervals are not the same as in previous CPTu tests. Here tests are performed each 10m.
2. Dissipation tests in lower layers are not performed the value $p_{50\%}$.
3. Taking into account the rapid increase of pore water pressure due to the mechanical penetration of the cone, the log time – most of pressure plots indicate the reasonable (up to 50kPa) increase of excess pore water pressure in the beginning of tests. It may be interpreted as the sign of light overconsolidation in soils.
4. The influence of factual surface level to the depth of each test is neglected.

Hydraulic permeabilities, calculated in the spreadsheets, are summarized in Table 23. Note that “Evaluation impossible” in this table means that the test was not performed properly.

Table 23 Values of hydraulic permeability for dissipation tests, approximated with the programmed spreadsheets

CPTu	Depth [m]	Estimated permeability k_h [m/s]	CPTu	Depth [m]	Estimated permeability k_h [m/s]
CPTu_135	10,04	2,4E-09	CPTu_136	10,26	1,9E-09
	15	2,6E-09		15	4,8E-09
	25	Extrapolation		25	Extrapolation
	35	Extrapolation		35	Extrapolation
CPTu_137	10	4,1E-07	CPTu_143	10,62	6,8E-09
	15	4,0E-09		15	6,9E-09
	25	Extrapolation		25	Extrapolation
	35	Extrapolation		35	Extrapolation
CPTu_144	10,06	1,9E-09	CPTu_145	10,04	Estimation impossible
	15	2,0E-09		15	6,9E-09
	25,02	Extrapolation		25,02	Extrapolation
	35	Extrapolation		35	Extrapolation
CPTu_151	11,58	2,2E-09	CPTu_152	10,18	Estimation impossible
	15	1,5E-08		15,18	1,7E-08
	25,26	Extrapolation		25	Extrapolation
	35	Extrapolation		35	Extrapolation

3.5.4.2 Comparison of results

The dissipation test results from recent CPTu tests can be compared only in the extent of the upper layer or so-called Formation A. Figure 73 serves this purpose.

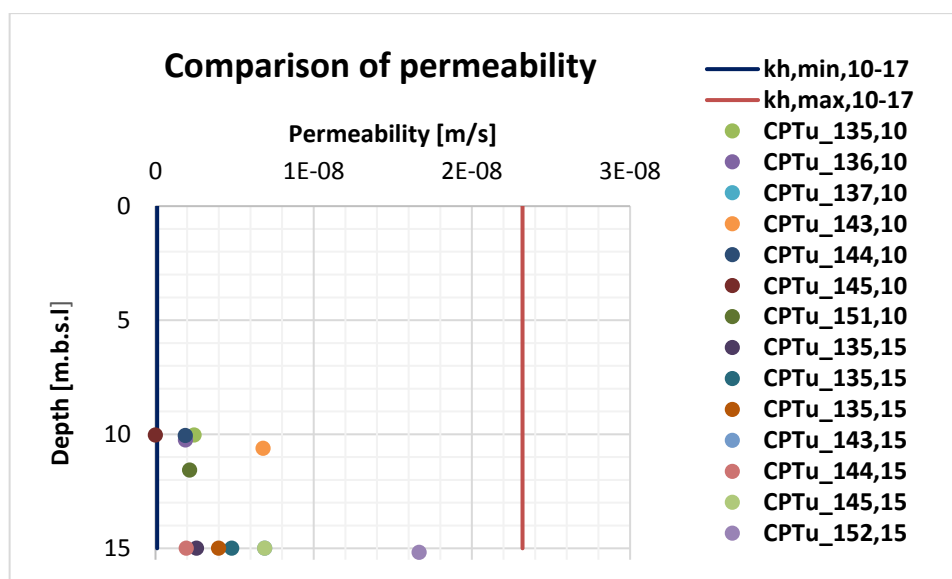


Figure 73 Comparison of dissipation tests for CPTu_132-152 with the delimitating lines

The horizontal coefficient of permeability estimated with CPTu_137 at the depth of 10m.b.s.l. is much higher than other values ($4,1E-07$ m/s) and does not fall into the estimated range (nor in this plot). Otherwise, the results of dissipation tests from the new eight CPTu tests show a very good agreement with the previously defined delimitating lines. Most of recently estimated values lay in the range within $1,9E-09$ – $6,8E-09$ m/s in the depth 10-12m.b.s.l. and $2,0E-09$ – $1,7E-08$ m/s in the depth 15-15,5m.b.s.l.

3.5.5 Comparison of time – settlement curves from the new CPTu data with the delimitating lines

The further settlement interpretation is performed with the horizontal hydraulic permeability, evaluated with the empiric correlations, due to the lack of data from dissipation tests. As well, higher values obtained with empiric correlations are considered as the conservative approach.

The settlement estimation for the new CPTu_135 – 152 is carried out in the same way as for previous CPTu tests. In the previous sections a good agreement of created constrained modulus M_{lc} and horizontal coefficient of permeability k_h with the delimitating lines was observed. Thus, the input values of stiffness and permeability were evaluated in the same way as for the first set of piezocone tests.

Input values for the new eight CPTu are summarized in Table 24 and Table 25. If the CPTu tests has not reached the depth 45m.b.s.l, the stiffness of previous sublayer is assigned to it.

Table 24 Input stiffness E [MPa] for CPTu_135- 152

Depth m.b.s.l.	CPTu_135	CPTu_136	CPTu_137	CPTu_143
0-10	4,5	5,2	5,4	5
10-12	3,2	3,6	2,7	2,7
12-14	3	4,3	3,3	2,8
14-15	3,1	4	3,3	3
15-20	2,9	3,4	3	2,7
20-25	3,3	3,3	3,1	3
25-30	3,8	3,6	3,4	3,5
30-35	4,1	4,1	3,8	3,9
35-40	4,4	4,5	4,2	4,4
40-45	4,8	4,8	4,4	4,8
45-50	4,8	4,8	4,4	4,8
Depth m.b.s.l.	CPTu_144	CPTu_145	CPTu_151	CPTu_152
0-10	4,9	5,1	5,2	5,3
10-12	2,7	3,6	3	3,6
12-14	3,2	3,6	2,7	3,1
14-15	3,4	3,5	3,3	3,9
15-20	2,8	3,6	2,8	3,3
20-25	3,2	3,8	3	3,5
25-30	3,6	4,2	3,4	3,8
30-35	4,1	4,6	3,7	4,2
35-40	4,7	5	4,1	4,6
40-45	5	5,3	4,4	5

Table 25 Input permeability k [m/s] for CPTu_135 – 152

Depth m.b.s.l.	CPTu_135	CPTu_136	CPTu_137	CPTu_143
0 - 25	4,2E-07	7,2E-07	3,8E-07	3,9E-07
25 - 35	2,6E-10	2,6E-10	1,9E-10	2,0E-10
35 - 50	1,9E-10	1,4E-10	1,6E-10	1,8E-10
Depth m.b.s.l.	CPTu_144	CPTu_145	CPTu_151	CPTu_152
0 - 25	3,5E-07	7,8E-07	4,8E-07	1,0E-06
25 - 35	2,2E-10	2,8E-10	1,9E-10	3,2E-10
35 - 50	2,0E-10	2,4E-10	1,7E-10	2,4E-10

In general, the approximated permeability in the upper 25m thick layer is 2 – 3 times higher than in the CPTu_1 – 8 and slightly lower in the lower layer (25-50m.b.s.l.).

The stiffness in the Formations A (0-15mb.s.l.) show similar values to the first eight CPTu tests. However, in the Formation B the stiffness approximated for the new eight CPTu tests is on average 10 – 20% lower than in the previous set of tests. Also, it should be noticed that the new tests were not performed to the depth below 45m.b.s.l. mark and the stiffness value for the lowest 5m thick layer is equal to the stiffness from the layer above.

The estimated log time – settlement curves for the eight new CPTu are compared with the delimitating lines in the next figure.

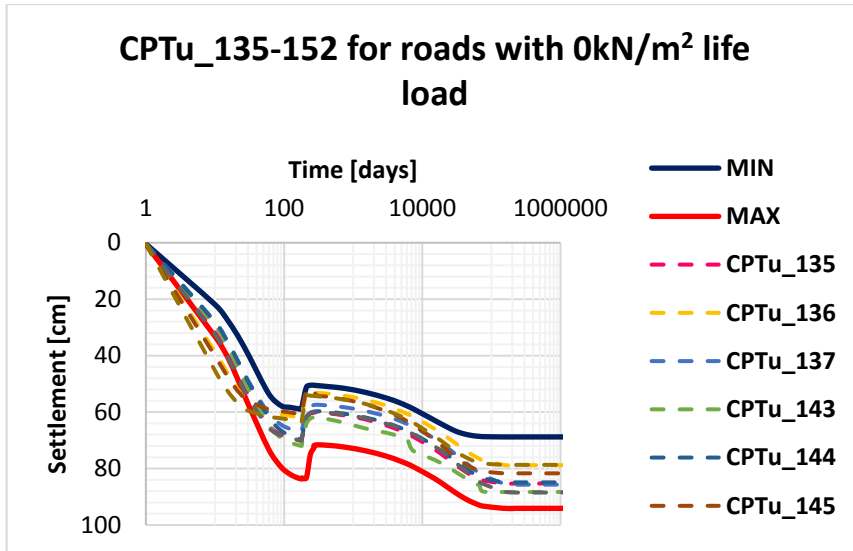


Figure 74 Comparison of log time - settlement curves for the eight new CPTu with the delimitating lines for roads with 0kN/m² life load

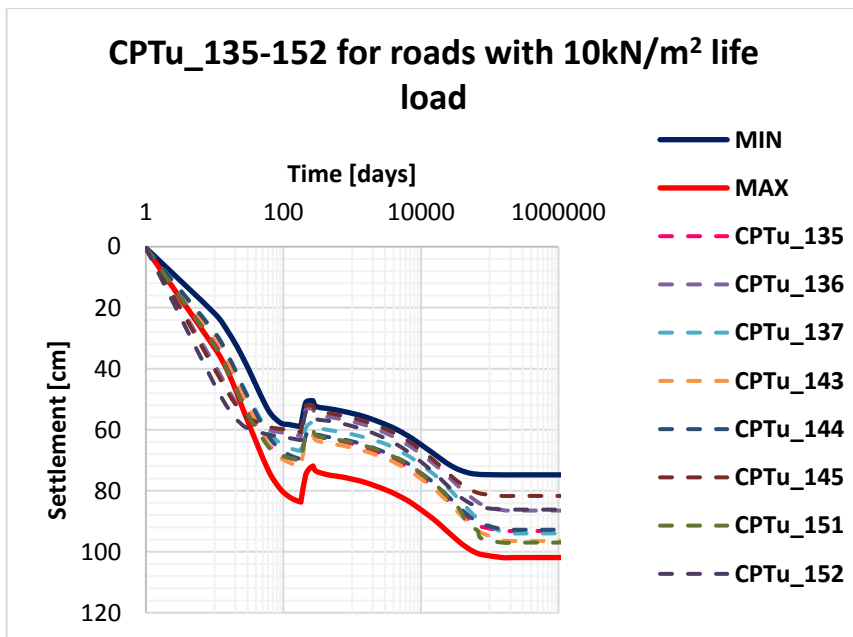


Figure 75 Comparison of log time - settlement curves for the eight new CPTu with the delimitating lines for roads with 10kN/m² life load

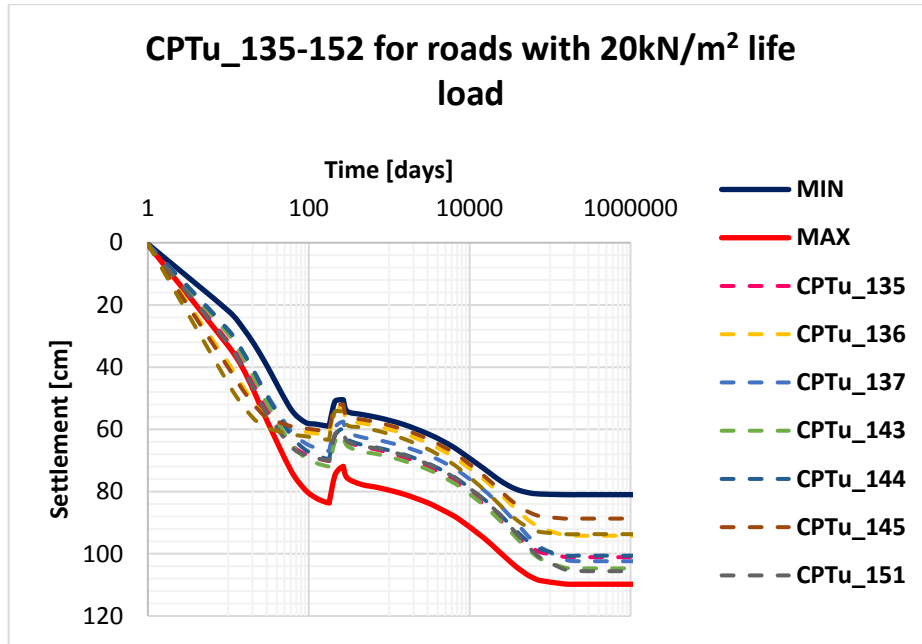


Figure 76 Comparison of log time - settlement curves for the eight new CPTu with the delimitating lines for roads with 20kN/m² life load

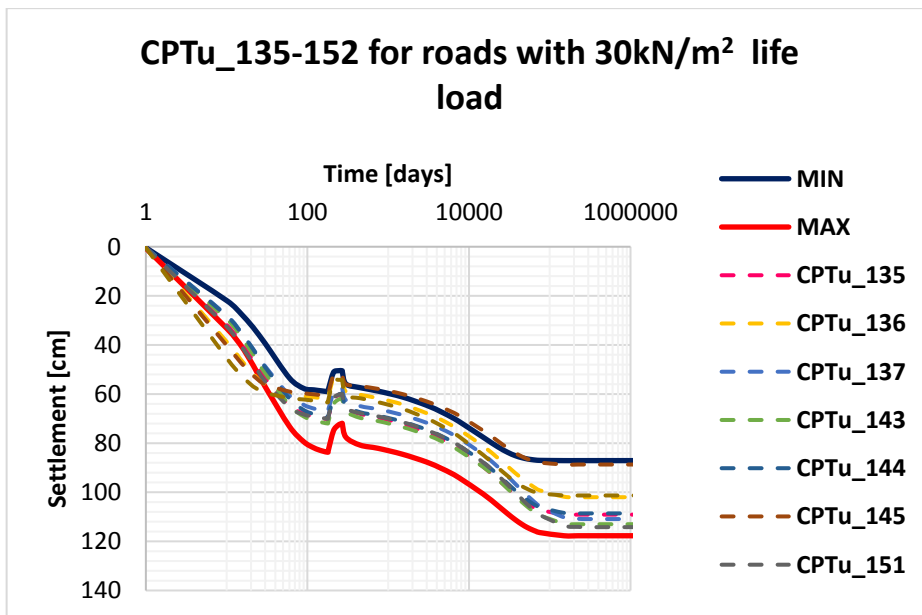


Figure 77 Comparison of log time - settlement curves for the eight new CPTu with the delimitating lines for roads with 30kN/m² life load

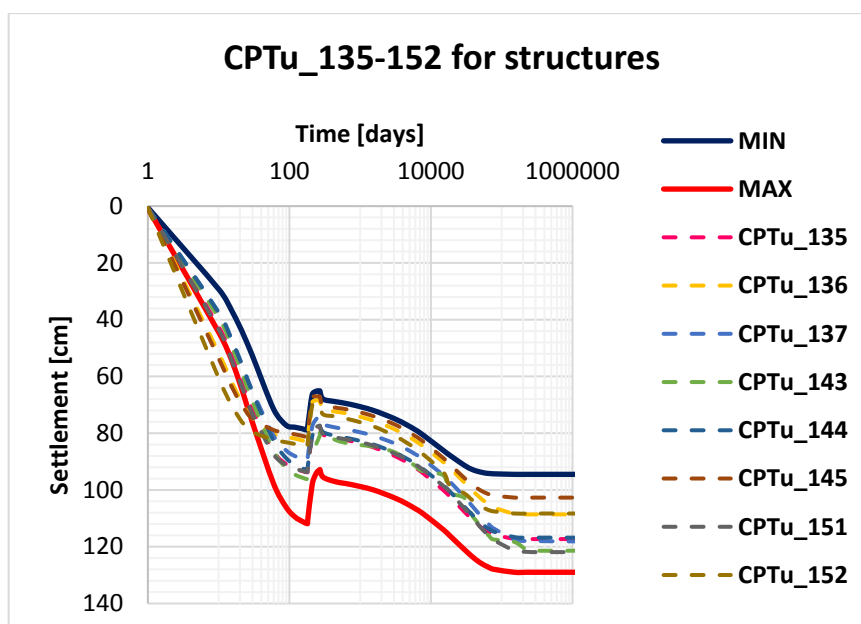


Figure 78 Comparison of log time - settlement curves for the eight new CPTu with the delimitating lines for structures with 16kN/m^2 life load

The eight new log time – settlement curves are compared with the delimitating lines and general observations state that:

- In all five cases the estimated settlement within the first several months for CPTu_136, CPTu_145 and CPTu_152 is outside the area, limited with the delimitating lines (they are below the red delimitating line). At the same time CPTu_135 and CPTu_151 overlap with the same red delimitating line. CPTu_137, CPTu_143 and CPTu_144 within the same time stay inside the area, marked by the delimitating lines.
- After approximately 3 months of the excess preloading, all eight log time –settlement curves of new CPTu tests stay inside the area, marked out by the delimitating lines.

The effective settlement of eight new CPTu is summarized in Table 26.

Table 26 Effective settlement [cm] approximated for CPTu_135 – 152 and the delimitating lines

Effective settlement [cm]	Corresponding life loads for roads				Structures
	0kN/m ²	10 kN/m ²	20 kN/m ²	30 kN/m ²	16 kN/m ²
CPTu_135	8,6	13,1	17,6	22,2	24,6
CPTu_136	8,6	12,8	17,1	21,3	23,6
CPTu_137	7,7	11,9	16,1	20,4	22,7
CPTu_143	7,8	12,2	16,6	21,1	20,1
CPTu_144	7,9	12,3	16,6	21,1	23,2
CPTu_145	8,5	12,6	16,7	21	23,7
CPTu_151	7,9	12,2	16,5	20,9	23,4
CPTu_152	9,5	13,9	18,4	22,9	28,2
Blue delimitating line (lower bound)	8,4	12,4	16,5	20,6	22,4
Red delimitating line (upper bound)	6,7	12,3	17,1	22,1	23,1

The comparison of provided graphs and data in Table 26 can be summarized with following statements:

- a) The evaluated effective settlement in the eight new CPTu tests CPTu135-152 shows a good agreement with the effective settlement, evaluated for the eight first CPTu tests, because the effective settlement estimated for two delimitating lines corresponds two critical cases from the first underground estimation with the piezocone tests (see comments in section 3.5.2.8).
- b) The CPTu_152 shows the highest effective settlement in comparison to other 7 tests. Even though the stiffness profile evaluated for this test varies in the same range as seven other stiffness profiles, the CPTu_152 has much higher permeability in the upper 25m thick layer. Despite the similar final settlement similar to other seven

CPTu tests, the rate of consolidation in CPTu_152 is much faster and consequently, results in faster generation of settlement.

- c) Within the approximately first three months CPTu_136 and CPTu_152 possess really similar log time – settlement curves. However, at the end of consolidation CPTu_136 has higher final settlement, It is likely to be influenced by the lower stiffness of the lower part in CPTu_136.
- d) Although in all five studied cases (four cases for roads and one for structures) the calculated effective settlement shows a reasonably good agreement for all eight new CPTu tests, it does not eliminate the risk of differential settlement. 9 months after preloading soils different amount of settlement is generated in soils due to the variable stiffness and permeability. The evaluation of eight new CPTu tests has shown that settlement 9 months after preloading in the investigated area may vary within the range of 52-62cm and soil is compacted up to different depth levels. The similar tendency is seen 20 or 50 years after the preloading stage has finished (see figures with log time – settlement curves for CPTu_135-152). This is likely to result in the occurrence of differential settlement. Thus, the level of the compacted soil from which the effective settlement is measured must be taken into account.

The acceleration of consolidation and consequently of settlement is dependent on the estimated hydraulic permeability. Note that above summarized results were estimated with the hydraulic permeability based on the empiric correlations. As it was discussed in the previous section, the permeability calculated with the empiric correlations is higher than the permeability estimated from the dissipation test. Thus, the above calculated effective settlement is likely to be either overestimated, or have a really similar value, but be based on the lower values of settlement 9 months and 249 months after the beginning of preloading.

3.6 Discussion

Some points of interest, as well as unanswered questions, arise from the results of settlement calculations and performed evaluation of piezocone tests. These points are summarized in this section.

1. The unloading – reloading stiffness in the software is evaluated through the defined ratio E_{ur}/E . The ratio $E_{ur}/E = 3$ was used in previously described simulations as the most practice – oriented value. The input ratio has a direct influence on the resulting settlement, because it controls the inclination of the re-compression line in the $e - \log \sigma'$ relationship plot (see Figure 8). The lower is the E_{ur}/E ratio, the steeper is the

inclination of this line. The steeper is the inclination of the re-compression line, the higher is the recovery of the void ratio e during the swelling.

The loading case for roads with 20 kN/m^2 life load is chosen to test the influence of the ratio E_{ur}/E on calculation results. The calculations are performed with two different ratios ($E_{ur}/E = 1$ and $E_{ur}/E = 5$) for two different drainage conditions assigned at the bottom of calculation model (see section about the drainage conditions 3.4.4).

Results are graphically presented in Figure 79 and Figure 80. Figure 79 corresponds calculations with the undrained bottom boundary, while Figure 80 shows the results of calculations with the drained bottom. Resulting effective settlement is compared in Figure 81.

Figure 79 and Figure 80 show that the ratio E_{ur}/E brings in the difference as soon as the unloading stage starts. The final settlement with the ratio $E_{ur}/E=3$ and $E_{ur}/E=5$ does not show the significant difference (0,5cm with the undrained bottom boundary and 0,7cm with the drained bottom boundary). However, it can be observed that the final settlement with the ratio $E_{ur}/E=1$ is more than 3cm lower than with the ratio $E_{ur}/E=3$.

Comparison of effective settlement shows the strong influence of the chosen ratio on results. The calculations with the ratio $E_{ur}/E=1$ estimated approximately 5cm higher effective settlement than with the ratio $E_{ur}/E=3$ in both cases. The ratio $E_{ur}/E=5$ has provided, as expected, lower values of effective settlement (approximately 1cm). Thus, it can be stated that the use of the lower ratio E_{ur}/E is considered as the conservative approach.

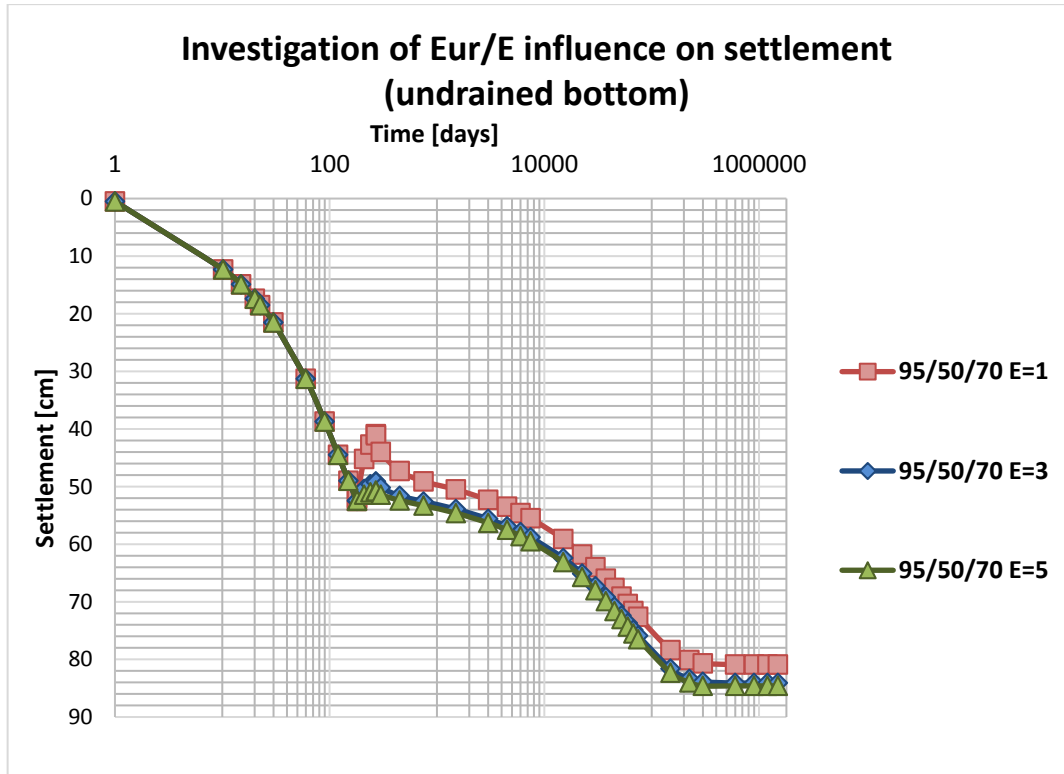


Figure 79 Influence of Eur/E ratio on settlement (undrained bottom of the model)

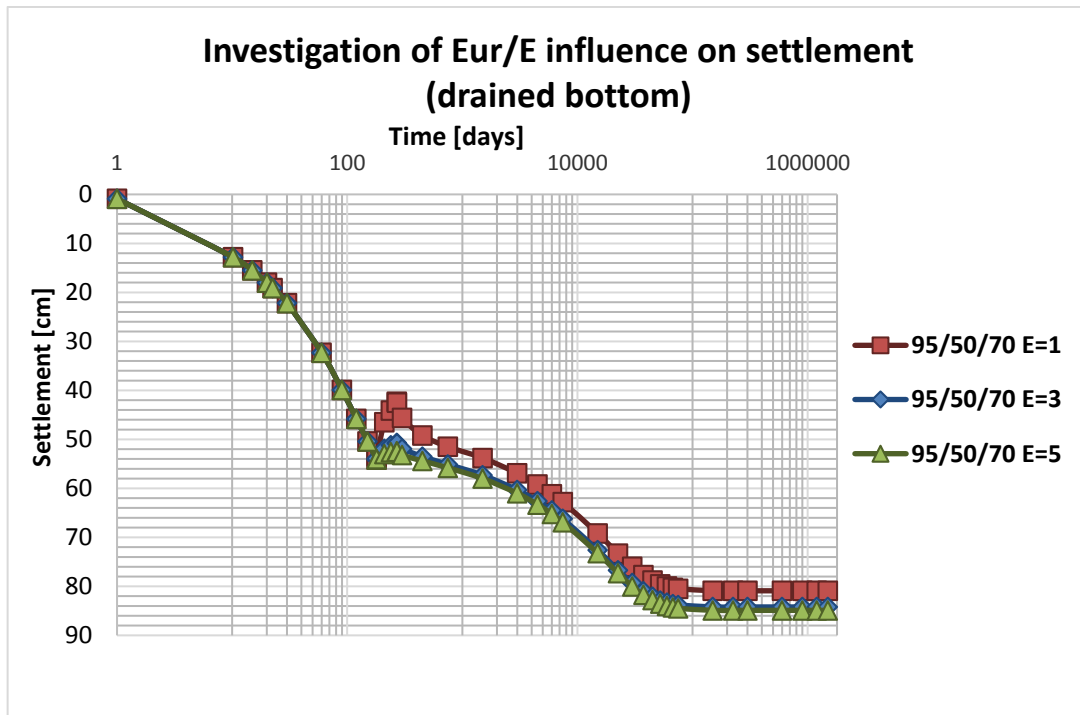


Figure 80 Influence of Eur/E ratio on settlement (drained bottom of the model)

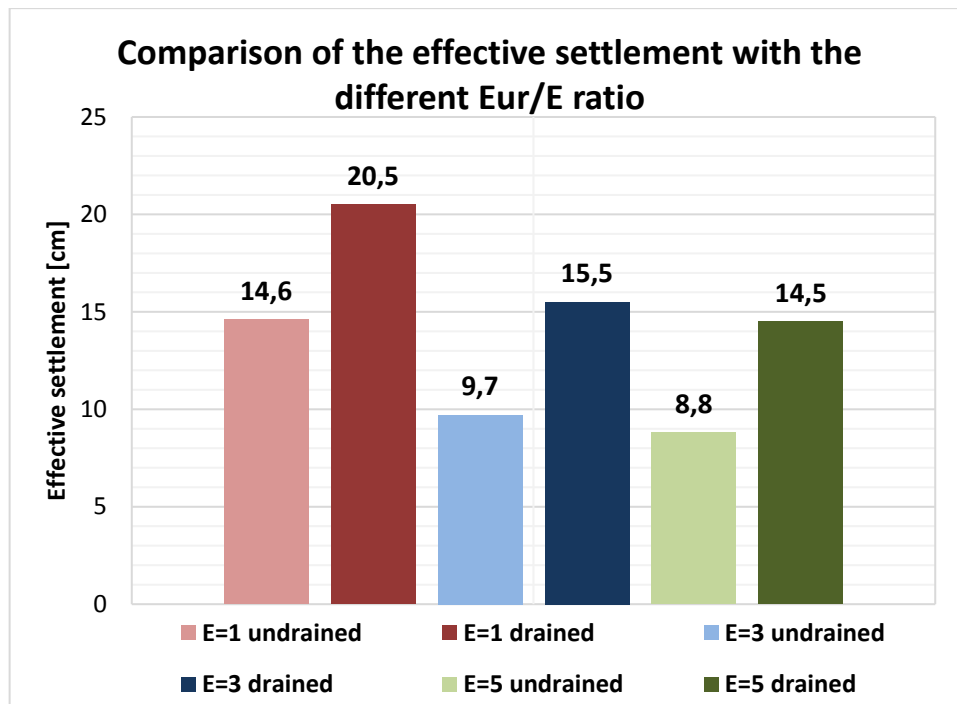
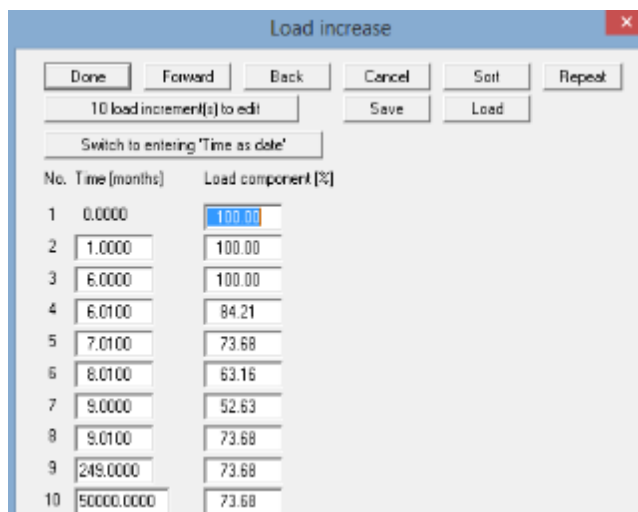


Figure 81 Comparison of effective settlement

- In settlement calculations described in section 3.4 loads in all construction stages are applied instantaneously. The influence of gradually decreasing loading is simulated for roads with 20kN/m^2 life load.

The loading variation with time for this simulation is illustrated in Figure 82. The following conditions are assigned: 1-6 months 95 kN/m^2 , 6-7 months 80 kN/m^2 , 7-8 months 60 kN/m^2 , 8-9 months 50 kN/m^2 and from 9 months 70 kN/m^2 . These values correspond the percentage in Figure 82.



No.	Time (months)	Load component (%)
1	0.0000	100.00
2	1.0000	100.00
3	6.0000	100.00
4	6.0100	84.21
5	7.0100	73.68
6	8.0100	63.16
7	9.0000	52.63
8	9.0100	73.68
9	249.0000	73.68
10	50000.0000	73.68

Figure 82 Gradual decrease of the applied loading

The resulting settlement 6, 9 and 249 months after the beginning of embankment construction are summarized in Table 27.

Table 27 Calculated settlement with gradually decreasing loading

Settlement after 6 months [cm]	Settlement after 9 months [cm]	Settlement after 249 months [cm]
52,5	51,1	59,2

This applied loading results in 8,1cm effective settlement (with the instantaneous applied loading this settlement 9,2cm). It means that instantaneous loading is a conservative approach and results in the higher effective settlement.

- The results of settlement calculations presented in section 2.4 are carried out for the area of great extent, where the stresses in soils are generated by embankments with the base area of $1.000.000\text{m}^2$ (1000m x 1000m). However, the embankment built on the Trial field has the base area of 22.500m^2 (150 x 150m). Thus, the lower stresses are generated in soils due to the lower loading. The comparison of two stress distribution models across the consolidation layers due to the different parameters of embankments is shown in Figure 83. On the left hand side of the picture the stress distribution due to the 1000m x 1000m base area is shown, while on the right hand side the stress distribution due to the 150m x 150m base area is presented.

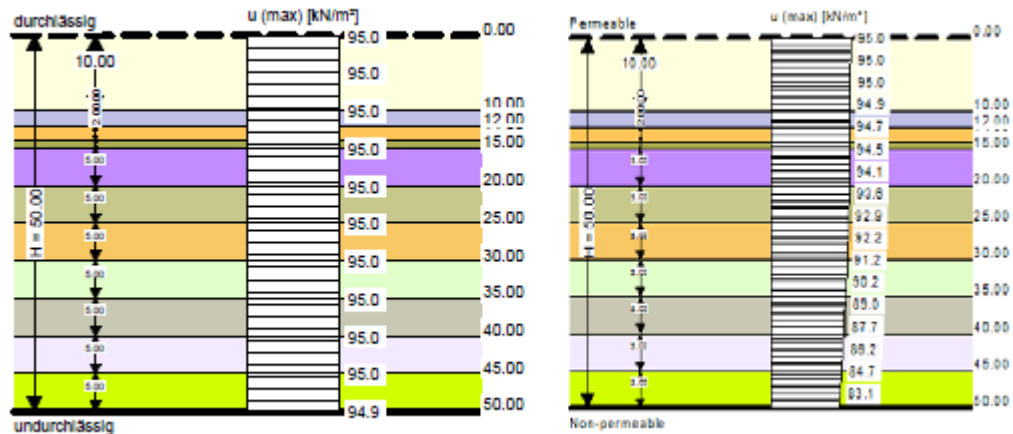


Figure 83 Stress distribution models due to different embankment' parameters

When the measured deformations in the Trial field are going to be compared to predicted settlement values, the influence of embankment size on the generated settlement must be taken into account.

- The used calculation model was simplified, when the CUR 191 (1997) approach was implemented. In order to implement this approach in calculations, the permeability of upper 10m thick layer was ignored (see section 3.4.2.3). For the whole 25m thick layer with vertical drains the lower value of permeability, estimated in Formation B, and was assigned. This solution is considered as conservative.

However, in order to perform the more precise settlement predictions, it would be useful to carry out simulations with the higher order software like PLAXIS, where the more detail underground model can be implemented into calculations. As well, the *GGU CONSOLIDATE 5* software calculates settlements based on the theory of elasticity. Using the higher order software would allow to calculate the settlement with the elasto-plastic model.

- The underground model, used in *GGU CONSOLIDATE 5* simulations, consists of eleven parallel soil layers and settlements are estimated under the assumption that the bottom boundary is a straight horizontal line (see Figure 43 Idealized underground model).

In the developed ground improvement strategy, the main portion of effective settlements comes from the lower layers, those without vertical drains. The concept of effective settlement is explained in section 3.3.1.3.

The length of the drainage path in the lower layers is influenced by their thickness. If a layer has a narrowing thickness, the drainage path shortens; if a layer thickens, the drainage path extends. The consolidation time varies with the length of the drainage path and influences the settlement rate (see chapter 2.1).

However, in reality the soil stratigraphy is more complex: soil layers may vary in thickness with respect to depth, contain multiple lenses or boulders or interlay with other deposits. As this Project covers a large area, the likelihood of a variable stratigraphy is high. This is especially important for the lower layers, because their thickness defines, how much effective settlement is generated. Also, the bottom boundary is not clearly defined. The worst case scenario would be the permeable bottom boundary in combination with the narrowing of these lower layers. This worst case scenario is illustrated in Figure 84.

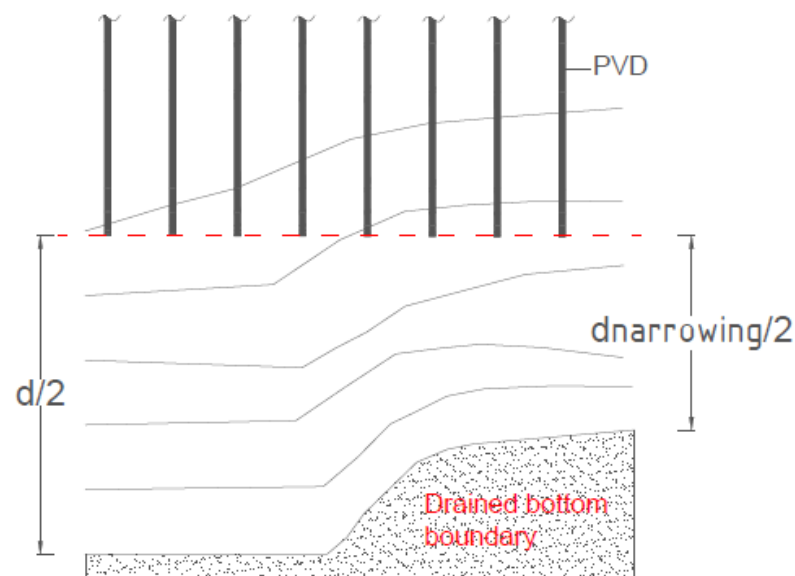


Figure 84 Influence of opened bottom boundary and narrowing of layers

Consequently, in such case the generated effective settlement would exceed the predicted value, leading to differential settlement.

6. The idealized underground model used for the settlement calculations in section 2.4 is a product of interpretations of eight CPTu tests performed during the Investigation-1. As it is explained in section 3.3.2, the stiffness assigned for this idealized model is a combination of two different empiric correlations: one proposed by Robertson (2012) and another proposed by Mayne (2001). This method was chosen by the geotechnical engineer, who was responsible for the evaluation. However, the reason why such interpretation method has been chosen is not provided in the report with the evaluation. The use of different evaluation methods would result in different soil parameters and different settlements. This shows the influence which a personal judgement has on the interpretation of CPTu results. As mentioned, prescribing only one value $\alpha = 6$ for two different formations with variable geotechnical properties is a questionable approach.
7. As it was explained in previous sections, the estimated permeability values with the empiric correlations by Robertson (2012) provide higher numbers as the results of dissipation test. Although hydraulic permeabilities evaluated with both methods are in the range of low permeability values ($1E-11 - 1E-9$), it has an influence on the settlement: the increasing permeability shifts the log time – settlement curve close to the y axis.

The influence of permeability is checked with CPTu_1, because as it was explained in section 3.5.2.8 the blue delimitating line (the lower boundary) mostly repeats the log time – settlement curve of CPTu_1. For calculations the same set of stiffness values has been used as in Table 20 for CPTu_1 and the simulations were performed with the same conditions as all previous calculations with the closed bottom boundary.

The log time – settlement curves for CPTu_1 with the permeability estimated with the empiric correlations and permeability estimated with the dissipations tests is shown in Figure 85. Comparison of effective and final settlements is shown in Table 28 and Table 29.

In this figure four cases with different life loads for roads are compared. Four continuous lines represent log time – settlement curves with empiric correlations and four solid lines represent log time – settlement curves with results from dissipation tests.

Table 28 Comparison of effective settlement for CPTu_1

Effective settlement [cm]	95/50/50	95/50/60	95/50/70	95/50/80
CPTu_1 with Robertson (2012)	8,4	12,4	16,5	20,6
CPTu_1 with dissipation test	2	4,9	7,8	11,3

Table 29 Comparison of final settlement for CPTu_1

Final settlement [cm]	95/50/50	95/50/60	95/50/70	95/50/80
CPTu_1 with Robertson (2012)	68,8	74,8	81	87,1
CPTu_1 with dissipation test	63,3	69,5	75,7	82,6

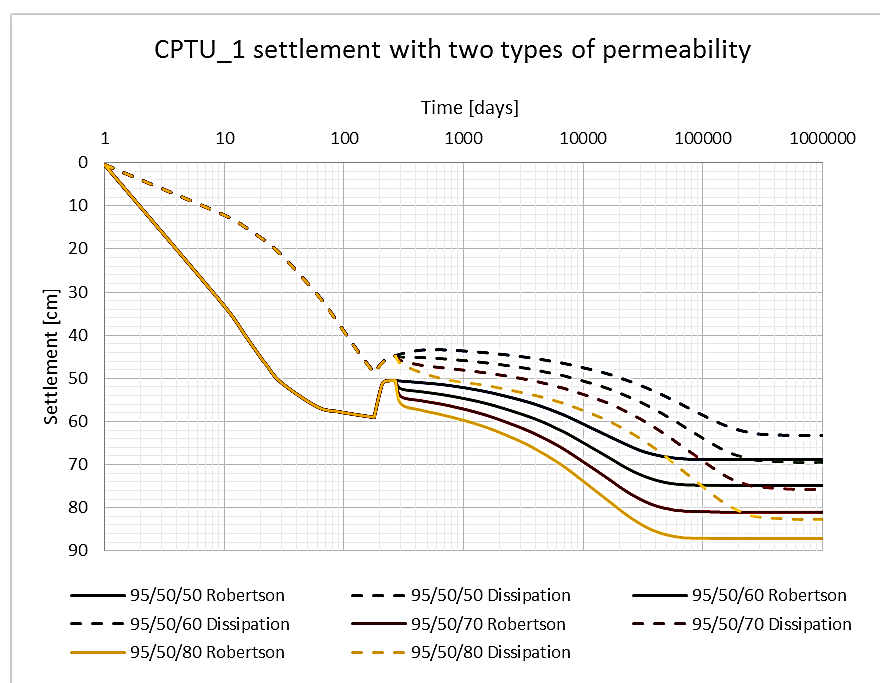


Figure 85 CPTu_1 settlement with two types of permeability

As it is seen from Figure 85, due to the reduced permeability the four cases with results from dissipation tests do not show such a rapid increase in settlement within the first six months. Due to the reduced permeability the influence of heave on the settlement is lower (the bend generated by the unloading within 6 and 9 months is less pronounced). In general, the effective settlement estimated with empiric equations is 2-4 times higher than the numbers estimated with the dissipation tests. However, the final settlement at the end of consolidation is approximately 5cm higher for cases with the empirical correlations.

4 Summary of results

Eight CPTu tests were performed in the Investigation-1 area (a parcel within the area of great extent, see Figure 33) and based on the results of this Investigation-1 the underground model was summarized. This summarized underground model was adopted for calculations of the effective settlement for the area of great extent (see section 3.4.2.3).

The effective settlement is calculated for two cases: with the closed bottom boundary (UNDR) and with the opened bottom boundary (DR) of the model. These results are compared in Table 30 and in Figure 86.

Table 30 Comparison of effective settlements with the closed and open bottom boundary

	Roads								Structures	
	0 kN/m ²		10 kN/m ²		20 kN/m ²		30 kN/m ²		16 kN/m ²	
	DR	UNDR	DR	UNDR	DR	UNDR	DR	UNDR	DR	UNDR
Upper part with PVD	2,1	-2	0,2	0,2	2,3	2,5	6,7	6,8	-0,2	-0,1
Lower part	8,9	4,9	11	6,1	13,2	7,2	15,3	8,4	21,2	12
Σ	6,8	2,9	11,2	6,3	15,5	9,7	22	15,2	21	11,9

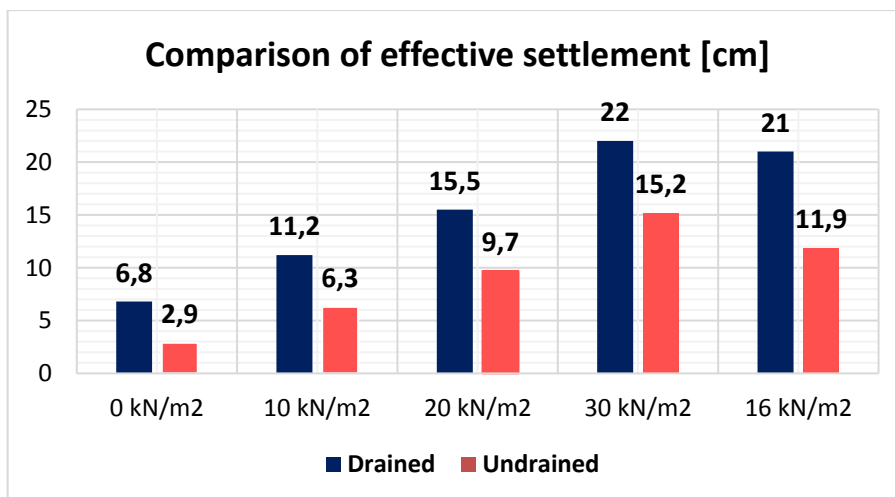


Figure 86 Comparison of effective settlement with the closed and opened bottom boundary

The comparison shows that the drained bottom boundary results in significantly higher settlement in the lower part and thus, the higher effective settlement. This is linked with the twice shorter drainage path in the lower part from 25 to 50m.b.s.l, when the drained bottom boundary is assigned to the model.

The next step in the evaluation is to mark out the extent of the data. The delimitating lines are created according the approximated data from the eight CPTus performed in the Investigatio-1 area. The delimitating lines is a quick way to see, if evaluated data from new piezocone tests fit within the range thus far considered.

The extent of data is marked out with two lines: the first line picks out the absolute lowest values of evaluated properties and the second consists of the absolute highest values from eight piezocone tests.

The three main types of delimitating lines are created on the basis of the eight programmed spreadsheets: for the constrained modulus M , horizontal coefficient of permeability k_h and soil behavior type (SBT) based on the soil behavior type index I_c . The fourth type of delimitating lines for settlement was obtained as a part of study, when the conservative approach (the permeability obtained from the empirical correlations) is applied.

In January, 2017 eight additional CPTu tests (Investigation-2) were performed as a part of extended underground exploration study. The tests are listed under following names:

CPTu_135, CPTu_136, CPTu_137, CPTu_143, CPTu_144, CPTu_145, CPTu_151 and CPTu_151.

The comparison of eight new CPTu tests with the three types of delimitating lines is shown in the next three figure.

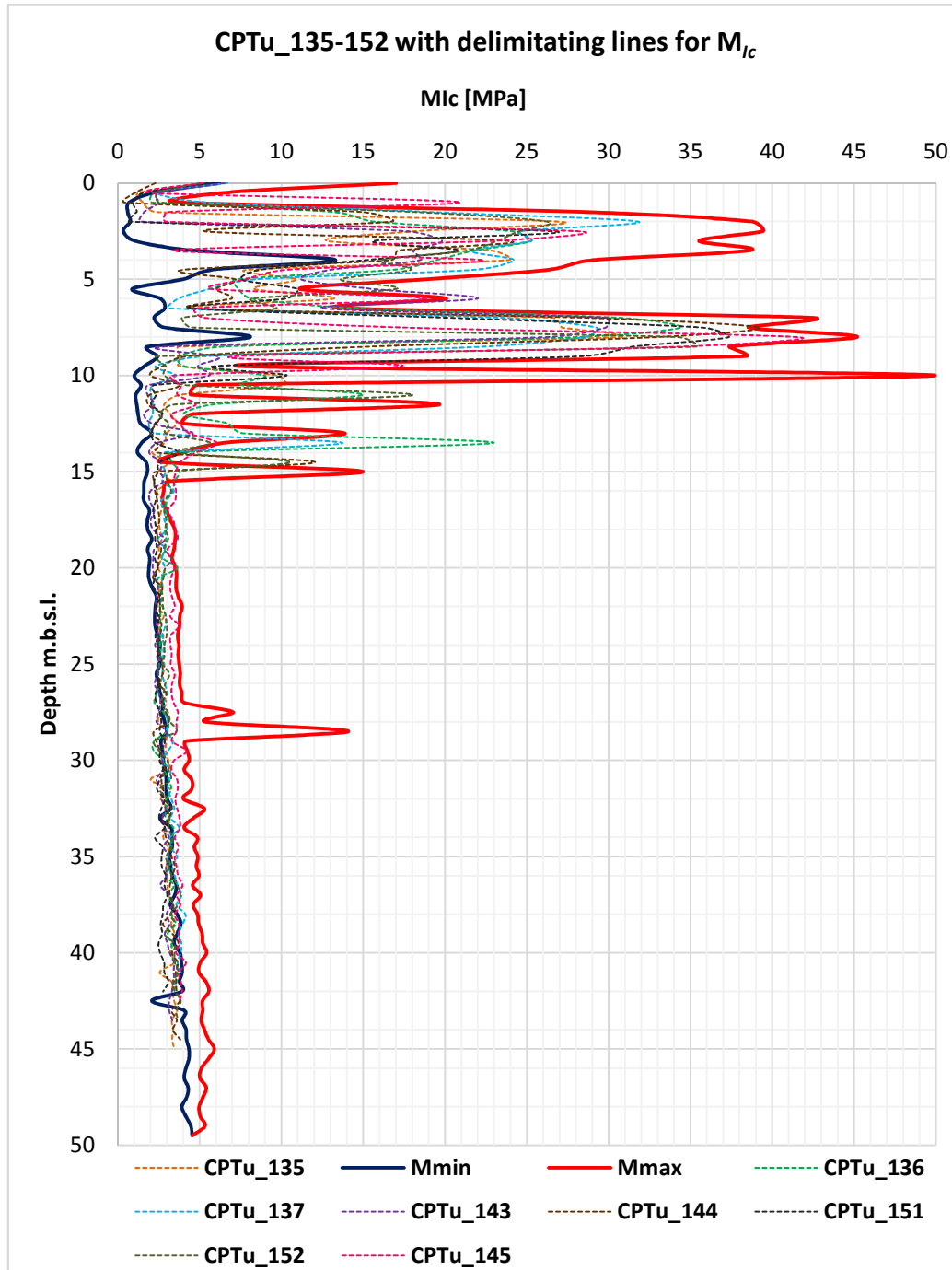


Figure 87 Comparison of new CPTu tests with the delimitating lines

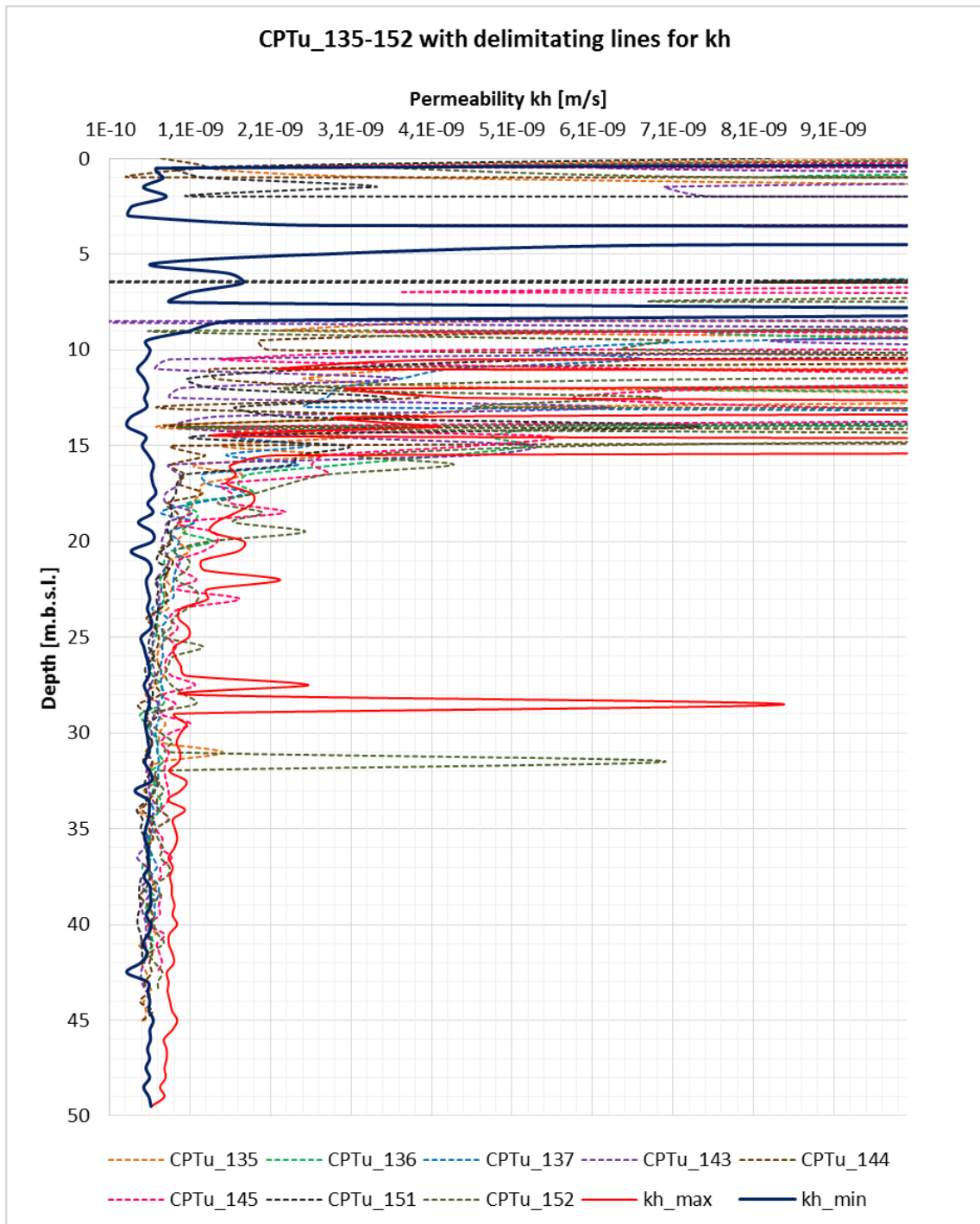


Figure 88 Comparison of new CPTu tests with delimitating lines

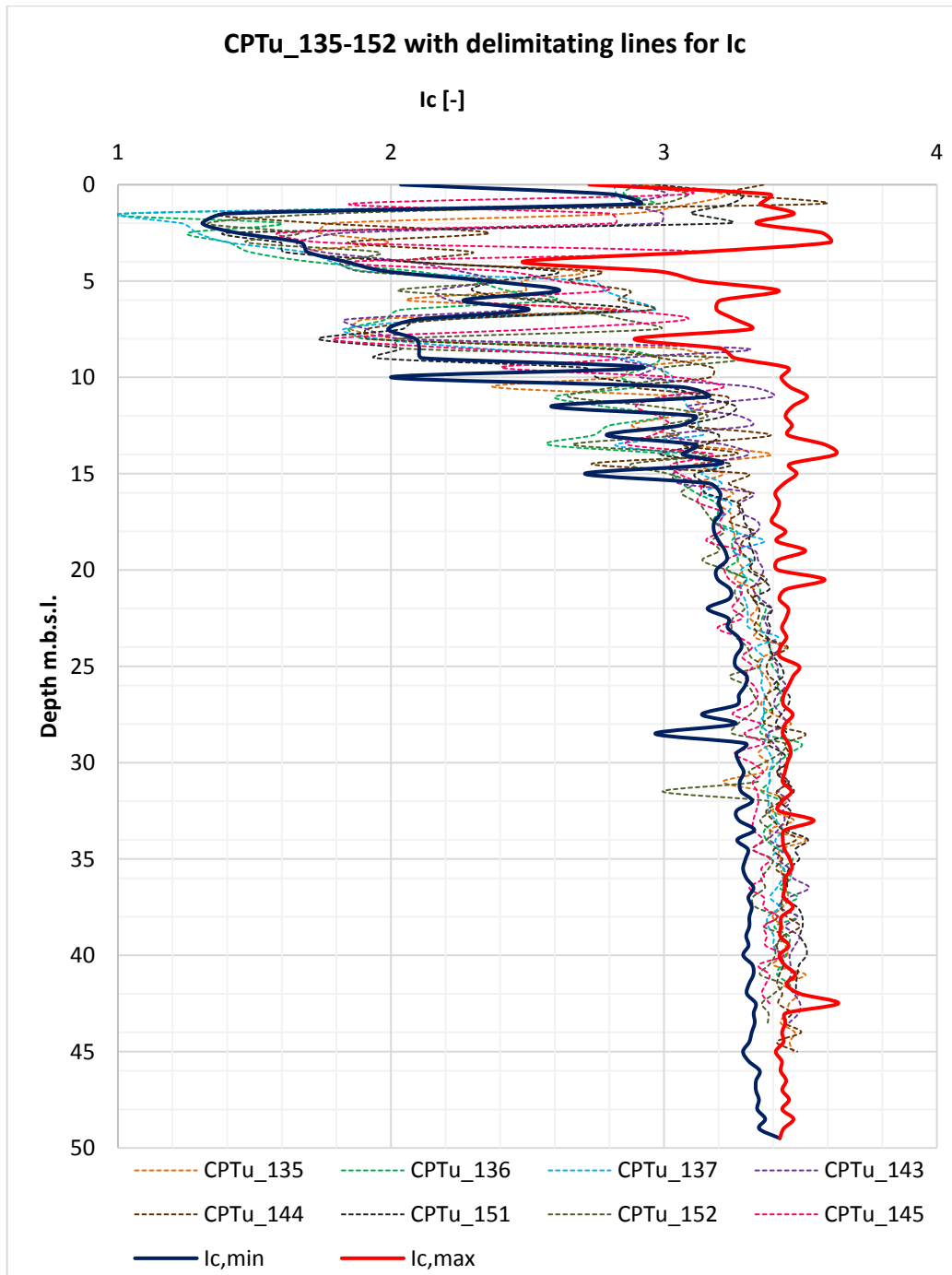


Figure 89 Comparison of generated soil behavior type (SBT) based on the soil behavior type index I_c graph for new CPTu tests with previously plotted delimitating lines

In general, the results of eight new piezocone tests fit in the range thus far considered. The new eight piezocone tests have as well indicated the presence of two sediment formations: the upper formation is about 15m thick and contains a variety of interlayers (this observation is based on the wide scatter of data point in all three above shown graphs); the lower formation with close to homogeneous soil profile. According to the

evaluations with the soil behavior type index I_c (Robertson 2012), the interlayering of silty clay/clayey silt with sands in the upper formation can be noticed, what shows a good agreement with the Investigation-1. In the lower formation the constant increase, which for some tests exceeds the red delimitating line, in the soil behavior type index I_c is noticed. According to the interpretation by Robertson (2012), this shows the increase of fines in the sediments. This could explain the decrease of permeability in the lower formation, shown in Figure 88.

The resulting effective settlement obtained from the eight new piezocones is compared to the effective settlement of delimitating lines in. In this section as a supplementary example to the Table 31, Figure 90 is given and it shows the resulting log time – settlement curves for roads with 20 kN/m². Other plots can be found in 3.5.2.7.

Table 31 Effective settlement [cm] approximated for CPTu_135 – 152 and the delimitating lines

Effective settlement [cm]	Corresponding life loads for roads				Structures	
	0kN/m ²	10 kN/m ²	20 kN/m ²	0kN/m ²	10 kN/m ²	
CPTu_135	8,6	13,1	CPTu_135	8,6	13,1	
CPTu_136	8,6	12,8	CPTu_136	8,6	12,8	
CPTu_137	7,7	11,9	CPTu_137	7,7	11,9	
CPTu_143	7,8	12,2	CPTu_143	7,8	12,2	
CPTu_144	7,9	12,3	CPTu_144	7,9	12,3	
CPTu_145	8,5	12,6	CPTu_145	8,5	12,6	
CPTu_151	7,9	12,2	CPTu_151	7,9	12,2	
CPTu_152	9,5	13,9	CPTu_152	9,5	13,9	
Blue delimitating line (lower bound)	8,4	12,4	Blue delimitating line (lower bound)	8,4	12,4	
Red delimitating line (upper bound)	6,7	12,3	Red delimitating line (upper bound)	6,7	12,3	

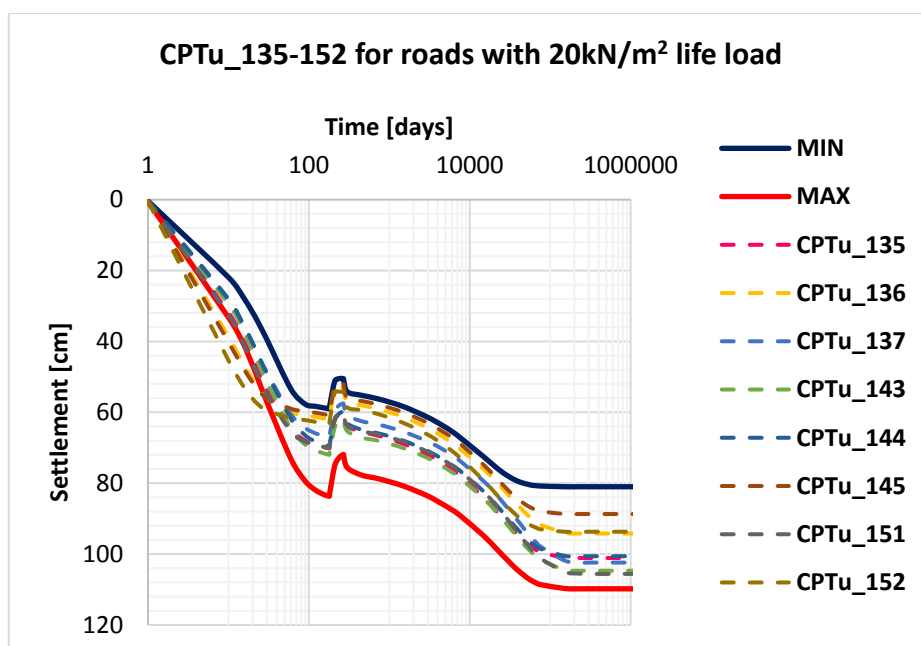


Figure 90 Comparison of log time - settlement curves for the eight new CPTu with the delimitating lines for roads with 20kN/m² life load

The main result of this comparison of effective settlement shows that even though the calculated effective settlements for the eight new piezocone tests are similar to the values obtained from the delimitating lines and the corresponding log time – settlement curves stay within the marked out area, the risk of differential settlement remains, because after preloading-unloading stage the soil is compacted up to different depth levels.

5 Conclusions

The concept of soil improvement for the area of great extent on about 50m of saturated weak silty clayey deposit has been presented in this Thesis. According to the boundary conditions of the project a combination of excess preloading with 25m vertical drains is used to accelerate the consolidation and increase the strength of soils.

As the starting point of this Thesis, the goal to gain the necessary theoretical background was set. The overview of this theory is presented in the four sections of chapter 2.

The settlement calculations for five different loading cases in the chapter 3 are carried out with the software *GGU CONSOLIDATE 5*. The CUR 191 (1997) approach is implemented in these calculations.

Settlement calculations for five different loading cases are carried out with two boundary conditions, related to the soil permeability underneath the 50m.b.s.l. depth: with the closed (undrained) boundary under assumption that underneath the 50m.b.s.l. depth the extend of low permeable clayey silty soil is located; with the opened (drained) bottom boundary under assumption that underneath the 50m.b.s.l. depth the stratum of permeable sand is located. The results are described in detail in sections 3.4.3, 3.4.4 and 3.4.5.

The evaluation of data obtained from piezocone tests is performed by means of programmed Excel sheets. The evaluation is carried out for two sets of data: the first set is gained from the Investigation-1; the second set is gained from the supplementary Investigation-2. Four different types of delimitating lines (for constrained modulus M , horizontal coefficient of hydraulic permeability k_h , soil behavior type index I_c and settlement) are obtained from the first set of data. The evaluated data from the second set is compared with these delimitating lines and these results are presented in section 3.5.3.

Some points of interest, as well as unanswered questions, arise from the results of settlement calculations and performed evaluation of piezocone tests. These points are summarized in the chapter 3.6.

Finally, the brief summary of the significant results is given in the chapter 0.

6 Literature

Arizona Geosynthetics (2017)

Available at: <http://arizonageosynthetics.com/products/tencate-polyfelt-alidrain-prefabricated-vertical-drain/> [Accessed: 5 January 2017]

Campanella, R G.; Gillespie, D.; Robertson, P. K. (1982)

Pore pressures during cone penetration testing, Proceedings of the 2nd European Symposium on Penetration Testing, ESOPT-2, Amsterdam, May 24 - 27, Vol. 2'

Carrillo, N. (1942)

Simple two and three dimensional consolidation. Jnl. Math. and Phys., vol 21, no.1.

Chu J.; Indraratna, B.; Yan, S.; Rujikiatkamjorn, C. (2014)

Overview of preloading methods for soil improvement [Online]. University of Wollongong: Research Online. Available at: <http://ro.uow.edu.au/cgi/viewcontent.cgi?article=3819&context=eispapers> [Accessed: 2 January 2017]

CUR 191 (1991)

Achtergronden bij numerieke modellering van geotechnische constructies, deel 2. Vertikal Drainage CUR-publikatie 191. Centre for Civil Engineering research Codes, Gouda, Netherlands

GDS (2017)

GDS Instruments [Online] Available at: <http://www.gdsinstruments.com/gds-products/gds-automatic-oedometer-system> [Accessed: 5 January 2017]

Geoengineering (2017)

Geoengineering.org [Online]. Available at: <http://www.geoengineer.org/education/web-based-class-projects/select-topics-in-ground-improvement/prefabricated-vertical-drains?start=2> [Accessed: 1 February 2017]

Hansbo, S.(1979)

Consolidation of clay by band-shaped prefabricated drains [Online]. Ground Engineering, July 1979. Available at: <https://www.geplus.co.uk/download?ac=1427292> [Accessed: 2 September 2016]

Holtz et al. (1991)

Prefabricated Vertical Drains: Design and Performance, CIRIA, London.

Indraratna, B.; Bamunawita C. I. (2002)

Soft Clay Stabilisation by Mandrel Driven Geosynthetic Vertical Drains [Online]. University of Wollongong: Research Online. Available at: <http://ro.uow.edu.au/engpapers/406/> [Accessed: 5 September 2016]

Indraratna B.; Rujikiatkamjorn, C.; Chu. J.(2007)

Soft Clay Stabilization with Geosynthetic Vertical Drains beneath Road and railway Embankments; A Critical review of Analytical Solutions and Numerical Analysis [Online]. University of Wollongong: Research Online. Available at: <http://ro.uow.edu.au/engpapers/334> [Accessed: 26 August 2016]

- Keller (2017)
Available at: <http://www.kellerholding.com/vertical-drains.html> [Accessed: 1 March 2017]
- Knappett, J.; Craig, R. F (2012)
Craig's Soil Mechanics, Eighth Edition. London: CRC Press.
- Mayne, P.W. (2000)
Enhanced geotechnical site characterization by seismic piezocone penetration tests [Online]. Available at: <http://geosystems.ce.gatech.edu/Faculty/Mayne/papers/Enhanced%20In-Situ%20Testing%202000.pdf> [Accessed: 19 February 2017]
- Mayne, P.W. (200)
Flow properties from piezocone dissipation tests [Online]. Available at: <http://geosystems.ce.gatech.edu/Faculty/Mayne/papers/PiezoDissipation.pdf> [Accessed: 19 December 2016]
- Menard (2017)
Vibro Menard [Online]. Available at: <http://www.vibromenard.co.uk/techniques/vertical-drains/> [Accessed: 7 January 2017]
- Robertson, P.K. (2006)
Guide to In-situ Testing [Online]. Gregg Drilling & Testing Inc. Available at: <http://www.geoplanning.it/test/wp-content/uploads/2012/02/Guide-to-in-situ-testing.pdf> [Accessed: 12 February 2017]
- Robertson, P.K. (2012)
Guide to Cone Penetration Testing [Online]. Gregg Drilling & Testing Inc. Available at: <http://www.novotechsoftware.com/downloads/PDF/en/Ref/CPT-Guide-5ed-Nov2012.pdf> [Accessed: 10 December 2016]
- Stapelfeldt, T. (2000)
Preloading and vertical drains [Online]. Helsinki University of Technology. Available at: http://civil.aalto.fi/fi/research/geoengineering/soil/theses/other/preloading_and_vertical_drains.pdf [Accessed: 2 January 2017]
- Tencate (2017)
Tencate [Online]. Available at: <http://www.tencate.com/apac/geosynthetics/product/infrastructure/tencate-polyfelt-alidrain-pvd.aspx> [Accessed: 3 February 2017]
- UMas Lowell (2013)
14.330 SOIL MECHANICS. Consolidation [Online]. University of Massachusetts Lowell. Available at: <http://faculty.uml.edu/ehajduk/teaching/14.330/documents/14.3302013consolidation.pdf> [Accessed: 2 January 2017]

UONBI

In-situ geotechnical tests [Online]. University of Nairobi. Department of Civil Engineering. Available at:
https://learning.uonbi.ac.ke/courses/FEB402/document/FEB_402-In-situ_geotechnical_tests.pdf [Accessed: 3 February 2017]Engin, H.K.; Andresen, L. (2011)

Veder, Ch.; Prinzi, F. (1983)

The avoidance of secondary settlements through overconsolidation. Proceedings of the Eight European Conference on Soil Mechanics and Foundation Engineering. Rotterdam.

Appendix A

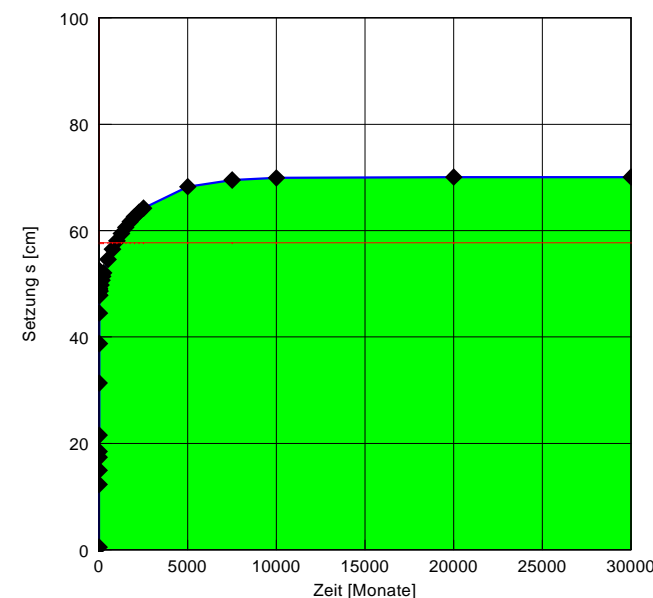
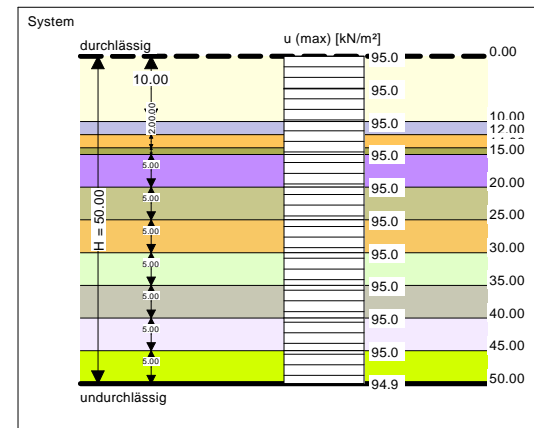
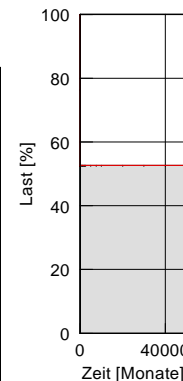
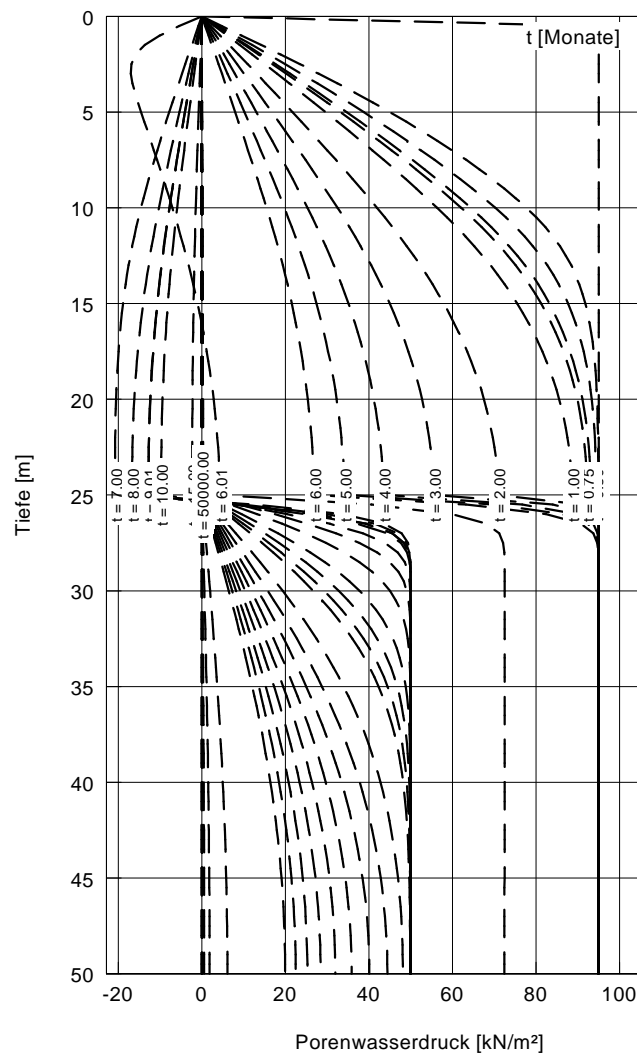
GGU CONSOLIDATE 5 calculations with the closed bottom boundary

(Contains 5 pages)

One-dimensional consolidation theory
 Settlement calculation for roads with 0kPa life load after 9 months
 Schrittweite (Tiefe) = 0.500 m
 Endsetzung = 109.7 cm

Boden	E_s [kN/m ²]	k [m/s]	c_v [m ² /s]	$E_{s(w)}/E_s$ [-]	Bezeichnung
	5000.0	$7.29 \cdot 10^{-8}$	$3.65 \cdot 10^{-5}$	3.00	Clayey Silt
	2600.0	$7.29 \cdot 10^{-8}$	$1.90 \cdot 10^{-5}$	3.00	Silty Clay
	2800.0	$7.29 \cdot 10^{-8}$	$2.04 \cdot 10^{-5}$	3.00	Silty Clay
	2900.0	$7.29 \cdot 10^{-8}$	$2.12 \cdot 10^{-5}$	3.00	Silty Clay
	3250.0	$7.29 \cdot 10^{-8}$	$2.37 \cdot 10^{-5}$	3.00	Silty Clay
	3750.0	$7.29 \cdot 10^{-8}$	$2.74 \cdot 10^{-5}$	3.00	Silty Clay
	4250.0	$8.04 \cdot 10^{-11}$	$3.42 \cdot 10^{-8}$	3.00	Silty Clay
	4750.0	$8.04 \cdot 10^{-11}$	$3.82 \cdot 10^{-8}$	3.00	Silty Clay
	5250.0	$8.04 \cdot 10^{-11}$	$4.22 \cdot 10^{-8}$	3.00	Silty Clay
	5750.0	$8.04 \cdot 10^{-11}$	$4.62 \cdot 10^{-8}$	3.00	Silty Clay
	6250.0	$8.04 \cdot 10^{-11}$	$5.02 \cdot 10^{-8}$	3.00	Silty Clay

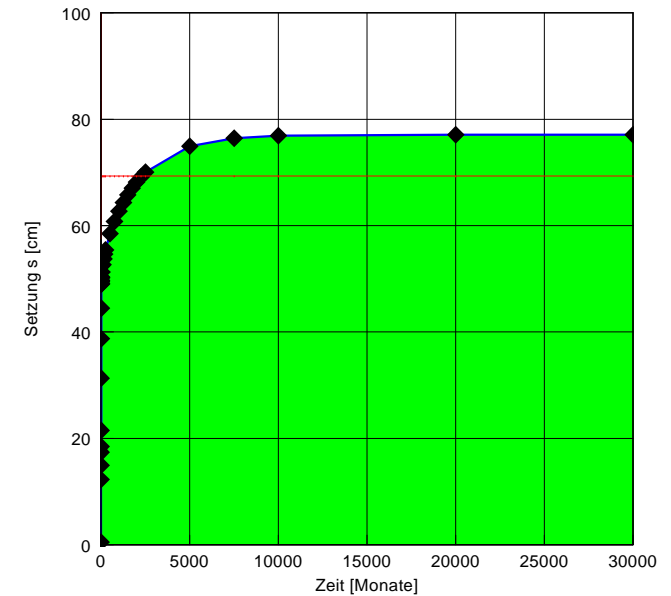
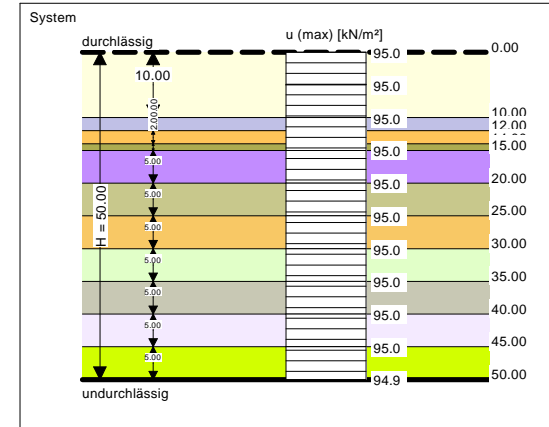
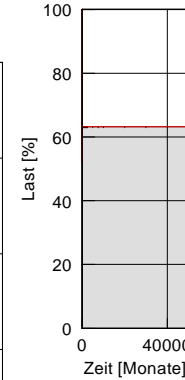
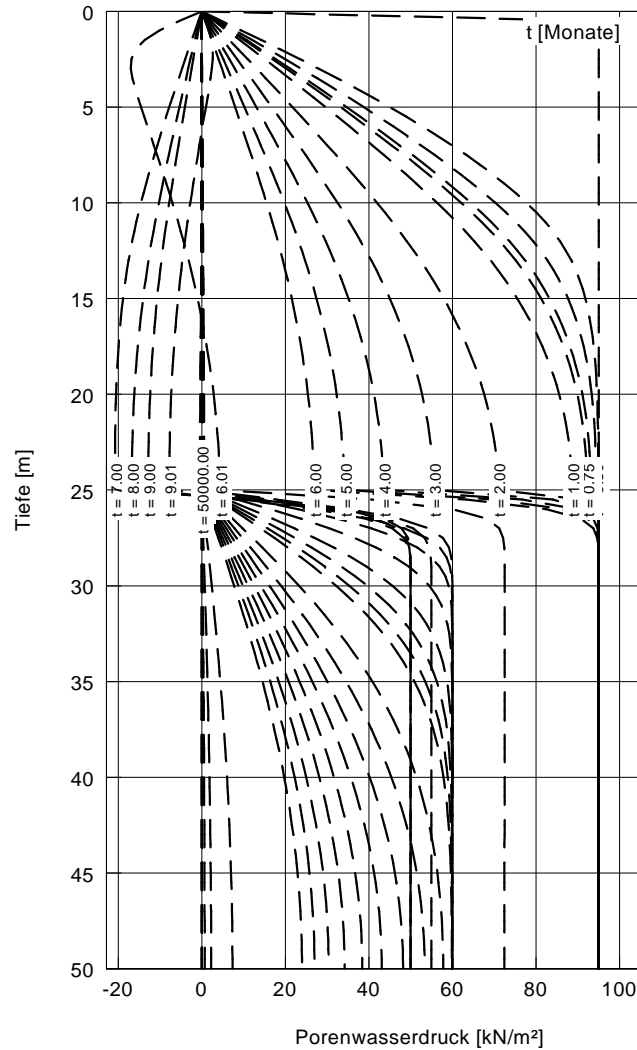
Zeit [Monate]	U [-]	s [cm]
0.00	0.004	0.5
0.34	0.112	12.3
0.50	0.136	14.9
0.67	0.159	17.4
0.75	0.168	18.5
1.00	0.196	21.5
2.00	0.286	31.3
3.00	0.353	38.7
4.00	0.406	44.5
5.00	0.446	49.0
6.00	0.478	52.5
6.01	0.477	52.4
7.00	0.459	50.4
8.00	0.452	49.6
9.00	0.448	49.1
9.01	0.448	49.1
10.00	0.444	48.7
15.00	0.436	47.8
25.00	0.436	47.8
50.00	0.443	48.6
100.00	0.454	49.8
150.00	0.462	50.7
200.00	0.468	51.4
249.00	0.474	52.0
500.00	0.498	54.6
750.00	0.515	56.5
1000.00	0.529	58.1
1250.00	0.542	59.4
1500.00	0.553	60.6
1750.00	0.562	61.7
2000.00	0.571	62.6
2250.00	0.578	63.5
2500.00	0.585	64.2
5000.00	0.622	68.3
7500.00	0.634	69.5
10000.00	0.637	69.9
20000.00	0.639	70.1
30000.00	0.639	70.1
40000.00	0.639	70.1
50000.00	0.639	70.1



One-dimensional consolidation theory
 Settlement calculation for roads with 10kPa life load after 9 months
 Schrittweite (Tiefe) = 0.500 m
 Endsetzung = 109.7 cm

Boden	E_s [kN/m ²]	k [m/s]	c_v [m ² /s]	E_{sw}/E_s [-]	Bezeichnung
	5000.0	$7.29 \cdot 10^{-8}$	$3.64 \cdot 10^{-5}$	3.00	Clayey Silt
	2600.0	$7.29 \cdot 10^{-8}$	$1.90 \cdot 10^{-5}$	3.00	Silty Clay
	2800.0	$7.29 \cdot 10^{-8}$	$2.04 \cdot 10^{-5}$	3.00	Silty Clay
	2900.0	$7.29 \cdot 10^{-8}$	$2.11 \cdot 10^{-5}$	3.00	Silty Clay
	3250.0	$7.29 \cdot 10^{-8}$	$2.37 \cdot 10^{-5}$	3.00	Silty Clay
	3750.0	$7.29 \cdot 10^{-8}$	$2.73 \cdot 10^{-5}$	3.00	Silty Clay
	4250.0	$8.04 \cdot 10^{-11}$	$3.42 \cdot 10^{-8}$	3.00	Silty Clay
	4750.0	$8.04 \cdot 10^{-11}$	$3.82 \cdot 10^{-8}$	3.00	Silty Clay
	5250.0	$8.04 \cdot 10^{-11}$	$4.22 \cdot 10^{-8}$	3.00	Silty Clay
	5750.0	$8.04 \cdot 10^{-11}$	$4.62 \cdot 10^{-8}$	3.00	Silty Clay
	6250.0	$8.04 \cdot 10^{-11}$	$5.02 \cdot 10^{-8}$	3.00	Silty Clay

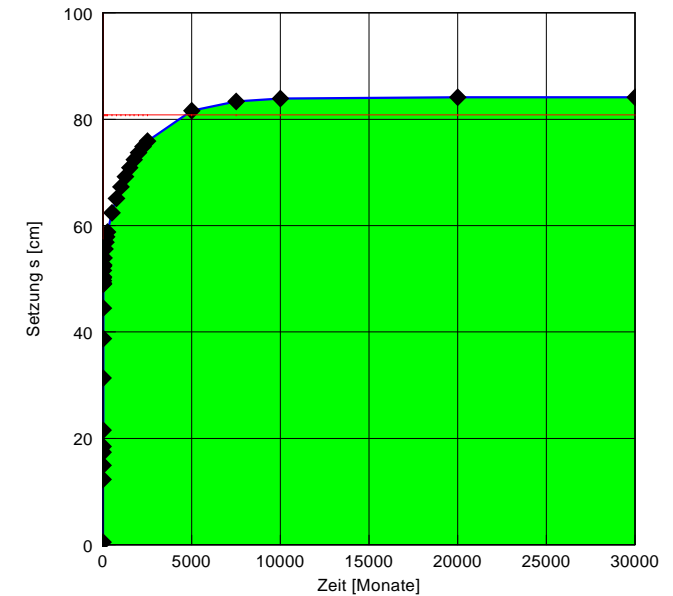
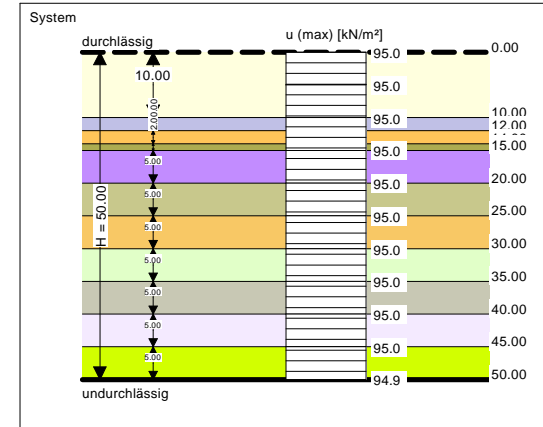
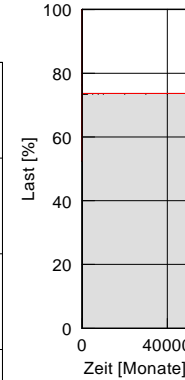
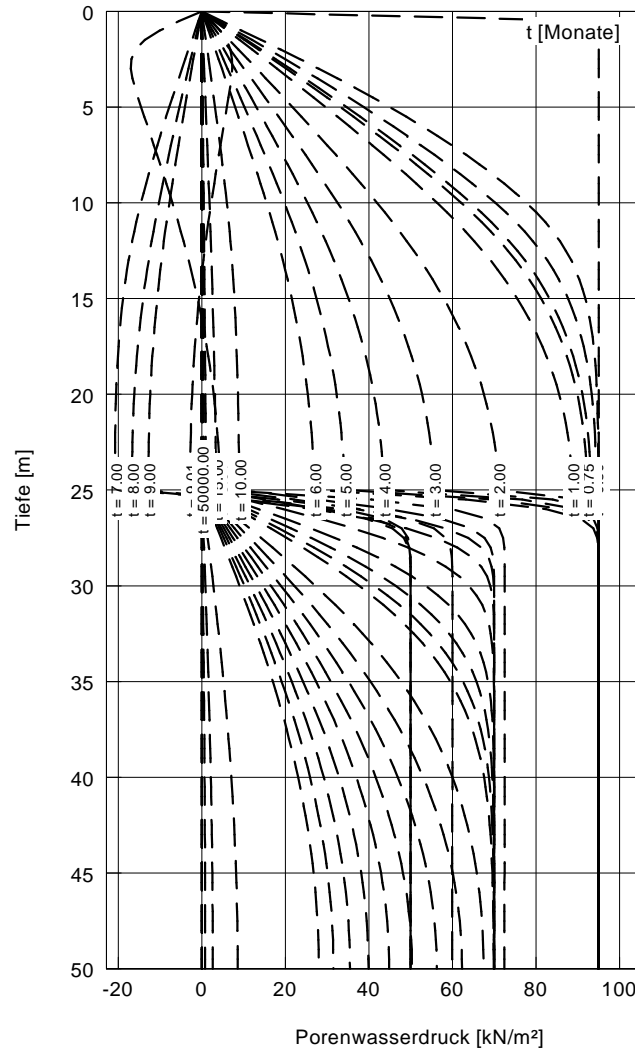
Zeit [Monate]	U [-]	s [cm]
0.00	0.004	0.5
0.34	0.112	12.3
0.50	0.136	14.9
0.67	0.159	17.4
0.75	0.168	18.5
1.00	0.196	21.5
2.00	0.286	31.3
3.00	0.353	38.7
4.00	0.406	44.5
5.00	0.446	49.0
6.00	0.478	52.5
6.01	0.477	52.4
7.00	0.459	50.4
8.00	0.452	49.6
9.00	0.447	49.1
9.01	0.448	49.1
10.00	0.451	49.4
15.00	0.453	49.7
25.00	0.458	50.2
50.00	0.467	51.3
100.00	0.480	52.7
150.00	0.490	53.8
200.00	0.498	54.7
249.00	0.505	55.4
500.00	0.533	58.5
750.00	0.554	60.8
1000.00	0.571	62.7
1250.00	0.586	64.3
1500.00	0.599	65.8
1750.00	0.611	67.0
2000.00	0.621	68.2
2250.00	0.630	69.2
2500.00	0.638	70.0
5000.00	0.683	74.9
7500.00	0.697	76.4
10000.00	0.701	76.9
20000.00	0.703	77.1
30000.00	0.703	77.1
40000.00	0.703	77.1
50000.00	0.703	77.1



One-dimensional consolidation theory
 Settlement calculation for roads with 20kPa life load after 9 months
 Schrittweite (Tiefe) = 0.500 m
 Endsetzung = 109.7 cm

Boden	E_s [kN/m ²]	k [m/s]	c_v [m ² /s]	$E_{s(w)}/E_s$ [-]	Bezeichnung
	5000.0	$7.29 \cdot 10^{-8}$	$3.65 \cdot 10^{-5}$	3.00	Clayey Silt
	2600.0	$7.29 \cdot 10^{-8}$	$1.90 \cdot 10^{-5}$	3.00	Silty Clay
	2800.0	$7.29 \cdot 10^{-8}$	$2.04 \cdot 10^{-5}$	3.00	Silty Clay
	2900.0	$7.29 \cdot 10^{-8}$	$2.12 \cdot 10^{-5}$	3.00	Silty Clay
	3250.0	$7.29 \cdot 10^{-8}$	$2.37 \cdot 10^{-5}$	3.00	Silty Clay
	3750.0	$7.29 \cdot 10^{-8}$	$2.74 \cdot 10^{-5}$	3.00	Silty Clay
	4250.0	$8.04 \cdot 10^{-11}$	$3.42 \cdot 10^{-8}$	3.00	Silty Clay
	4750.0	$8.04 \cdot 10^{-11}$	$3.82 \cdot 10^{-8}$	3.00	Silty Clay
	5250.0	$8.04 \cdot 10^{-11}$	$4.22 \cdot 10^{-8}$	3.00	Silty Clay
	5750.0	$8.04 \cdot 10^{-11}$	$4.62 \cdot 10^{-8}$	3.00	Silty Clay
	6250.0	$8.04 \cdot 10^{-11}$	$5.02 \cdot 10^{-8}$	3.00	Silty Clay

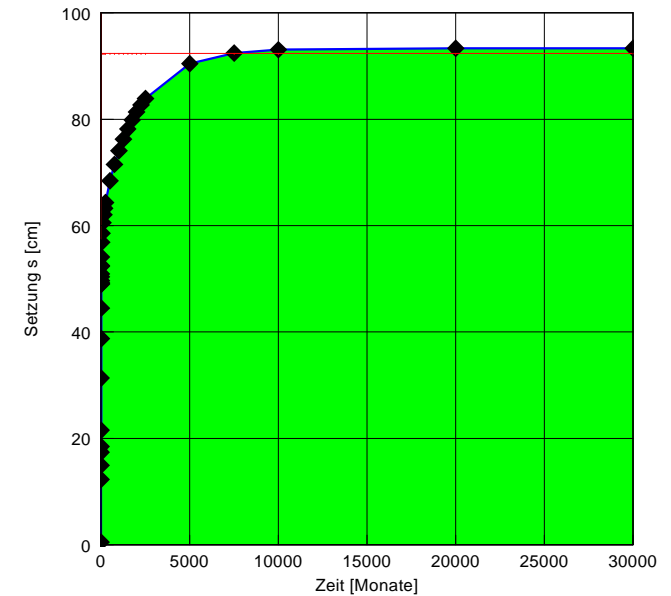
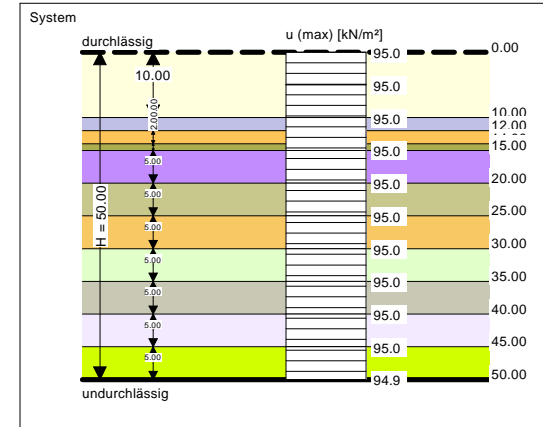
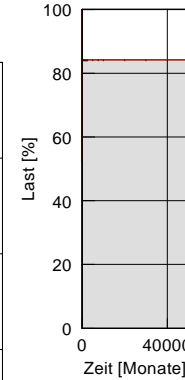
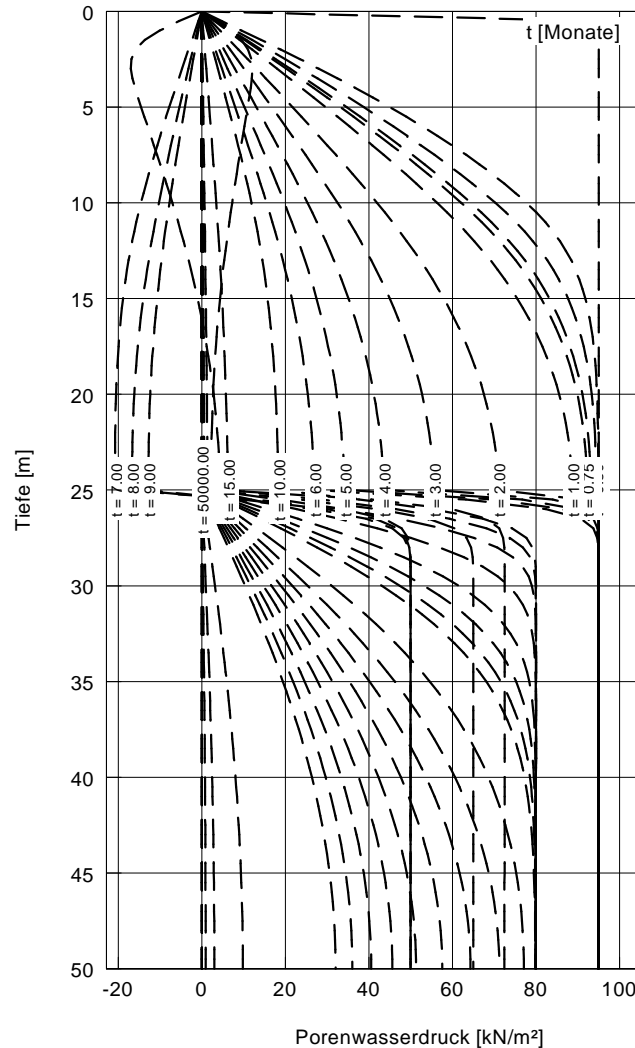
Zeit [Monate]	U [-]	s [cm]
0.00	0.004	0.5
0.34	0.112	12.3
0.50	0.136	14.9
0.67	0.159	17.4
0.75	0.168	18.5
1.00	0.196	21.5
2.00	0.286	31.3
3.00	0.353	38.7
4.00	0.406	44.5
5.00	0.446	49.0
6.00	0.478	52.5
6.01	0.477	52.4
7.00	0.459	50.4
8.00	0.452	49.6
9.00	0.448	49.1
9.01	0.448	49.2
10.00	0.457	50.2
15.00	0.470	51.6
25.00	0.480	52.6
50.00	0.491	53.9
100.00	0.507	55.6
150.00	0.518	56.9
200.00	0.528	57.9
249.00	0.536	58.8
500.00	0.569	62.4
750.00	0.593	65.1
1000.00	0.613	67.3
1250.00	0.631	69.2
1500.00	0.646	70.9
1750.00	0.660	72.4
2000.00	0.672	73.7
2250.00	0.682	74.9
2500.00	0.692	75.9
5000.00	0.744	81.6
7500.00	0.760	83.4
10000.00	0.765	83.9
20000.00	0.767	84.1
30000.00	0.767	84.1
40000.00	0.767	84.1
50000.00	0.767	84.1



One-dimensional consolidation theory
 Settlement calculation for roads with 30kPa life load after 9 months
 Schrittweite (Tiefe) = 0.500 m
 Endsetzung = 109.7 cm

Boden	E_s [kN/m ²]	k [m/s]	c_v [m ² /s]	$E_{s(w)}/E_s$ [-]	Bezeichnung
	5000.0	$7.29 \cdot 10^{-8}$	$3.65 \cdot 10^{-5}$	3.00	Clayey Silt
	2600.0	$7.29 \cdot 10^{-8}$	$1.90 \cdot 10^{-5}$	3.00	Silty Clay
	2800.0	$7.29 \cdot 10^{-8}$	$2.04 \cdot 10^{-5}$	3.00	Silty Clay
	2900.0	$7.29 \cdot 10^{-8}$	$2.12 \cdot 10^{-5}$	3.00	Silty Clay
	3250.0	$7.29 \cdot 10^{-8}$	$2.37 \cdot 10^{-5}$	3.00	Silty Clay
	3750.0	$7.29 \cdot 10^{-8}$	$2.74 \cdot 10^{-5}$	3.00	Silty Clay
	4250.0	$8.04 \cdot 10^{-11}$	$3.42 \cdot 10^{-8}$	3.00	Silty Clay
	4750.0	$8.04 \cdot 10^{-11}$	$3.82 \cdot 10^{-8}$	3.00	Silty Clay
	5250.0	$8.04 \cdot 10^{-11}$	$4.22 \cdot 10^{-8}$	3.00	Silty Clay
	5750.0	$8.04 \cdot 10^{-11}$	$4.62 \cdot 10^{-8}$	3.00	Silty Clay
	6250.0	$8.04 \cdot 10^{-11}$	$5.02 \cdot 10^{-8}$	3.00	Silty Clay

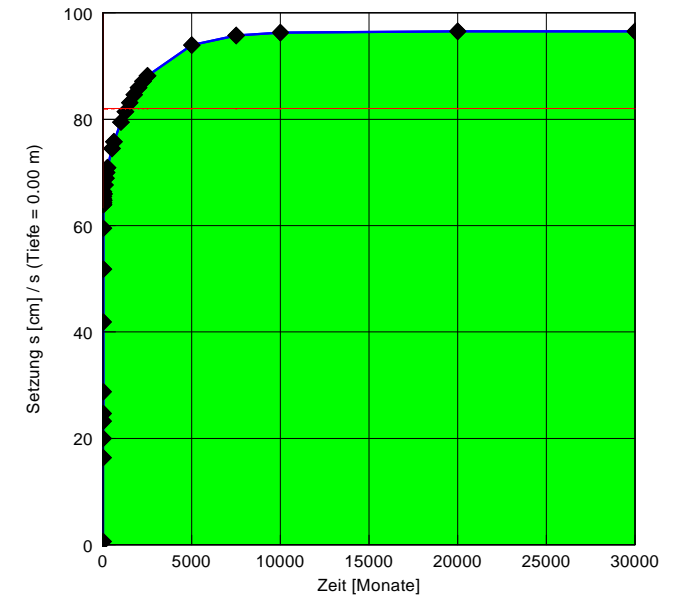
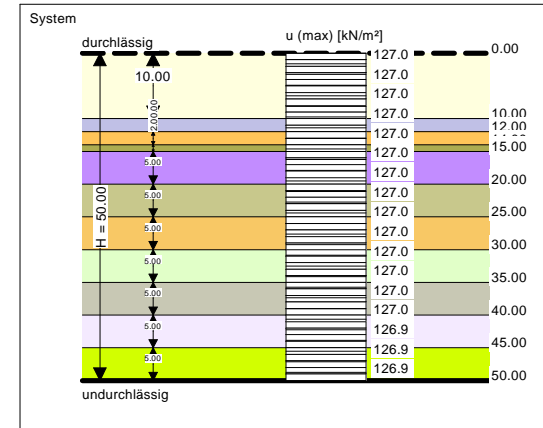
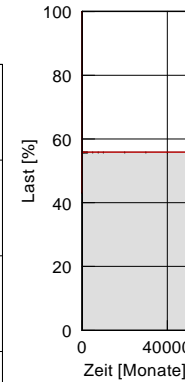
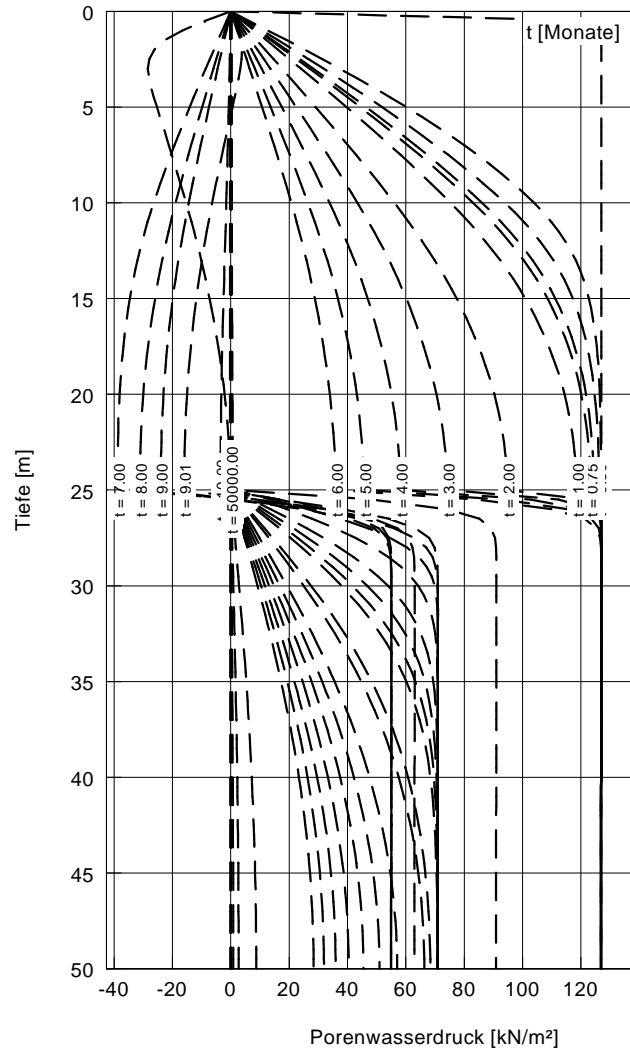
Zeit [Monate]	U [-]	s [cm]
0.00	0.004	0.5
0.34	0.112	12.3
0.50	0.136	14.9
0.67	0.159	17.4
0.75	0.168	18.5
1.00	0.196	21.5
2.00	0.286	31.3
3.00	0.353	38.7
4.00	0.406	44.5
5.00	0.446	49.0
6.00	0.478	52.5
6.01	0.477	52.4
7.00	0.459	50.4
8.00	0.452	49.6
9.00	0.448	49.1
9.01	0.449	49.2
10.00	0.464	50.9
15.00	0.493	54.1
25.00	0.518	56.8
50.00	0.534	58.6
100.00	0.552	60.6
150.00	0.566	62.0
200.00	0.577	63.3
249.00	0.586	64.3
500.00	0.624	68.4
750.00	0.652	71.5
1000.00	0.675	74.1
1250.00	0.695	76.3
1500.00	0.712	78.2
1750.00	0.728	79.9
2000.00	0.742	81.4
2250.00	0.754	82.7
2500.00	0.765	83.9
5000.00	0.824	90.4
7500.00	0.843	92.5
10000.00	0.848	93.1
20000.00	0.851	93.3
30000.00	0.851	93.3
40000.00	0.851	93.3
50000.00	0.851	93.3



One-dimensional consolidation theory
 Settlement calculation for structures with 16kPa life and structural loads after 9 months
 Schrittweite (Tiefe) = 0.500 m
 Endsetzung = 146.7 cm

Boden	E_s [kN/m ²]	k [m/s]	c_v [m ² /s]	$E_{s(w)}/E_s$ [-]	Bezeichnung
	5000.0	$7.29 \cdot 10^{-8}$	$3.65 \cdot 10^{-5}$	3.00	Clayey Silt
	2600.0	$7.29 \cdot 10^{-8}$	$1.90 \cdot 10^{-5}$	3.00	Silty Clay
	2800.0	$7.29 \cdot 10^{-8}$	$2.04 \cdot 10^{-5}$	3.00	Silty Clay
	2900.0	$7.29 \cdot 10^{-8}$	$2.12 \cdot 10^{-5}$	3.00	Silty Clay
	3250.0	$7.29 \cdot 10^{-8}$	$2.37 \cdot 10^{-5}$	3.00	Silty Clay
	3750.0	$7.29 \cdot 10^{-8}$	$2.74 \cdot 10^{-5}$	3.00	Silty Clay
	4250.0	$8.04 \cdot 10^{-11}$	$3.42 \cdot 10^{-8}$	3.00	Silty Clay
	4750.0	$8.04 \cdot 10^{-11}$	$3.82 \cdot 10^{-8}$	3.00	Silty Clay
	5250.0	$8.04 \cdot 10^{-11}$	$4.22 \cdot 10^{-8}$	3.00	Silty Clay
	5750.0	$8.04 \cdot 10^{-11}$	$4.62 \cdot 10^{-8}$	3.00	Silty Clay
	6250.0	$8.04 \cdot 10^{-11}$	$5.02 \cdot 10^{-8}$	3.00	Silty Clay

Zeit [Monate]	U [-]	s [cm]
0.00	0.004	0.6
0.34	0.112	16.4
0.50	0.136	20.0
0.67	0.159	23.3
0.75	0.168	24.7
1.00	0.196	28.8
2.00	0.286	41.9
3.00	0.353	51.8
4.00	0.406	59.5
5.00	0.446	65.5
6.00	0.478	70.2
6.01	0.477	70.0
7.00	0.452	66.4
8.00	0.443	65.0
9.00	0.436	63.9
9.01	0.436	64.0
10.00	0.439	64.3
15.00	0.438	64.3
25.00	0.442	64.8
50.00	0.450	66.0
100.00	0.461	67.6
150.00	0.470	68.9
200.00	0.477	70.0
250.00	0.483	70.9
500.00	0.508	74.5
609.00	0.516	75.8
1000.00	0.542	79.5
1250.00	0.555	81.4
1500.00	0.567	83.1
1750.00	0.577	84.6
2000.00	0.586	85.9
2250.00	0.594	87.1
2500.00	0.601	88.2
5000.00	0.641	94.0
7500.00	0.653	95.7
10000.00	0.656	96.3
20000.00	0.658	96.5
30000.00	0.658	96.5
40000.00	0.658	96.5
50000.00	0.658	96.5



Appendix B

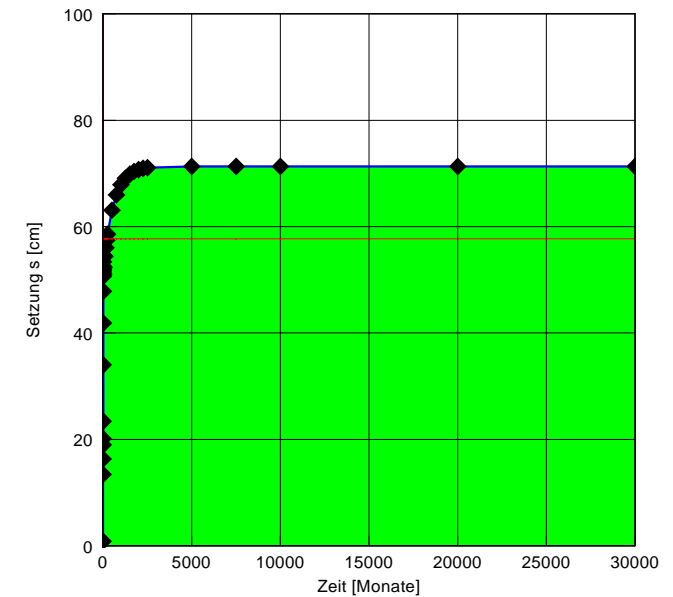
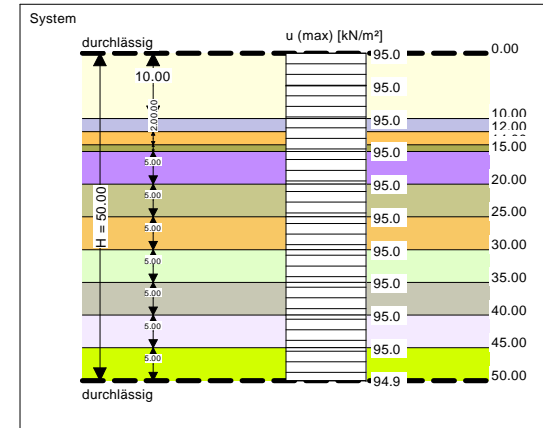
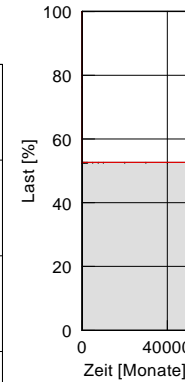
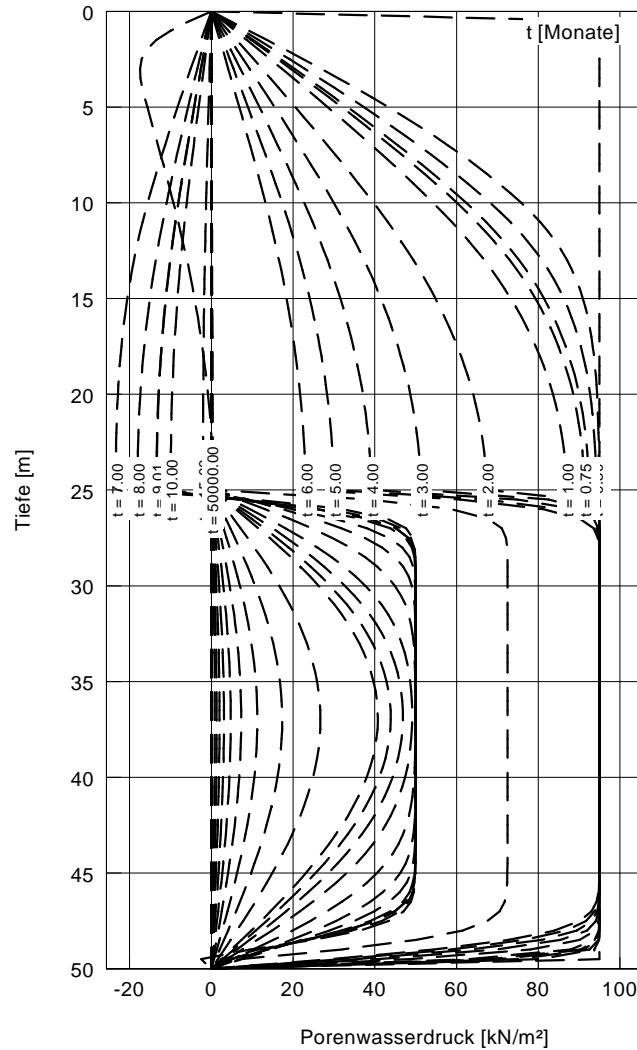
GGU CONSOLIDATE 5 calculations with the opened bottom boundary

(Contains 5 pages)

One-dimensional consolidation theory
 Settlement calculation for roads with 0kPa life load after 9 months
 Schrittweite (Tiefe) = 0.500 m
 Endsetzung = 109.7 cm

Boden	E_s [kN/m ²]	k [m/s]	c_v [m ² /s]	E_{sw}/E_s [-]	Bezeichnung
	5000.0	$8.07 \cdot 10^{-8}$	$4.03 \cdot 10^{-5}$	3.00	Clayey Silt
	2600.0	$8.07 \cdot 10^{-8}$	$2.10 \cdot 10^{-5}$	3.00	Silty Clay
	2800.0	$8.07 \cdot 10^{-8}$	$2.26 \cdot 10^{-5}$	3.00	Silty Clay
	2900.0	$8.07 \cdot 10^{-8}$	$2.34 \cdot 10^{-5}$	3.00	Silty Clay
	3250.0	$8.07 \cdot 10^{-8}$	$2.62 \cdot 10^{-5}$	3.00	Silty Clay
	3750.0	$8.07 \cdot 10^{-8}$	$3.03 \cdot 10^{-5}$	3.00	Silty Clay
	4250.0	$8.04 \cdot 10^{-11}$	$3.42 \cdot 10^{-8}$	3.00	Silty Clay
	4750.0	$8.04 \cdot 10^{-11}$	$3.82 \cdot 10^{-8}$	3.00	Silty Clay
	5250.0	$8.04 \cdot 10^{-11}$	$4.22 \cdot 10^{-8}$	3.00	Silty Clay
	5750.0	$8.04 \cdot 10^{-11}$	$4.62 \cdot 10^{-8}$	3.00	Silty Clay
	6250.0	$8.04 \cdot 10^{-11}$	$5.02 \cdot 10^{-8}$	3.00	Silty Clay

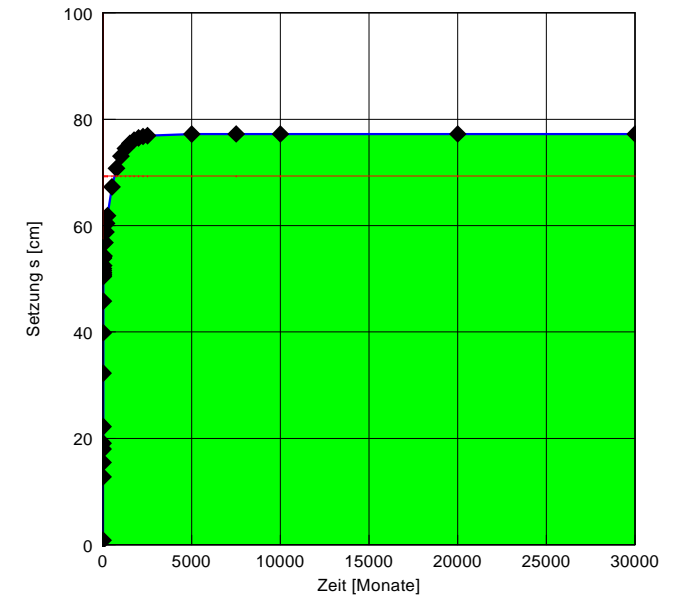
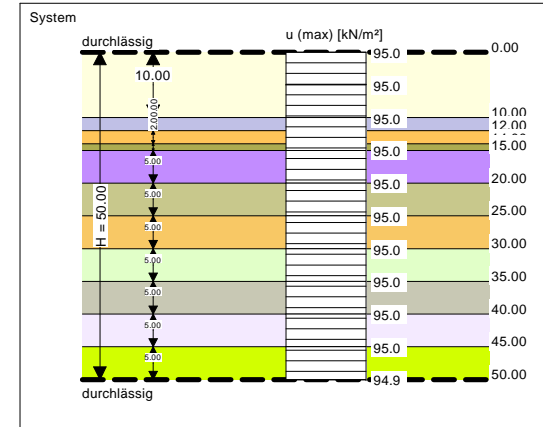
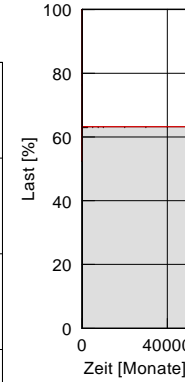
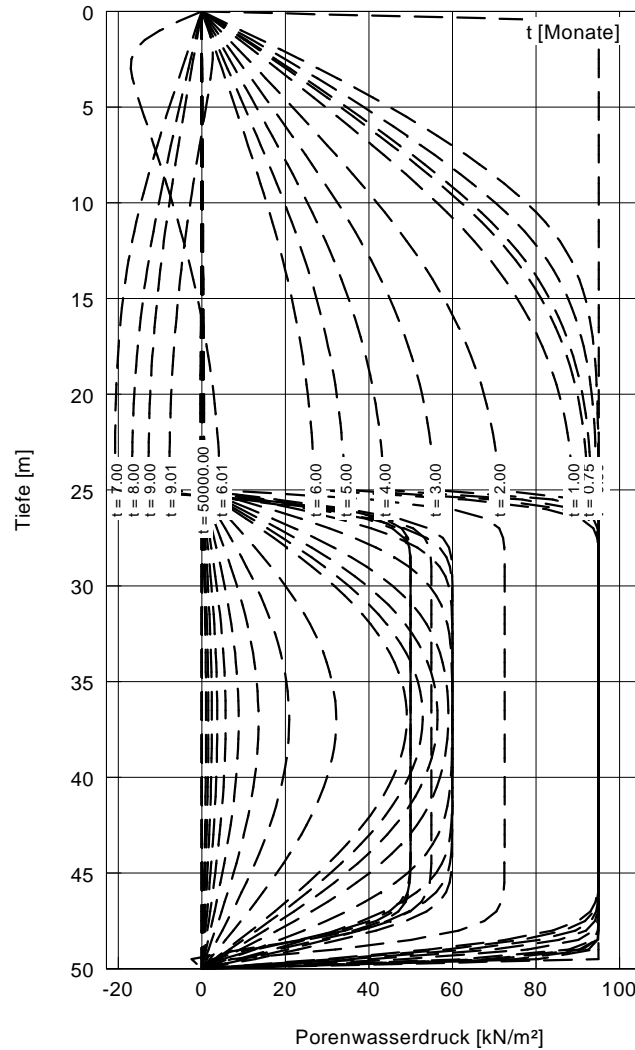
Zeit [Monate]	U [-]	s [cm]
0.00	0.008	0.9
0.34	0.122	13.4
0.50	0.149	16.3
0.67	0.173	19.0
0.75	0.183	20.1
1.00	0.214	23.4
2.00	0.310	34.0
3.00	0.382	41.9
4.00	0.436	47.8
5.00	0.477	52.4
6.00	0.509	55.9
6.01	0.508	55.7
7.00	0.486	53.4
8.00	0.479	52.5
9.00	0.473	51.9
9.01	0.473	51.9
10.00	0.469	51.5
15.00	0.462	50.7
25.00	0.465	51.0
50.00	0.477	52.4
100.00	0.496	54.4
150.00	0.511	56.0
200.00	0.523	57.4
249.00	0.534	58.6
500.00	0.575	63.1
750.00	0.601	66.0
1000.00	0.619	67.9
1250.00	0.630	69.1
1500.00	0.637	69.9
1750.00	0.642	70.4
2000.00	0.645	70.7
2250.00	0.647	70.9
2500.00	0.648	71.1
5000.00	0.650	71.3
7500.00	0.650	71.3
10000.00	0.650	71.3
20000.00	0.650	71.3
30000.00	0.650	71.3
40000.00	0.650	71.3
50000.00	0.650	71.3



One-dimensional consolidation theory
 Settlement calculation for roads with 10kPa life load after 9 months
 Schrittweite (Tiefe) = 0.500 m
 Endsetzung = 109.7 cm

Boden	E_s [kN/m ²]	k [m/s]	c_v [m ² /s]	$E_{s(w)}/E_s$ [-]	Bezeichnung
	5000.0	$7.29 \cdot 10^{-8}$	$3.65 \cdot 10^{-5}$	3.00	Clayey Silt
	2600.0	$7.29 \cdot 10^{-8}$	$1.90 \cdot 10^{-5}$	3.00	Silty Clay
	2800.0	$7.29 \cdot 10^{-8}$	$2.04 \cdot 10^{-5}$	3.00	Silty Clay
	2900.0	$7.29 \cdot 10^{-8}$	$2.12 \cdot 10^{-5}$	3.00	Silty Clay
	3250.0	$7.29 \cdot 10^{-8}$	$2.37 \cdot 10^{-5}$	3.00	Silty Clay
	3750.0	$7.29 \cdot 10^{-8}$	$2.74 \cdot 10^{-5}$	3.00	Silty Clay
	4250.0	$8.04 \cdot 10^{-11}$	$3.42 \cdot 10^{-8}$	3.00	Silty Clay
	4750.0	$8.04 \cdot 10^{-11}$	$3.82 \cdot 10^{-8}$	3.00	Silty Clay
	5250.0	$8.04 \cdot 10^{-11}$	$4.22 \cdot 10^{-8}$	3.00	Silty Clay
	5750.0	$8.04 \cdot 10^{-11}$	$4.62 \cdot 10^{-8}$	3.00	Silty Clay
	6250.0	$8.04 \cdot 10^{-11}$	$5.02 \cdot 10^{-8}$	3.00	Silty Clay

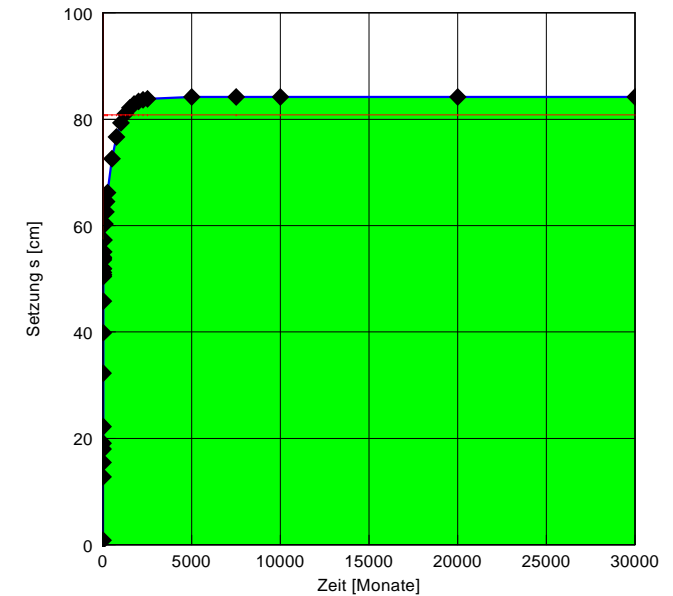
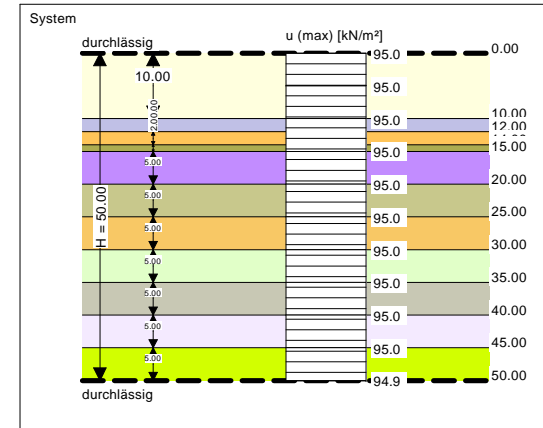
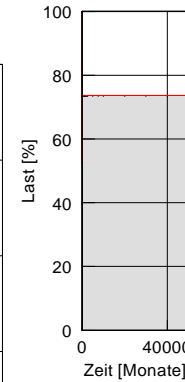
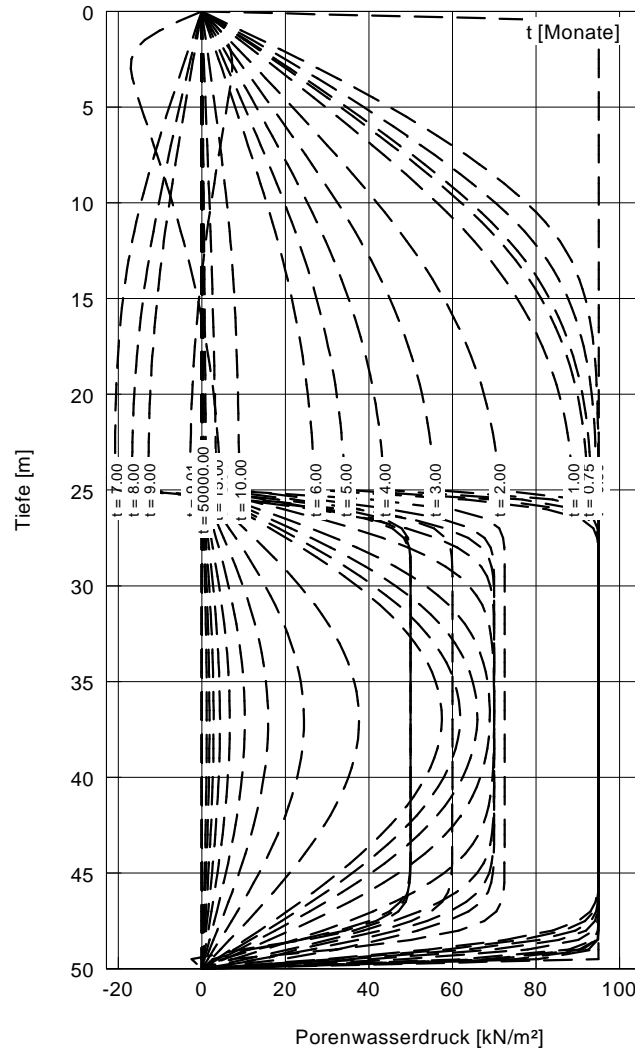
Zeit [Monate]	U [-]	s [cm]
0.00	0.008	0.9
0.34	0.116	12.8
0.50	0.141	15.5
0.67	0.164	18.0
0.75	0.174	19.1
1.00	0.203	22.2
2.00	0.294	32.3
3.00	0.363	39.9
4.00	0.417	45.8
5.00	0.459	50.4
6.00	0.493	54.1
6.01	0.491	53.9
7.00	0.473	51.9
8.00	0.467	51.2
9.00	0.462	50.7
9.01	0.463	50.8
10.00	0.466	51.1
15.00	0.470	51.6
25.00	0.478	52.5
50.00	0.495	54.3
100.00	0.518	56.8
150.00	0.536	58.8
200.00	0.551	60.4
249.00	0.564	61.9
500.00	0.613	67.3
750.00	0.645	70.8
1000.00	0.666	73.0
1250.00	0.679	74.5
1500.00	0.688	75.5
1750.00	0.693	76.1
2000.00	0.697	76.5
2250.00	0.700	76.8
2500.00	0.701	76.9
5000.00	0.704	77.2
7500.00	0.704	77.2
10000.00	0.704	77.2
20000.00	0.704	77.2
30000.00	0.704	77.2
40000.00	0.704	77.2
50000.00	0.704	77.2



One-dimensional consolidation theory
 Settlement calculation for roads with 20kPa life load after 9 months
 Schrittweite (Tiefe) = 0.500 m
 Endsetzung = 109.7 cm

Boden	E_s [kN/m ²]	k [m/s]	c_v [m ² /s]	$E_{s(w)}/E_s$ [-]	Bezeichnung
	5000.0	$7.29 \cdot 10^{-8}$	$3.65 \cdot 10^{-5}$	3.00	Clayey Silt
	2600.0	$7.29 \cdot 10^{-8}$	$1.90 \cdot 10^{-5}$	3.00	Silty Clay
	2800.0	$7.29 \cdot 10^{-8}$	$2.04 \cdot 10^{-5}$	3.00	Silty Clay
	2900.0	$7.29 \cdot 10^{-8}$	$2.12 \cdot 10^{-5}$	3.00	Silty Clay
	3250.0	$7.29 \cdot 10^{-8}$	$2.37 \cdot 10^{-5}$	3.00	Silty Clay
	3750.0	$7.29 \cdot 10^{-8}$	$2.74 \cdot 10^{-5}$	3.00	Silty Clay
	4250.0	$8.04 \cdot 10^{-11}$	$3.42 \cdot 10^{-8}$	3.00	Silty Clay
	4750.0	$8.04 \cdot 10^{-11}$	$3.82 \cdot 10^{-8}$	3.00	Silty Clay
	5250.0	$8.04 \cdot 10^{-11}$	$4.22 \cdot 10^{-8}$	3.00	Silty Clay
	5750.0	$8.04 \cdot 10^{-11}$	$4.62 \cdot 10^{-8}$	3.00	Silty Clay
	6250.0	$8.04 \cdot 10^{-11}$	$5.02 \cdot 10^{-8}$	3.00	Silty Clay

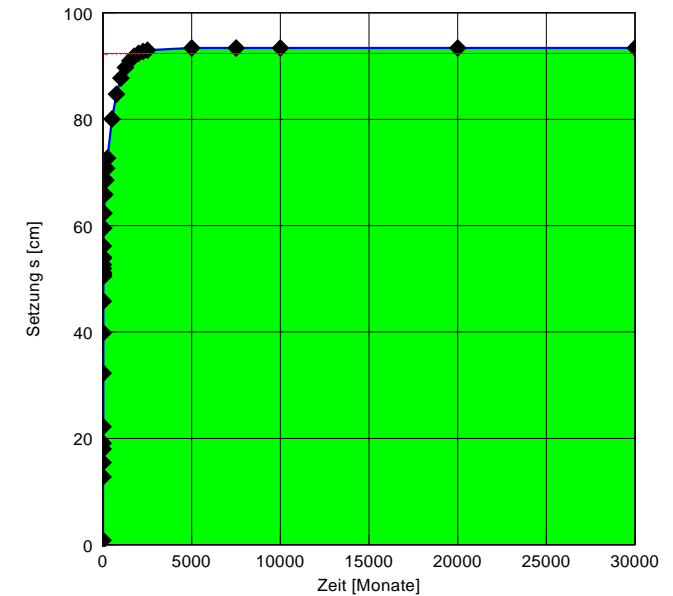
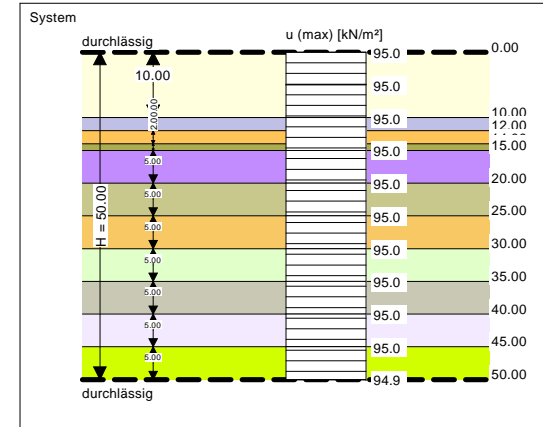
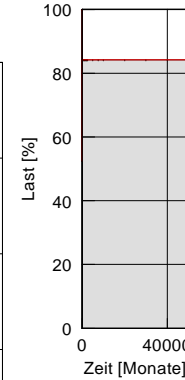
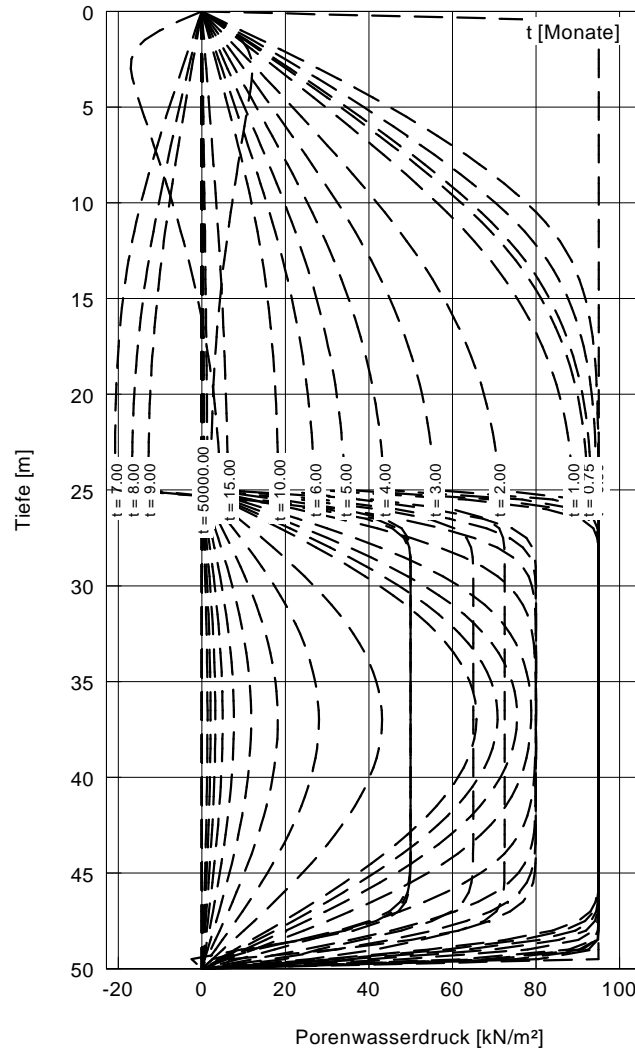
Zeit [Monate]	U [-]	s [cm]
0.00	0.008	0.9
0.34	0.116	12.8
0.50	0.141	15.5
0.67	0.164	18.0
0.75	0.174	19.1
1.00	0.203	22.2
2.00	0.294	32.3
3.00	0.363	39.9
4.00	0.417	45.8
5.00	0.459	50.4
6.00	0.493	54.1
6.01	0.491	53.9
7.00	0.473	51.9
8.00	0.467	51.2
9.00	0.462	50.7
9.01	0.463	50.8
10.00	0.473	51.9
15.00	0.488	53.5
25.00	0.502	55.1
50.00	0.522	57.3
100.00	0.550	60.3
150.00	0.570	62.6
200.00	0.588	64.5
249.00	0.603	66.2
500.00	0.661	72.6
750.00	0.699	76.7
1000.00	0.723	79.3
1250.00	0.738	81.0
1500.00	0.749	82.1
1750.00	0.755	82.9
2000.00	0.760	83.3
2250.00	0.762	83.6
2500.00	0.764	83.8
5000.00	0.767	84.2
7500.00	0.768	84.2
10000.00	0.768	84.2
20000.00	0.768	84.2
30000.00	0.768	84.2
40000.00	0.768	84.2
50000.00	0.768	84.2



One-dimensional consolidation theory
 Settlement calculation for roads with 30kPa life load after 9 months
 Schrittweite (Tiefe) = 0.500 m
 Endsetzung = 109.7 cm

Boden	E_s [kN/m ²]	k [m/s]	c_v [m ² /s]	$E_{s(w)}/E_s$ [-]	Bezeichnung
	5000.0	$7.29 \cdot 10^{-8}$	$3.65 \cdot 10^{-5}$	3.00	Clayey Silt
	2600.0	$7.29 \cdot 10^{-8}$	$1.90 \cdot 10^{-5}$	3.00	Silty Clay
	2800.0	$7.29 \cdot 10^{-8}$	$2.04 \cdot 10^{-5}$	3.00	Silty Clay
	2900.0	$7.29 \cdot 10^{-8}$	$2.12 \cdot 10^{-5}$	3.00	Silty Clay
	3250.0	$7.29 \cdot 10^{-8}$	$2.37 \cdot 10^{-5}$	3.00	Silty Clay
	3750.0	$7.29 \cdot 10^{-8}$	$2.74 \cdot 10^{-5}$	3.00	Silty Clay
	4250.0	$8.04 \cdot 10^{-11}$	$3.42 \cdot 10^{-8}$	3.00	Silty Clay
	4750.0	$8.04 \cdot 10^{-11}$	$3.82 \cdot 10^{-8}$	3.00	Silty Clay
	5250.0	$8.04 \cdot 10^{-11}$	$4.22 \cdot 10^{-8}$	3.00	Silty Clay
	5750.0	$8.04 \cdot 10^{-11}$	$4.62 \cdot 10^{-8}$	3.00	Silty Clay
	6250.0	$8.04 \cdot 10^{-11}$	$5.02 \cdot 10^{-8}$	3.00	Silty Clay

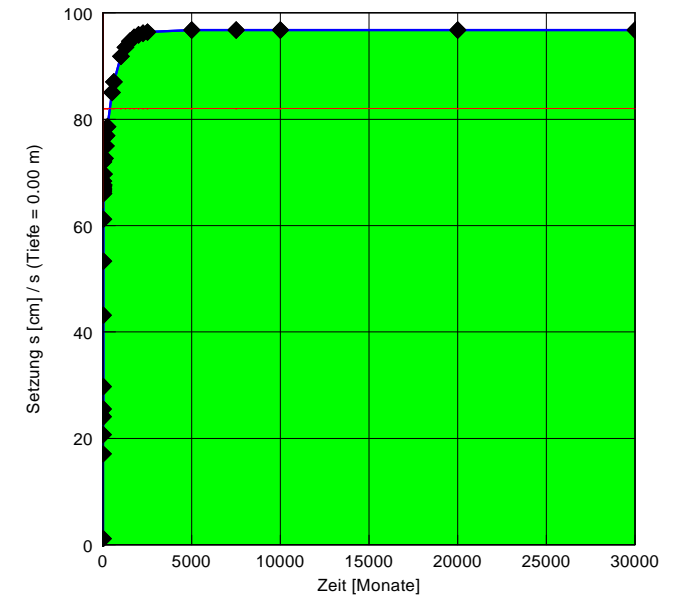
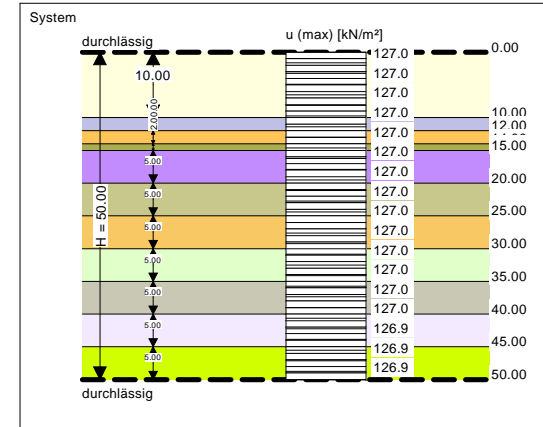
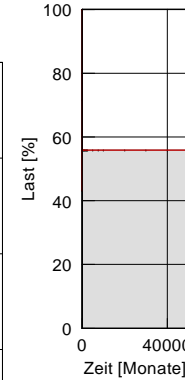
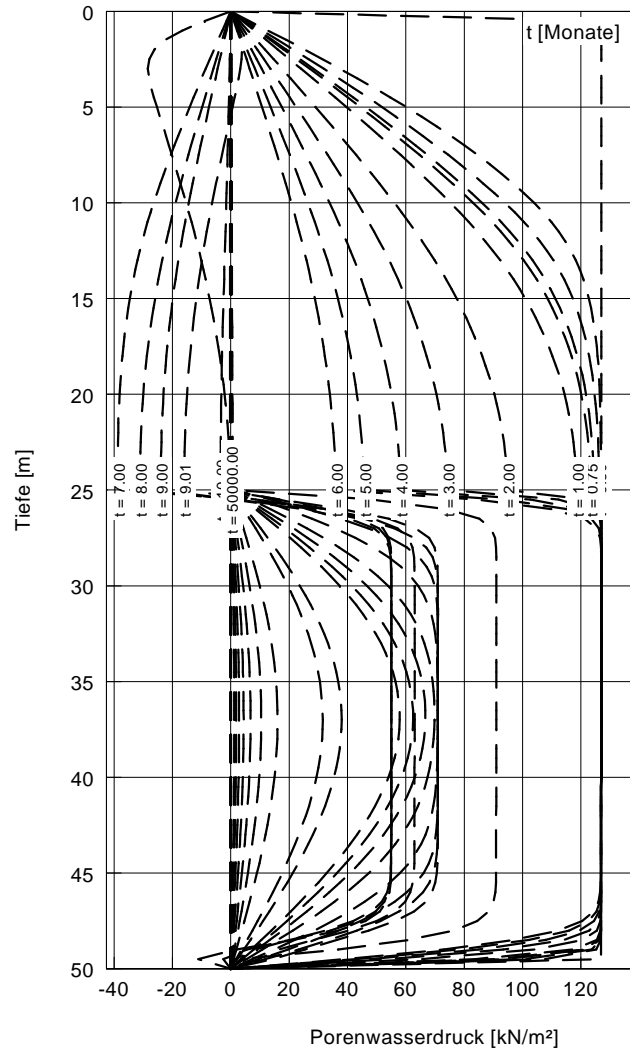
Zeit [Monate]	U [-]	s [cm]
0.00	0.008	0.9
0.34	0.116	12.8
0.50	0.141	15.5
0.67	0.164	18.0
0.75	0.174	19.1
1.00	0.203	22.2
2.00	0.294	32.3
3.00	0.363	39.9
4.00	0.417	45.8
5.00	0.459	50.4
6.00	0.493	54.1
6.01	0.491	53.9
7.00	0.473	51.9
8.00	0.467	51.2
9.00	0.462	50.7
9.01	0.463	50.8
10.00	0.480	52.7
15.00	0.512	56.2
25.00	0.542	59.5
50.00	0.568	62.3
100.00	0.600	65.9
150.00	0.625	68.5
200.00	0.645	70.8
249.00	0.662	72.7
500.00	0.729	80.0
750.00	0.772	84.7
1000.00	0.800	87.7
1250.00	0.818	89.7
1500.00	0.829	91.0
1750.00	0.837	91.8
2000.00	0.842	92.4
2250.00	0.845	92.7
2500.00	0.847	93.0
5000.00	0.851	93.4
7500.00	0.851	93.4
10000.00	0.851	93.4
20000.00	0.851	93.4
30000.00	0.851	93.4
40000.00	0.851	93.4
50000.00	0.851	93.4



One-dimensional consolidation theory
 Settlement calculation for structures with 16kPa life and structural loads after 9 months
 Schrittweite (Tiefe) = 0.500 m
 Endsetzung = 146.7 cm

Boden	E_s [kN/m ²]	k [m/s]	c_v [m ² /s]	$E_{s(w)}/E_s$ [-]	Bezeichnung
	5000.0	$7.29 \cdot 10^{-8}$	$3.65 \cdot 10^{-5}$	3.00	Clayey Silt
	2600.0	$7.29 \cdot 10^{-8}$	$1.90 \cdot 10^{-5}$	3.00	Silty Clay
	2800.0	$7.29 \cdot 10^{-8}$	$2.04 \cdot 10^{-5}$	3.00	Silty Clay
	2900.0	$7.29 \cdot 10^{-8}$	$2.12 \cdot 10^{-5}$	3.00	Silty Clay
	3250.0	$7.29 \cdot 10^{-8}$	$2.37 \cdot 10^{-5}$	3.00	Silty Clay
	3750.0	$7.29 \cdot 10^{-8}$	$2.74 \cdot 10^{-5}$	3.00	Silty Clay
	4250.0	$8.04 \cdot 10^{-11}$	$3.42 \cdot 10^{-8}$	3.00	Silty Clay
	4750.0	$8.04 \cdot 10^{-11}$	$3.82 \cdot 10^{-8}$	3.00	Silty Clay
	5250.0	$8.04 \cdot 10^{-11}$	$4.22 \cdot 10^{-8}$	3.00	Silty Clay
	5750.0	$8.04 \cdot 10^{-11}$	$4.62 \cdot 10^{-8}$	3.00	Silty Clay
	6250.0	$8.04 \cdot 10^{-11}$	$5.02 \cdot 10^{-8}$	3.00	Silty Clay

Zeit [Monate]	U [-]	s [cm]
0.00	0.008	1.1
0.34	0.116	17.1
0.50	0.141	20.7
0.67	0.164	24.1
0.75	0.174	25.5
1.00	0.203	29.7
2.00	0.294	43.1
3.00	0.363	53.3
4.00	0.417	61.2
5.00	0.459	67.4
6.00	0.493	72.3
6.01	0.491	72.0
7.00	0.466	68.4
8.00	0.457	67.0
9.00	0.450	66.0
9.01	0.451	66.1
10.00	0.453	66.5
15.00	0.455	66.7
25.00	0.461	67.6
50.00	0.475	69.7
100.00	0.495	72.7
150.00	0.511	75.0
200.00	0.524	76.9
250.00	0.536	78.6
500.00	0.580	85.0
609.00	0.593	87.0
1000.00	0.626	91.8
1250.00	0.638	93.5
1500.00	0.645	94.7
1750.00	0.650	95.4
2000.00	0.654	95.9
2250.00	0.656	96.2
2500.00	0.657	96.4
5000.00	0.660	96.7
7500.00	0.660	96.8
10000.00	0.660	96.8
20000.00	0.660	96.8
30000.00	0.660	96.8
40000.00	0.660	96.8
50000.00	0.660	96.8



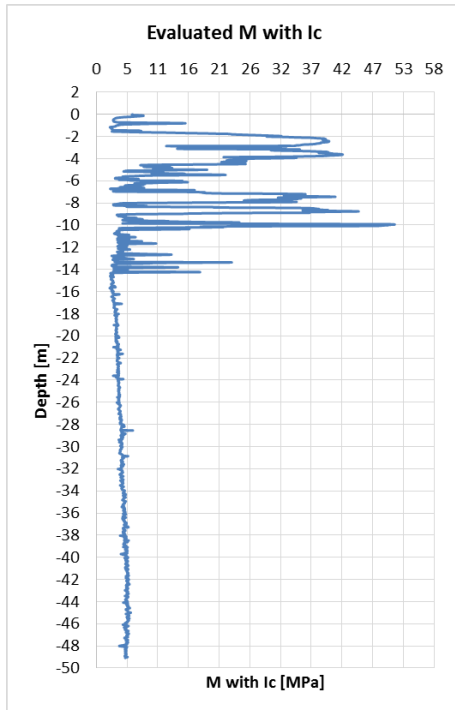
Appendix C

**Recreated with the Excel spreadsheets graphs for the
Investigation-1 (CPTu_1 – CPTu_8)**

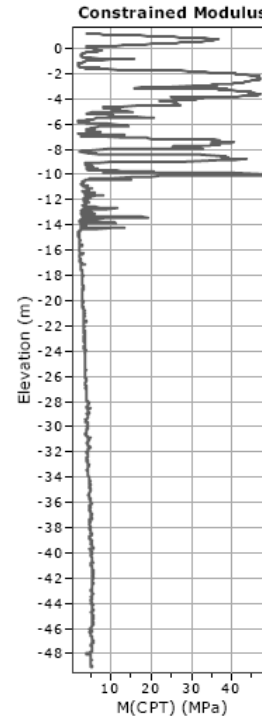
(Contains 24 pages)

1. CPTu_1

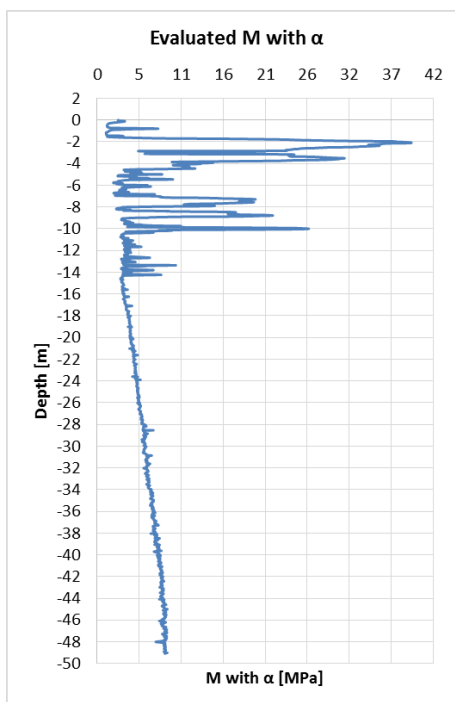
Evaluated constrained modulus M_{Ic}



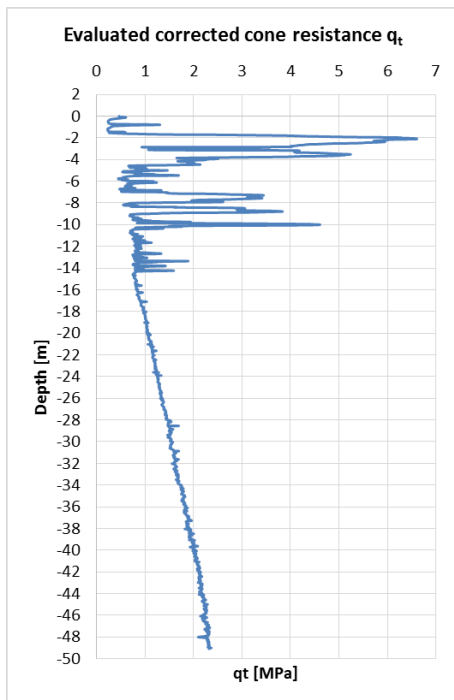
Constrained modulus M_{Ic} from the report



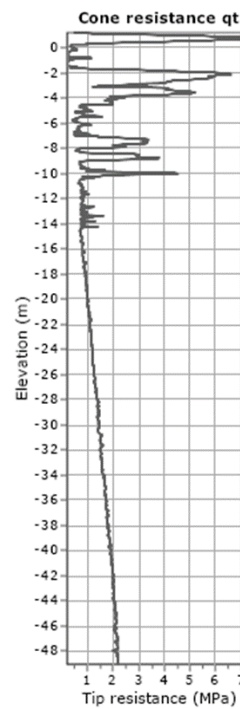
Evaluated constrained modulus $M_{\alpha M}$



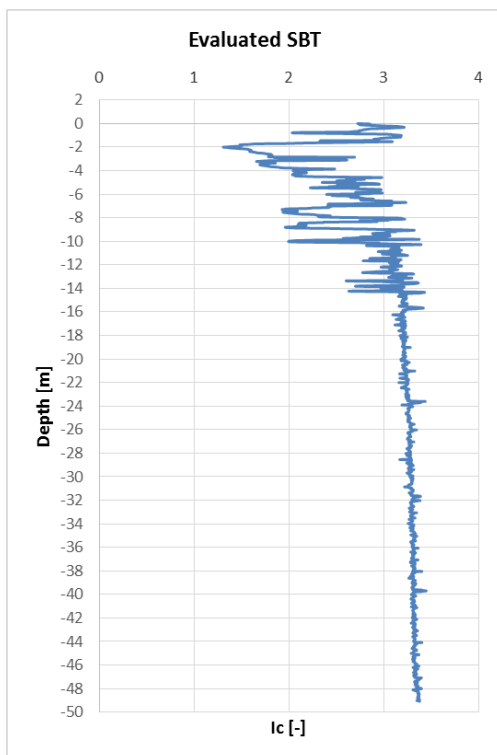
Evaluated corrected cone resistance q_t



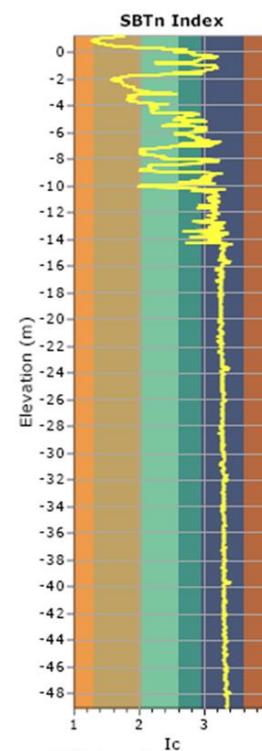
Corrected cone resistance q_t from the report



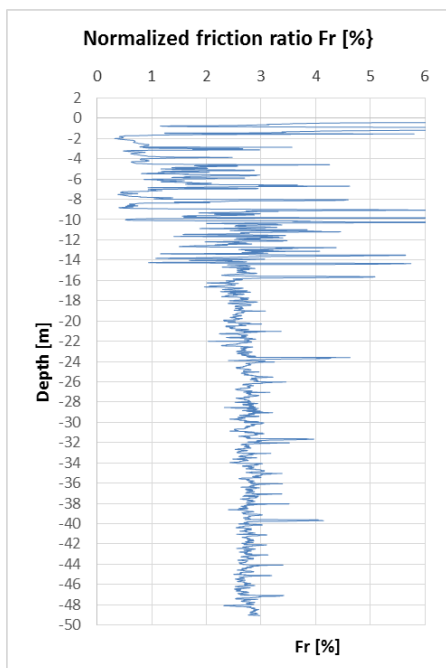
Evaluated soil behavior type index I_c



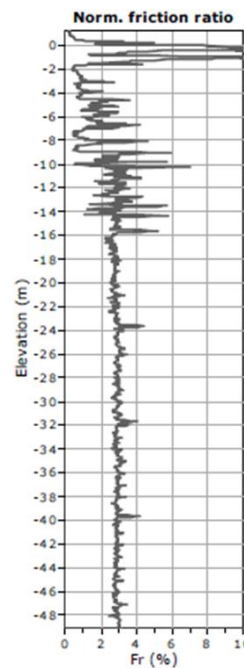
Soil behavior type index I_c from the report



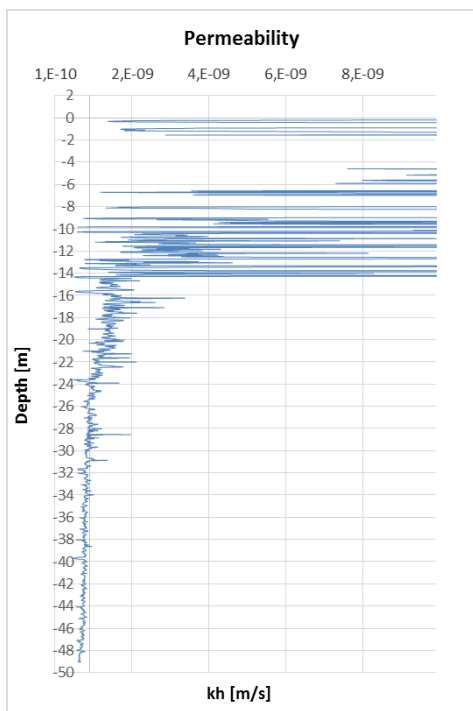
Evaluated normalized friction ratio Fr



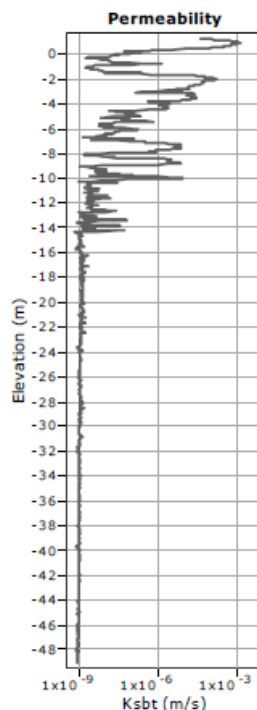
Normalized friction ratio Fr from the report



Evaluated permeability k_h

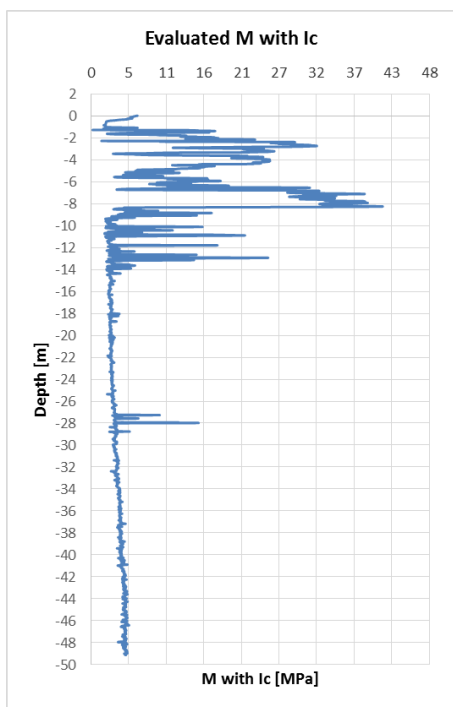


Permeability k_h from the report

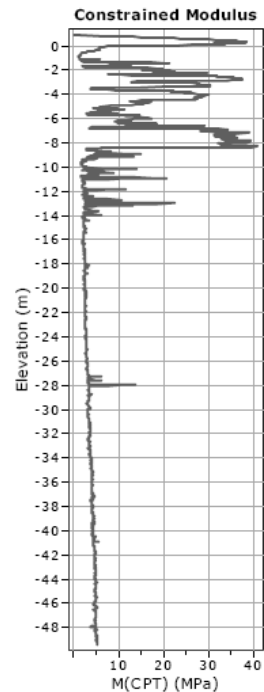


2. CPTu_2

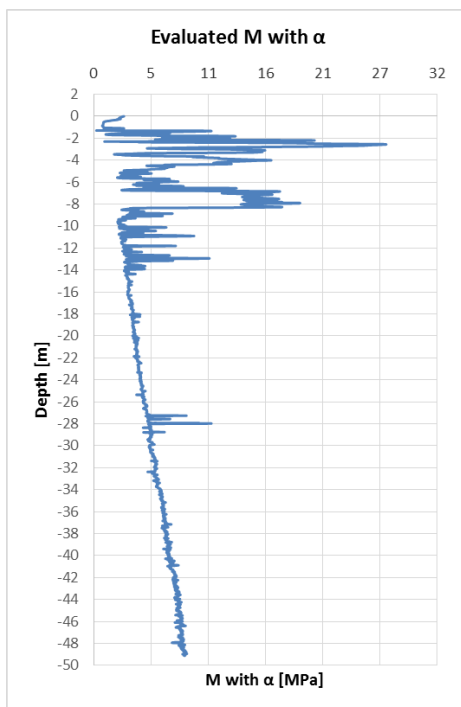
Evaluated constrained modulus M_{Ic}



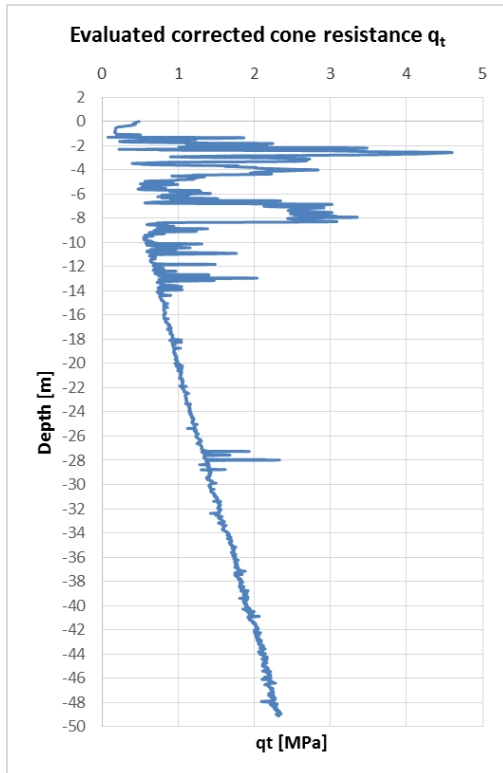
Constrained modulus M_{Ic} from the report



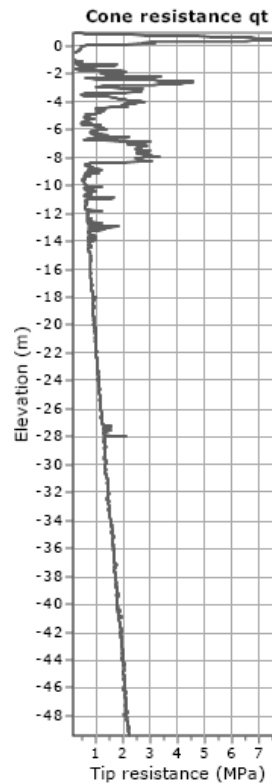
Evaluated constrained modulus $M_{\alpha M}$



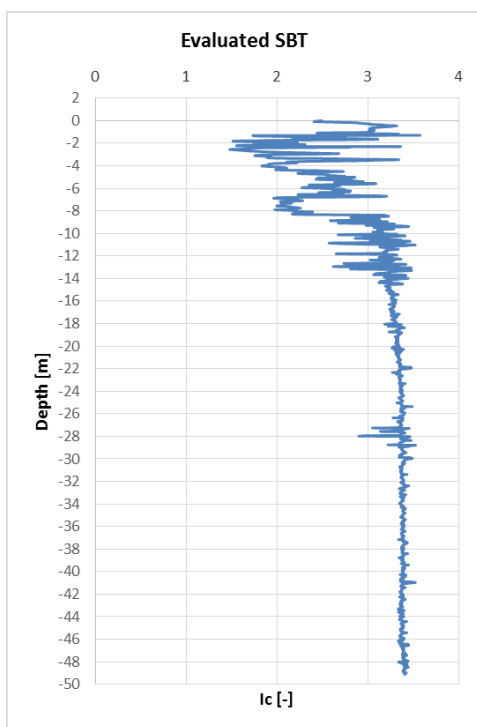
Evaluated corrected cone resistance
 q_t



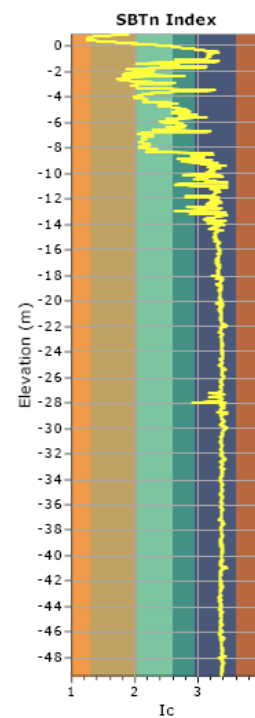
Corrected cone resistance q_t from the report



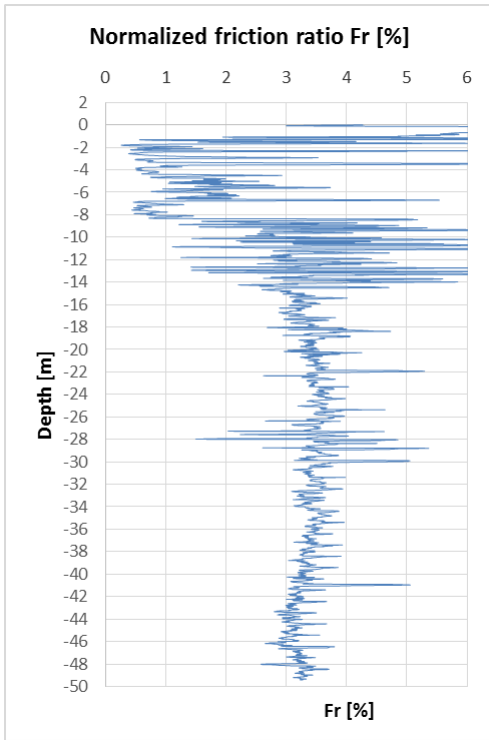
Evaluated soil behavior type index I_c



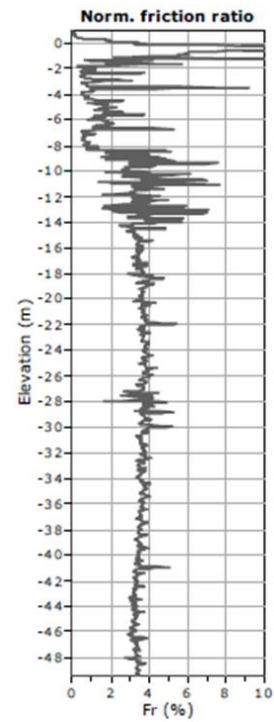
Soil behavior type index I_c from the report



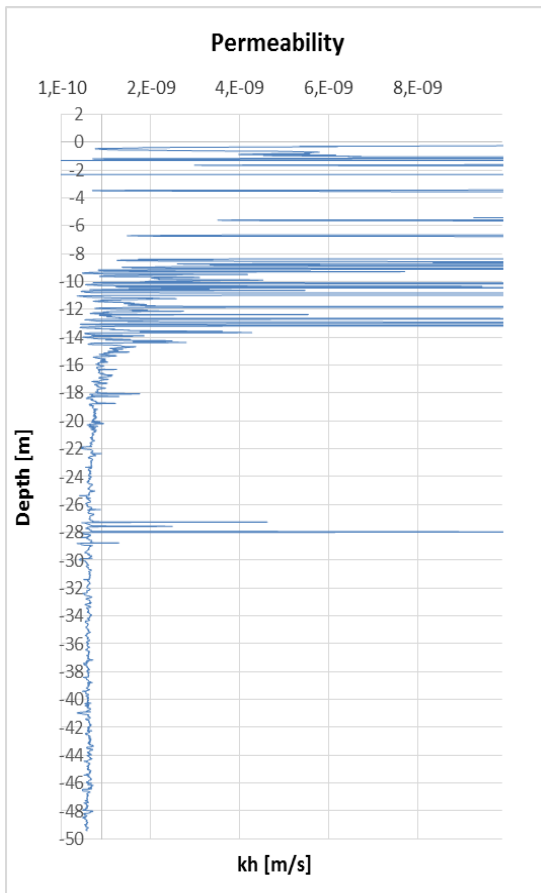
Evaluated normalized friction ratio F_r



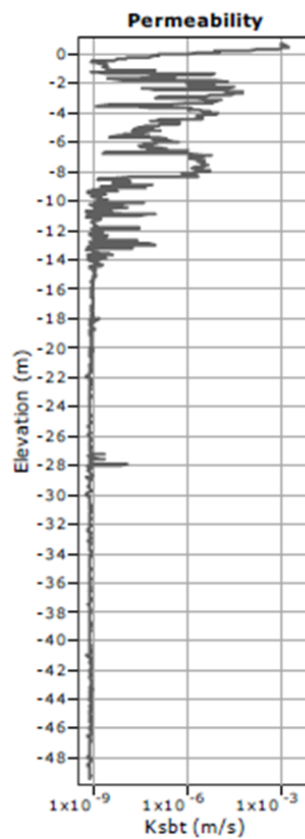
Normalized friction ratio F_r from the report



Evaluated permeability k_h

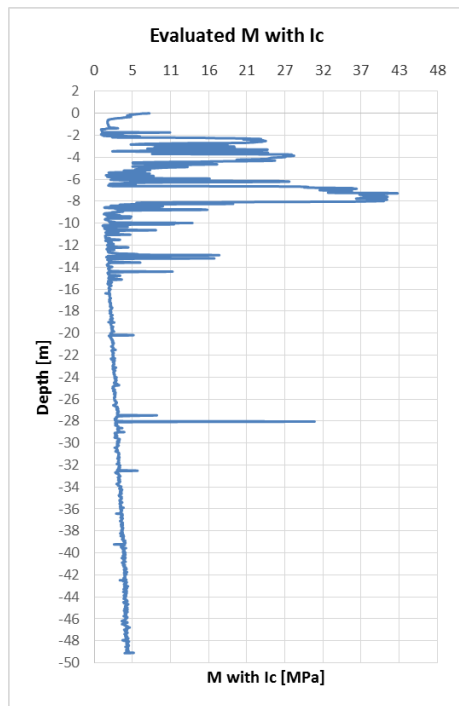


Permeability k_h from the report

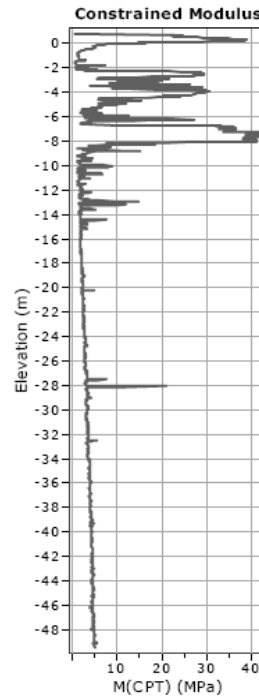


3. CPTu_3

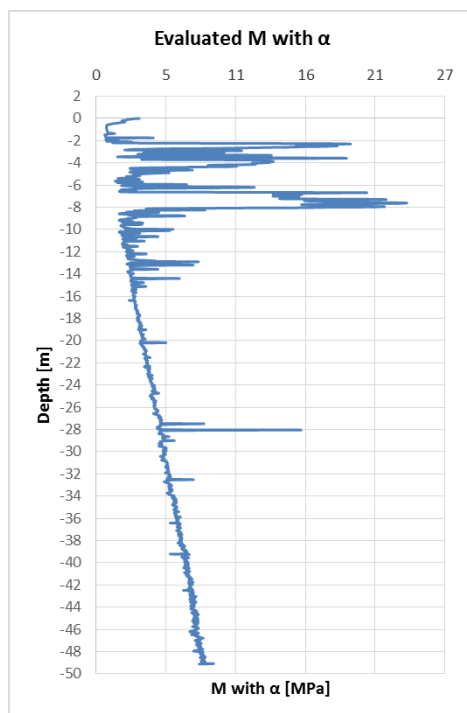
Evaluated constrained modulus M_{Ic}



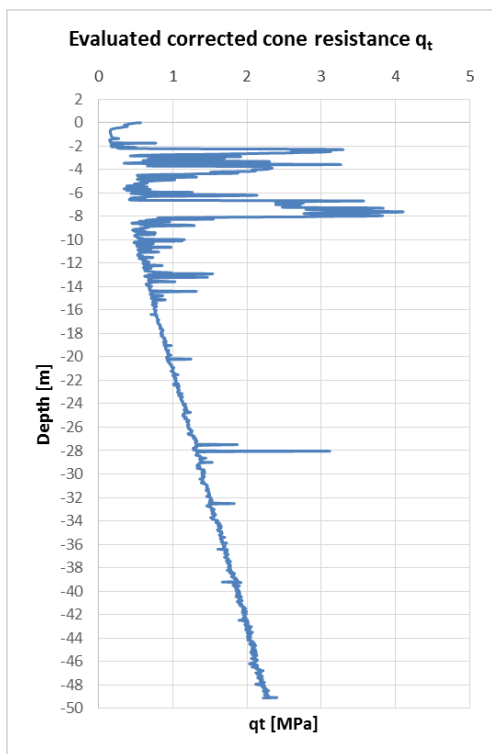
Constrained modulus M_{Ic} from the report



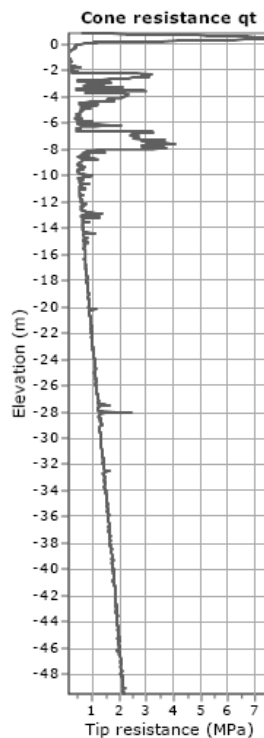
Evaluated constrained modulus $M_{\alpha M}$



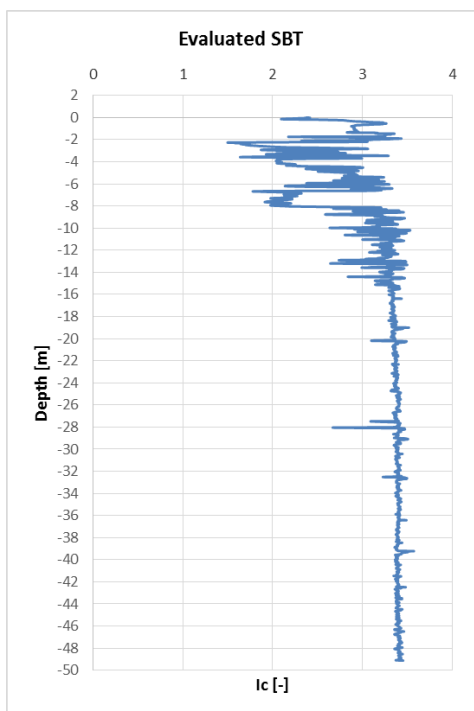
Evaluated corrected cone resistance q_t



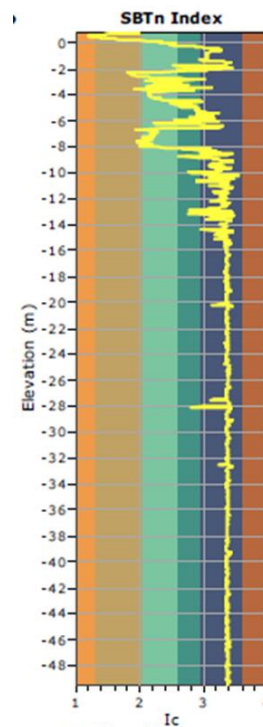
Corrected cone resistance q_t from the report



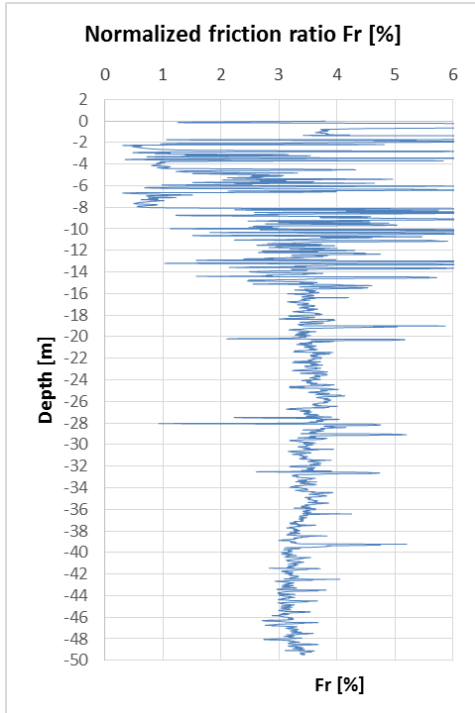
Evaluated soil behavior type index I_c



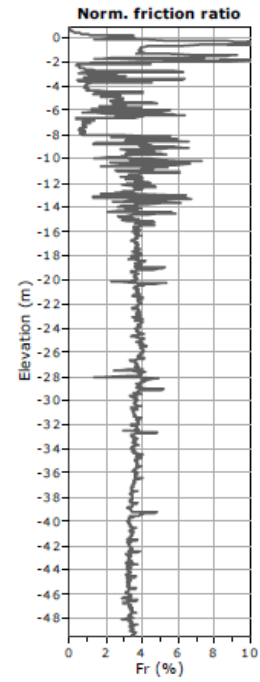
Soil behavior type index I_c from the report



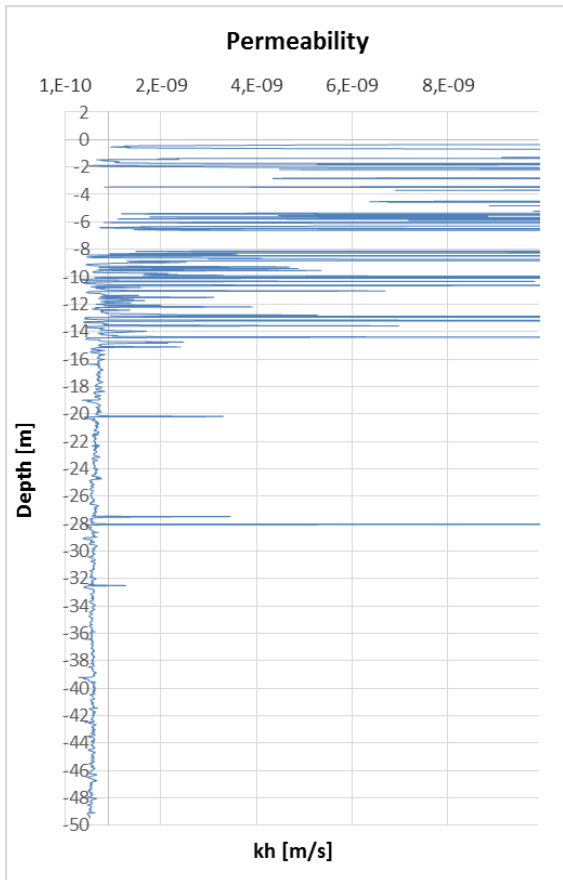
**Evaluated normalized
friction ratio Fr**



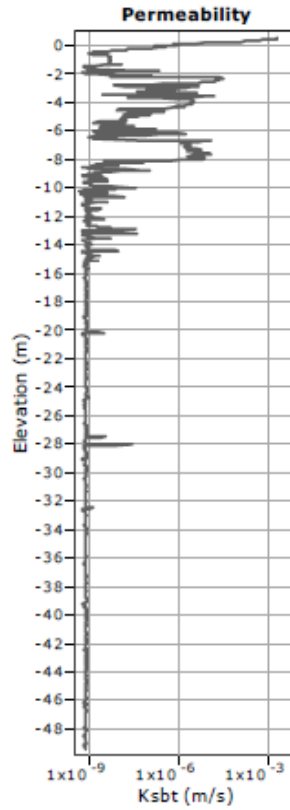
**Normalized friction ratio Fr
from the report**



Evaluated permeability k_h

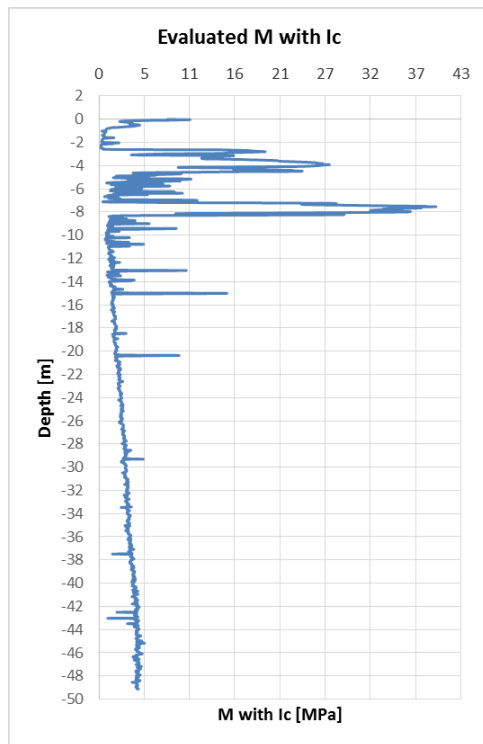


Permeability k_h from the report

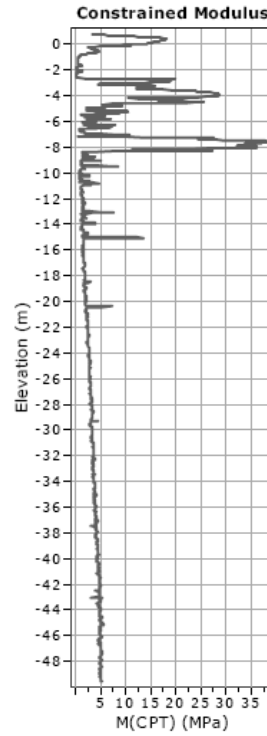


4. CPTu_4

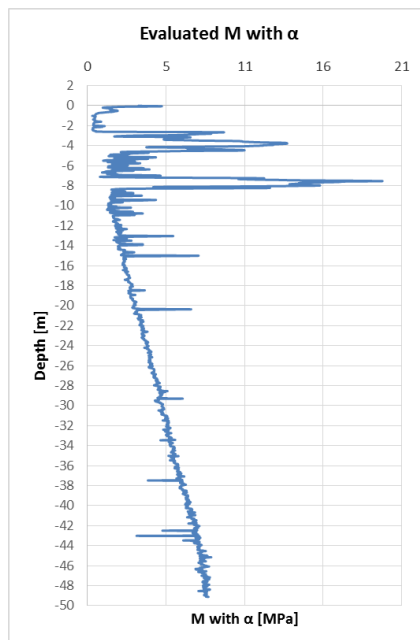
Evaluated constrained modulus M_{Ic}



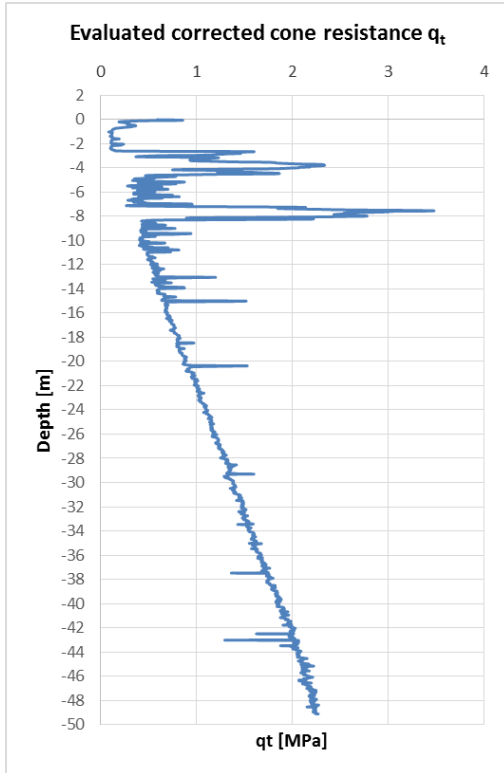
Constrained modulus M_{Ic} from the report



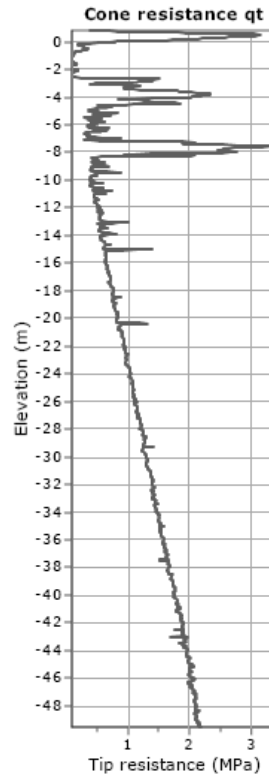
Evaluated constrained modulus $M_{\alpha M}$



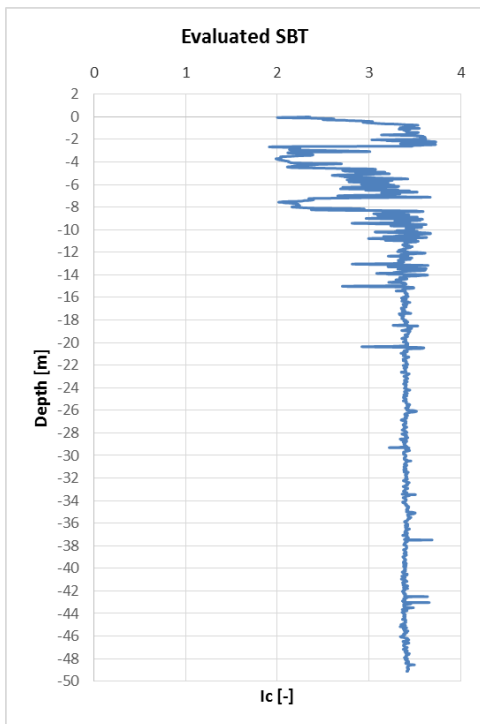
Evaluated corrected cone resistance q_t



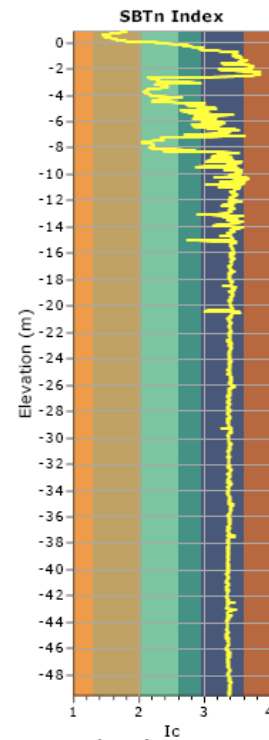
Corrected cone resistance q_t from the report



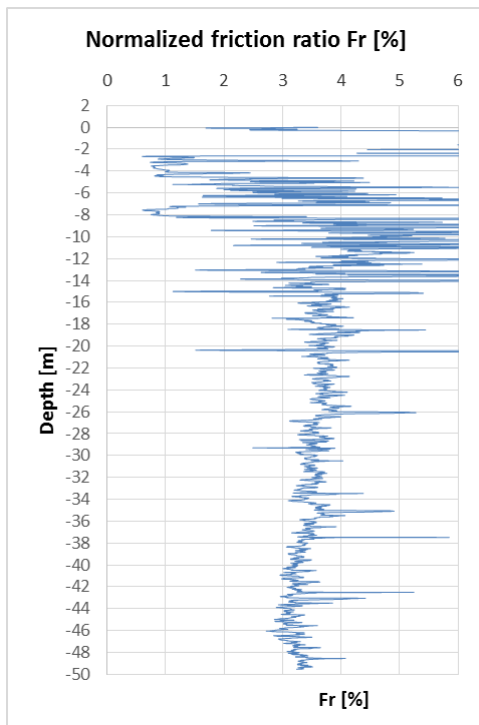
Evaluated soil behavior type index I_c



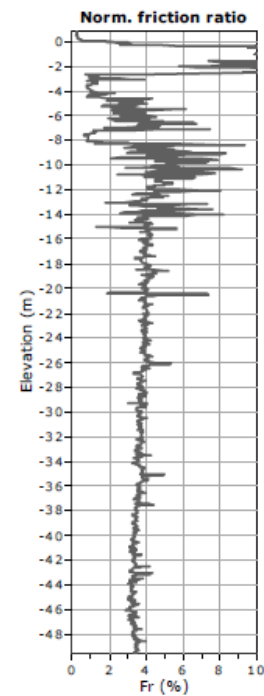
Soil behavior type index I_c from the report



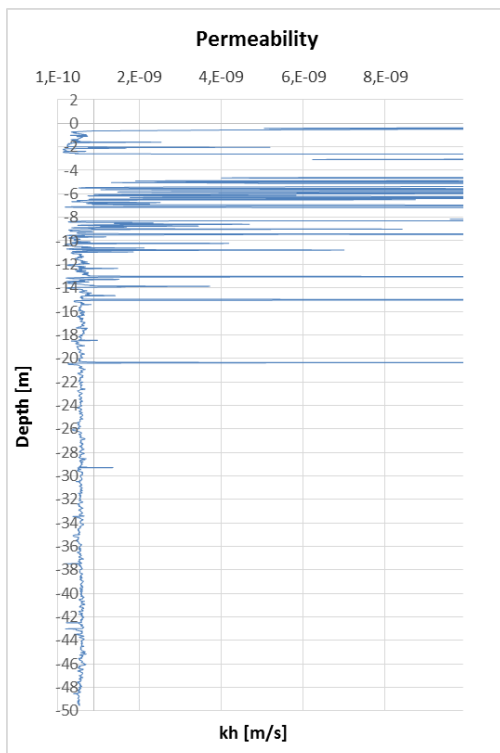
Evaluated normalized friction ratio Fr



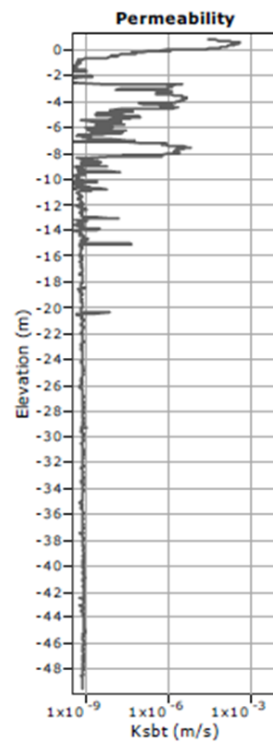
Normalized friction ratio Fr from the report



Evaluated permeability k_h



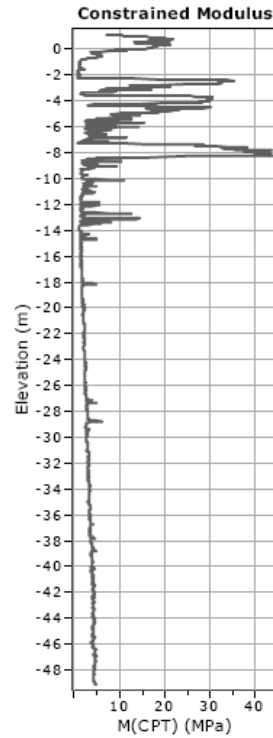
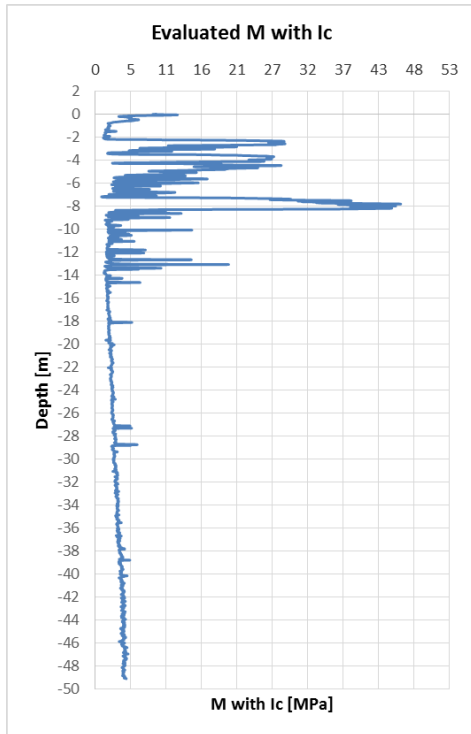
Permeability k_h from the report



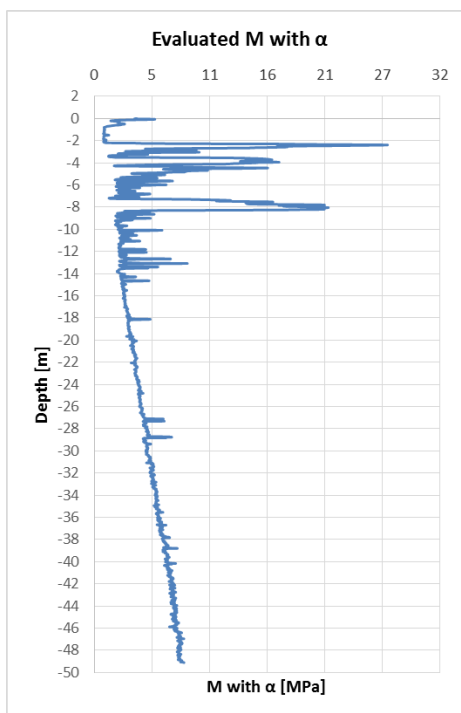
5. CPTu_5

**Evaluated constrained
modulus M_{Ic}**

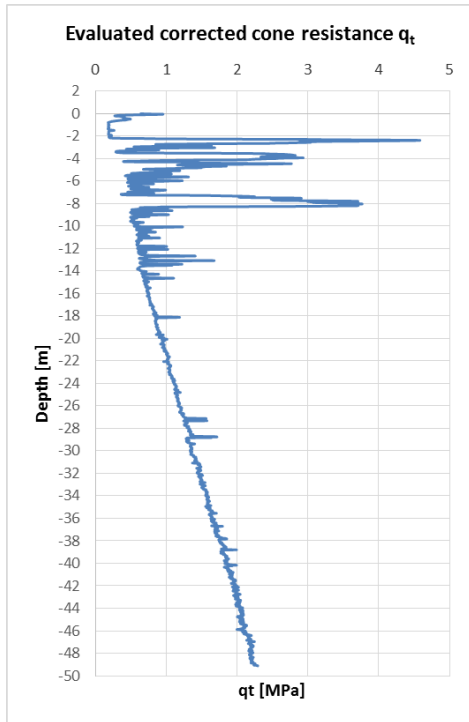
**Constrained modulus M_{Ic} from the
report**



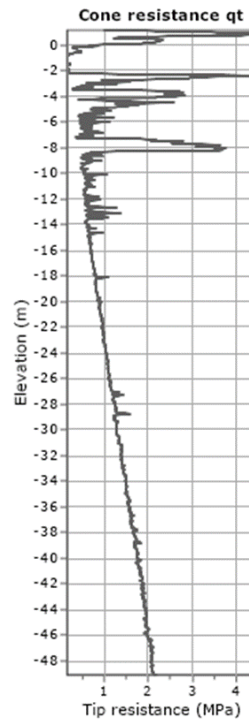
Evaluated constrained modulus $M_{\alpha M}$



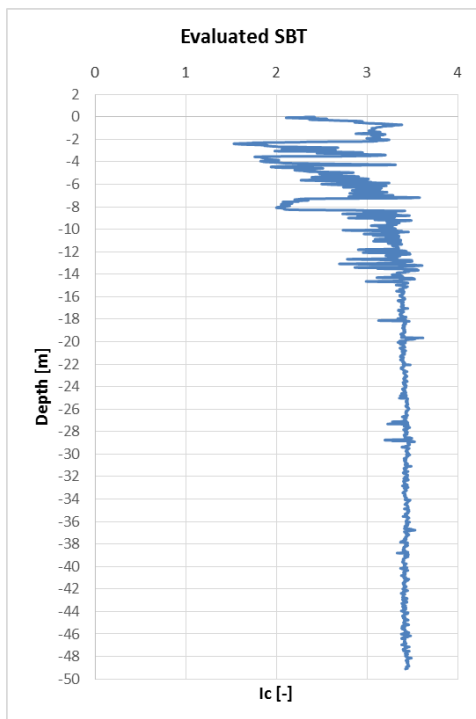
Evaluated corrected cone resistance q_t



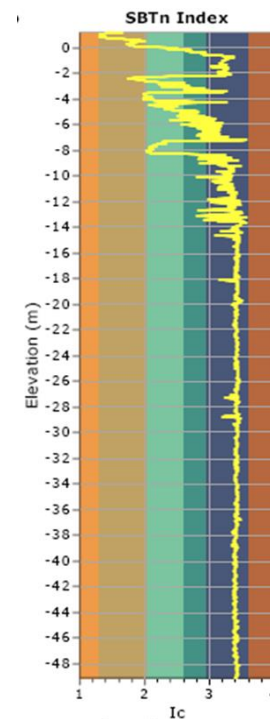
Corrected cone resistance q_t from the report



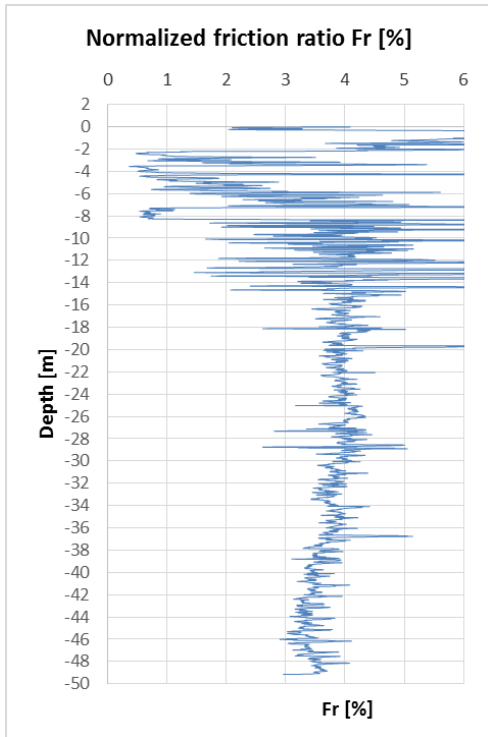
Evaluated soil behavior type index I_c



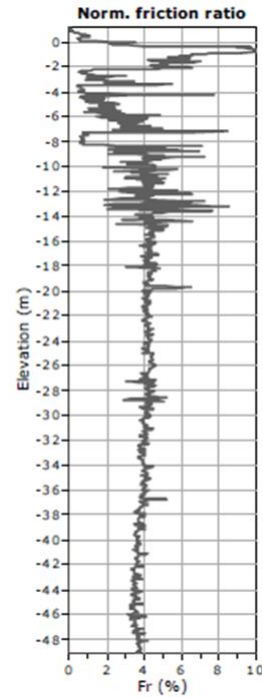
Soil behavior type index I_c from the report



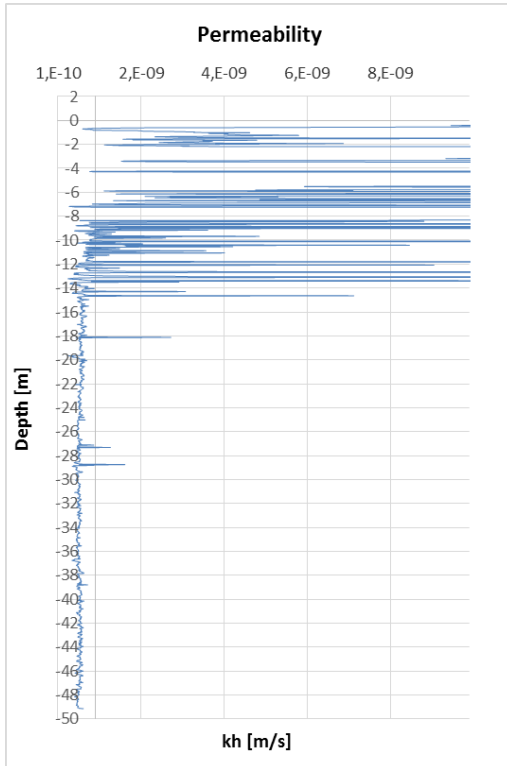
Evaluated normalized friction ratio Fr



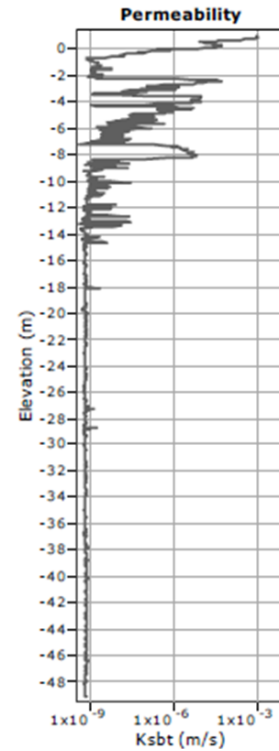
Normalized friction ratio Fr from the report



Evaluated permeability k_h

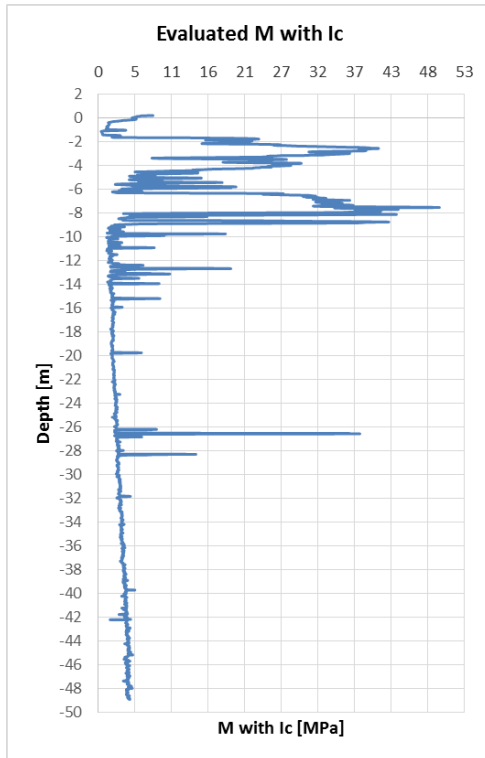


Permeability k_h from the report

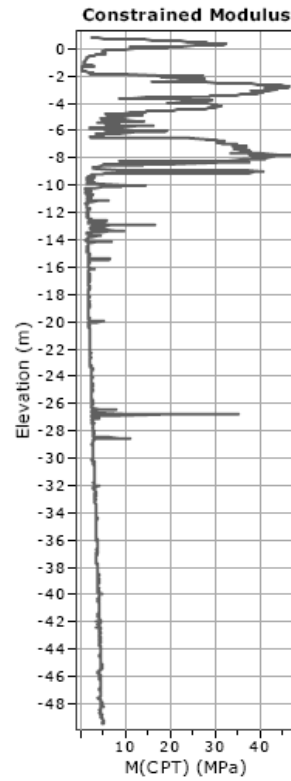


6. CPTu_6

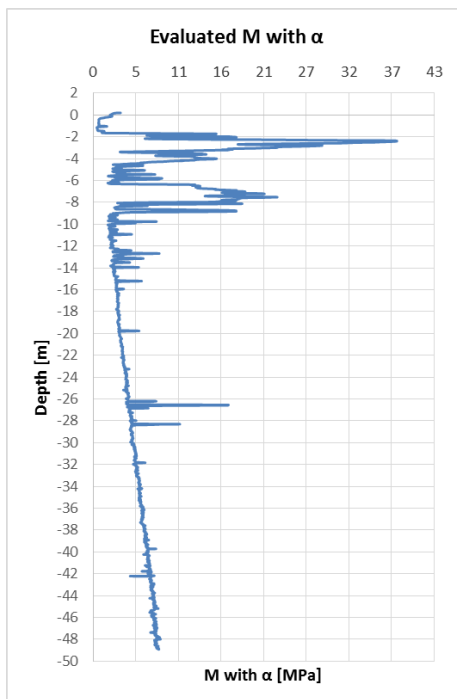
Evaluated constrained modulus M_{Ic}



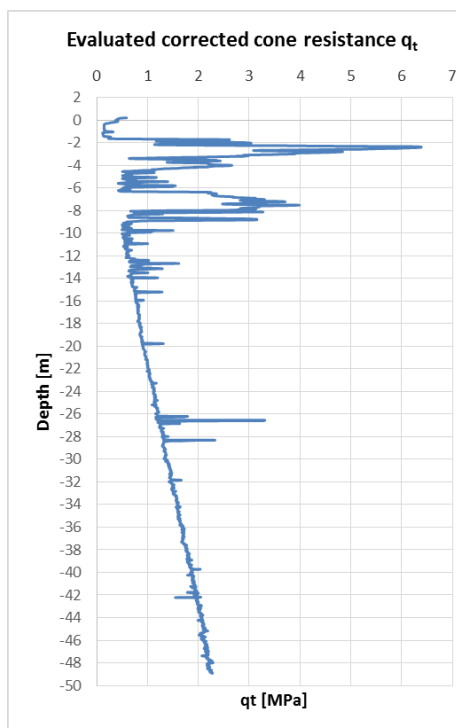
Constrained modulus M_{Ic} from the report



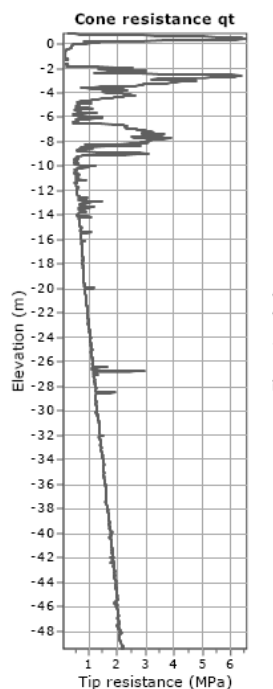
Evaluated constrained modulus $M_{\alpha M}$



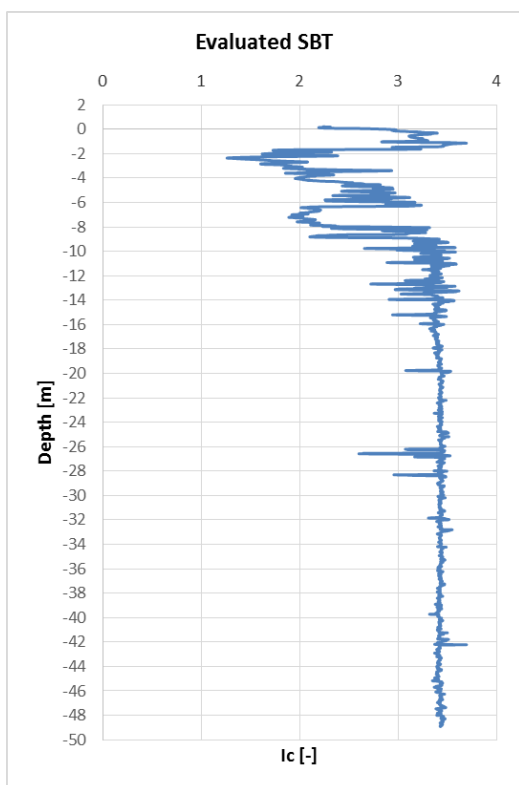
Evaluated corrected cone resistance q_t



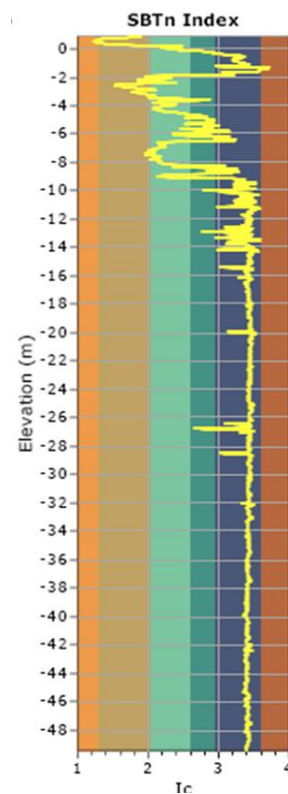
Corrected cone resistance q_t from the report



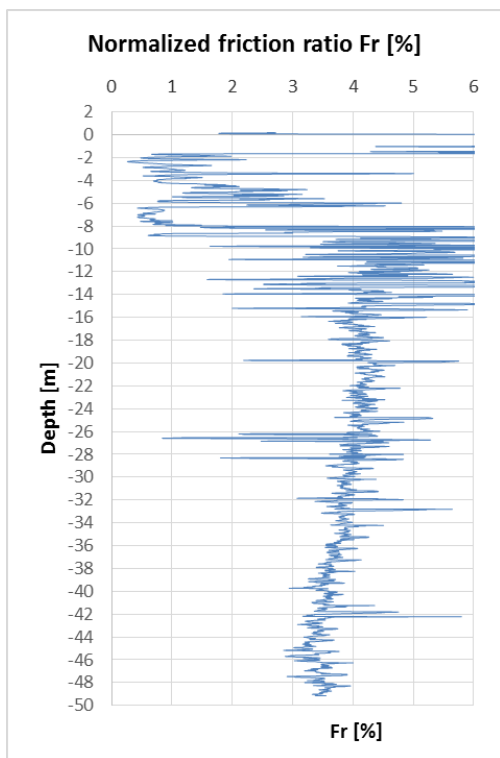
Evaluated soil behavior type index I_c



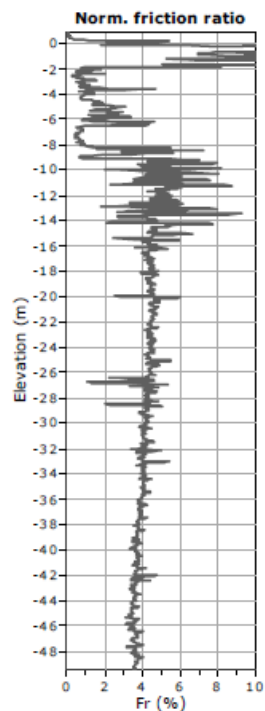
Soil behavior type index I_c from the report



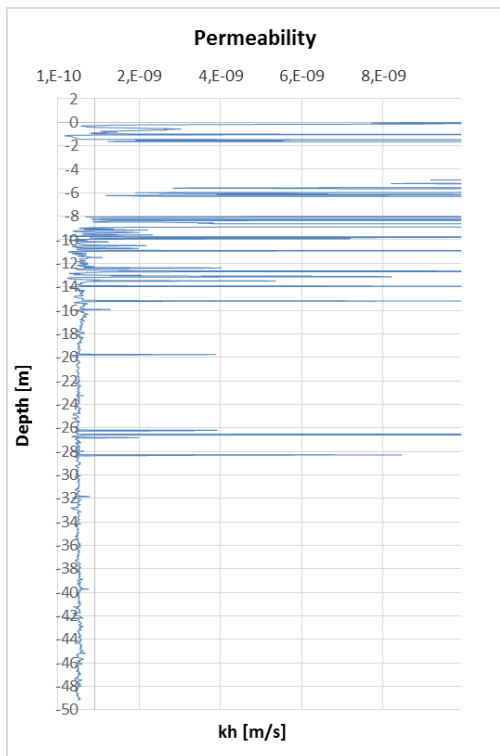
Evaluated normalized friction ratio Fr



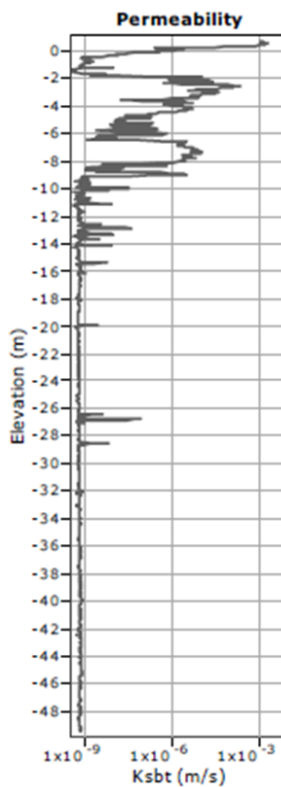
Normalized friction ratio Fr from the report



Evaluated permeability k_h

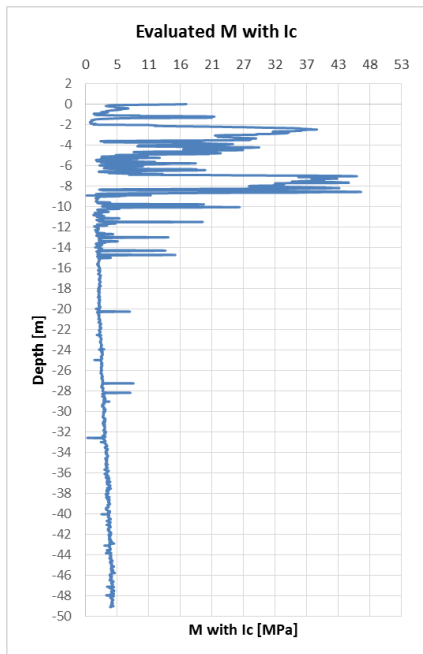


Permeability k_h from the report

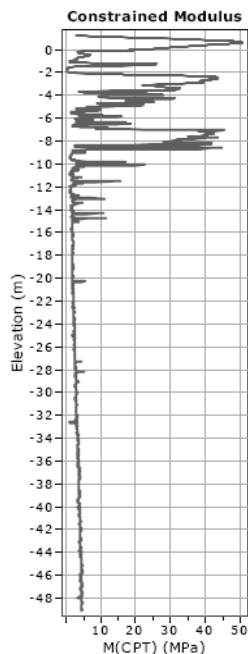


7. CPTu_7

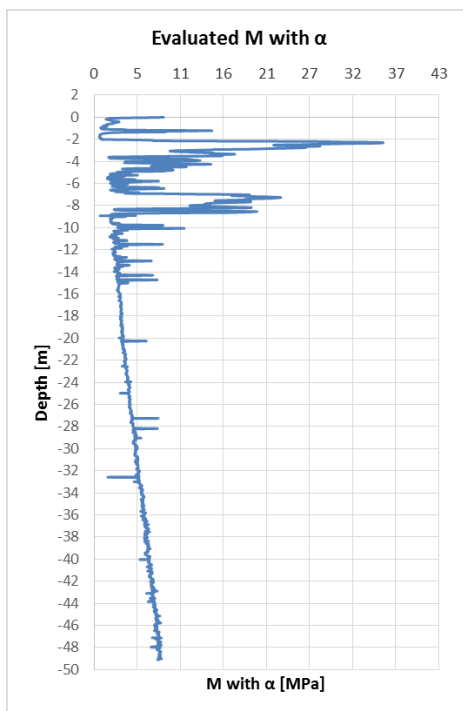
Evaluated constrained modulus M_{Ic}



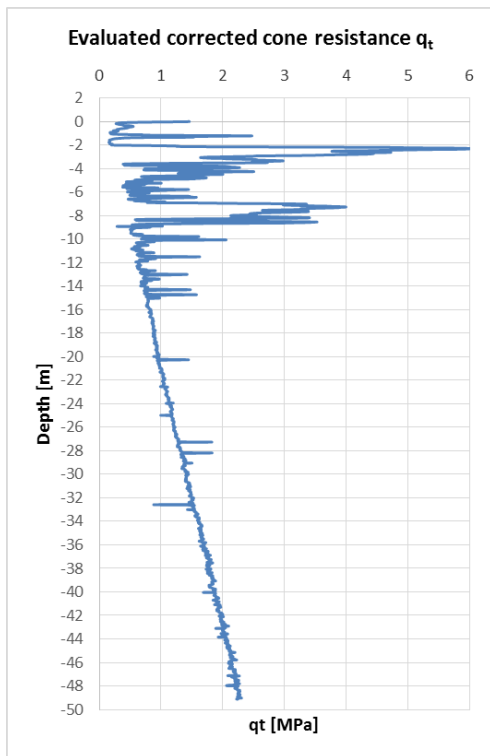
Constrained modulus M_{Ic} from the report



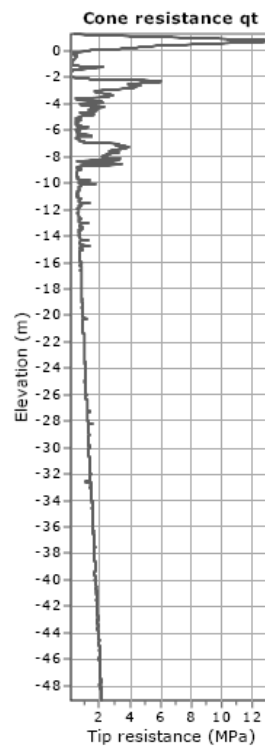
Evaluated constrained modulus $M_{\alpha M}$



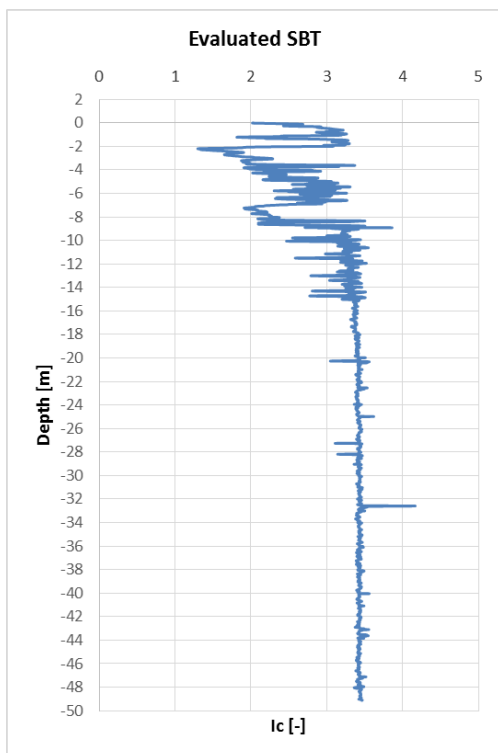
Evaluated corrected cone resistance q_t



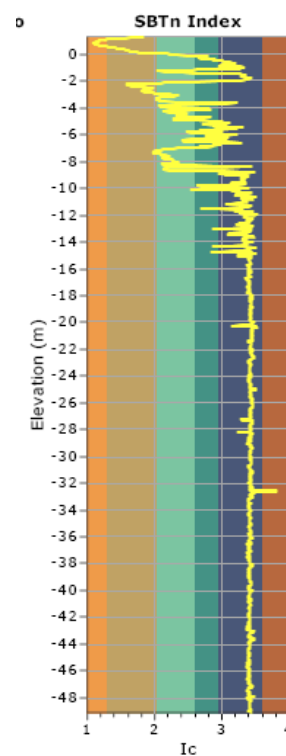
Corrected cone resistance q_t from the report



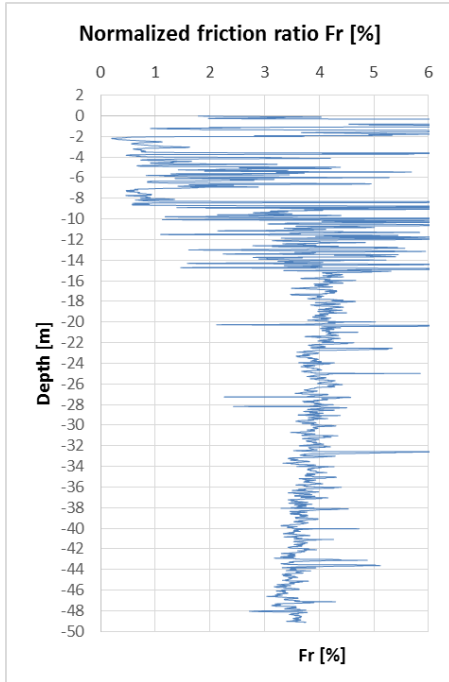
Evaluated soil behavior type index I_c



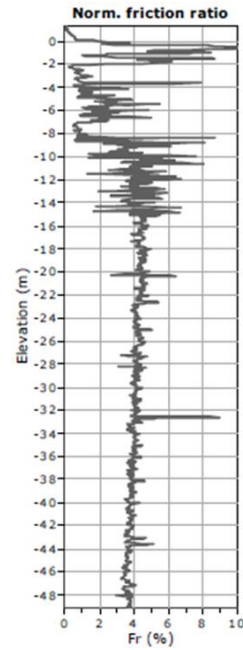
Soil behavior type index I_c from the report



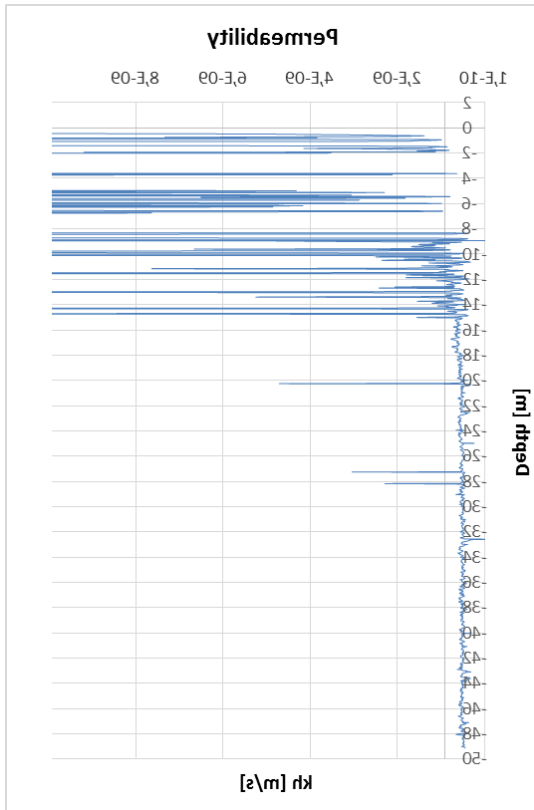
Evaluated normalized friction ratio Fr



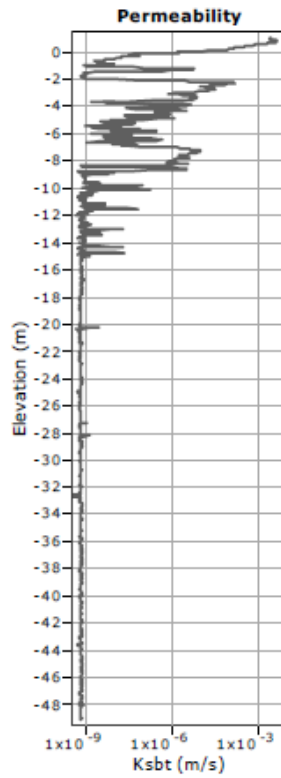
Normalized friction ratio Fr from the report



Evaluated permeability k_h

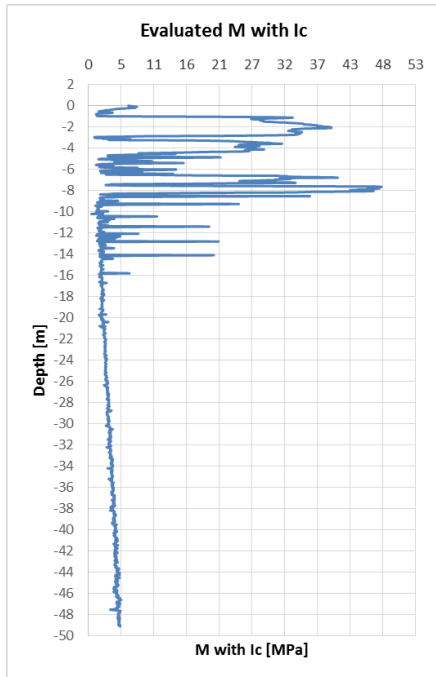


Permeability k_h from the report

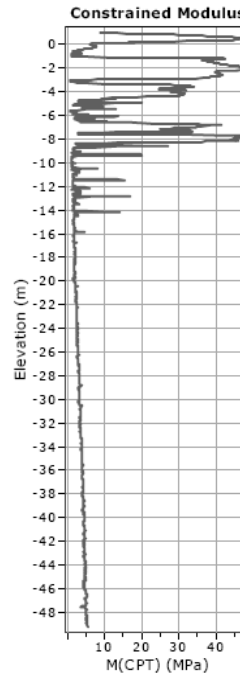


8. CPTu_8

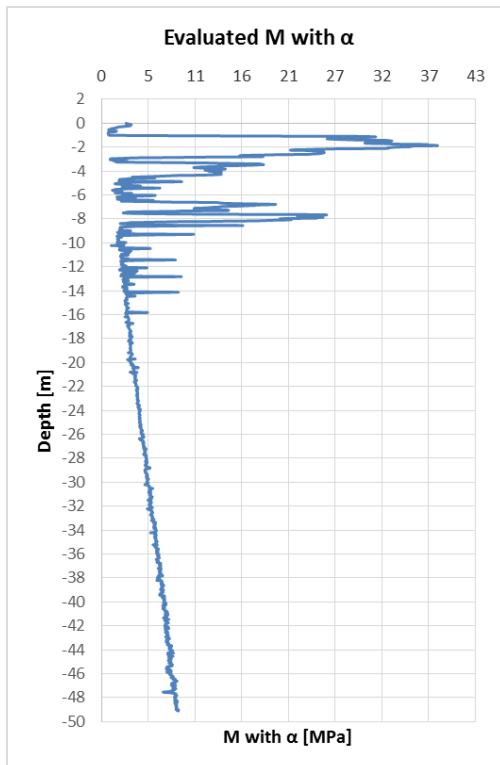
Evaluated constrained modulus M_{Ic}



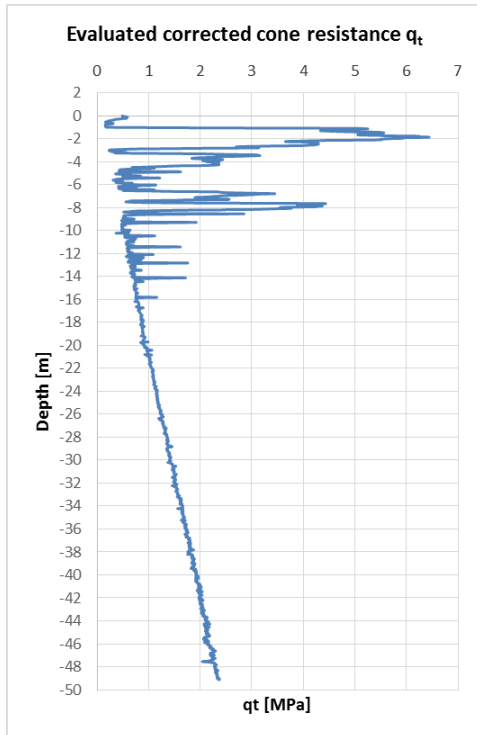
Constrained modulus M_{Ic} from the report



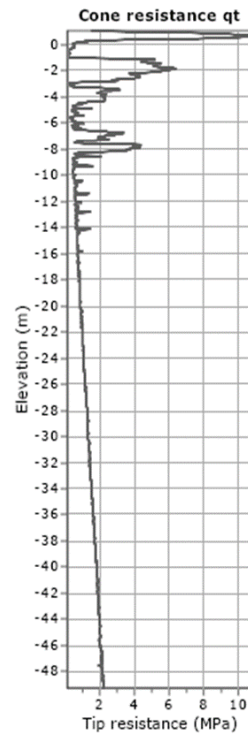
Evaluated constrained modulus $M_{\alpha M}$



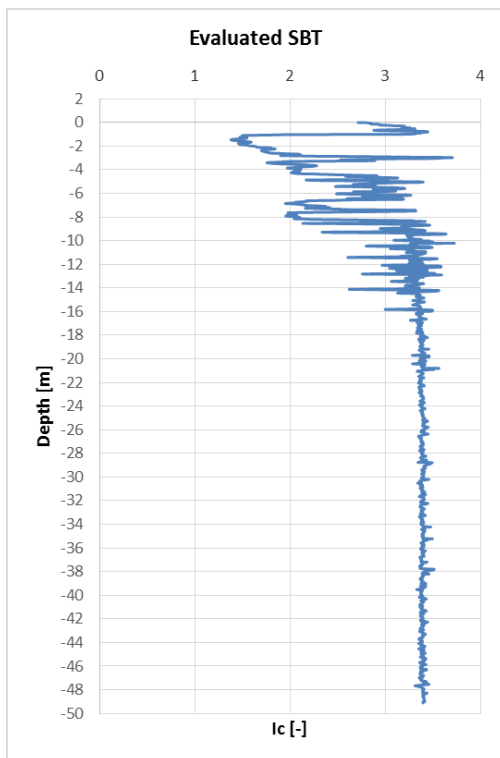
Evaluated corrected cone resistance q_t



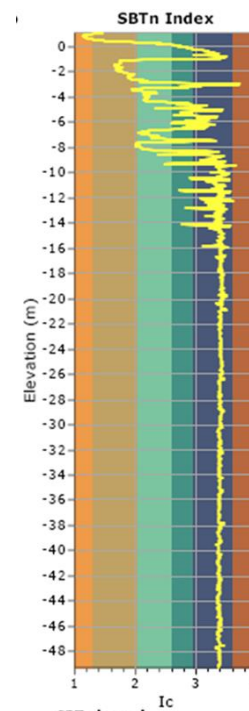
Corrected cone resistance q_t from the report



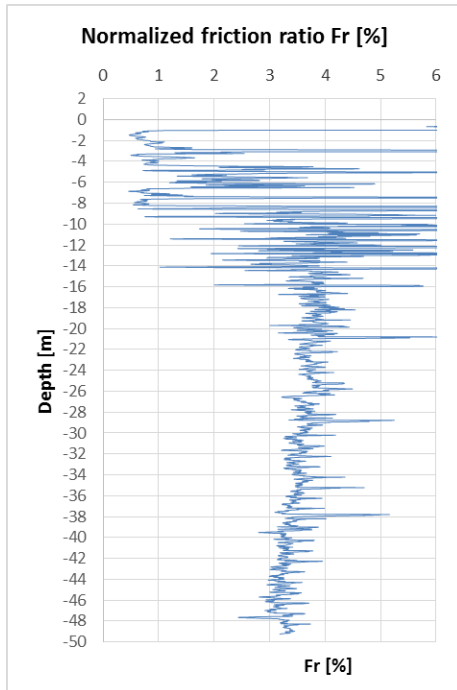
Evaluated soil behavior type index I_c



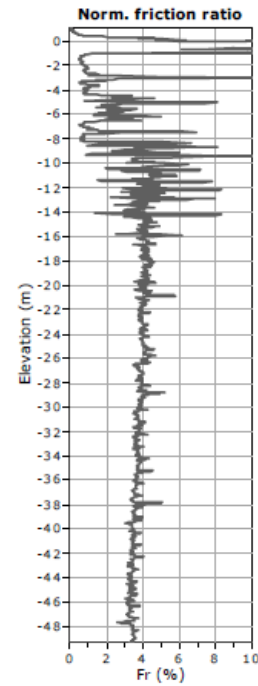
Soil behavior type index I_c from the report



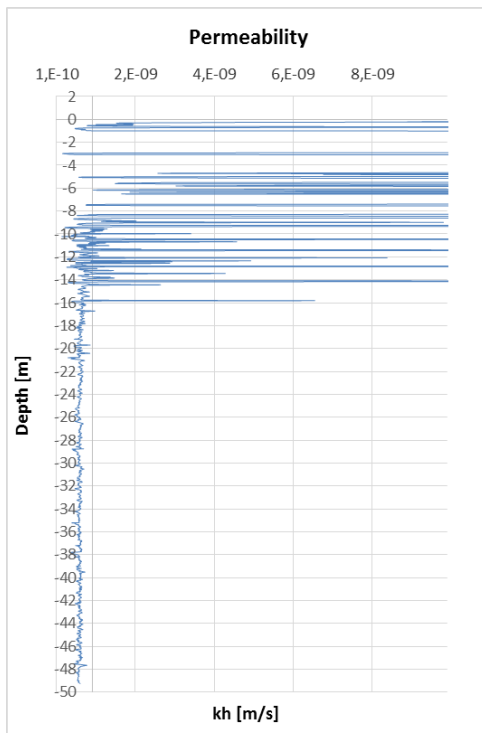
Evaluated normalized friction ratio Fr



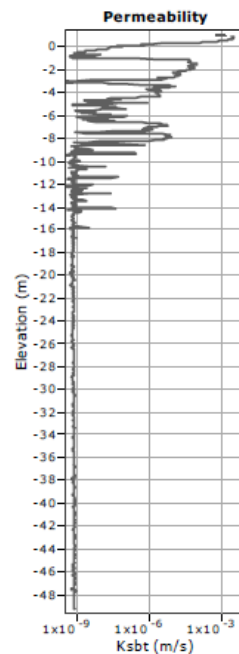
Normalized friction ratio Fr from the report



Evaluated permeability k_h



Permeability k_h from the report

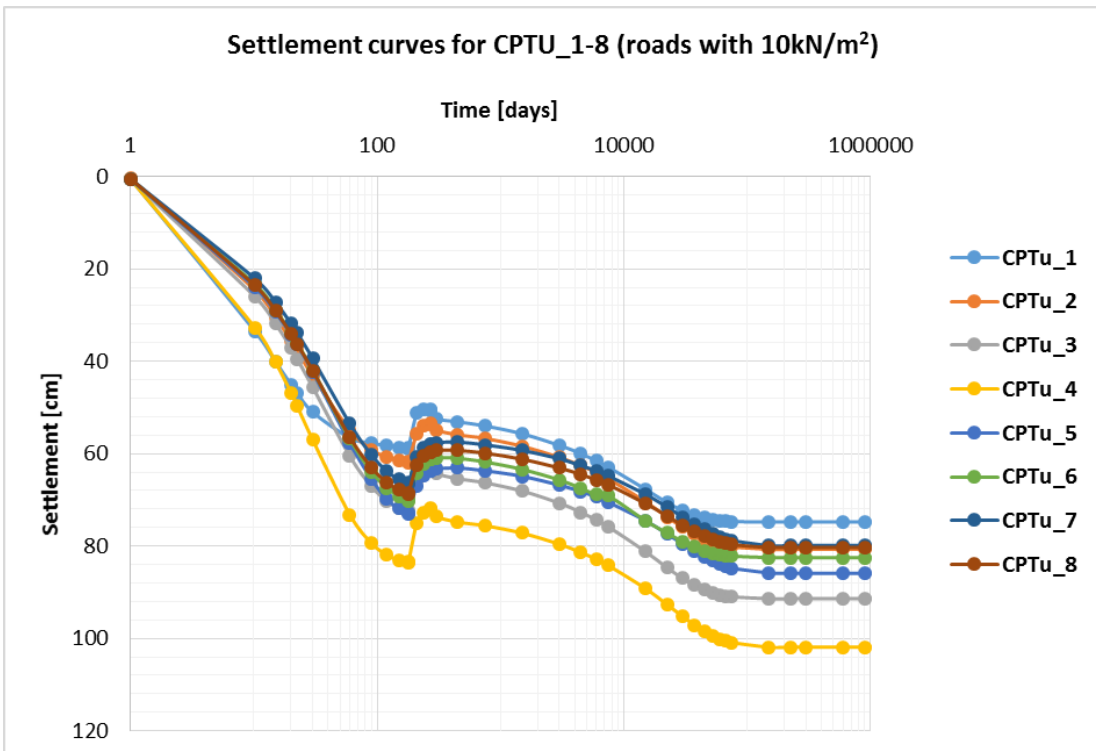
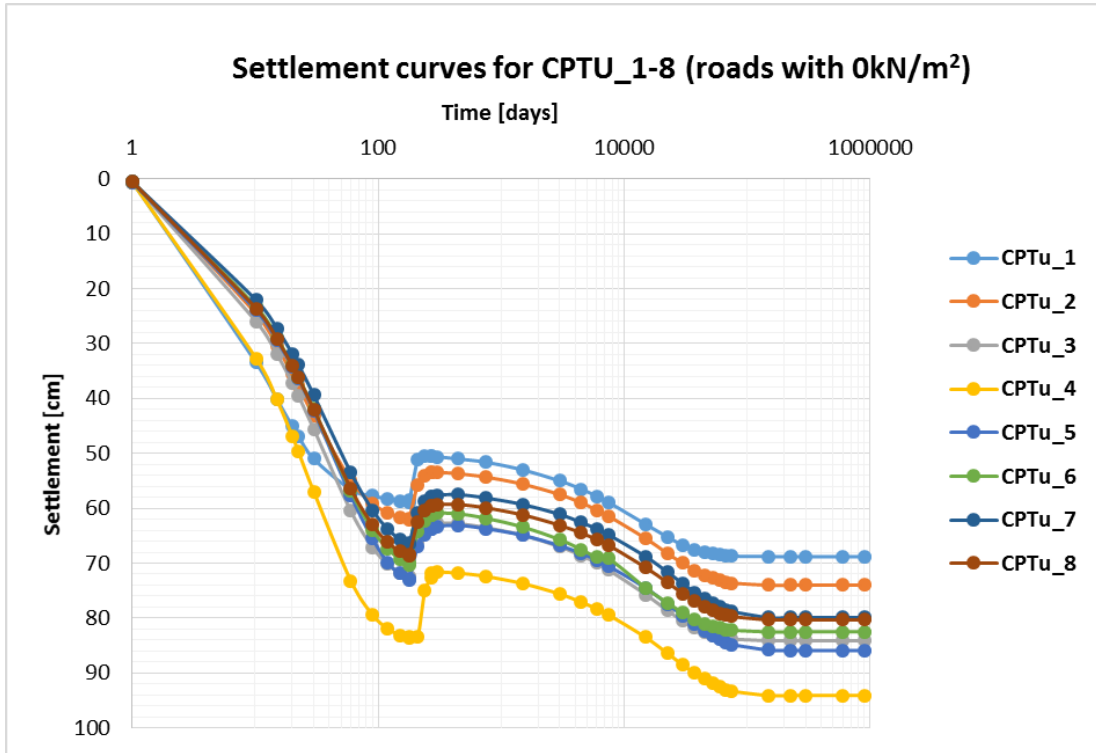


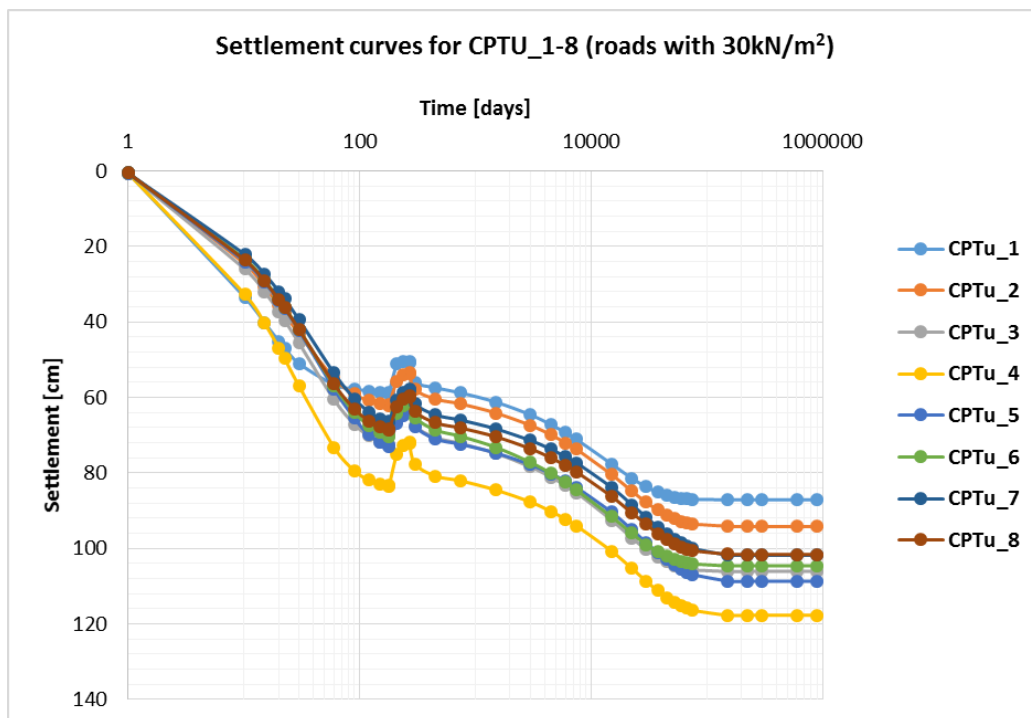
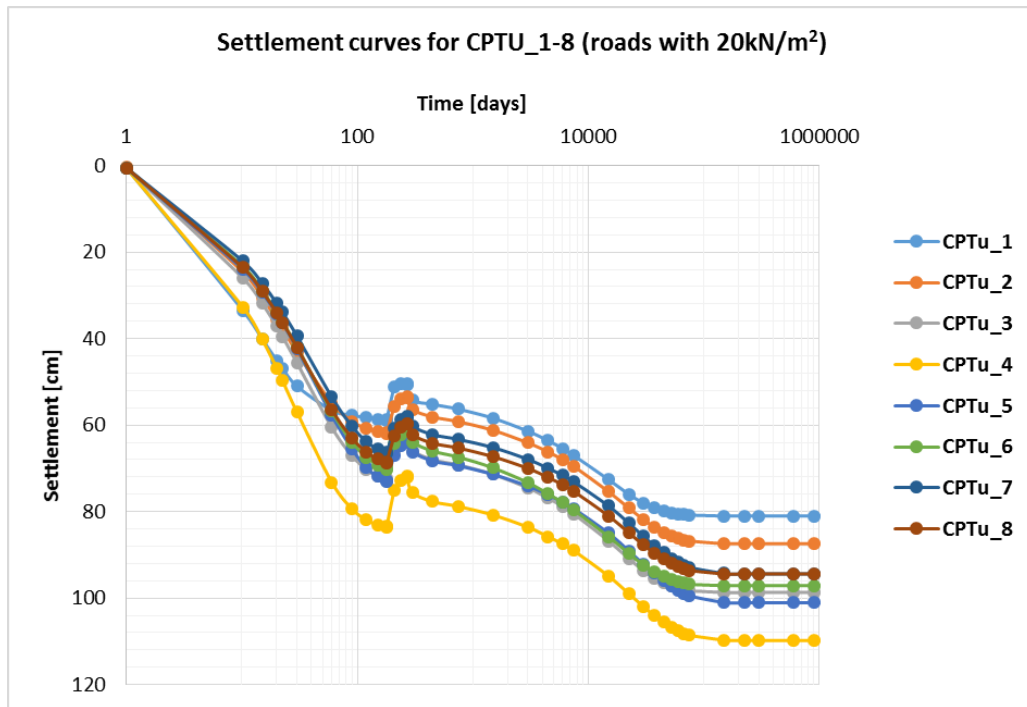
Appendix D

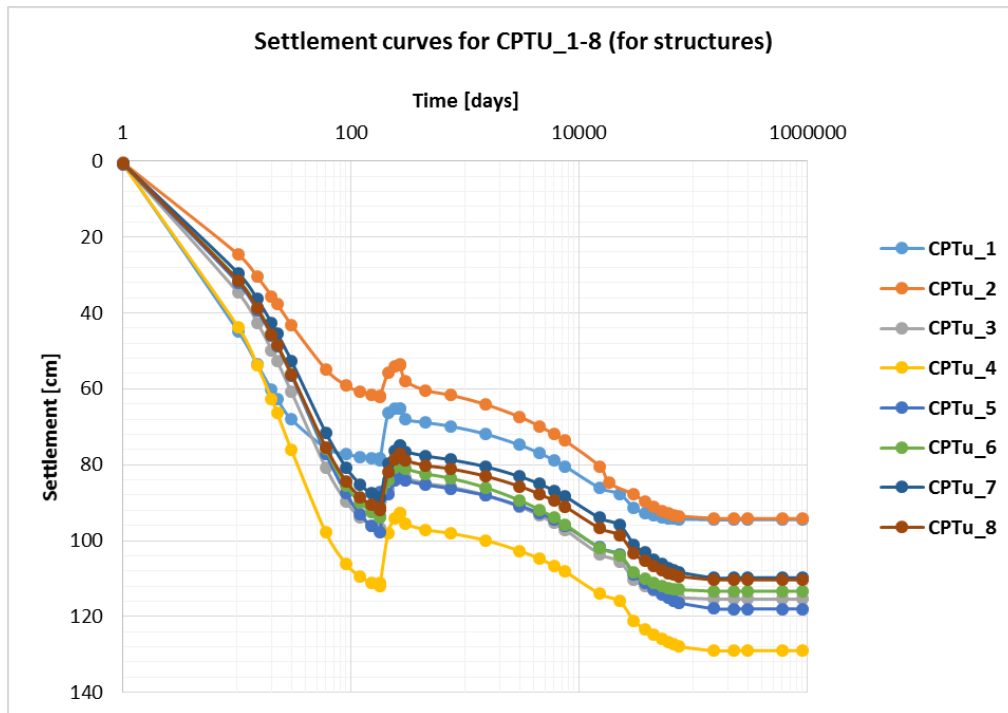
Settlement curves for the Investigation-1

(CPTu_1 – CPTu_8)

(Contains 3 pages)







Appendix E

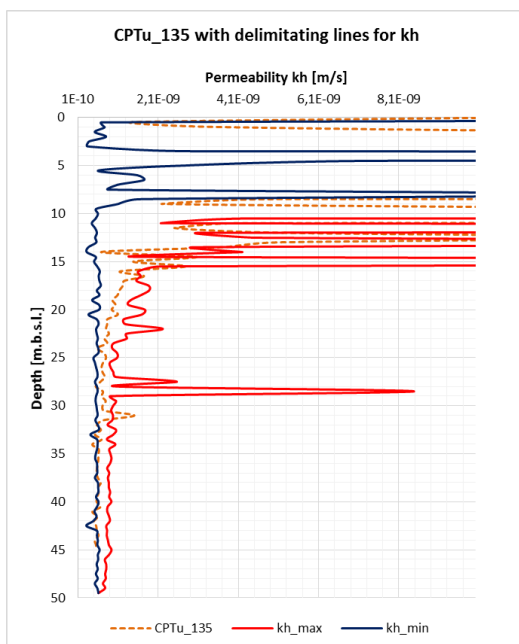
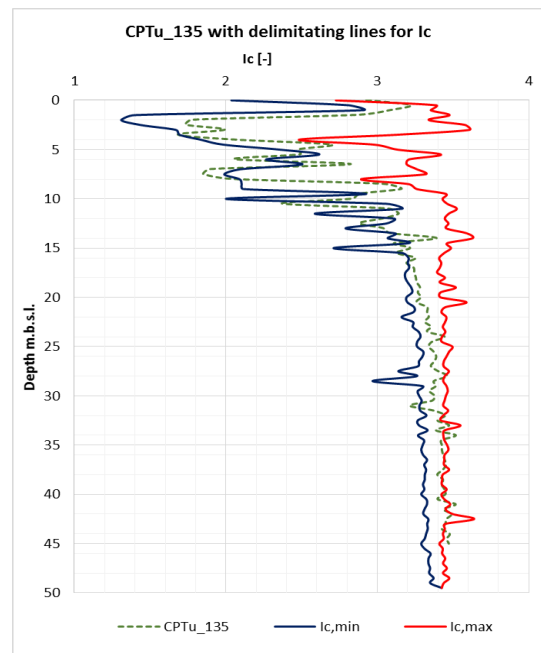
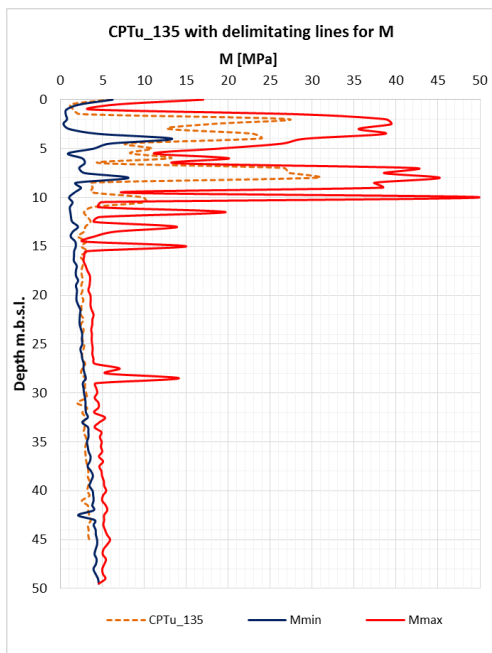
Comparison of results from Investigation-2

with delimitating lines

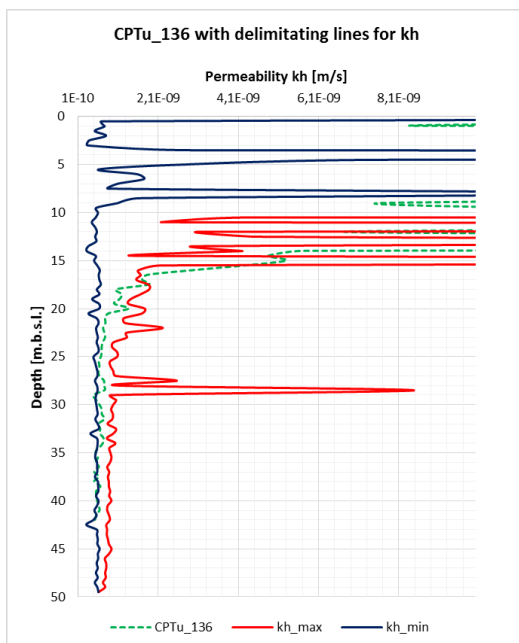
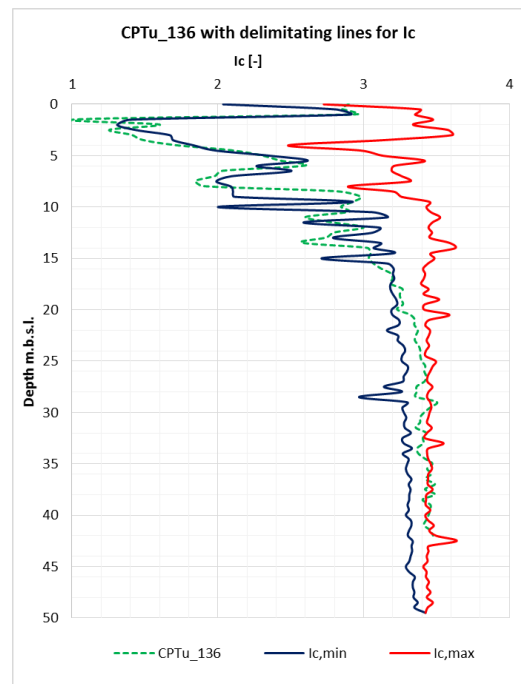
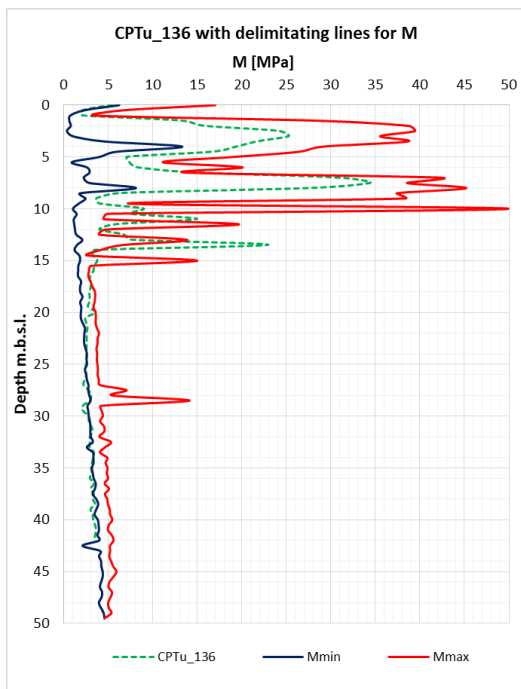
(CPTu_135 – CPTu_152)

(Contains 8 pages)

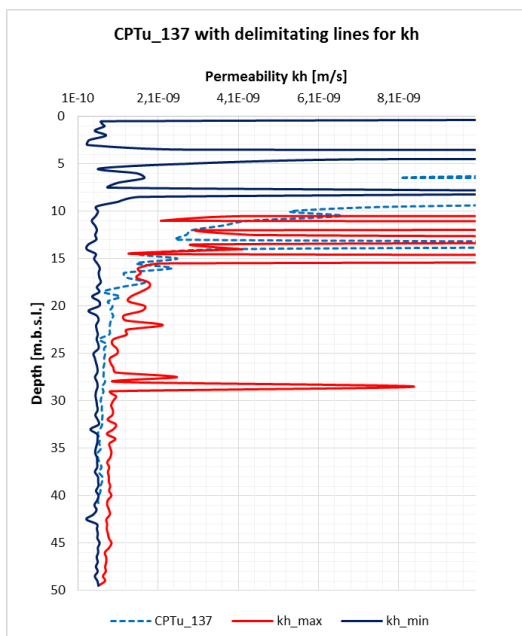
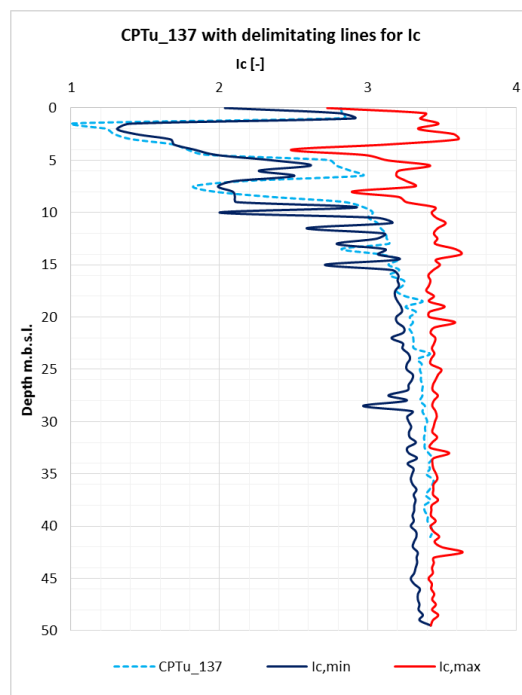
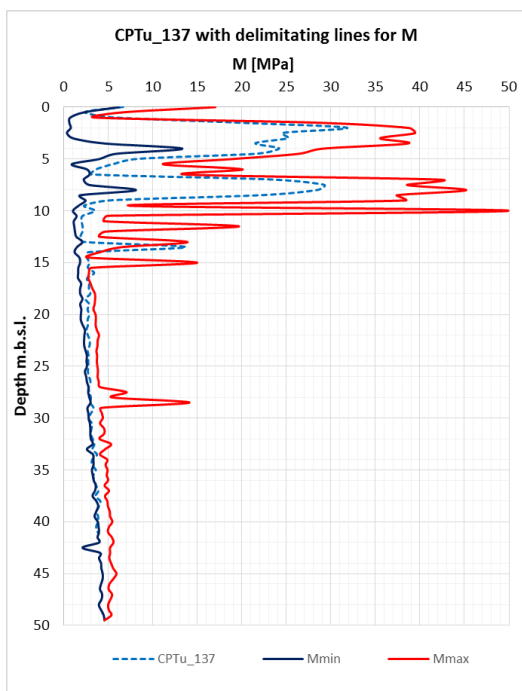
CPTu_135



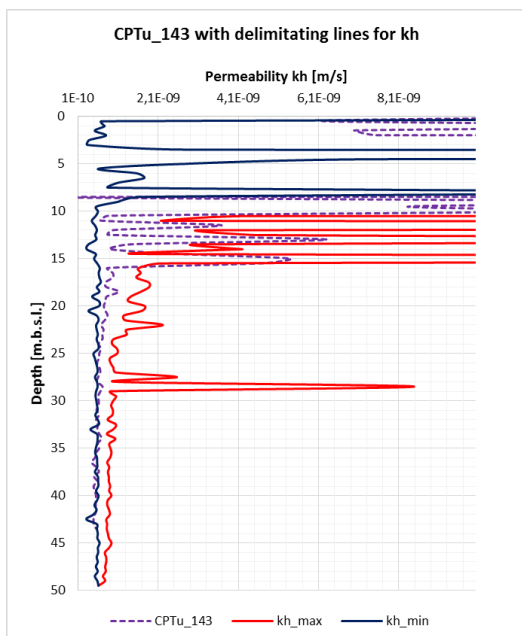
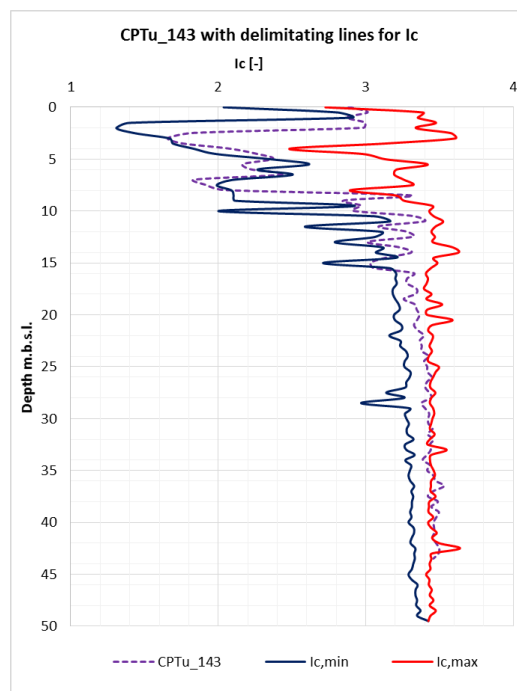
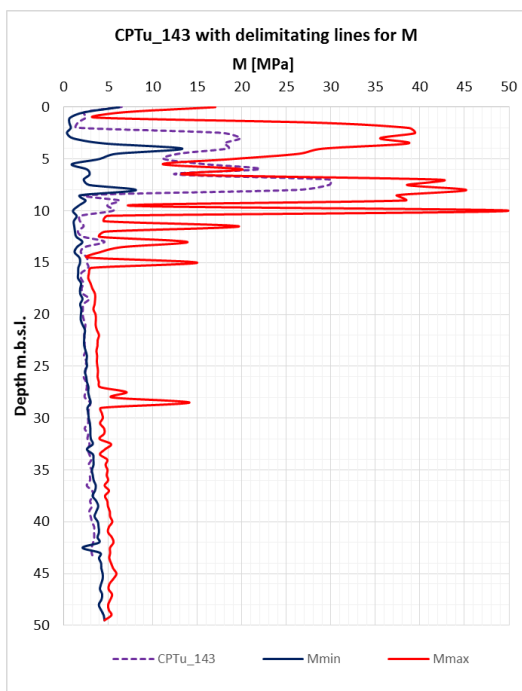
CPTu_136



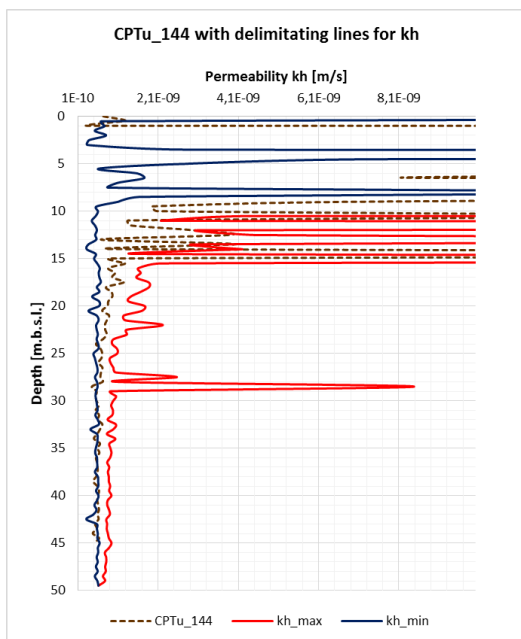
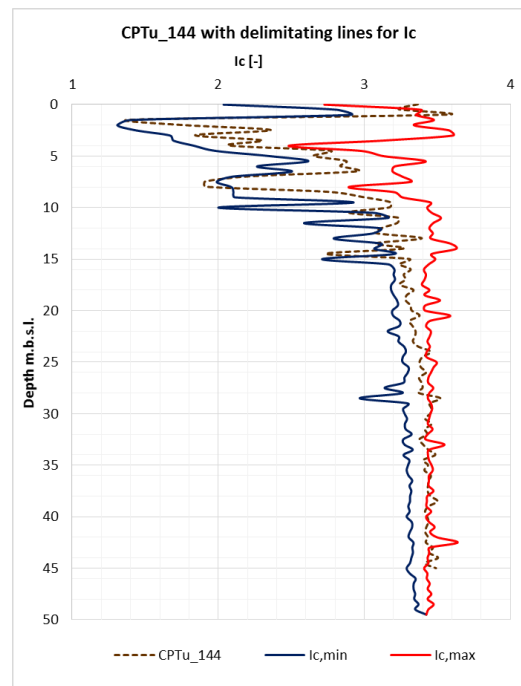
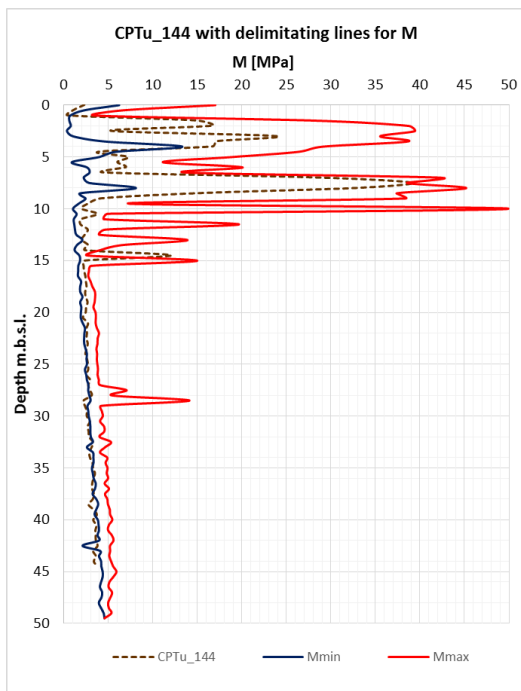
CPTu_137



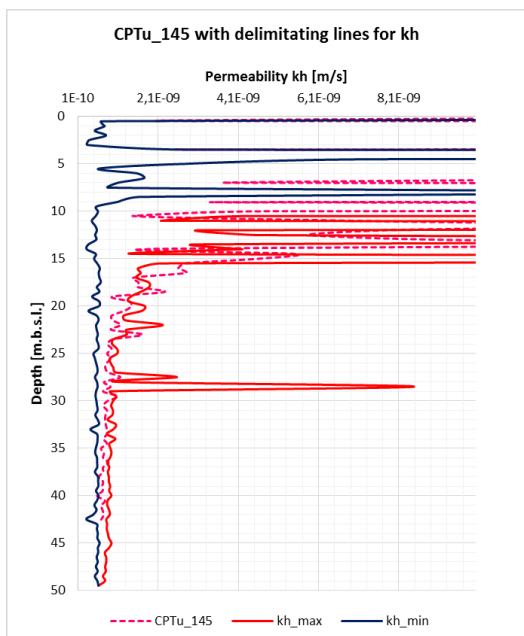
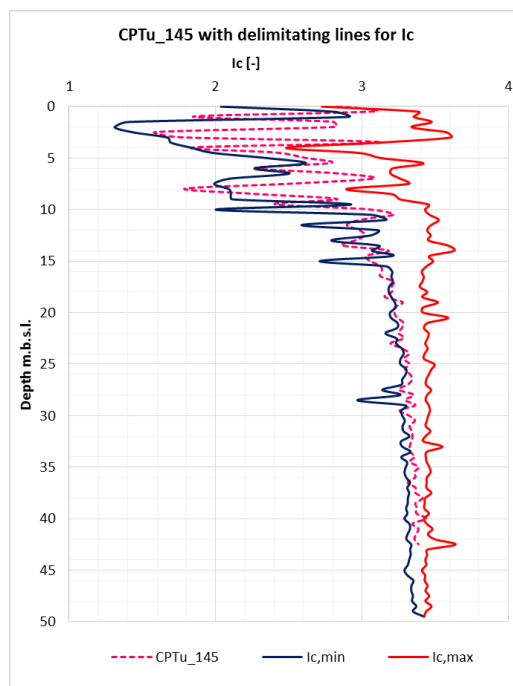
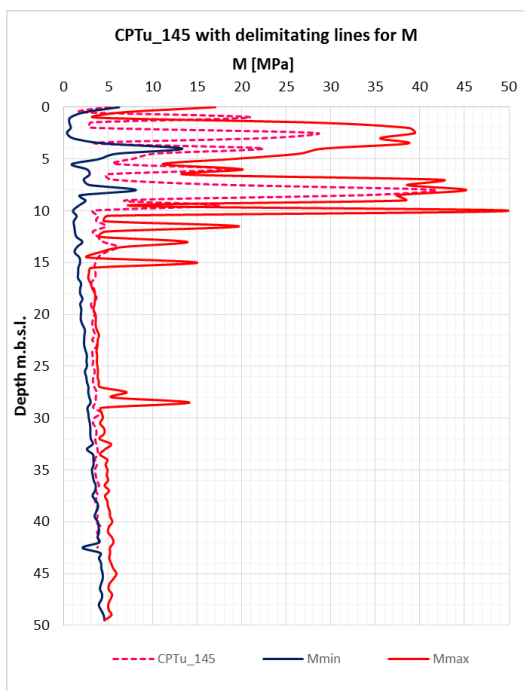
CPTu_143



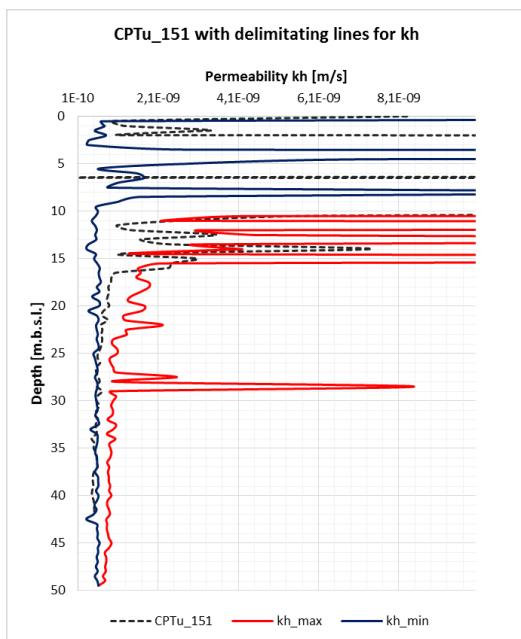
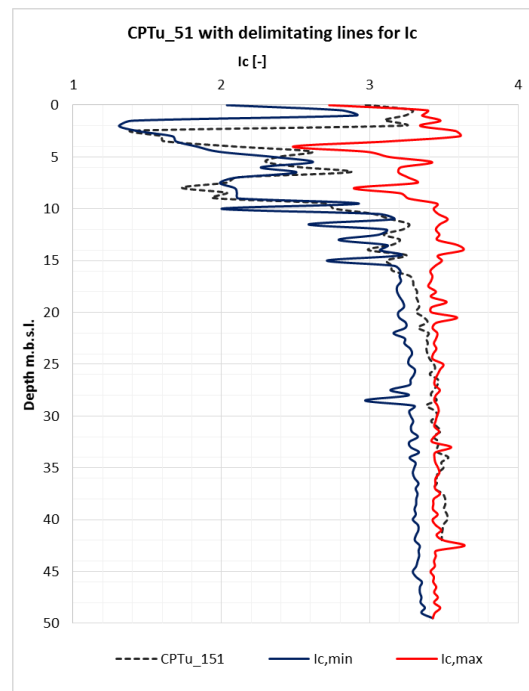
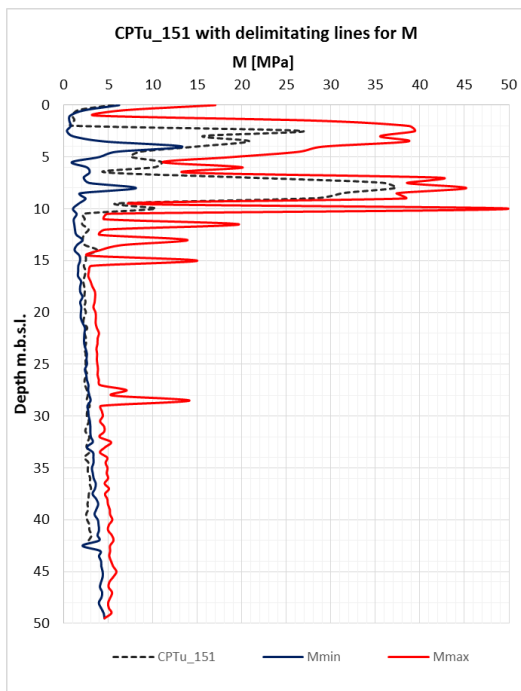
CPTu_144



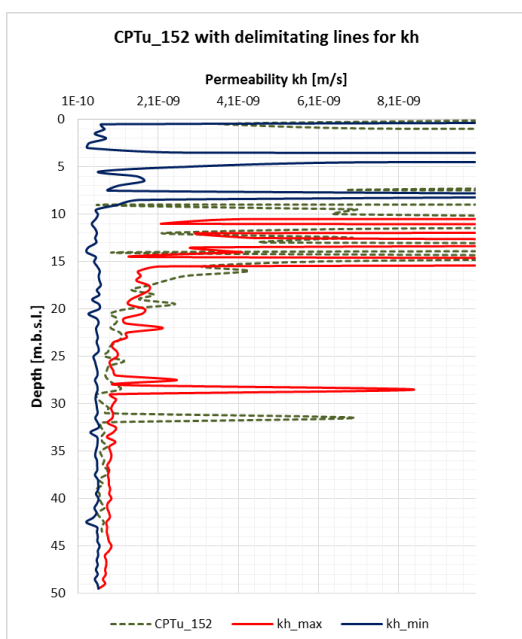
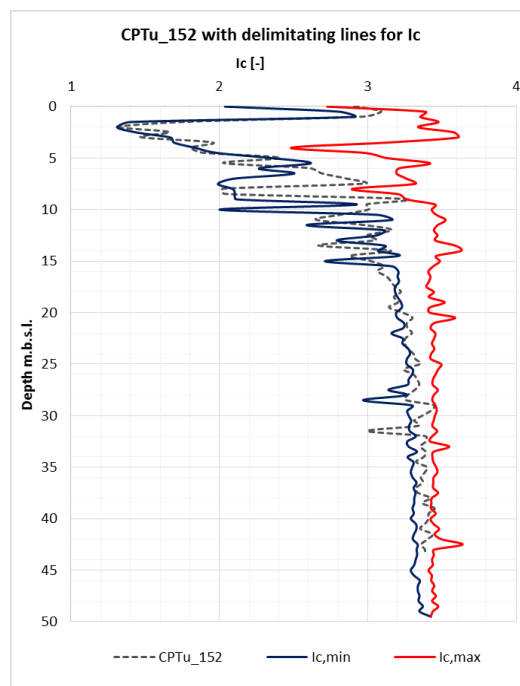
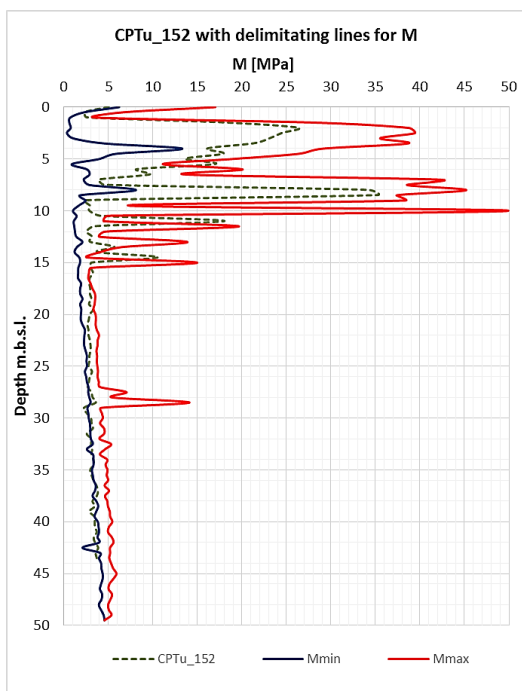
CPTu_145



CPTu_151



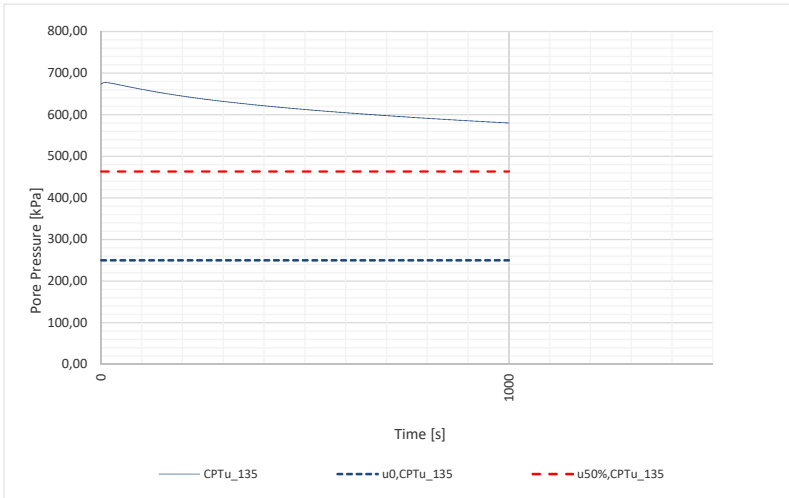
CPTu_152



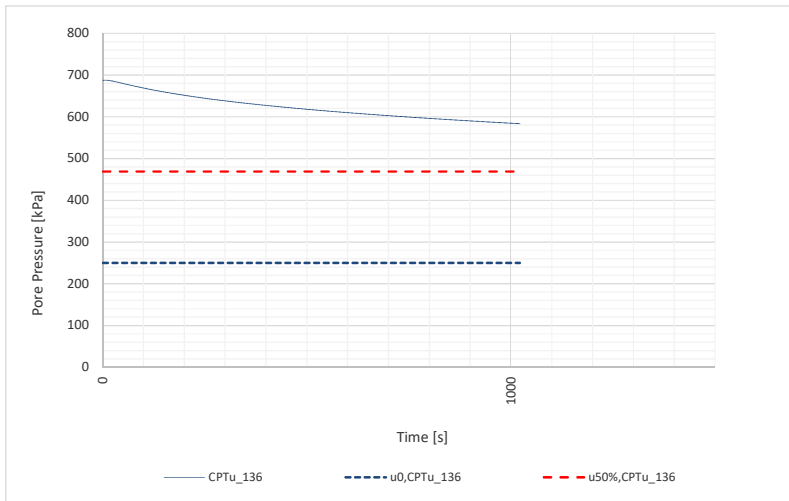
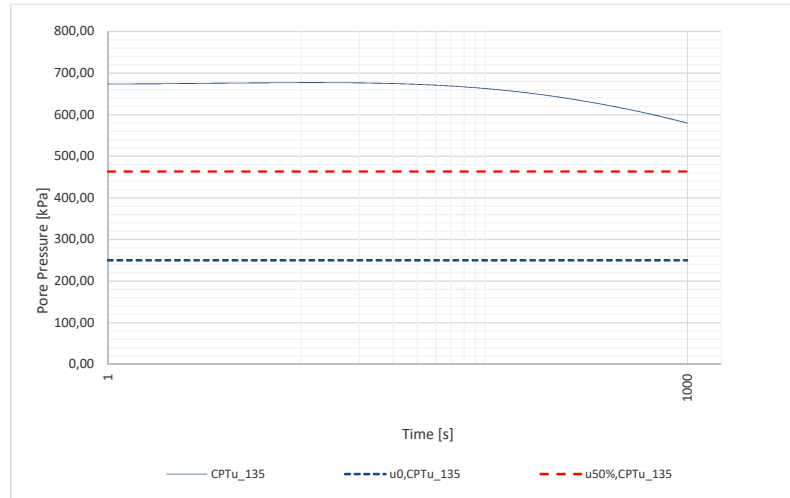
Appendix F

Results of programmed Excel spreadsheets of the dissipation tests for the Investigation-2 (CPTu_135 – CPTu_152)

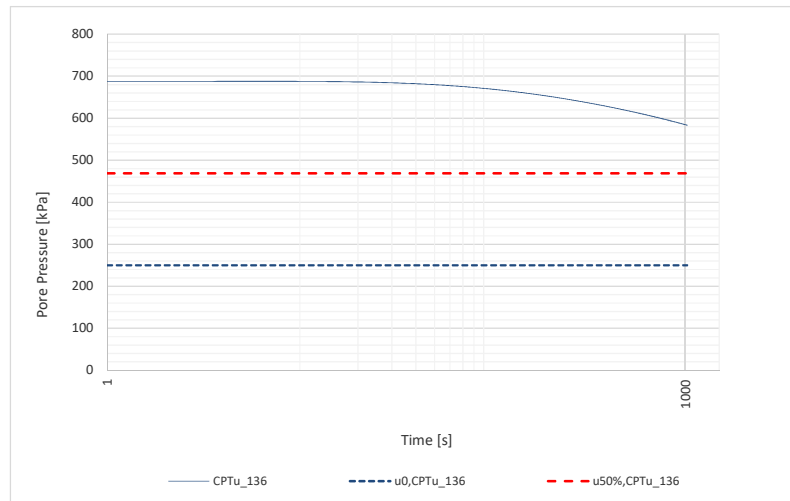
(Contains 16 pages)

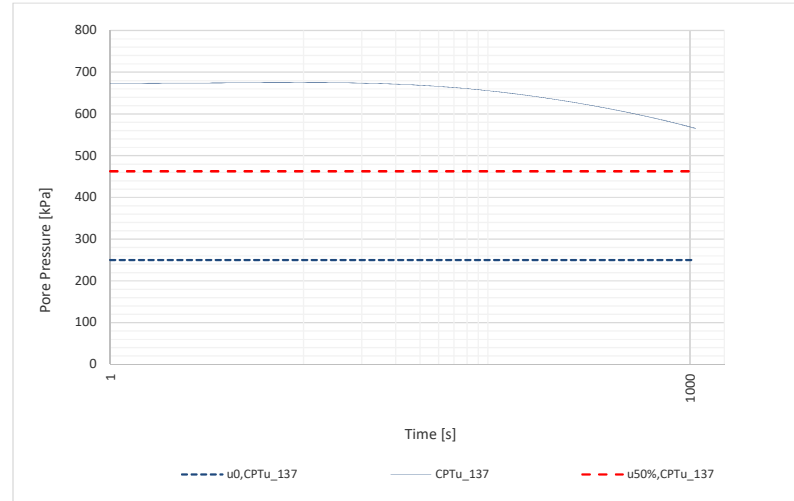
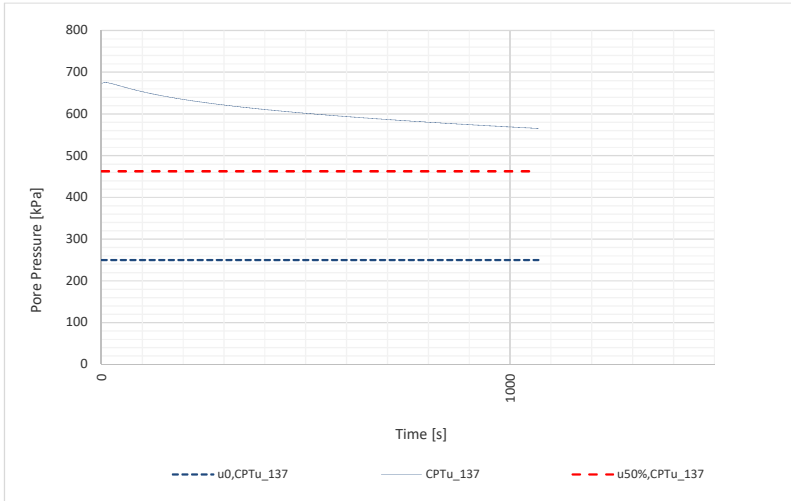


t_50 [s]	k [m/s]
0	#DIV/0!

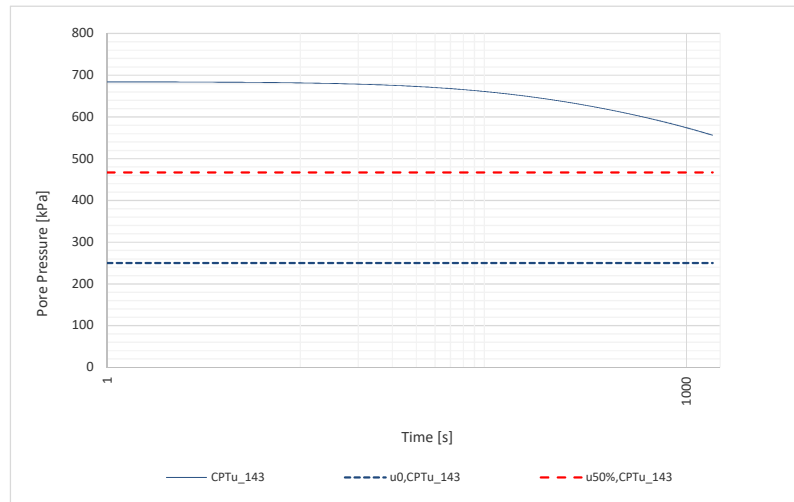
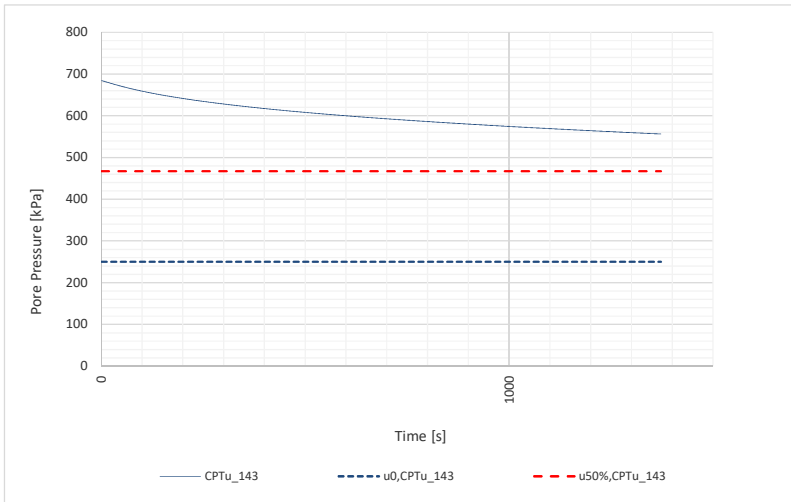


t_50 [s]	k [m/s]
0	#DIV/0!

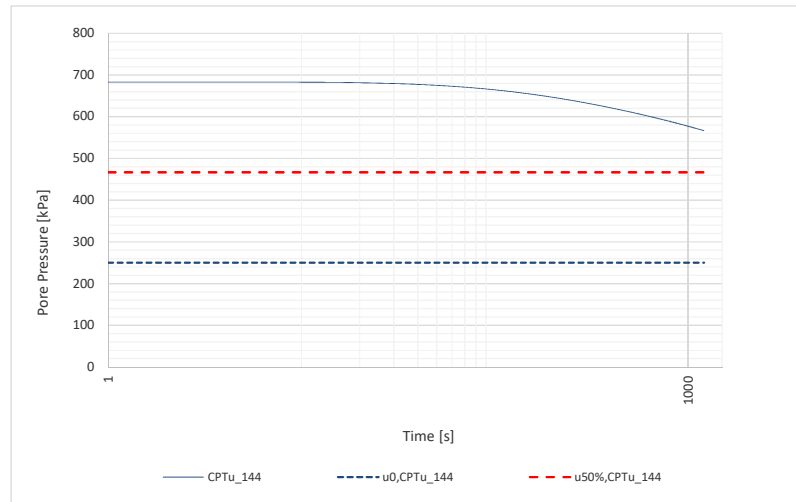
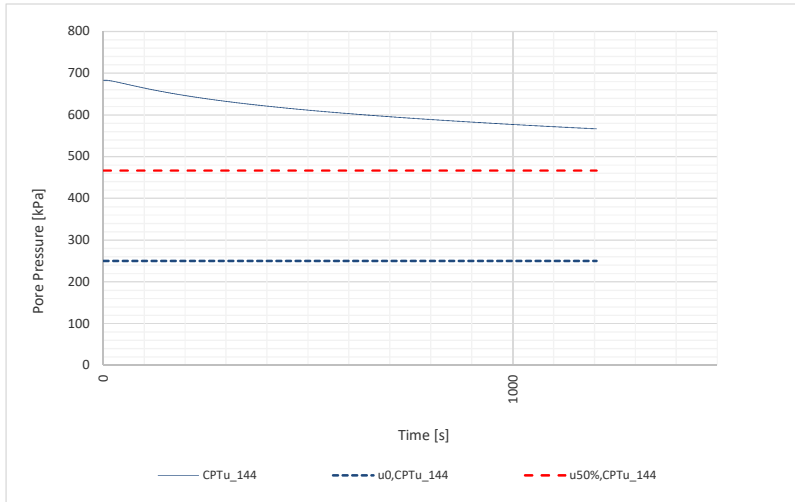




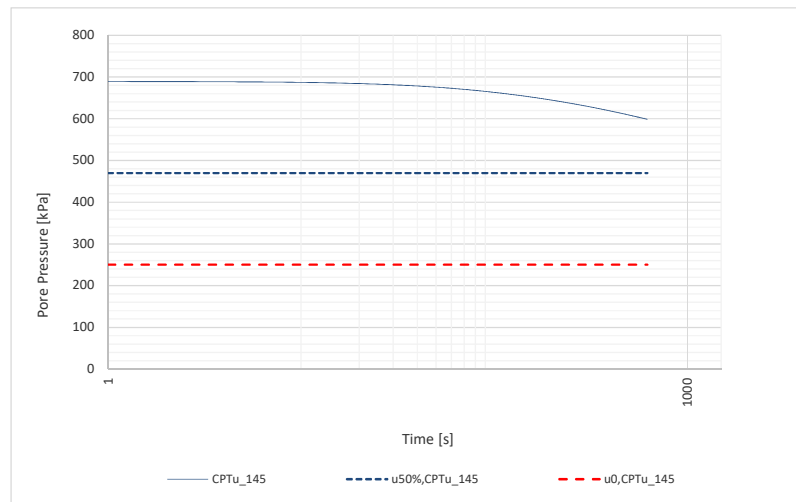
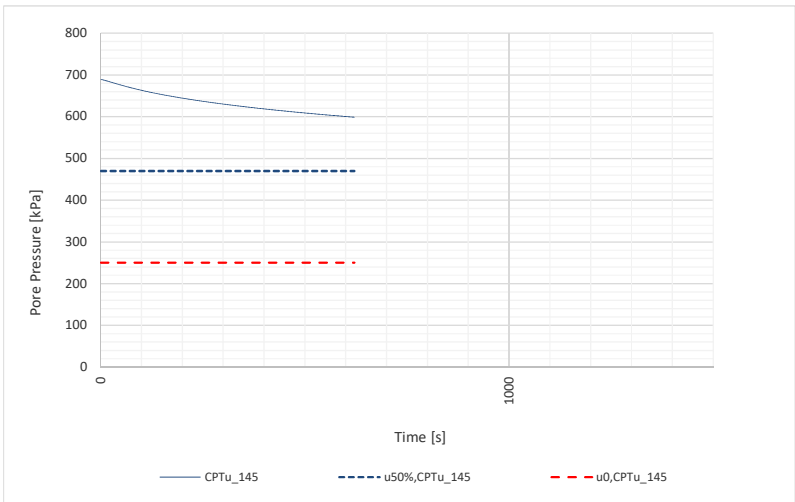
t_50 [s]	k [m/s]
0	#DIV/0!



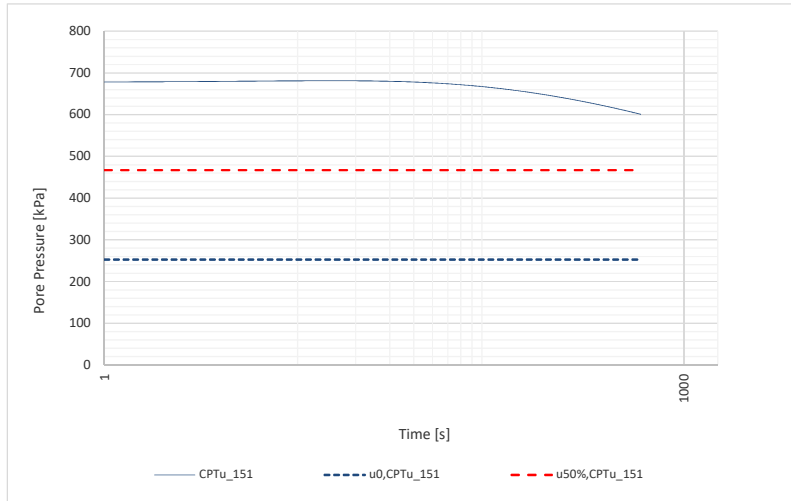
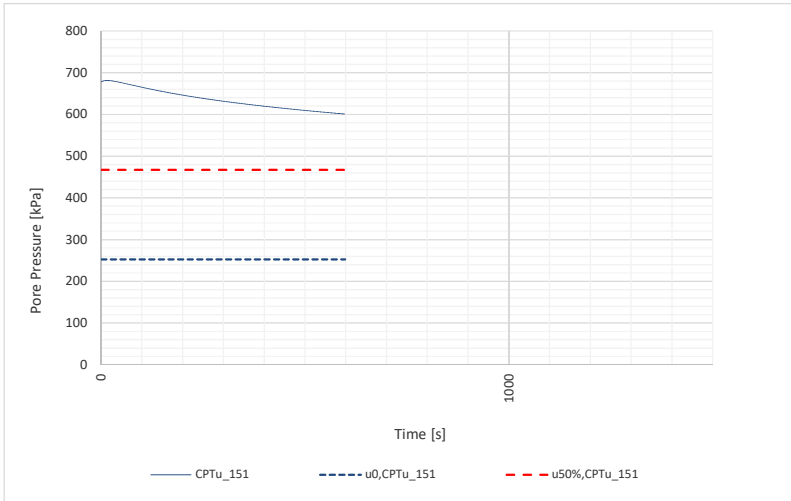
t_50 [s]	k [m/s]
0	#DIV/0!



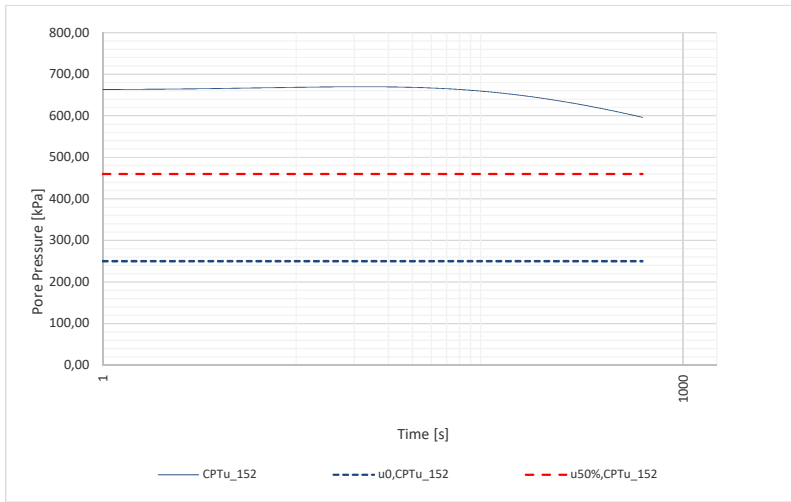
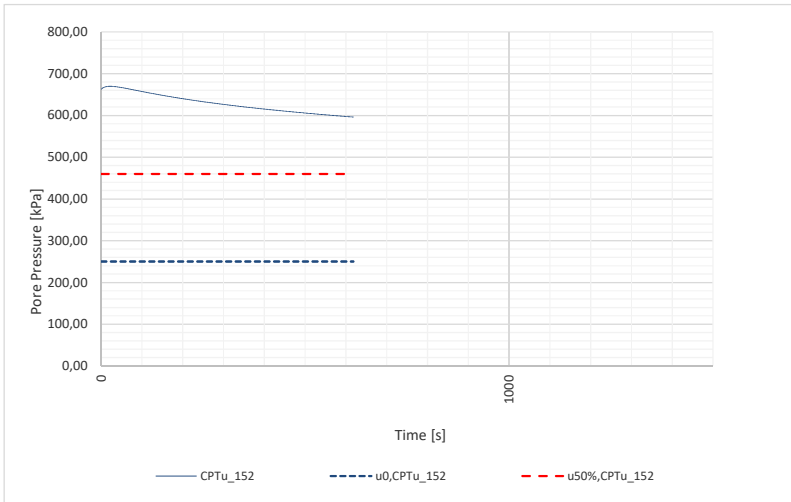
t_{50} [s]	k [m/s]
0	#DIV/0!



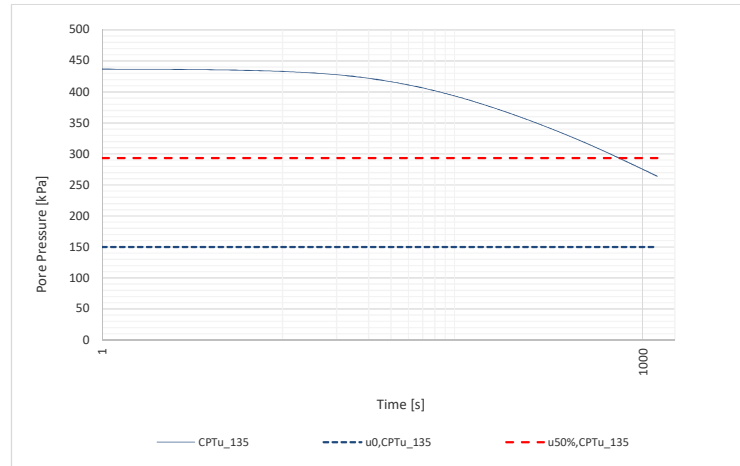
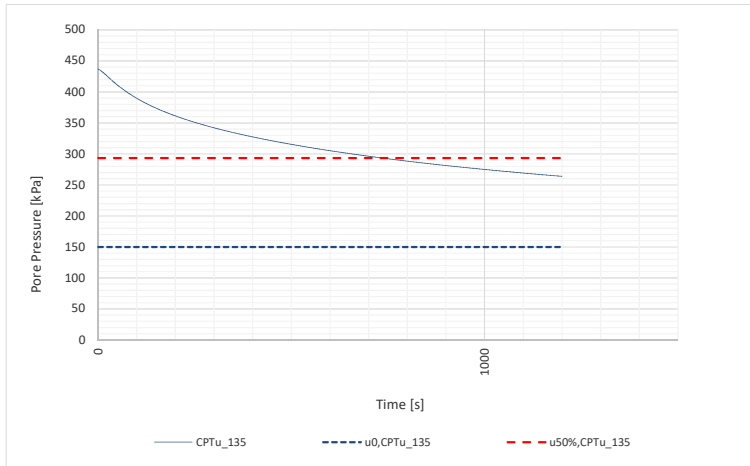
t_{50} [s]	k [m/s]
0	#DIV/0!



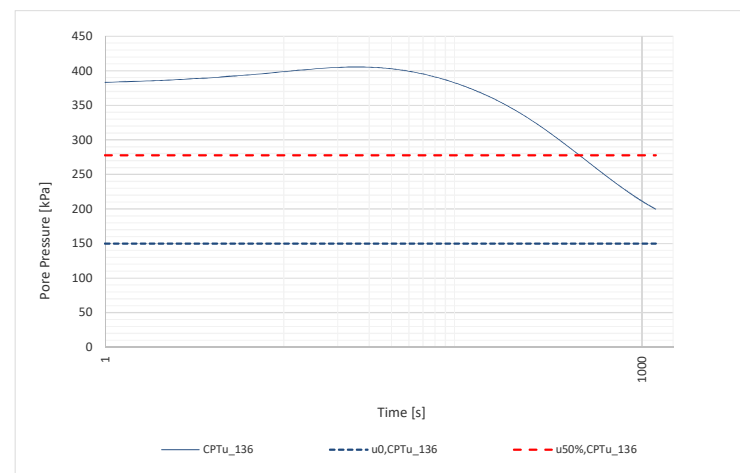
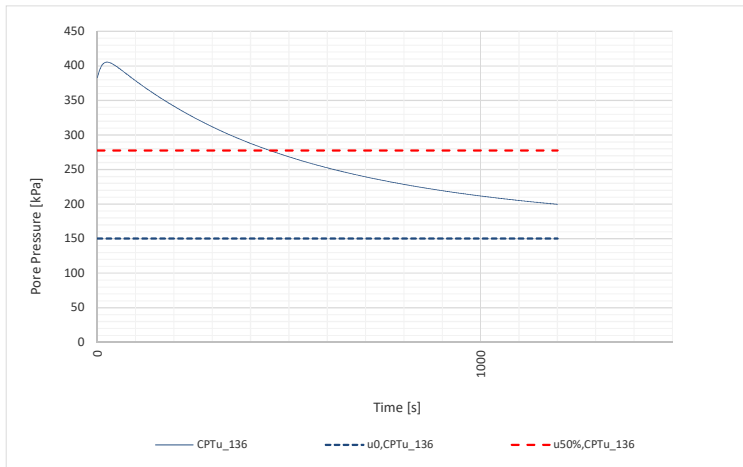
t ₅₀ [s]	k [m/s]
0	#DIV/0!



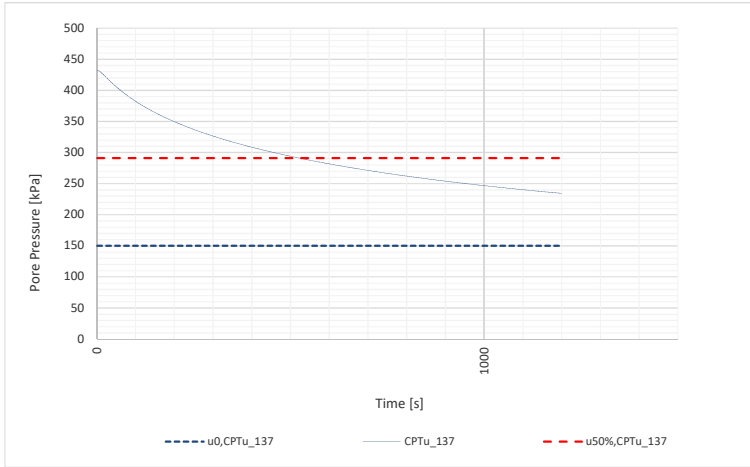
t ₅₀ [s]	k [m/s]
0	#DIV/0!



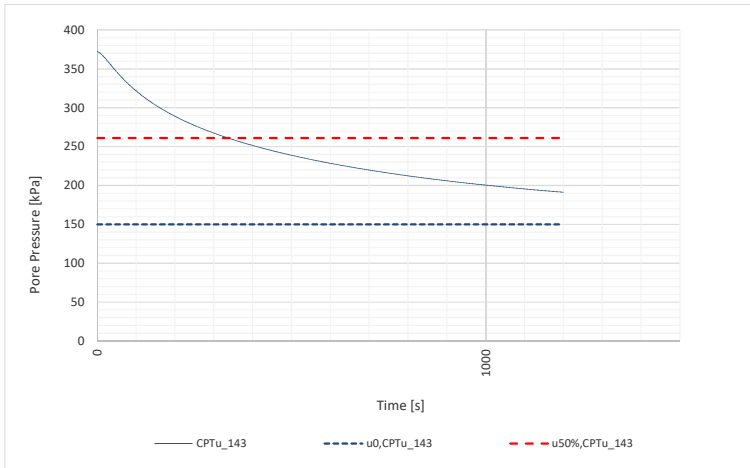
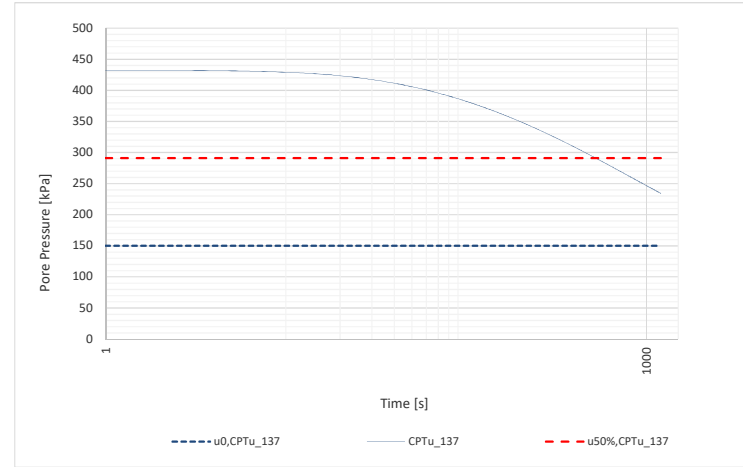
t_50 [s]	k [m/s]
738	2,60E-09



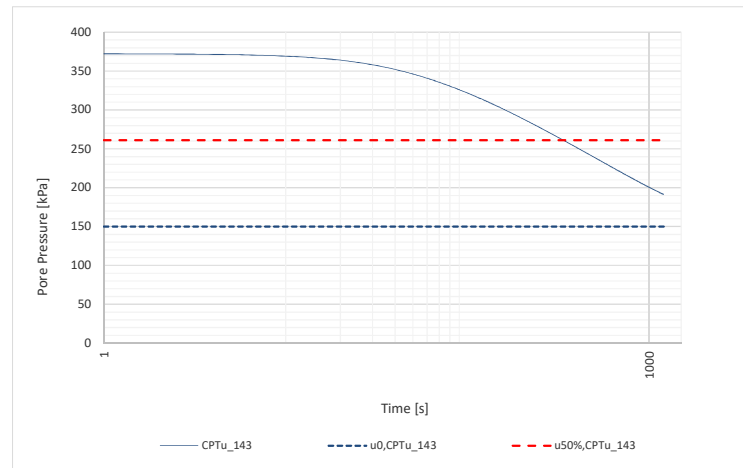
t_50 [s]	k [m/s]
450	4,83E-09

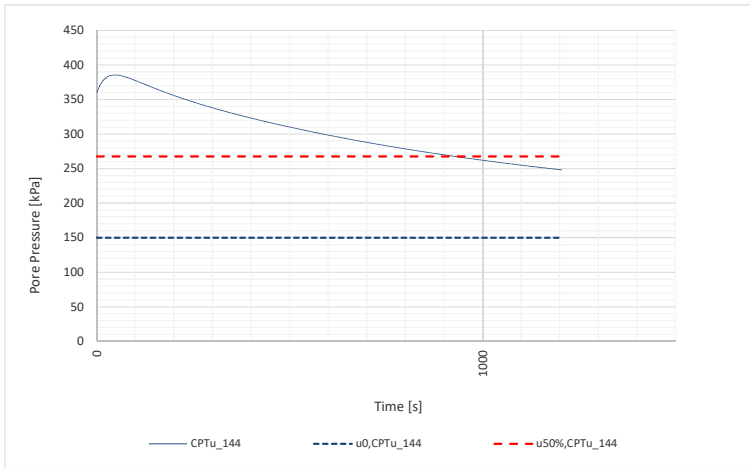


t ₅₀ [s]	k [m/s]
524	3,99E-09

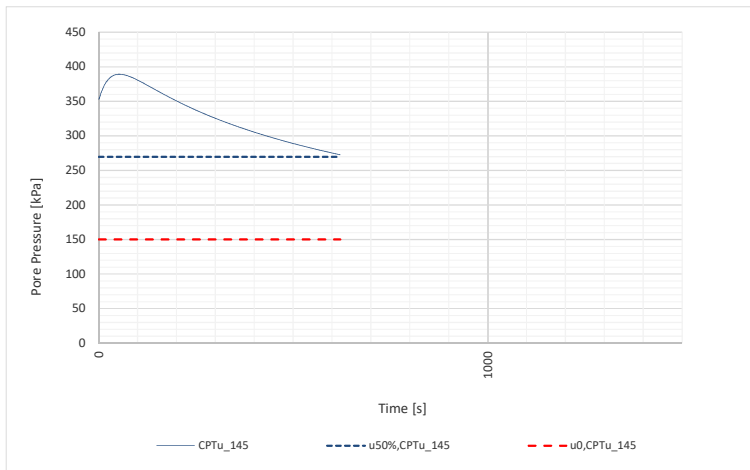
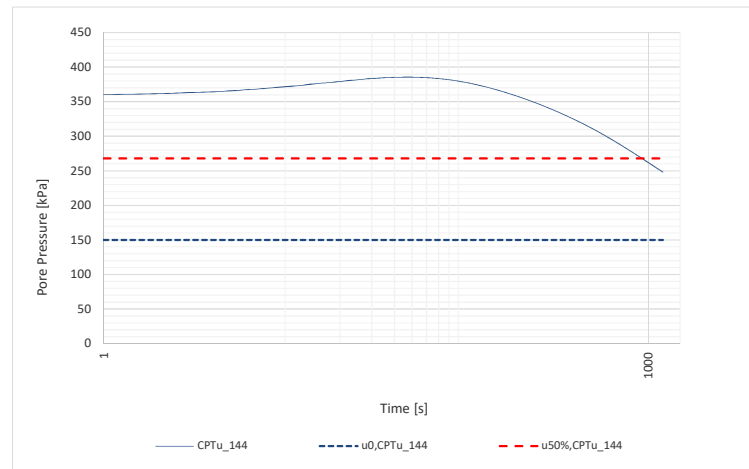


t ₅₀ [s]	k [m/s]
338	6,91E-09

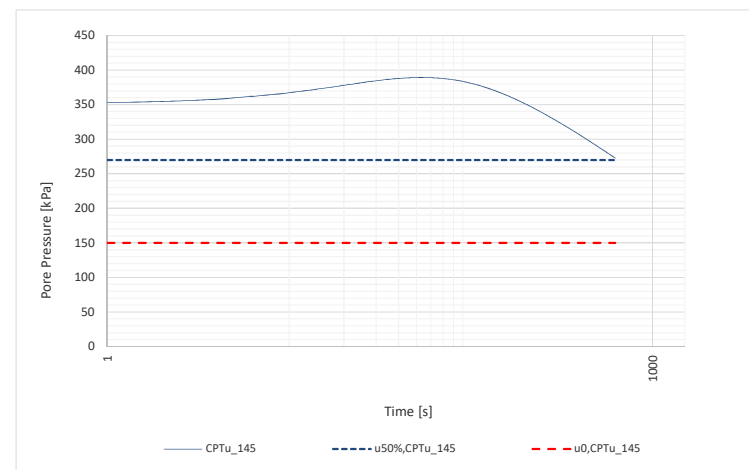


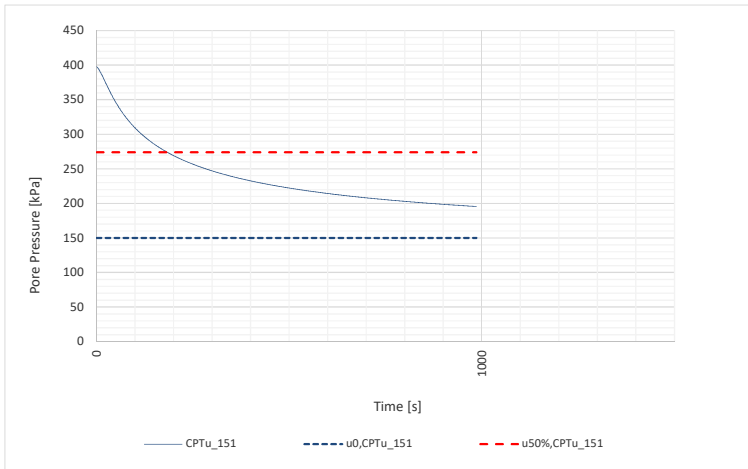


t_50 [s]	k [m/s]
929	1,95E-09

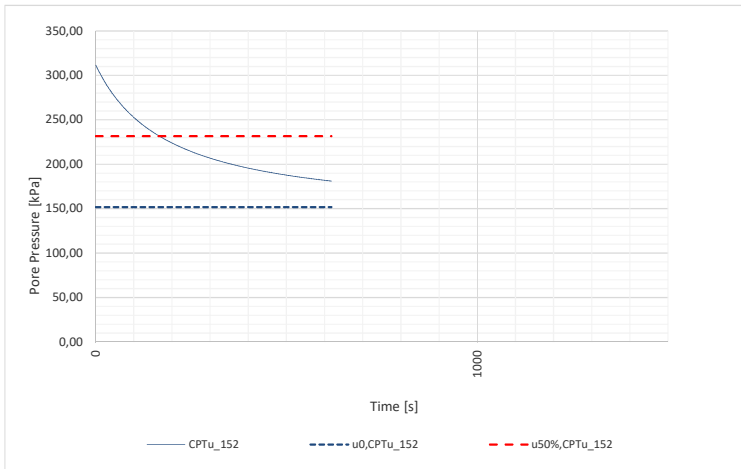
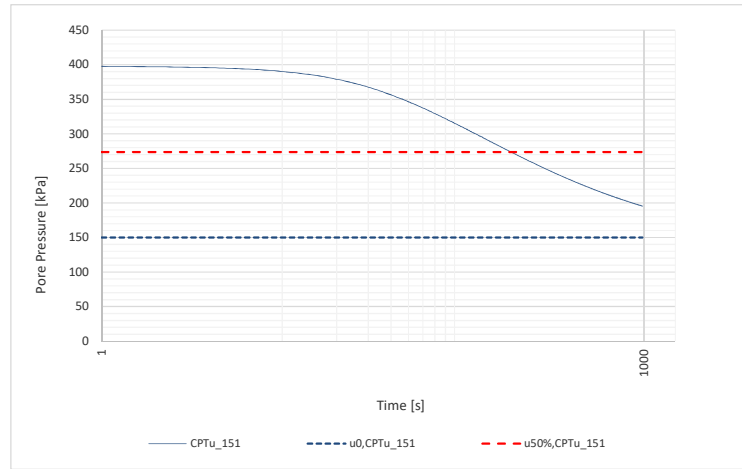


t_50 [s]	k [m/s]
0	#DIV/0!

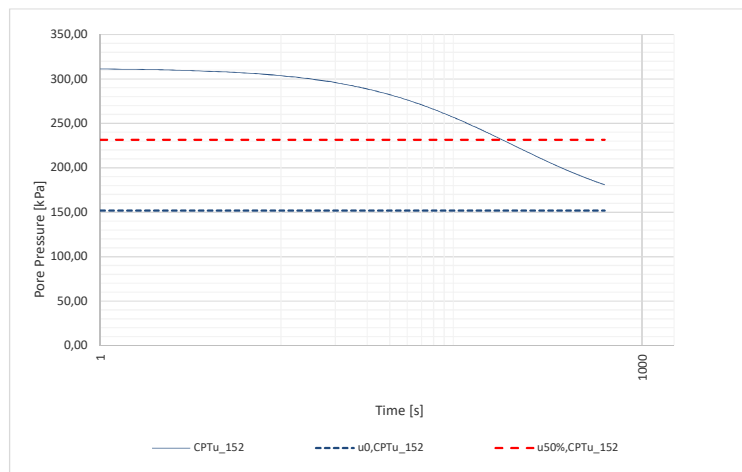


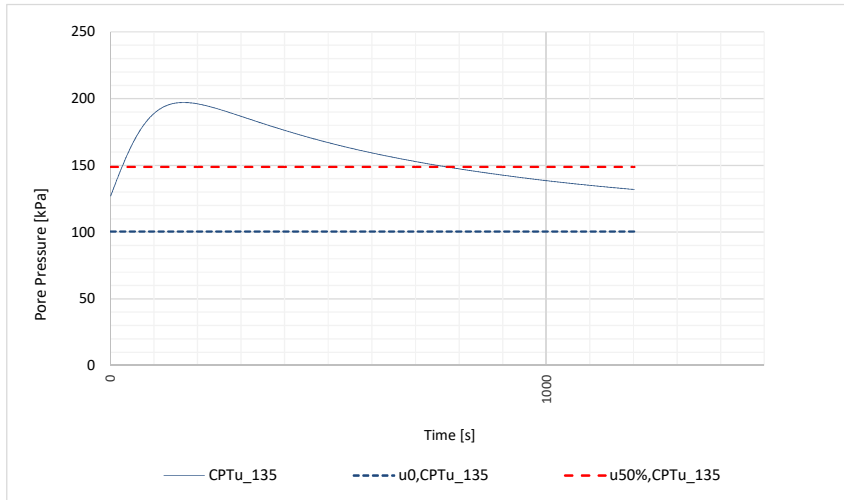


t ₅₀ [s]	k [m/s]
185	1,47E-08

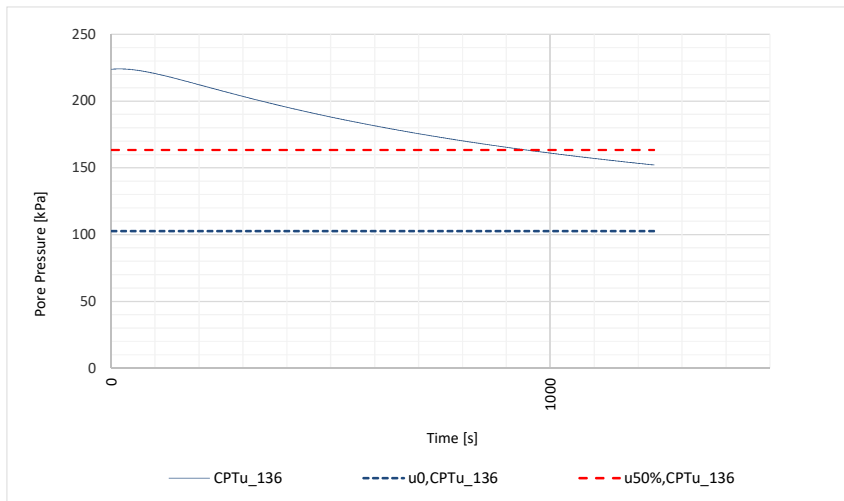
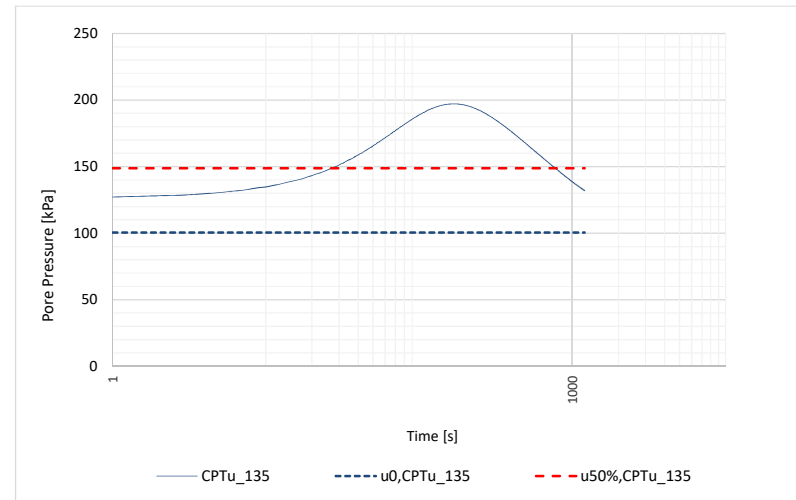


t ₅₀ [s]	k [m/s]
167	1,67E-08

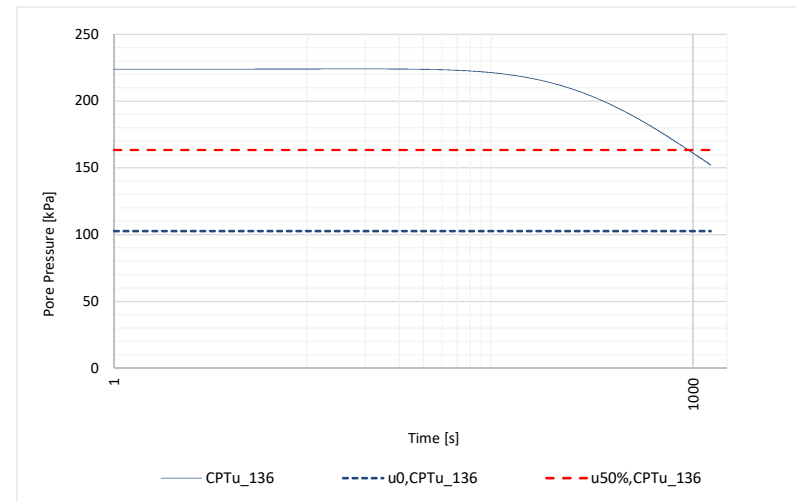


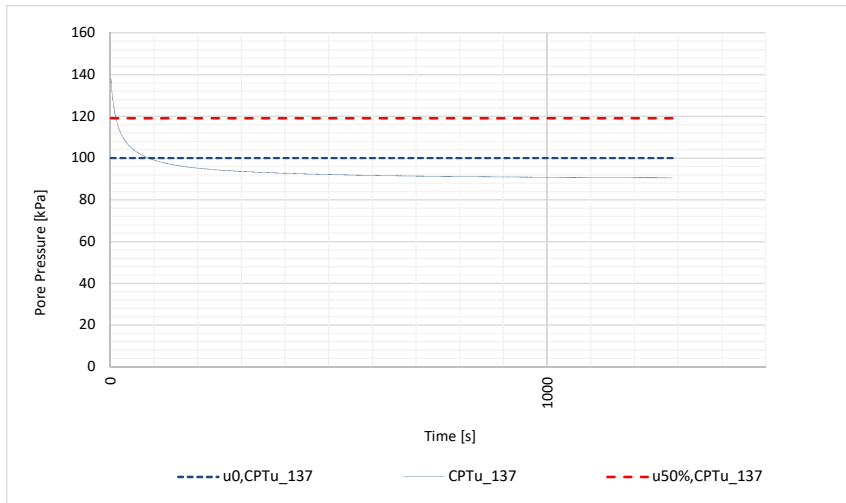


t_50 [s]	k [m/s]
776	2,44E-09

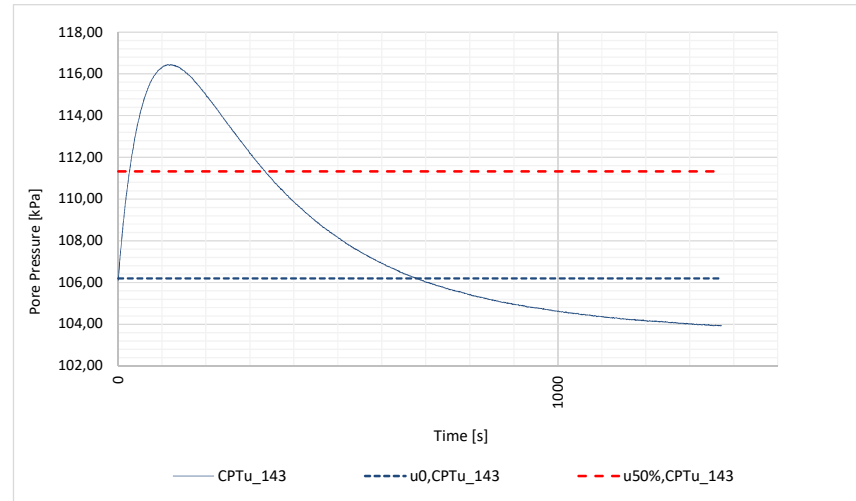
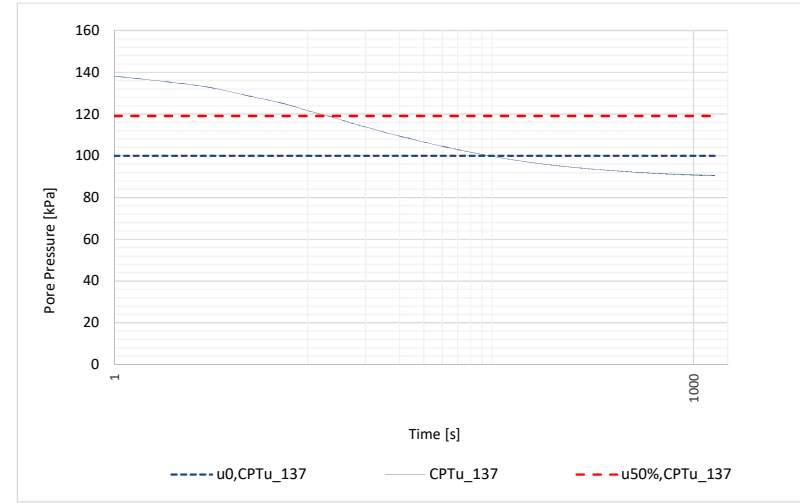


t_50 [s]	k [m/s]
950	1,90E-09

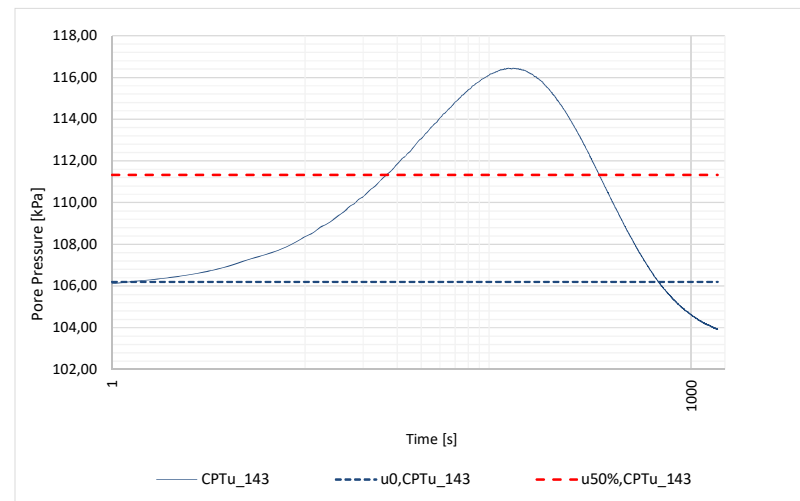


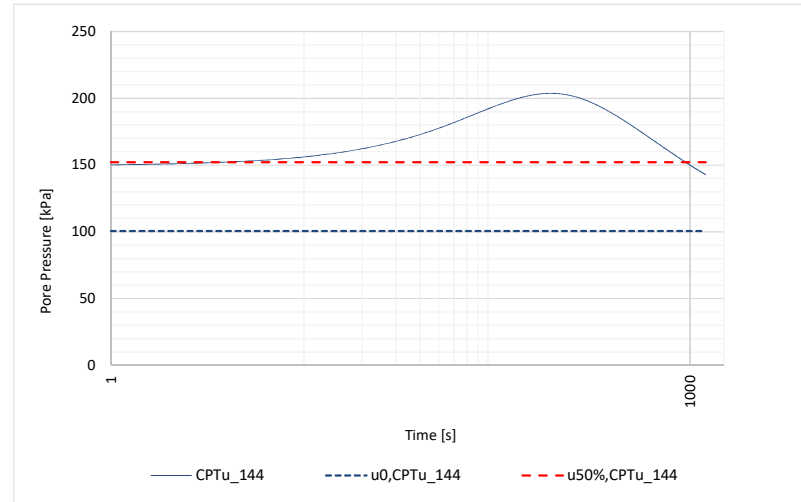
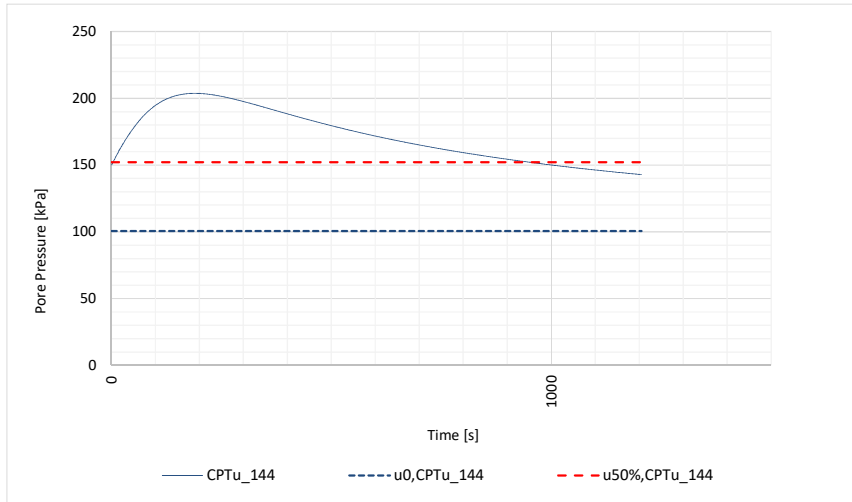


t_50 [s]	k [m/s]
13	4,05E-07

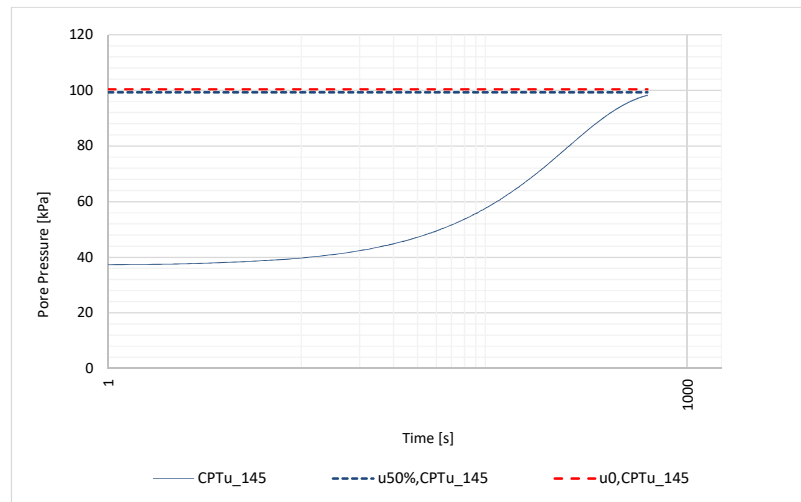
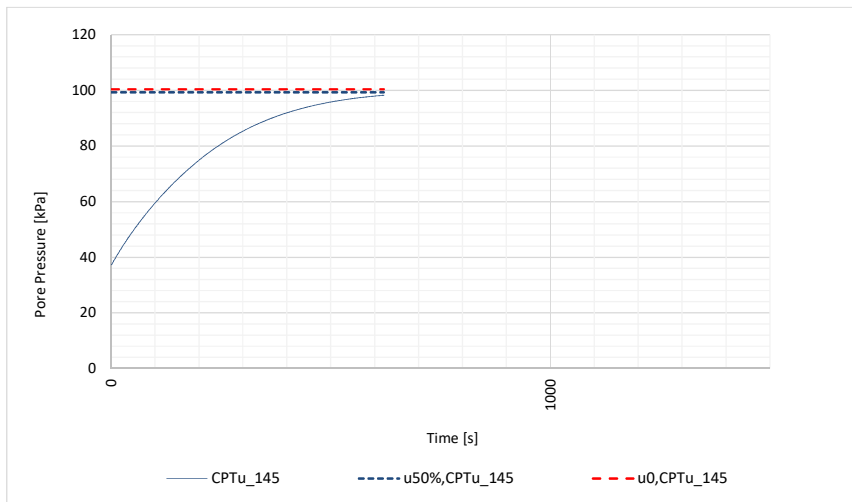


t_50 [s]	k [m/s]
342	6,81E-09

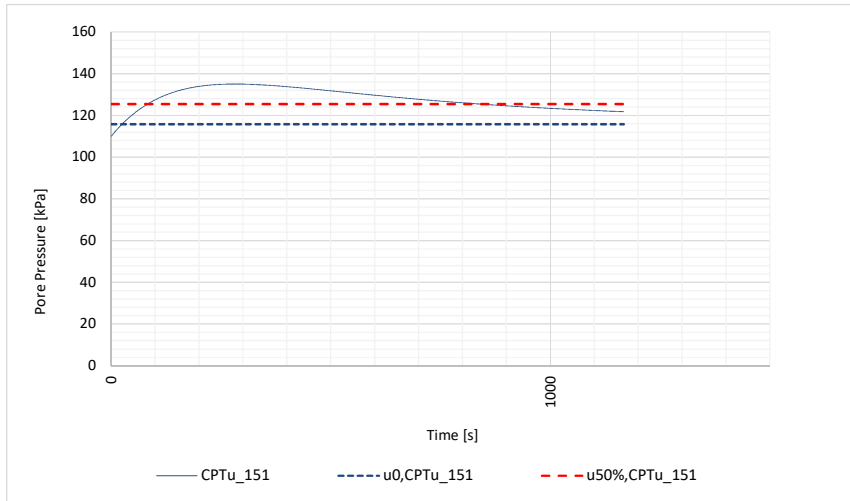




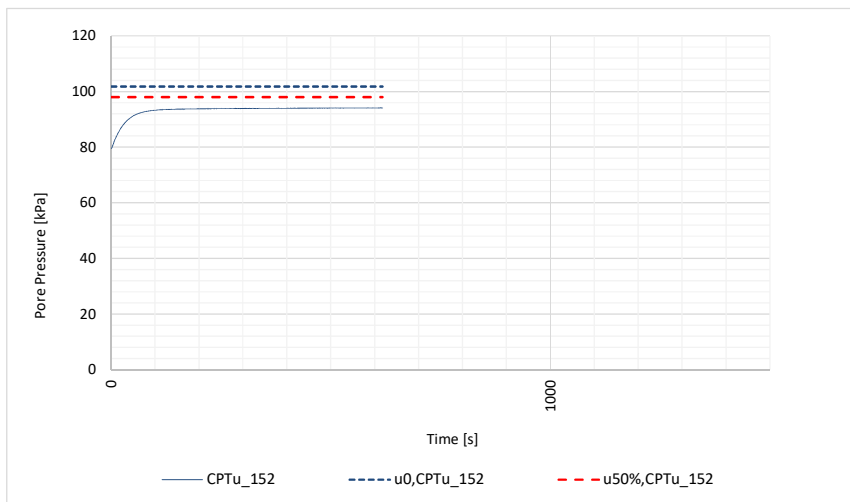
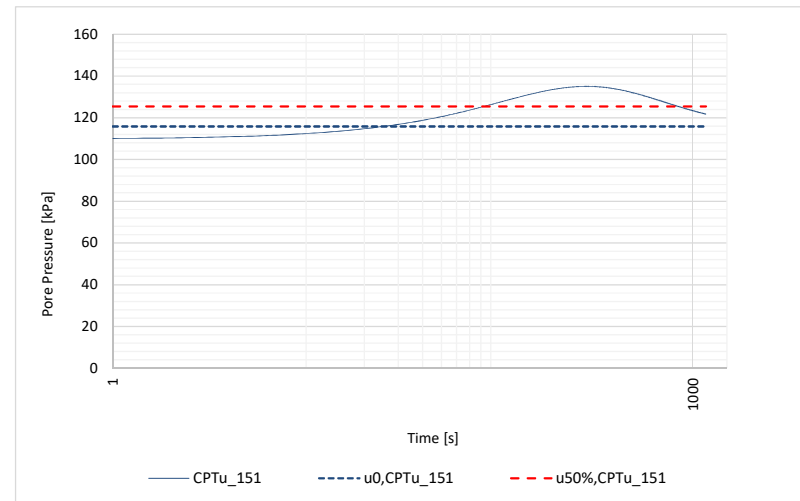
t₅₀ [s]	k [m/s]
954	1,89E-09



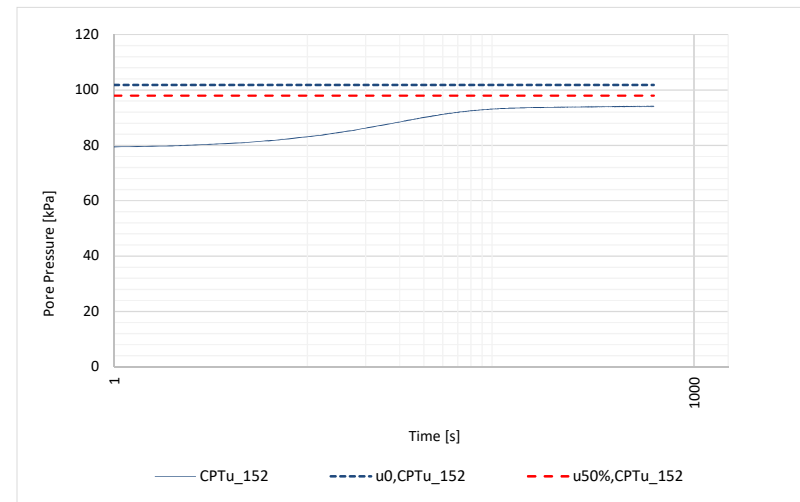
t₅₀ [s]	k [m/s]
	#DIV/0!

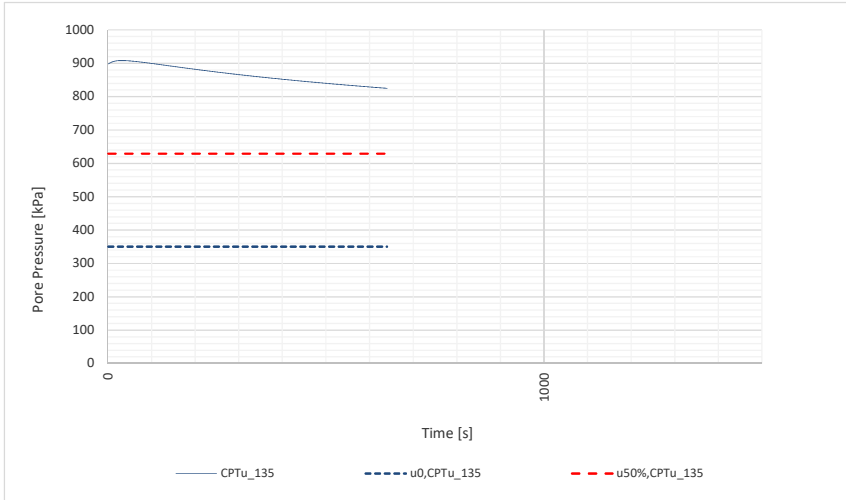


t_{50} [s]	k [m/s]
855	2,16E-09

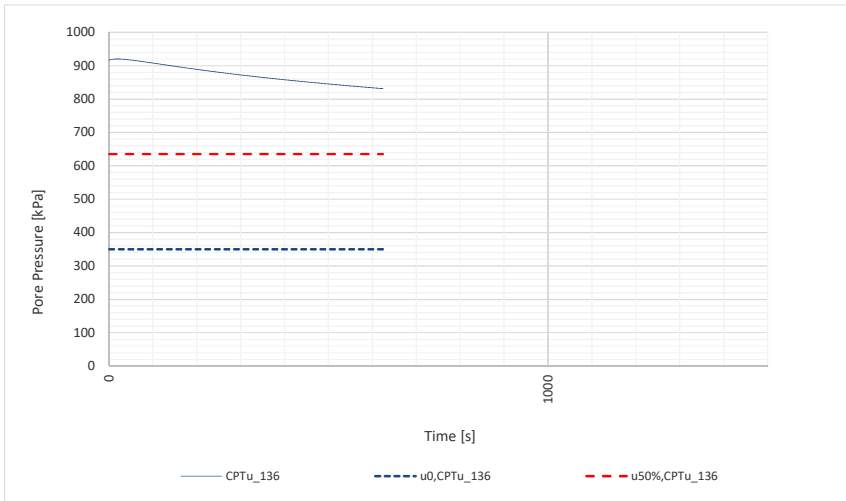
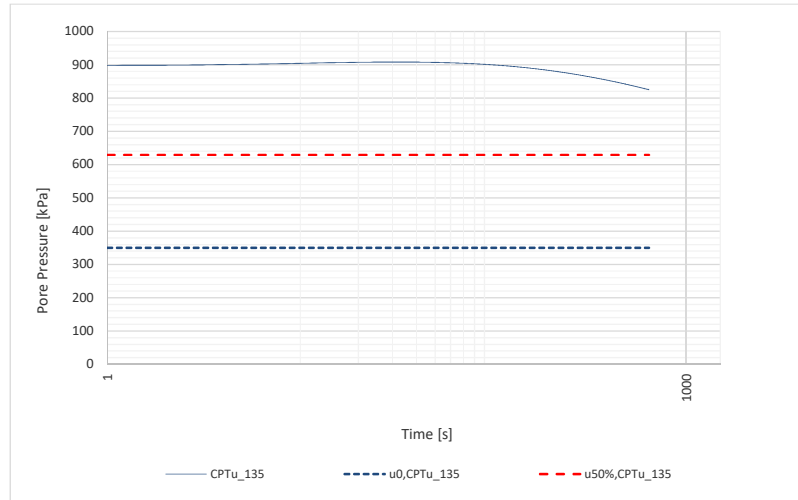


t_{50} [s]	k [m/s]
0	#DIV/0!

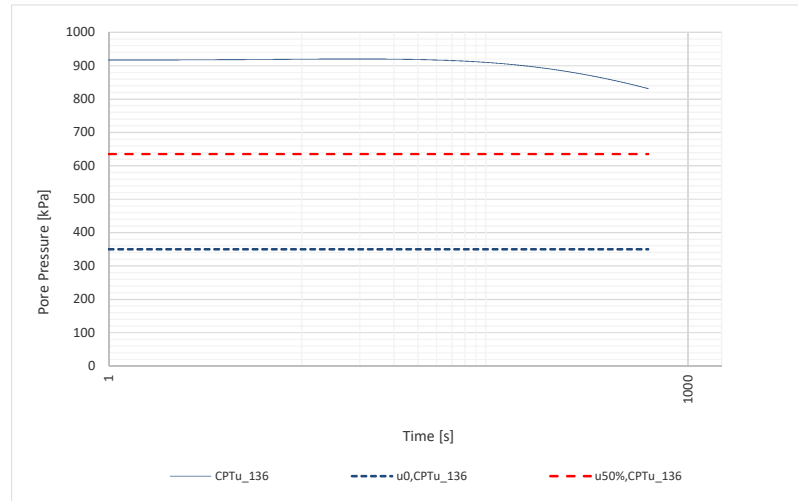


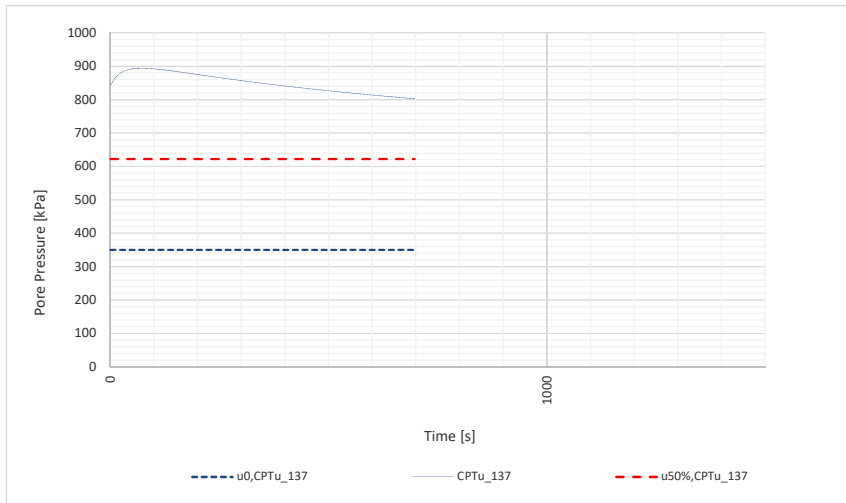


t_50 [s]	k [m/s]
0	#DIV/0!

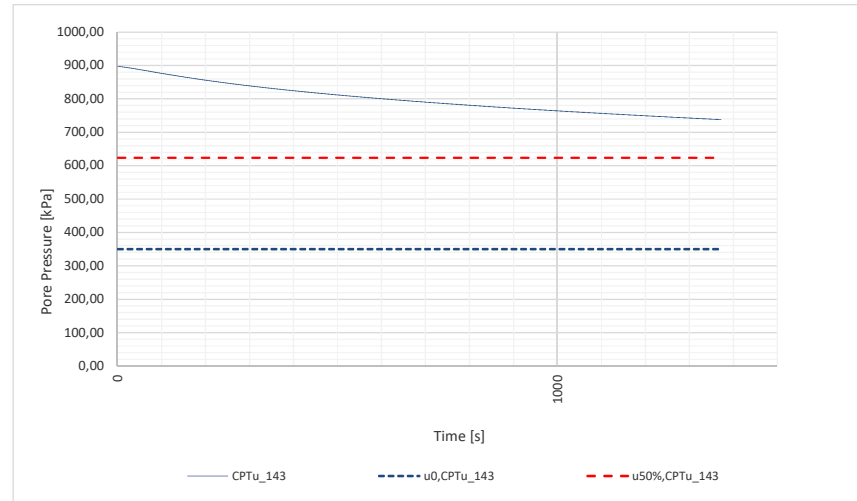
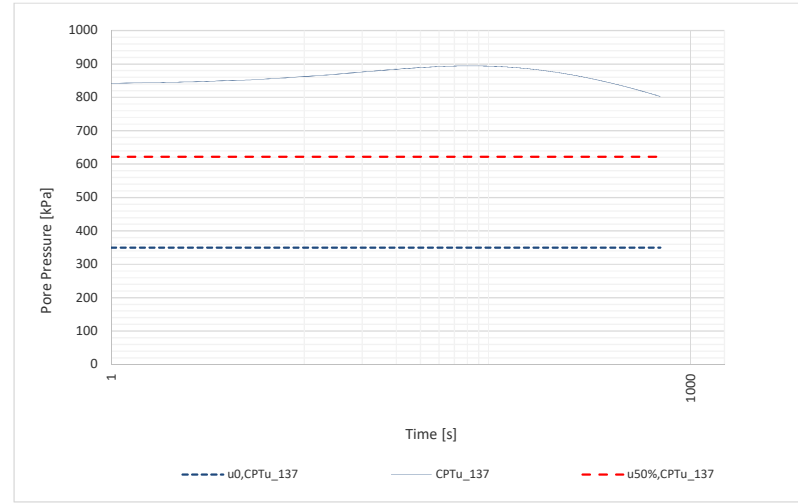


t_50 [s]	k [m/s]
0	#DIV/0!

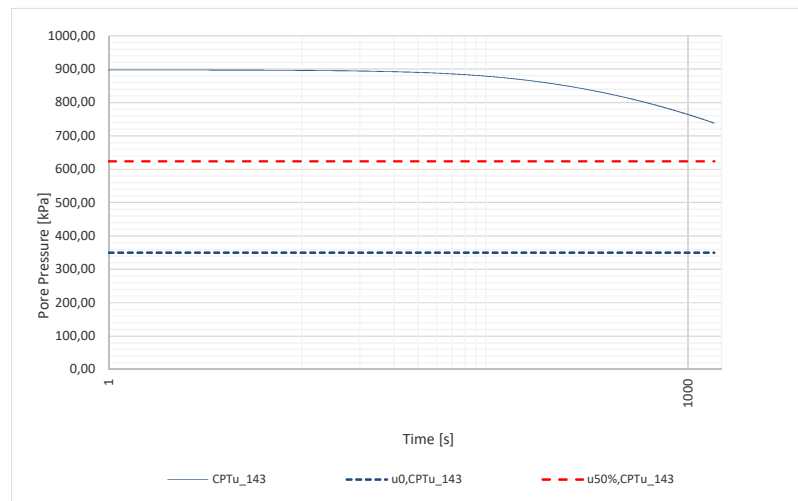


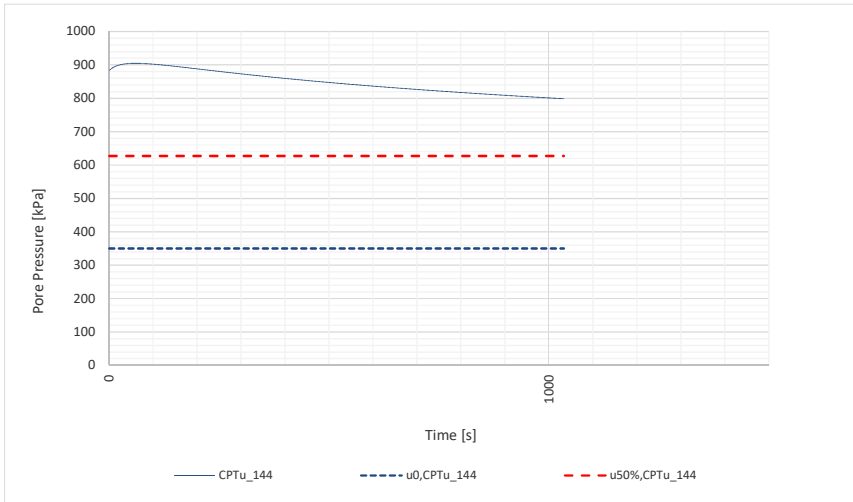


t_50 [s]	k [m/s]
0	#DIV/0!

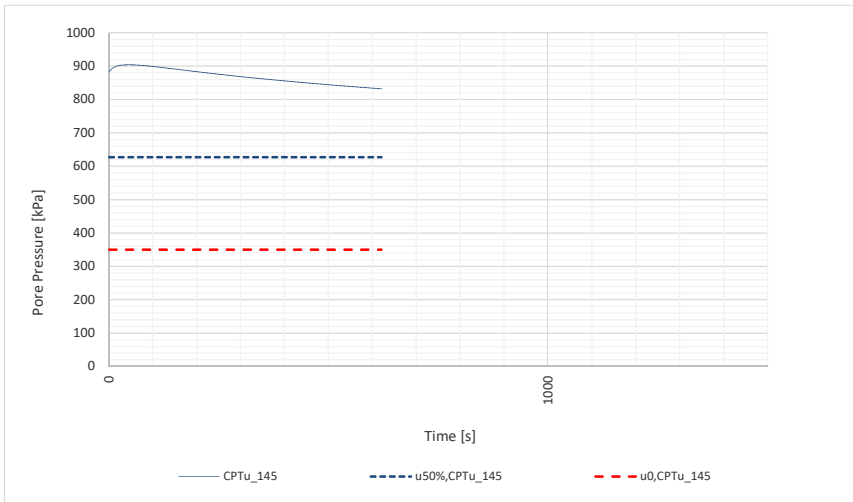
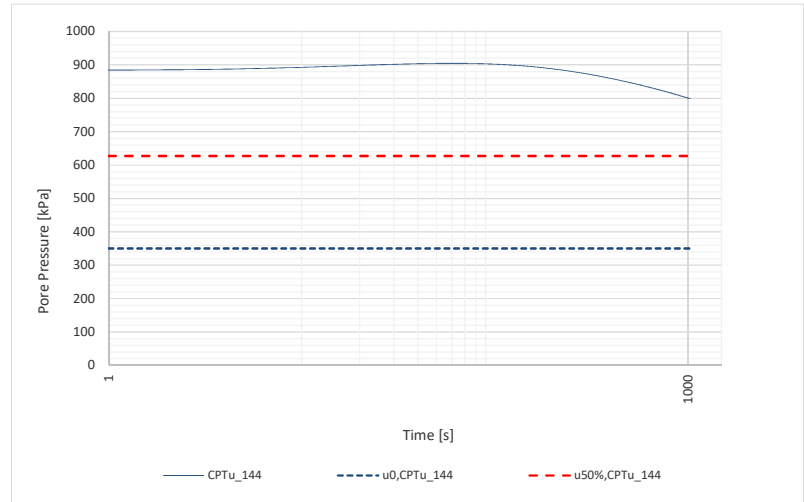


t_50 [s]	k [m/s]
0	#DIV/0!

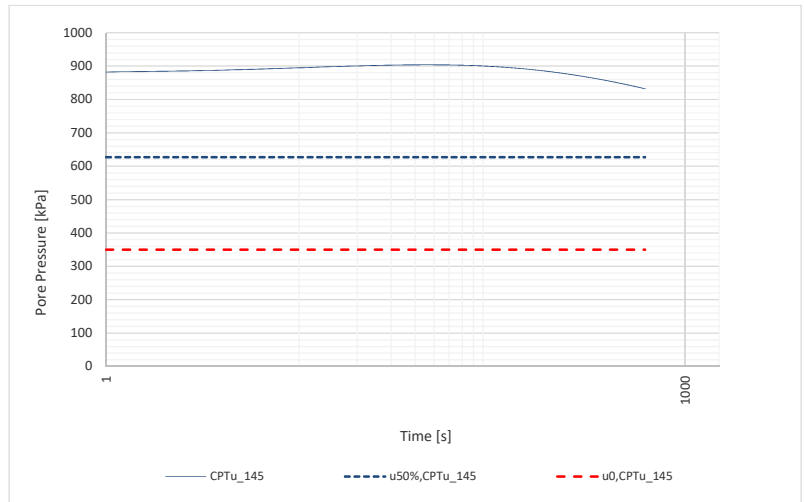


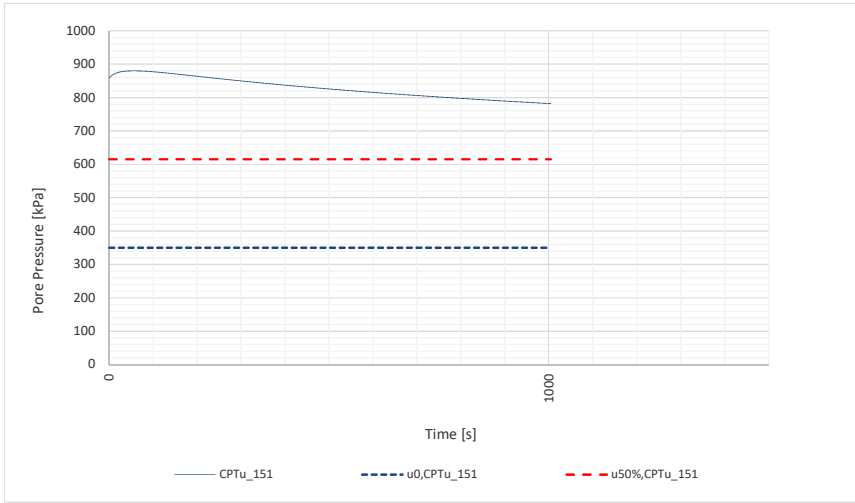


t_50 [s]	k [m/s]
0	#DIV/0!

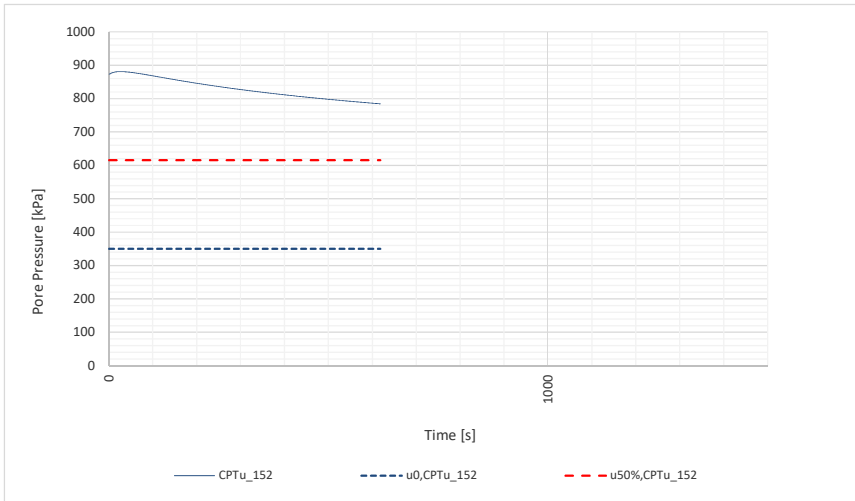
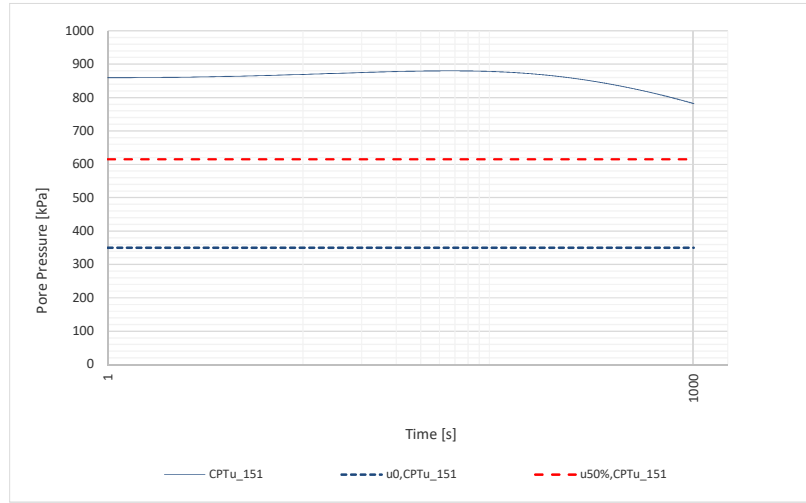


t_50 [s]	k [m/s]
	#DIV/0!





t_50 [s]	k [m/s]
0	#DIV/0!



t_50 [s]	k [m/s]
0	#DIV/0!

